



UNIL | Université de Lausanne

Unicentre

CH-1015 Lausanne

<http://serval.unil.ch>

---

Year : 2020

## Geomorphological characteristics as predictors for vegetation models in alpine environment

Giaccone Elisa

Giaccone Elisa, 2020, Geomorphological characteristics as predictors for vegetation models in alpine environment

Originally published at : Thesis, University of Lausanne

Posted at the University of Lausanne Open Archive <http://serval.unil.ch>

Document URN : urn:nbn:ch:serval-BIB\_EF887773E6157

### **Droits d'auteur**

L'Université de Lausanne attire expressément l'attention des utilisateurs sur le fait que tous les documents publiés dans l'Archive SERVAL sont protégés par le droit d'auteur, conformément à la loi fédérale sur le droit d'auteur et les droits voisins (LDA). A ce titre, il est indispensable d'obtenir le consentement préalable de l'auteur et/ou de l'éditeur avant toute utilisation d'une oeuvre ou d'une partie d'une oeuvre ne relevant pas d'une utilisation à des fins personnelles au sens de la LDA (art. 19, al. 1 lettre a). A défaut, tout contrevenant s'expose aux sanctions prévues par cette loi. Nous déclinons toute responsabilité en la matière.

### **Copyright**

The University of Lausanne expressly draws the attention of users to the fact that all documents published in the SERVAL Archive are protected by copyright in accordance with federal law on copyright and similar rights (LDA). Accordingly it is indispensable to obtain prior consent from the author and/or publisher before any use of a work or part of a work for purposes other than personal use within the meaning of LDA (art. 19, para. 1 letter a). Failure to do so will expose offenders to the sanctions laid down by this law. We accept no liability in this respect.



UNIL | Université de Lausanne

Faculty of Geosciences and Environment  
Institute of Earth Surface Dynamics

# GEOMORPHOLOGICAL CHARACTERISTICS AS PREDICTORS FOR VEGETATION MODELS IN ALPINE ENVIRONMENT

**Ph.D. thesis**

Presented at the  
Faculty of Geosciences and Environment of the University of Lausanne

by

**Elisa Giaccone**

B.Sc. and M.Sc. at the University of Turin (Italy)

to obtain the grade of  
Ph.D. in Geography

## **Jury**

Dr. Christophe Lambiel	Thesis director
Prof. Grégoire Mariéthoz	Thesis co-director
Dr. Christophe Randin	Expert
Prof. Miska Luoto	Expert
Prof. Derek Karssenber	Expert
Prof. Marie-Elodie Perga	Jury president

Lausanne 2020



## IMPRIMATUR

Vu le rapport présenté par le jury d'examen, composé de

Présidente de la séance publique :	Mme la Professeure Marie-Elodie Perga
Présidente du colloque :	Mme la Professeure Marie-Elodie Perga
Co-directeur de thèse :	M. le Docteur Christophe Lambiel
Co-directeur de thèse :	M. le Professeur Grégoire Mariéthoz
Expert interne :	M. le Docteur Christophe Randin
Expert externe :	M. le Professeur Miska Luoto
Expert externe :	M. le Professeur Derek Karssenber

Le Doyen de la Faculté des géosciences et de l'environnement autorise l'impression de la thèse de

### **Madame Elisa GIACCONE**

Titulaire d'un  
*Master en biologie environnementale*  
*De l'Université de Turin*

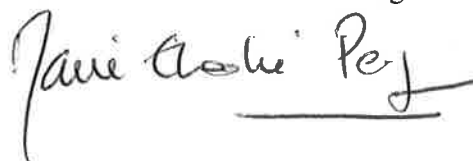
intitulée

## **Geomorphological characteristics as predictors for vegetation models in Alpine environment**

Lausanne, le 31 janvier 2020

Pour le Doyen de la Faculté des géosciences et de  
l'environnement

Professeure Marie-Elodie Perga







“Great things are done when men and mountains meet”

*William Blake*



Alla mia famiglia, radice di ogni cosa



# Acknowledgement

Questo capitolo della mia vita sta giungendo a termine e, volgendomi indietro, tante sono le persone che mi hanno aiutato, sostenuto, incoraggiato o semplicemente che hanno reso migliori piccoli momenti della mia vita. Quello che oggi siamo è frutto di tutti i nostri giorni passati. È quindi giusto ringraziare, fin dove possibile, uno per uno tutti quanti. I will write the acknowledgement in many languages to be understood by each single person concerned.

Je commence par le français pour pouvoir remercier en premier mon directeur de thèse dr. Christophe Lambiel et mon co-directeur Prof. Grégoire Mariéthoz. Merci pour la confiance que vous m'avez donnée dès mon entretien, pour votre présence, pour votre soutien, pour vos innombrables commentaires et suggestions tout le long de ma thèse, merci pour m'avoir poussée plus à fond dans le milieu de la recherche de montagne mais aussi dans les géostatistiques et merci aussi pour les moments de détente partagés avec les équipes.

I gratefully acknowledge my three co-examiners, Prof. Miska Luoto, Prof. Derek Karssenbergh and Dr. Christophe Randin, who accepted to read and evaluate my thesis.

Vifs remerciements à Prof. Antoine Guisan, dr. Pascal Vittoz, dr. Mary Tonini et dr. Fabio Oriani. Comme coordinateur du projet IntegrAlp le premier, comme co-auteurs de mes publications tous vous, pour vos apports scientifiques, vos discussions stimulantes et pour m'avoir accompagnée le long de ces quatre années de thèse, un grand merci.

Merci à tous mes collègues de l'IDYST et de l'ISTE, avec lesquels j'ai partagé des très beaux moments avec des bbqs, des bières, des pizzas, des journées en montagne, des innombrables pauses café, des conseils et des aides pratiques sur logiciels pas toujours appréciés. Merci beaucoup Federico, Gilles, Pascal E., Matteo, Lionel, Inigo, Moctar, Mathieu, Gustavo, Gelare, Clémence, Charlotte, Harsh, Anthony, Tom, Ignes, Sassi, Isabella, Carmen, Benjamin, Nadja, Joanne, Pascal P., Gabriel, Mike, Zoncibe, Filippo, Raphaël N.

Muchas gracias Seb por todos los momentos compartidos junto, grazie per il nostro itañol, per la tua amicizia, per il tuo supporto morale, psicologico, fisico (l'ufficio della plank e dello yoga!), alcoolico e culinario. Grazie Nicola per i primi due anni della mia tesi passati insieme e per aver cercato di non dimenticare del tutto i tuoi vecchi colleghi.

Merci Aline, collègue mais surtout amie, pour tous nos rencontres, discussions, bières, moment de danse bourrée partagée, discours sur les chats et sur plain d'autres choses. Pour m'avoir mieux fait comprendre ce monde suisse et pour m'avoir élargi mille conseils.

Un grand remerciement chaleureux à toutes les personnes qui m'ont aidé pendant mes travaux sur le terrain, en partageant fatigue, paysages magnifiques, nuitées en cabane avec « douche partagée », chutes, sourires et nourriture: Laurianne, Raphaël V., Régis, Anthoni, Cynthia, Boris et une fois de plus Gelare, Lionel et Aline (et les bains). Ça a été un plaisir énorme de travailler avec vous, de partager tous ses moments inoubliables entre fossiles et cristaux et merci aussi pour avoir amélioré mon niveau de français en parlant de mille et un sujets! Merci à l'équipe Otemma avec laquelle j'ai partagé quelques inoubliables journées de camping sauvage: Lila, Hannah et encore Boris, Matteo et Tom.

Grazie Magali, la mia bella franco-piemontesina: anche tu da collega e amica hai saputo darmi tanti consigli e tanti spunti di riflessione sia per la vita lavorativa sia per la vita privata. E te ne ringrazio tanto!

Un remerciement à Carole et Sabrina pour leur travail infatigable et continu.

Come posso non ringraziare tutti i miei amici più o meno esterni a Losanna e all'università che mi hanno accompagnato nel corso di questi anni? Vielen danken Corinne for your friendship, le group des jeunes géomorphologues suisses et en particulier Julia, Mario, Dorota, Monica, Jonathan et Chantal (come annunciato, grazie Chantal per il tuo “sostegno culinario e alcolico”), Andrea il motivatore personale per la piscina e cuoco provetto, Norma il mio raggio di sole e compagna di risate tra una pioggia losannese e l'altra.

Italiana sono e italiana resto nell'anima. Un grazie di cuore a tutta la mia famiglia, Matteo, mia mamma e mio papà, per aver sempre creduto in me e nel fatto che potessi sentirmi realizzata anche oltralpe. Alle mie due care nonne Luciana e Giovanna che mi hanno sempre sostenuta con manicaretti cucinati amorevolmente, attività sartoriali, contribuzione nelle pulizie domestiche, tante preghiere, qualche lacrima e tantissimo amore. Grazie anche ai miei due cari nonni, Romeo ed Eraldo, che da lassù, o da qualunque parte essi siano, hanno sempre vegliato sulla loro nipote, ne sono sicura. E un pensiero va anche a zia Ida, partita a ritrovare zio Toni e nonno. Grazie Simone per essere parte integrante della mia vita, per aver lottato e combattuto con e contro di me su svariati aspetti e di essere ancora qua, circondati da peli di Leo, a condividere questa vita che chissà cosa ci riserva ancora. E grazie anche alla tua famiglia.

Grazie a Gaia la mia storica amica dal liceo, a Cecilia e Valentina le mie sorelle acquisite d'università, a Marco e Vanessa, compagni di coppia e compagni di sventure dottorali, alla mia finta sorellina Giulia con la quale girerei il mondo, e all'altra Giulia ritrovata perché è sempre bello ricordare le proprie origini valcasottesesi e le costellazioni gelato, ad Antonellina che si è aggiunta con la sua solarità alla mia famiglia. E ancora a Riccardo, Mattia, Nicola, Cristina, Anna, Irene. Alle flamenquitas per la loro grinta ed energia e per avermi fatto dimenticare per un'ora a settimana tutto il resto.

Et je voudrais encore remercier de tout cœur toutes les personnes qu'ici je n'ai pas nommé mais qui ont contribué à la réussite de ce travail. Un très grand merci.

Elisa

Lausanne, 5 novembre 2019

## **Financial Support**

The author is grateful to the Swiss National Science Foundation for funding this project (CR23I2\_162754) entitled “Integrating spatial predictions of vegetation, soils, geomorphology and hydrology for improved assessment of ecosystem services under climate change”.

## **Credits and copyright**

Giaccone E. (2020). Geomorphological predictor for vegetation models in alpine environment. Thesis, University of Lausanne. Posted at the University of Lausanne Open Archive (<http://serval.unil.ch>)

## **Copyright**

The University of Lausanne expressly draws the attention of users to the fact that all documents published in the SERVAl Archive are protected by copyright in accordance with federal law on copyright and similar rights (LDA). Accordingly it is indispensable to obtain prior consent from the author and/or publisher before any use of a work or part of a work for purposes other than personal use within the meaning of LDA (art. 19, para. 1 letter a). Failure to do so will expose offenders to the sanctions laid down by this law. We accept no liability in this respect.

## **Droits d’auteur**

L’Université de Lausanne attire expressément l’attention des utilisateurs sur le fait que tous les documents publiés dans l’Archive SERVAl sont protégés par le droit d’auteur, conformément à la loi fédérale sur le droit d’auteur et les droits voisins (LDA). A ce titre, il est indispensable d’obtenir le consentement préalable de l’auteur et/ou de l’éditeur avant toute utilisation d’une oeuvre ou d’une partie d’une oeuvre ne relevant pas d’une utilisation à des fins personnelles au sens de la LDA (art. 19, al. 1 lettre a). A défaut, tout contrevenant s’expose aux sanctions prévues par cette loi. Nous déclinons toute responsabilité en la matière.



# Abstract

The alpine environments are composed of numerous natural elements, interconnected between them and involved in different processes. However, the alpine areas are highly sensitive to actual global warming and it becomes crucial to study these elements at fine scale and to implement models at large scale to better understand their interactions and their future evolution. While the relationships between plants and soil-topo-climatic variables have been yet highlighted, specific aspects of the relationships between plant and geomorphic remained unclear, in particular at high elevations. Consequently, the aim of the present thesis is to investigate how geomorphic processes and landforms influence alpine vegetation communities and thus provide geomorphic predictors for plant species distribution models. To meet this purpose, statistical and quantitative approaches coupled with data analysis has been developed and three sub-objectives have been established.

The first sub-objective is the study of the fine scale effects of geomorphic processes on vegetation communities in the alpine environment. To this end, 72 vegetation plots across three focus sites in the Vaud Alps are carried out, coupled with ground microclimate monitoring with iButtons and evaluation of landform morphodynamics and earth surface processes (solifluction, rill erosion, nivation and frost weathering). The relationships between plant communities and environmental variables are analysed using non-metric multi-dimensional scaling (NMDS) and multivariate regression techniques. Landform morphodynamics, growing degree days (sum of degree days above 5 °C) and mean ground surface temperature are the most important explanatory variables of plant community composition. Furthermore, the regression models for species cover and species richness are significantly improved by adding the morphodynamics variable. This thesis section provided complementary support that landform morphodynamics is a key factor, together with ground temperature, to explain alpine plant distribution and community composition.

The second sub-purpose is the development of a methodology to analyse debris size on extended surfaces and perform debris size distribution maps, which can be employed as predictor variable on plant species distribution models. Indeed, grain size is an important factor influencing the type of plant communities and the ground thermal regime in alpine environments. The developed methodology is based on high-resolution optical imagery, acquired by drones, which are processed with the Basegrain algorithm to identify the grain size. The debris size detected by the algorithm is validated and calibrated before proceeding with the elaboration. Artefacts related to the presence of shadows, vegetation, or snow are generated during the grain detection phase, and they are corrected before the computation of the debris size distribution map. This methodology is applied in two focus sites in the Vaud Alps, but it can be exploited in another context where debris are visible.

The third sub-objective is to implement a methodology to perform semi-automated geomorphological maps, which can constitute an important environmental predictor at large scale for plant species models. Particularly, two different methodologies are applied: the geostatistical approach Direct Sampling (DS) and the machine learning algorithm Random Forest (RF). Both approaches are tested with 13 environmental predictor variables to simulate a geomorphological classification of 8 classes. Results are compared with a classical geomorphological map based on field data acquisition. Both methods present a similar accuracy and a Cohen's Kappa of 0.46. Late Glacial deposits, glaciers, rock outcrops and rock walls are identified with high precision, while alluvial fans and alluvial plains show the highest misclassification errors. The results suggest that

DS and RF are both suitable techniques to simulate semi-automated geomorphological maps in alpine environments and on regional scale.

# Résumé

Les environnements alpins sont composés de nombreux éléments naturels, qui sont interconnectés et impliqués dans différents processus. Cette complexité rend nécessaire une étude à échelle locale ainsi que la mise en œuvre de modèles régionaux pour mieux comprendre les interactions qui façonnent ces environnements, surtout sous les effets du réchauffement climatique actuel. Tandis que les relations parmi les plantes et les variables sol-topo-climatiques ont été largement investiguées, les aspects spécifiques des relations entre plantes et processus géomorphologiques sont restés dans l'ombre, en particulier à haute altitude. Pour cette raison, le but de la présente thèse est d'étudier comment les processus géomorphologiques et les formes géomorphologiques influencent les communautés végétales alpines et, ainsi, d'identifier des prédicteurs géomorphologiques pour les modèles de distribution d'espèces végétales. Cet objectif principal est scindé en trois sous-objectifs qui sont traités selon une approche statistique et quantitative.

Le premier sous-objectif est l'étude à petite échelle des effets des processus géomorphologiques sur les communautés végétales en milieu alpin. Pour cela, 72 relevés de végétation répartis sur trois sites des Alpes Vaudoises ont été effectués et couplés d'une part à un suivi du microclimat du sol avec des capteurs de température (iButtons), et d'autre part à une évaluation de la morphodynamique du relief et des processus superficiels. Les relations entre les communautés végétales et les variables environnementales sont analysées à l'aide de techniques de positionnement multidimensionnel non-métrique (NMDS) et de régression multivariée. Il ressort de ces analyses que la morphodynamique du relief, les degrés-jours de croissance (somme des degrés-jours au-dessus de 5 °C) et la température moyenne au sol sont les variables explicatives les plus importantes pour la composition des communautés végétales. Ceci implique que l'ajout d'une variable morphodynamique améliore considérablement les modèles de régression pour la couverture végétale et la richesse spécifique.

Le deuxième sous-objectif consiste à développer une méthode d'analyse de la taille des débris sur des surfaces étendues. Ceci permet de réaliser des cartes de distribution de cette variable, qui peut alors être utilisée comme variables prédictives dans les modèles de distribution d'espèces végétales. En effet, dans les environnements alpins, la taille des débris est un facteur important qui influence le type de communauté végétale et le régime thermique du sol. La méthodologie développée est basée sur des images optiques à haute résolution, acquises par des drones et traitées avec l'algorithme Basegrain afin d'identifier la taille des débris. Cette taille détectée par l'algorithme est validée et calibrée par comparaison avec des mesures à la main. Des artefacts liés à la présence d'ombres, de végétation ou de neige apparaissent lors de la phase de détection des grains mais ils sont corrigés avant le calcul de la carte de répartition de la taille des débris. Cette méthodologie est appliquée à deux sites tests dans les Alpes Vaudoises, mais elle peut facilement être généralisée à tout site où des débris sont visibles.

Le troisième sous-objectif vise à générer des cartes géomorphologiques semi-automatisées, qui constituent un important prédicteur environnemental à grande échelle pour les modèles d'espèces végétales. Deux approches distinctes ont été appliquées à la création de cartes géomorphologiques: l'approche géostatistique Direct Sampling (DS) et l'algorithme d'apprentissage automatique Random Forest (RF). Ces deux approches sont testées avec 13 variables environnementales prédictives afin de simuler une classification géomorphologique en 8 classes. Les résultats sont comparés à une carte géomorphologique classique basée sur l'acquisition de données de terrain.

Les deux méthodes testées présentent une précision similaire et une valeur modérée de Kappa de Cohen de 0,46. Les dépôts glaciaires datant du Tardiglaciaire, les glaciers, les affleurements rocheux et les parois rocheuses sont identifiés avec une haute précision, tandis que les cônes de déjection et les plaines alluviales présentent une erreur de classification plus élevée. Ces résultats suggèrent que DS et RF sont deux techniques appropriées pour la simulation semi-automatisée de cartes géomorphologiques dans les environnements alpins et à l'échelle régionale.

# Riassunto

Gli ambienti alpini sono composti da numerosi elementi naturali, interconnessi tra loro e coinvolti in diversi processi. Tuttavia, poiché le aree alpine sono estremamente sensibili all'attuale riscaldamento globale, diventa cruciale studiare questi elementi su scala locale e sviluppare modelli su scala regionale per poter comprendere meglio le loro interazioni e la loro futura evoluzione. Mentre le relazioni tra piante e variabili edafiche-topografiche-climatiche sono state ampiamente affrontate, aspetti specifici delle relazioni tra piante e processi geomorfici sono rimasti poco noti, soprattutto ad alta quota. Di conseguenza, lo scopo della presente tesi è di studiare come i processi geomorfici e le forme del terreno influenzino le comunità di vegetazione alpina e, quindi, di fornire predittori geomorfici per i modelli di distribuzione delle specie vegetali. Per raggiungere questo scopo, è stato sviluppato un approccio statistico e quantitativo, associato all'analisi dei dati, e sono stati fissati tre sotto-obiettivi.

Il primo sotto-obiettivo è lo studio a scala locale degli effetti dei processi geomorfici sulle comunità vegetali in ambiente alpino. A tal fine, 72 rilievi di vegetazione sono stati eseguiti in tre siti di studio nelle Alpi del Canton Vaud e sono stati accompagnati dal monitoraggio del microclima del suolo con sensori di temperatura (iButtons) e dalla valutazione della morfodinamica del terreno e dei processi superficiali terrestri. Le relazioni tra le comunità vegetali e le variabili ambientali sono state analizzate tramite tecniche di ridimensionamento multidimensionale non metrico (NMDS) e di regressione multivariata. Il risultato di queste analisi mostra che la morfodinamica del terreno, la somma termica (somma dei gradi giorno superiori a 5 °C) e la temperatura media della superficie del suolo sono le variabili esplicative più importanti per la composizione delle comunità vegetali. Inoltre, i modelli di regressione per la copertura vegetale e la ricchezza specifica sono significativamente migliorati aggiungendo la variabile morfodinamica.

Il secondo sotto-obiettivo è lo sviluppo di una metodologia per analizzare la dimensione dei detriti su superfici estese ed eseguire, successivamente, una mappa di distribuzione della taglia degli stessi. Tale mappa può essere impiegata come variabile predittiva nei modelli di distribuzione di specie vegetali. Infatti, la dimensione del detrito è un fattore importante che influenza il tipo di comunità vegetali e il regime termico del suolo negli ambienti alpini. La metodologia sviluppata si basa su immagini ottiche ad alta risoluzione, acquisite da droni, che vengono elaborate dall'algoritmo Basegrain per identificare la dimensione del detrito. La dimensione dei detriti rilevata dall'algoritmo viene in seguito validata e calibrata prima di procedere con l'elaborazione. Alcuni artefatti, relativi alla presenza di ombre, vegetazione o neve, vengono generati durante la fase di identificazione del detrito e vengono corretti prima dell'elaborazione della mappa di distribuzione delle dimensioni dei detriti. Questa metodologia è stata applicata in due aree di studio nelle Alpi del Canton Vaud, ma può essere sfruttata in altri contesti in cui sono visibili i detriti.

Il terzo sotto-obiettivo è l'implementazione di una metodologia per elaborare mappe geomorfologiche semi-automatizzate, che possono costituire un importante predittore ambientale su larga scala per i modelli di specie vegetali. Per raggiungere questo obiettivo, due diverse metodologie sono state applicate: l'approccio geostatistico Direct Sampling (DS) e l'algoritmo di apprendimento automatico Random Forest (RF). Entrambi gli approcci sono testati con 13 variabili predittive ambientali per simulare una classificazione geomorfologica di 8 classi. I risultati sono stati confrontati con una classica mappa geomorfologica basata sull'acquisizione dei dati in campo. Entrambi i metodi presentano una precisione simile e un valore moderato di Kappa di

Cohen pari a 0,46. Depositi glaciali datati al Tardoglaciale, ghiacciai, affioramenti rocciosi e pareti rocciose sono identificati con maggiore precisione, mentre i coni di detrito e le pianure alluvionali mostrano un più alto errore di classificazione. I risultati suggeriscono che DS e RF sono entrambe tecniche adatte per simulare mappe geomorfologiche semi-automatizzate in ambienti alpini e su scala regionale.

# Contents

<b>Acknowledgement</b> .....	<b>i</b>
<b>Abstract</b> .....	<b>iv</b>
<b>Résumé</b> .....	<b>vi</b>
<b>Riassunto</b> .....	<b>viii</b>
<b>List of Figures</b> .....	<b>xiii</b>
<b>List of Tables</b> .....	<b>xvii</b>
<b>List of Abbreviations</b> .....	<b>xix</b>
<b>1. Introduction</b> .....	<b>1</b>
1.1 Motivation.....	1
1.2 Research context.....	2
1.2.1 Geomorphic processes and landforms.....	2
1.2.1.1 <i>Classification of geomorphic processes</i> .....	2
1.2.1.2 <i>Landform mapping</i> .....	5
1.2.1.3 <i>Climate change acting on sediment fluxes</i> .....	5
1.2.2 Vegetation on alpine environment.....	8
1.2.2.1 <i>Alpine plant life conditions and controlling factors</i> .....	8
1.2.2.2 <i>Disturbance factors and their involvement on plant models</i> .....	9
1.2.2.3 <i>Plant – geomorphological system: joint conceptualization</i> .....	11
1.3 The IntegrAlp project .....	12
1.4 Objectives of the thesis.....	14
1.5 Thesis outline .....	15
<b>2. Influence of microclimate and geomorphological factors on alpine vegetation in the Western Swiss Alps</b> .....	<b>18</b>
2.1 Introduction.....	20
2.2 Material and methods.....	21
2.2.1 Study area.....	21
2.2.2 Vegetation plot surveys .....	24
2.2.3 Ground surface temperature monitoring.....	26
2.2.4 Statistical analysis .....	26
2.3 Results .....	28
2.3.1 Plant communities.....	28
2.3.2 Ground Surface Temperatures.....	30
2.3.3 Vegetation–environment relationships .....	32

2.4	Discussion.....	37
2.5	Conclusion.....	40
2.6	Acknowledgements.....	41
2.7	Supplementary material.....	42
<b>3.</b>	<b>Large scale debris size mapping in alpine environment using UAVs imagery .....</b>	<b>57</b>
3.1	Introduction.....	59
3.2	Methods.....	60
3.2.1	Study area and data acquisition.....	61
3.2.2	Grain detection.....	63
3.2.3	Validation and calibration.....	64
3.2.4	Debris size distribution map.....	64
3.2.5	Innovative aspects.....	65
3.3	Results and discussion.....	65
3.3.1	Validation test and calibration.....	65
3.3.2	Debris size map results.....	66
3.3.3	Limitations.....	68
3.4	Data and code availability.....	72
3.5	Conclusions.....	72
3.6	Acknowledgments.....	74
<b>4.</b>	<b>Semi-automated geomorphological mapping in mountain environment.....</b>	<b>75</b>
4.1	Introduction.....	77
4.2	Material and Methods.....	78
4.2.1	Direct Sampling.....	78
4.2.2	Random Forest.....	79
4.2.3	Test design and dataset.....	79
4.2.4	Landform classification.....	81
4.2.5	Model validation.....	83
4.3	Results.....	84
4.3.1	Direct Sampling.....	84
4.3.2	Random Forest.....	85
4.4	Discussion.....	90
4.5	Conclusion.....	92
4.6	Acknowledgments.....	92
<b>5.</b>	<b>Outcomes at larger temporal and spatial scale .....</b>	<b>93</b>
5.1	Microclimate monitoring.....	93
5.2	Permafrost distribution in the Vaud Alps.....	95



5.3	Semi-automated geomorphological map in the Vaud Alps .....	98
<b>6.</b>	<b>Synthesis and conclusions .....</b>	<b>102</b>
6.1	General discussion.....	102
6.2	Conclusions and perspectives .....	105
<b>7.</b>	<b>Bibliography.....</b>	<b>107</b>
<b>8.</b>	<b>Appendices.....</b>	<b>124</b>

# List of Figures

<b>Figure 1.1</b> - Permafrost stratigraphy and ground thermal profile (modified from French, 2007).	.3
<b>Figure 1.2</b> - Temperature anomalies from the mean 1961-1990 in Switzerland (period 1864-2018). Modified from ©MeteoSwiss.	7
<b>Figure 1.3</b> - Schematic representation about a sediment flux on paraglacial environment. Adapted from Cossart (2014).	7
<b>Figure 1.4</b> - Representation of the three upper vegetation belts in European Alps.	8
<b>Figure 1.5</b> - Structure of the IntegrAlp project, with the four thematic modules, their interactions and the module about data integration. The output model aims assessing the mountain ecosystem services, the landscape aesthetic value and the water provision/regulation.	13
<b>Figure 1.6</b> - Location of the regional study area (Vaud Alps, left) and the local study area (Vallon de Nant, right).	14
<b>Figure 1.7</b> - Conceptual figure summarizing the research questions, the used data sets and the main methods.	17
<b>Figure 2.1</b> - A) Locations of the three selected sites. The red star indicates the location of Pont de Nant (1253 m a.s.l.) B) Topographic map of Les Martinets and Col des Perris Blancs. C) Topographic map of Les Outans. D) Detailed picture of Les Martinets, seen from the Col des Perris Blancs (August 2016); a: The Glacier des Martinets; b: LIA moraine; c: Holocene moraines; d1: rock glacier, upper lobe; d2: rock glacier, lower lobe; e: talus slope. E) Detailed picture of Col des Perris Blancs, seen from the namesake alpine pass (September 2018); f: debris slope; g: alpine grassland. F) Detailed picture of Les Outans; h: steep latero-frontal moraines of the debris-covered glacier; i: debris slope (September 2018). SwissMapRaster © swisstopo (DV084371).	23
<b>Figure 2.2</b> - Location of vegetation plots, grouped based on cluster analysis. Colors indicate the value of the Freezing degree days index (01.10.2016 - 30.09.2018) for Les Outans, Col des Perris Blancs and Les Martinets. SwissImage © swisstopo (DV084371).	31
<b>Figure 2.3</b> - NMDS biplot of the vegetation plots, based on the Bray–Curtis dissimilarity matrix, with fitted vectors of all environmental factors. The plot data are regrouped in 5 groups. Ordination stress = 0.22. GSL = Growing Season Length; GDD = Growing Degree Day; FDD = Freezing Degree Day; MGST = Mean Annual Ground Surface Temperature; TVDI = Temperature Vegetation Dryness Index.	33
<b>Figure 2.4</b> - Relationship between the plant community (black points; ordination conducted using NMDS) and the environmental variables that are the most significant. The blue vectors indicate the direction of maximum linear correlation (ordination score reported in percentage). The red smoothed surface fits represent the change of the variable between the plots. The <i>p-value</i> of vectors is < 0.001 for (a)-(g) and < 0.05 for (h)-(i). GSL = Growing Season Length; GDD = Growing Degree Day; FDD = Freezing Degree Day; TVDI = Temperature Vegetation Dryness Index.	35
<b>Figure 2.5</b> - Species cover (a-c) and species richness (d-g) models conducted using GAMs. (a-b) and (d-f) represent the baseline explanatory variables, (c) and (g) the environmental variables added to improve models. The x-axis represents the environmental variables and the y-axis the smoothed factor of the variable with estimated degrees of freedom. Shaded area represents the confidence interval. GDD = Growing Degree Day. FDD = Freezing Degree Day. Symbols between [ ] indicate statistical significance. [***] = p-value < 0.001; [*] = p-value < 0.05; [.] = p-values < 0.1; [ns] = not significant.	36
<b>Figure 2.6</b> - Longitudinal electrical resistivity tomography (ERT) profile realized the 16 <sup>th</sup> August 2016 on Les Martinets rock glacier. The x-axis represents the longitudinal distance in meters from	

the profile starting point and the y-axis the elevation (m a.s.l.). The ERT profile was carried out with 48 electrodes and an inter-electrode spacing of 5 m from the upper lobe (UL) to the half part of the lower lobe (LL). The apparent resistivity were measured with the Syscal Pro Switch 96 (Iris Instruments). Salt-water saturated sponges were used to improve the contact between the electrodes and the ground because the surface was characterized by plurimetric blocks. Collected data were analysed with the Prosys II software, in which the surface topography measured with dGPS was inserted. The inversion was carried out with the RES2DINV software. We choose least-square inversion and robust parameters, providing a good visualization of high resistivity contrasts (for further details in the methodology see (Bosson et al., 2015; Marecot, 2006). A high resistivity body (30 kΩm on average with maximum of 300-500 kΩm) is present in the upper part of the UL up to a depth of 30 m. This can be interpreted as a permafrost layer. In the lower part of the UL, no permafrost is detected, considering low resistivity values (< 5 kΩm). In the LL, small patches of very high resistivities (300-500 kΩm) are interpreted as permafrost lenses. However, care have to be taken in the interpretation because of the relatively high error value (12.4%).....42

**Figure 2.7** - Left. Frequency of species cover [%]. Center. Frequency of species richness [n°]. Right. Frequency of evenness.....45

**Figure 2.8** - Temperature distributions (period from 1<sup>st</sup> October 2016 to 30<sup>th</sup> September 2018) of iButtons, grouped according to plant composition. The box-plot delimit the 1<sup>st</sup> and the 3<sup>rd</sup> quantiles and the median (bold segment). The dotted line indicates the extremes and the small circle the outliers.....46

**Figure 2.9** - Examples of temperature evolution during one year. RD = basal-ripening data; MD = melt-out date. iButton n°2 is located at 2300 m a.s.l. in Les Martinets, in a debris area composed of ancient rock fall deposit and avalanche deposit. It does not have RD because of lack of ground freezing during the winter. iButton n°63 is situated in the upper part of the creeping talus slope in Col des Perris Blancs site, at 2426 m of elevation. In this case, both RD and MD were detected. ....47

**Figure 2.10** - Correlation matrix between explanatory variables based on Spearman's rank correlation coefficient. Spearman correlation coefficient was set to  $|ρ| > 0.7$  as criterion to limit collinearity between the variables. MGST = Mean Annual Ground Surface Temperature; Tmin = minimum temperature; Tmax = maximum temperature; FDD = Freezing Degree Day; GDD = Growing Degree Day; GSL = Growing season length; TVDI = Temperature Vegetation Dryness Index.....48

**Figure 2.11** - Baseline GLM of species cover, with normal explanatory variables, family argument “Quasipoisson”. Residuals vs Fitted, Normal Q-Q, Scale-Location and Residuals vs Leverage plots are shown.....49

**Figure 2.12** - Baseline GLM of species cover, with quadratic explanatory variables, family argument “Quasipoisson”. Residuals vs Fitted, Normal Q-Q, Scale-Location and Residuals vs Leverage plots are shown.....50

**Figure 2.13** - Advanced GLM of species cover, with normal explanatory variables, family argument “Quasipoisson”. Residuals vs Fitted, Normal Q-Q, Scale-Location and Residuals vs Leverage plots are shown.....51

**Figure 2.14** - Advanced GLM of species cover, with quadratic explanatory variables, family argument “Quasipoisson”. Residuals vs Fitted, Normal Q-Q, Scale-Location and Residuals vs Leverage plots are shown.....52

**Figure 2.15** - Baseline GLM of species cover, with normal explanatory variables, family argument “Quasibinomial”. Residuals vs Fitted, Normal Q-Q, Scale-Location and Residuals vs Leverage plots are shown.....53

**Figure 2.16** - Baseline GLM of species cover, with quadratic explanatory variables, family argument “Quasibinomial”. Residuals vs Fitted, Normal Q-Q, Scale-Location and Residuals vs Leverage plots are shown.....54

**Figure 2.17** - Advanced GLM of species cover, with normal explanatory variables, family argument “Quasibinomial”. Residuals vs Fitted, Normal Q-Q, Scale-Location and Residuals vs Leverage plots are shown.....55

**Figure 2.18** - Advanced GLM of species cover, with quadratic explanatory variables, family argument “Quasibinomial”. Residuals vs Fitted, Normal Q-Q, Scale-Location and Residuals vs Leverage plots are shown.....56

**Figure 3.1** - Flowchart showing the developed methodology. UAVs: Unmanned Aerial Vehicles. ....61

**Figure 3.2** - A) Location of the study area. B) Orthomosaic of Les Martinets (eBee RTK UAV, October 2016); a: Les Martinets glacier; b: LIA moraine; c: Holocene moraines; d: rock glacier; e: talus slope; f: rock falls / avalanche deposits. C) Orthomosaic of les Outans (Phantom 3 professional UAV, September 2016); g: debris-covered glacier; h: debris slope; i: bedrock outcrop. D) Digital Surface Model of Les Martinets. E) Digital Surface Model of Les Outans. ....62

**Figure 3.3** – Validation and calibration curves for Les Martinets (left side) and Les Outans (right side) images. The y-axis represents the ellipse size estimated in Basegrain (square meters SQM), the x-axis the real size (square meters SQM) of debris measured manually in ArcGIS. The equation of the curves is shown in the top part in black and it was employed to calibrate data before proceeding with the computing of the median area. R = Spearman’s rank correlation;  $p$  = p-value. In red, the equation after the calibration. The 200 black dots are the grain size values before calibration, the 200 red dots the values after calibration. ....66

**Figure 3.4** - DSD map with median values (a and d on the top), standard deviation values (b and e in the middle) and the original orthophoto with the main landforms delimited by colored contours (c and f on the bottom) for Les Martinets and Les Outans focus sites. The red square in a indicates the zoom reported in Figure 3.6. Landforms explanation in c) and f): a: Les Martinets glacier; b: LIA moraine; c: Holocene moraines; d: rock glacier; e: talus slope; f: rock falls / avalanche deposits; g: debris-covered glacier; h: debris slope; i: bedrock outcrop. ....69

**Figure 3.5** - Zoom of Figure 3.4, DSD map - Les Martinets - Median. Examples of large boulders divided in smaller blocks (circles red, orange, fuchsia and green). DSD map - Median: mobile mean values (sqm) developed starting from the density map of the debris size values. DSD map – Standard Deviation: mobile standard deviation values (sqm) developed starting from the density map of the debris size values. Basegrain estimation: processed tile with delineated ellipses in correspondence to the debris. Orthophoto: original part of the tile from UAV campaign.....70

**Figure 3.6** - Example of Basegrain results (a, c and e) and original images (b, d and f). The scale is represented in pixel. In a-d 1 px = 5.75 cm; in e-f 1 px = 3 cm. In a and b, the red ovals indicate incorrect grain identification, the green ones a correct identification and the yellow ones the areas where no grain was detected. In c and d, the red oval indicates a snowfield identified as debris and the yellow one a portion with small granulometry. In e and f, the red oval underlines a grassland patches, where debris were wrongly recognized.....71

**Figure 3.7** - Final map with mask application for Les Martinets (left side) and Les Outans (right side). The vegetation mask is colored in green, the snow mask and/or the area with low roughness and/or the glacier in white.....73

**Figure 4.1** - Focus site where the traditional geomorphological map was elaborated realized by Lambiel et al. (2016) (left side). On the right side, the area selected for calibrating and running the algorithms to produce the SAGM. The area was divided in two part, the training image (upper part) and the simulation grid (lower part). Legend of the selected area: 1) talus slope; 2) active-inactive

rock glacier, debris-covered glacier, Little Ice Age moraine deposit; 3) rockslide, landslide, relict rock glacier; 4) alluvial fan; 5) alluvial plain; 6) Late Glacial deposit; 7) glacier and permanent snow; 8) rock outcrop, rock wall. White zones are excluded from all the calculations.....	80
<b>Figure 4.2</b> - Conceptual model of the test design. The study area is split in two parts, the training image (TI) and the Simulation Grid (SG). Both are composed of the same number of variables with equal resolution grid. In the TI the geomorphological classification is represented because it serves to train the model, in the SG it is absent because it is the variable to simulate. ....	82
<b>Figure 4.3</b> - A) Reference geomorphological map for the selected study area. In white the areas not considered for classification. B) Semi-automated geomorphological map obtained from one DS realisation. C) Semi-automated geomorphological map obtained from the mode of 100 DS realisations. D) Uncertainty map of the 100 DS realisations, showing the frequency of detection of the class corresponding to the mode. The higher is the probability, the more certain is the estimation. E) Semi-automated geomorphological map obtained through RF. F) Uncertainty map of the RF result. G) Aerial orthophoto mosaic SwissMapRaster © swisstopo (DV084371). H) Histograms of the uncertainty maps. Legend: 1) talus slope; 2) active-inactive rock glacier, debris-covered glacier, Little Ice Age moraine deposit; 3) rockslide, landslide, relict rock glacier; 4) alluvial fan; 5) alluvial plain; 6) Late Glacial deposit; 7) glacier and permanent snow; 8) rock outcrop, rock wall.....	86
<b>Figure 4.4</b> - Error evolution of RF model trained on the TI, through 500 trees. OOB indicates out of bag error. Numbers from 1 to 8 correspond to geomorphological classes listed in Table 4.3. .	89
<b>Figure 4.5</b> - Importance of the 12 predictor variables expressed with mean decrease of Gini index. ....	89
<b>Figure 5.1</b> - Comparison between the vegetation plots classified in 5 groups based on cluster analysis and the 3 years of ground thermal monitoring. MGST: Mean Ground Surface Temperature [°C]; FDD: Freezing Degree Day [degree day]; GDD: Growing Degree Day [degree day]; GSL: Growing Season Length [day]. ....	95
<b>Figure 5.2</b> - PERMAL probability of permafrost occurrence map elaborated through Random Forest classification for the Vaud Alps (A). Detailed focus on Les Martinets – Col des Perris Blancs (B) and Les Outans (C) sites. ....	96
<b>Figure 5.3</b> - Workflow of the PERMAL modelling, from data collection to permafrost prediction. Modified from Deluigi (2018). ....	97
<b>Figure 5.4</b> - A) Semi-automated geomorphological map obtained from the mode of 100 DS realisations. Legend: 1) talus slope; 2) active-inactive rock glacier, debris-covered glacier, Little Ice Age moraine deposit; 3) rockslide, landslide, relict rock glacier; 4) alluvial fan; 5) alluvial plain; 6) Late Glacial deposit; 7) glacier and permanent snow; 8) rock outcrop, rock wall. On black the areas lower than 1500 m; B) uncertainty map showing the frequency of detection of the class corresponding to the mode; C) aerial orthophoto mosaic; D) topographic map, SwissMapRaster © swisstopo (DV084371). ....	100
<b>Figure 5.5</b> - A) Zoom of the SAGM obtained from the mode of 100 DS realisations for Les Martinets and Col des Perris Blancs focus sites; B) classical geomorphological map; C) aerial orthophoto mosaic and topographic map of Les Martinets and Col des Perris Blancs; D) Zoom of the SAGM for Les Outans; E) classical geomorphological map F) aerial orthophoto mosaic and topographic map of Les Outans. Legend: 1) talus slope; 2) active-inactive rock glacier, debris-covered glacier, Little Ice Age moraine deposit; 3) rockslide, landslide, relict rock glacier; 4) alluvial fan; 5) alluvial plain; 6) Late Glacial deposit; 7) glacier and permanent snow; 8) rock outcrop, rock wall.....	101
<b>Figure 6.1</b> - Conceptualization figure about the main outcomes of the present thesis in relation to the research objectives.....	103

# List of Tables

<b>Table 2.1</b> - Braun-Blanquet scale (Braun-Blanquet, 1932) and its transformations used in the analyses.....	24
<b>Table 2.2</b> - Guidelines to assign the morphodynamics index to each plot (based on Randin et al., 2009).....	25
<b>Table 2.3</b> - Alliances (Delarze et al., 2015) to which the plots belong and their characteristics. ..	28
<b>Table 2.4</b> - Number of plots and community characteristics observed in the different ESP categories (absence of ESP, solifluction, rill erosion, nivation and frost weathering). Mean values and standard deviation are reported. Species cover: percentage of vascular plant cover [%]. Species richness: number of species per plot. Evenness: biodiversity index measuring the dominance of one species above the others in the same survey.....	29
<b>Table 2.5</b> - Environmental characteristics of the five vegetation groups. Mean values and standard deviations are reported. Species richness: number of species per plot. Evenness: biodiversity index measuring the dominance of one species above the others in the same plot. Elevation: [meters]. Aspect: North (-1) South (+1) gradient. Slope: [degrees]. MGST: Mean Ground Surface Temperature [°C]. Tmax: mean maximum temperature [°C]. Tmin: mean minimum temperature [°C]. FDD: Freezing Degree Day [degree day]. GDD: Growing Degree Day [degree day]. GSL: Growing Season Length [day]. .....	30
<b>Table 2.6</b> - Correlations between NMDS axes and explained variables. NMDS1 and NMDS2 are the axis scores about the 2D ordination space. $R^2$ = linear fit of correlation. Signif.: indicate the <i>p</i> -value. *** $\leq 0.001$ ; ** $\leq 0.01$ ; * $\leq 0.05$ ; . $\leq 0.1$ ; ns = not significant. GSL = Growing Season Length; GDD = Growing Degree Day; FDD = Freezing Degree Day; TVDI = Temperature Vegetation Dryness Index; MGST = Mean Ground Surface Temperature; Tmax and Tmin = maximum and minimum temperature. ....	34
<b>Table 2.7</b> - List of plots with topographic information (elevation [meters], aspect [North (-1) South (+1) gradient] and slope [degrees]), landforms type, species cover (percentage of vascular plant cover - %), and species richness (number of species per plot).....	43
<b>Table 3.1</b> - Technical data about tiles characteristics, overlapping, minimum and maximum debris size and final area investigated for both focus sites. ....	67
<b>Table 4.1</b> - Dataset composition. ....	81
<b>Table 4.2</b> - Main classes of the geomorphological map of the University of Lausanne and example of typical landforms. ....	82
<b>Table 4.3</b> - Geomorphological classification selected for testing in DS and RF algorithms. ....	83
<b>Table 4.4</b> - Confusion matrices about DS and RF data. ....	87
<b>Table 4.5</b> - Quality indexes showing the DS and the RF performance for each modeled class. PPV: positive predicted value. ....	88
<b>Table 4.6</b> - Error for each simulated class, obtained from RF model training on the TI. ....	88
<b>Table 5.1</b> - Environmental characteristics of the five vegetation groups (2018-2019 year). Mean values and standard deviations are reported. MGST: Mean Ground Surface Temperature [°C]; Tmax: mean maximum temperature [°C]; Tmin: mean minimum temperature [°C]; FDD: Freezing Degree Day [degree day]; GDD: Growing Degree Day [degree day]; GSL: Growing Season Length [day]. ....	93
<b>Table 7.1</b> - iButtons data for the year 01-10-2016/30-09-2017. MGST: Mean Ground Surface Temperature [°C]; Tmax: mean maximum temperature [°C]; Tmin: mean minimum temperature	

[°C]; RD: basal-Ripening Date; MD: Melt-out Date; FDD: Freezing Degree Day [degree day]; GDD: Growing Degree Day [degree day]; GSL: Growing Season Length [day].....125

**Table 7.2** - iButtons data for the year 01-10-2017/30-09-2018. MGST: Mean Ground Surface Temperature [°C]; Tmax: mean maximum temperature [°C]; Tmin: mean minimum temperature [°C]; RD: basal-Ripening Date; MD: Melt-out Date; FDD: Freezing Degree Day [degree day]; GDD: Growing Degree Day [degree day]; GSL: Growing Season Length [day].....127

**Table 7.3** - iButtons data for the year 01-10-2018/30-09-2019. MGST: Mean Ground Surface Temperature [°C]; Tmax: mean maximum temperature [°C]; Tmin: mean minimum temperature [°C]; RD: basal-Ripening Date; MD: Melt-out Date; FDD: Freezing Degree Day [degree day]; GDD: Growing Degree Day [degree day]; GSL: Growing Season Length [day].....129

**Table 7.4** - List of plant species identified in the 72 vegetation plots and their species cover. Species cover values are reported according to the Braun-Blanquet scale (Braun-Blanquet, 1932). ‘?’: absent; ‘r’: 1-2 individuals; ‘+’: cover < 5 %, few individuals; ‘1’: cover < 5 %; ‘2’: cover 5-25 %; ‘3’: cover 25-50 %; ‘4’: cover 50-75 %; ‘5’: cover 75-100 %.....131

# List of Abbreviations

<b>BTS</b>	Bottom Temperature of the winter Snow cover
<b>DEM</b>	Digital Elevation Model
<b>DS</b>	Direct Sampling
<b>DSD</b>	Debris Size Distribution
<b>DSM</b>	Digital Surface Model
<b>ESP</b>	Earth Surface Processes
<b>FCIR</b>	False-Color InfraRed
<b>FDD</b>	Freezing Degree Day
<b>FN</b>	False Negative
<b>FP</b>	False Positive
<b>GAM</b>	Generalized Additive Model
<b>GDD</b>	Growing Degree Day
<b>GIS</b>	Geographic Information System
<b>GLM</b>	Generalized Linear Model
<b>GSL</b>	Growing Season Length
<b>GST</b>	Ground Surface Temperature
<b>LGM</b>	Last Glacial Maximum
<b>LIA</b>	Little Ice Age
<b>LL</b>	Low Lobe
<b>MD</b>	Melt-out Date
<b>MGST</b>	Mean Ground Surface Temperature
<b>MPS</b>	Multiple-Point Geostatistics
<b>NDVI</b>	Normalized Difference Vegetation Index
<b>NMDS</b>	Non-Metric multi-Dimensional Scaling
<b>OOB</b>	Out Of Bag
<b>PERMAL</b>	PERmafrost modelling with MACHine Learning
<b>PPV</b>	Positive Predicted Value
<b>RD</b>	Basal Ripening Date



<b>RF</b>	Random Forest
<b>SAGM</b>	Semi-Automated Geomorphological map
<b>SDM</b>	Species Distribution Modelling
<b>SG</b>	Simulation Grid
<b>TI</b>	Training Image
<b>TN</b>	True Negative
<b>TP</b>	True Positive
<b>TVDI</b>	Temperature Vegetation Dryness Index
<b>UAV</b>	Unmanned Aerial Vehicle
<b>UL</b>	Upper Lobe

# CHAPTER 1

## 1. Introduction

### 1.1 Motivation

Under actual global warming, some natural environments are more sensible than other, such as for example the alpine environments (Beniston et al., 2018; Terzi et al., 2019). They are natural laboratories where it is possible to observe and seek to understand the natural processes with few human interactions. Indeed, alpine areas are composed of numerous elements (flora, fauna, hydric resources, atmosphere, cryosphere, soil, bedrock), interconnected between them and involved in different processes. For this reason, they are key factors that could help us to understand the future evolution of actual landscape (Gobiet et al., 2014). Several studies about single elements such as alpine vegetation, water resources, glacier retreat or natural hazard on slopes were carried out in last decades (e.g. Beniston et al., 2018; Ravelin et al., 2017; Viviroli et al., 2011; Wipf et al., 2013). However, few are the researches about interactions of different components, in particular between geomorphic processes and alpine vegetation. This doctoral thesis aims to improve this knowledge, applying statistical-quantitative methodologies coupled with data analysis. But why focus on geomorphic processes and vegetation in alpine environment?

The geomorphic processes shape the most part of visible surface, modifying the landscape and its aesthetic value based on human vision. Their action, coupled with climatic, geological and hydrological setting, conditions the life of flora and fauna, originates a great diversity of ecosystems and is suitable for the study of interactions with the other system components. As well, the flora is one of the elements the most visible in an alpine environment, attracting the attention not only of the scientists. In addition, alpine vegetation is subject to modifications on the colonization pattern and on the community composition because of the temperature warming.

Global warming is acting on different environments (IPCC, 2018) and the scientific community has to deepen the current knowledge about its effect and to improve our capacities to face up to the changes, trying to better understand them and to adopt strategies to reduce their impacts.

Studying at local scale the relations between different components, in this case between geomorphological characteristics and vegetation, is the basis to understand their connections and, afterwards, to expand the results on extended areas. At this stage, models can help to improve the knowledge between geomorphic processes and vegetation on coarse scale, using data collected on local areas.

The present thesis revolves around these topics and aspires first to analyse in details at fine scale the relations between geomorphological processes and vegetation. Secondly, it aims to implement methodologies to realize extended maps about geomorphological characteristics, especially debris size and type of geomorphological class.

## 1.2 Research context

### 1.2.1 Geomorphic processes and landforms

#### *1.2.1.1 Classification of geomorphic processes*

The geomorphic processes are the responsible of the Earth's surface shape and of its evolution. They vary with the position on the Earth and with time due to changes in the climate, and they mark the landscape with specific signature based on the principal active processes (Anderson and Anderson, 2010). But what are the geomorphic processes and what drives them?

The geomorphic processes are the whole of processes that occur in the surficial zone, where rock, air, water and life interact, and they shape the surface of the Earth. They are driven primary by the atmosphere. Indeed, the atmosphere controls wind, precipitation and temperature that vary extremely depending on Earth location and its related solar radiation. One of the most evident temporal variation is represented by the ice ages, which shaped extensively the landscape. Other drivers are the tectonic, which acts directly on the shape of the Earth through collisions, subductions, trusts and related earthquakes, and the geology. Based on geology and consequently on lithology and structure, rocks have different resistance to the weathering processes that disintegrate and transport rocks, eroding them (Gilbert, 1877). In their turn, tectonic, geology and weathering processes condition the topography, acting actively on elevation, aspect, slope and shape concavity or convexity of the landform. Consequently, the geomorphic processes will be affected also by these topographical elements.

The processes are distinguished into several categories depending on the main acting agent.

The **glacial processes** are driven by glaciers. The glaciers erode landscape and deposit the eroded materials in distinctive landforms called moraines (Iverson, 2002). The moraines, characterized by stratification absence, can be modeled by consequently water fusion and originate fluvio-glacial deposits.

In **periglacial processes**, the actions of frost and freezing temperatures create landscapes shaped by frost heave and soil that alternates semi-liquid and solid states. Coined first by Lozinski, (1909), the word “periglacial” describes the non-glacial freeze-thaw processes in any setting. One of the fundamental processes is the frost weathering, which acts on rocks where temperature fluctuations across freezing point and moisture are present. The freeze-thaw cycles promote the disintegration of superficial rocks and the release of debris that can be transported and deposited by other processes (Matsuoka and Murton, 2008). The periglacial processes act on surficial ground and product patterned ground, solifluction lobes, block field and block stream, pingos and thaw lakes (French, 2007). The solifluction lobes take their name from solifluction, the creep process of saturated soil associated with freeze-thaw action (Ballantyne and Harris, 1994). Climate, topography, ground characteristics, water content, depth and thickness of ice lenses present in the soil, and freeze–thaw frequency are the major controlling factors on the spatial variation in solifluction processes. Depending on the abundance of vegetation, solifluction can be classified in turf-banked lobes or stone-banked lobes.

Below the surface, perennial frozen ground may be present. If ground temperatures are below 0°C for at least two consecutive years, this negative thermal state is called *permafrost* (Harris et al., 2009; Washburn, 1980). Ground surface temperatures are not permanently negative but they change seasonally as shown in Figure 1.1.

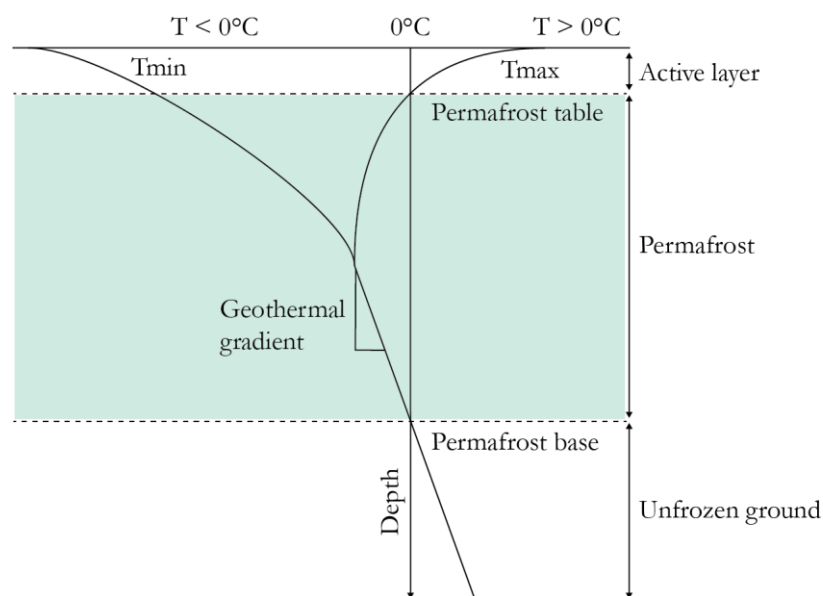


**Figure 1.1** - Permafrost stratigraphy and ground thermal profile (modified from French, 2007).

The *active layer* is located between the ground surface and the *permafrost table* and it is characterized by seasonal thaw and freeze cycles. Instead, the *body of permafrost* is a permanently frozen layer limited by the *permafrost base*. From this threshold, the geothermal gradient increases the temperature and does not allow the maintenance of negative temperatures in the ground.

Typical permafrost landforms are the rock glaciers, visible especially on alpine regions (Barsch, 2012). They are characterized by an internal mixture of ice and sediments and they are subjected to a gravity-induced movement of creep, which may result in surface compression ridges and furrows (Arenson et al., 2002). The characteristics and the distribution of mountain permafrost are indirectly controlled by debris size (Haeberli, 2000, 1975). Indeed, the debris size acts on

microtopography, heat exchange processes between surface and air, and consequently on the ground temperature (Rödder and Kneisel, 2012; Zhang, 2005).

The water action is part of **fluvial processes**. Once rainwater hits the ground, runoff collects into rivers and starts to carve the landscape and sweep away debris. Water drives many geomorphic processes, such as rill erosion, landslide, debris flows, karst and soil formation. It transports solutes and sediments across and within hillslopes and originates deposit landforms, such as alluvial plains and alluvial fans, and erosional landforms, such as valley incisions and terraces (Leopold et al., 2012).

Wind is the key factor of **eolian processes**, common on coastland and desert areas but also at high latitude and altitude. Erosion and deposit product ripples, dunes and loess. The loess is a mineral eolian dust deposit, which potentially provides important information about past climates (Rost, 2001). It derives, indeed, from terrestrial sediments reworked during Quaternary glaciations and it is widely distributed on alpine soils (Martignier et al., 2013).

On high latitude and altitude regions, snow is the main factor concerning the **nival processes**. Especially on glacially-oversteepened slopes, avalanches may occur involving not only snow but, in some cases, also sediments, rocks and soils (French, 2007). In these cases, to an erosion process in the top hill correspond a deposit in the downhill area. The word “nivation”, instead, includes combined processes correlated to snow accumulation in depressions, controlled by prevailing winds and topography (Christiansen, 1998; French, 2007). The erosion in the upper part of the depression, due to freeze-thaw cycles, and the subsequent loosening and downward transport of eroded material produce a gradually formation of nivation hollows.

**Gravitational processes** are generated by gravity, shear strength and stability state. Acting on rock fractures and sliding surfaces, helped by water, freeze-thaw processes, pressure change, and earthquakes, they generate rockfalls, landslides, block slides, topples, debris avalanches and creep (Varnes, 1978).

Often these processes are triggered by several between the before-mentioned factors and they have also feedback mechanisms that product polygenetic landforms. It is the case, for example, of a moraine that is subject to fluvial erosion and gravitational processes. Generally, geomorphic processes operate on longtime scales, but sometimes rapid sudden events, such as a landslide or flood, can cause accelerated changes to the environment, affecting also human activities especially in alpine valleys. All these processes produce landforms, shaping the landscape, and influence the texture (or grain size) of the ground. In a complex system like the Earth, the geomorphic processes are not independent between them but, together with climate, geology, topography, ground and superficial ice, they influence the other terrestrial components such as vegetation, soil and water resource. Furthermore, they can be influenced also by the other terrestrial components, confirming the interactions between the Earth components.

In the present thesis, the focus is centered on alpine environment. In a relatively small geographical area, characterized by a complex topography (Beniston, 2005), a great diversity of geomorphic processes and, consequently, of landforms is observable, allowing for the reconstruction of the history of the area. The alpine environments are highly susceptible to the impact of a rapid climate change. However they provide locations and tools for the detection and the study of the climate change and its impact on ecological, hydrological, geomorphological and biological systems (Gobiet et al., 2014; Haeberli and Beniston, 1998).

### ***1.2.1.2 Landform mapping***

The landform diversity, produced by the geomorphic processes, is usually represented in geomorphological maps. According to scale map and to the purpose of utilisation, three forms of geomorphological map exist (Lee, 2001):

- Regional surveys for general investigations, land use planning or baseline studies;
- General assessments of resources or geohazards;
- Local scale surveys to characterize specific landform at fine scale.

The first modern geomorphological maps started in the early 1950s. They required physical site visits, in order to record landform position and composition, as well as manual elaborations. Soon multiple legends developed in the different countries and still now a universal legend is unlikely, even if some agreements were achieved, for example the use of colors to represent the landforms shaped by the same family of processes (Verstappen, 2011). In this case, the importance is pointed on the landform morphogenesis and many researchers adopted this kind of approach (e.g. Schoeneich and Reynard, 1993). In the last decades, the availability of new data sources (aerial photographs and satellite data) allowed performing rapid mapping on geographic information system (GIS) without field mapping in remote areas (Smith et al., 2011). Furthermore, the development of numerical approaches permitted the implementation of semi-automated methods for the identification and classification of terrestrial features.

Especially using high-resolution Digital Elevation Models (DEMs), from which it is possible to extract morphometric factors such as aspect and slope, landforms can be extracted automatically and the “classical” geomorphological maps can be used to train and validate these methods (Seijmonsbergen et al., 2011). These semi-automated methods showed fast improvement but their development and applicability is still ongoing. Furthermore, in the recent years, more advanced techniques based on machine learning and geostatistics are implemented. Between the employed methods, the Random Forest (RF - Breiman, 2001) offers accurate applicability on geomorphological classification, even if it is applied to a reduced number of geomorphological classes (Marmion et al., 2008; Stumpf and Kerle, 2011; Veronesi and Hurni, 2014). For this reason, this scientific field is still in progress and new methods can be developed and applied.

### ***1.2.1.3 Climate change acting on sediment fluxes***

Especially in the Alps, during the last century a rapid increase of the minimum air temperatures of up to 2°C was registered, together with a more modest rise in maximum temperatures (Acquaotta et al., 2015; Beniston, 2005 - Figure 1.2). This warming was twice than the temperature change in Europe and caused an acceleration of ice and snow melt, an upshift of the snowline and changes in water resources availability (Auer et al., 2007; Beniston et al., 2018). Although a trend for the liquid precipitation is not so clear because of its high spatial and temporal variability, a reduction of snow depth and snow cover duration has been well documented in the Alps thanks to the long-term observations (Klein et al., 2016). The climate forcing has indirect effects on the geomorphic processes, generating an augmentation of geomorphological hazard with a consequently increase on landslides, mudflows, debris flow and other slope instability phenomena (Keiler et al., 2010).

These changes on geomorphological activity and landscape development are strictly correlated to the alpine catchment sensitivity towards the climate change, evident overall in water availability and sediment fluxes (Carrivick et al., 2013).

Sediment fluxes are at the basis of the geomorphic processes and their production is complicated because of mountain glaciers react in a heterogeneous way to regional and local climate (Carrivick and Chase, 2011). Following glacier retreat, indeed, new surfaces are exposed to weathering and to paraglacial processes reworking the sediments (Ballantyne, 2002). “Paraglacial” refers to “...nonglacial processes that are directly conditioned by glaciation”, and “...it refers both to proglacial processes, and to those occurring around and within the margins of a former glacier that are the direct result of the former presence of ice” (Church and Ryder, 1972). Paraglacial processes include interrill erosion, gullying, debris flows, landslide, solifluction and frost creep (Rose, 1991). Depending on local topography, sediments can be stored or made available for erosion and transferred from one landform to another one creating a sediment cascade (Otto et al., 2008). In a hypothetical alpine catchment, after the Last Glacial Maximum (LGM), the glacier retreat leads to a glacial decompression of valley slopes, causing possible rockslide or landslide, also triggered by intense precipitations.

The summits, free of ice, are exposed to air temperature and weathering processes. If temperature are below 0°C for at least two consecutive years, permafrost conditions can establish. In presence of rock cracks, infiltrating water can turn into ice due to negative temperature. Following daily and seasonally freeze-thaw cycles, cracks can open and generate rockfalls. Equally, avalanches during winter are responsible of sediment transport. These sediments accumulate at the foot of the rock walls and can be subjected to periglacial conditions, forming visible landforms indicating permafrost presence, such as rock glaciers (Haeberli, 1985), or coarse and heterometric talus slopes. Both landforms, as well as the moraines of the LGM or the Little Ice Age (LIA), depending on topography and position, can be reworked by fluvial activity, which erodes the available material connecting the sediment cascade to the bottom part of the catchment. Alluvial or lacustrine deposits in valley-fill deposit act, finally, as sinks for transported sediments (Figure 1.3).

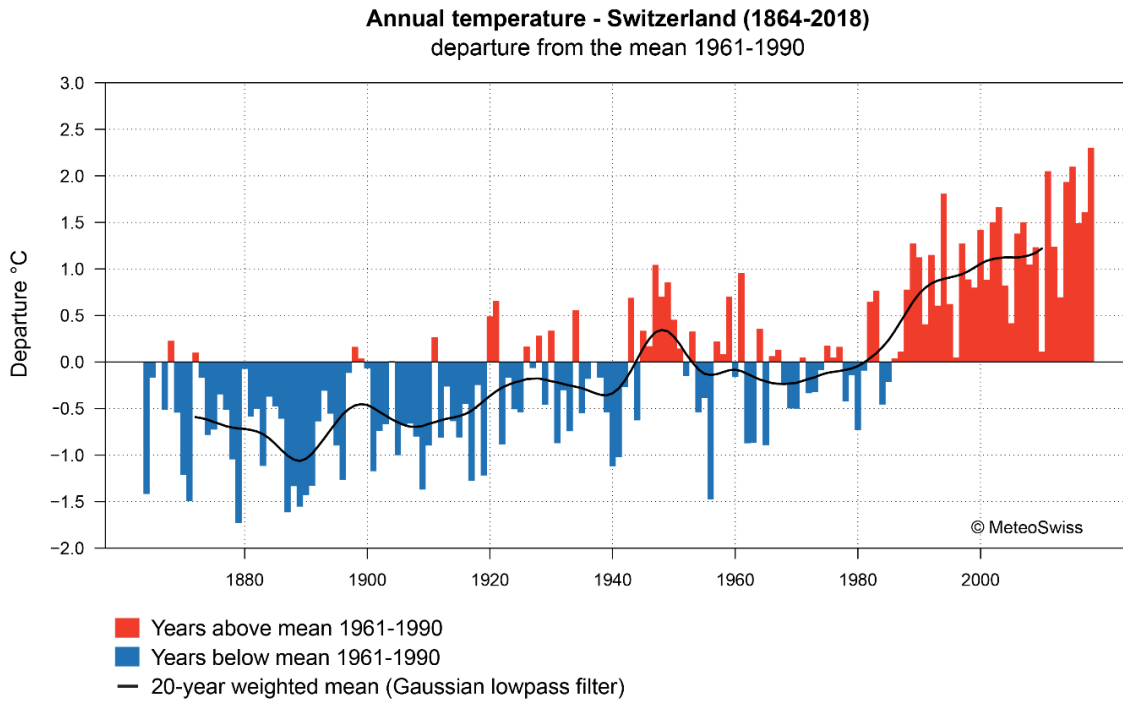


**Figure 1.2** - Temperature anomalies from the mean 1961-1990 in Switzerland (period 1864-2018). Modified from ©MeteoSwiss.

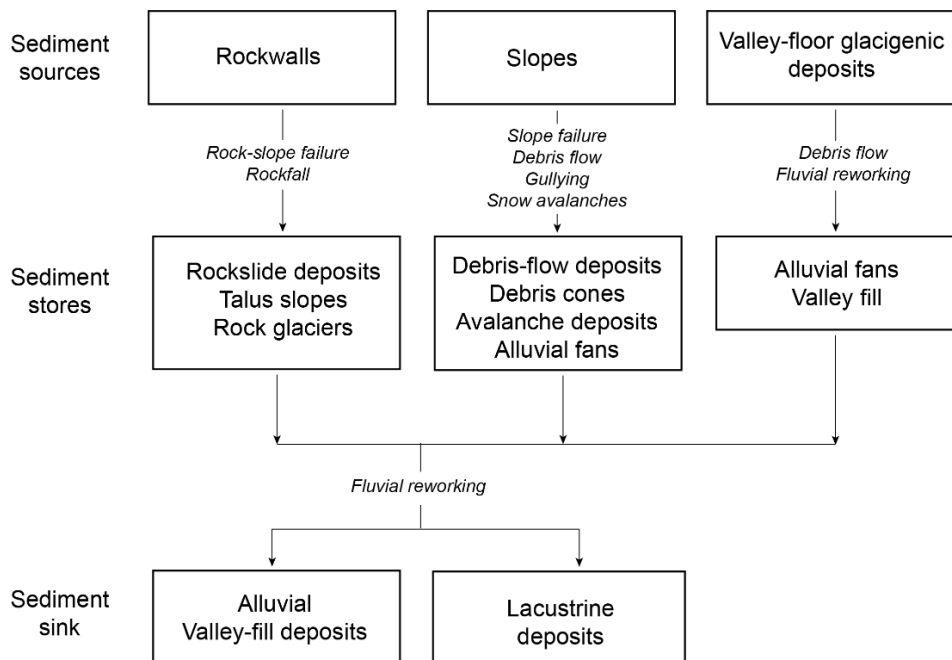


**Figure 1.3** - Schematic representation about a sediment flux on paraglacial environment. Adapted from Cossart (2014).



## 1.2.2 Vegetation on alpine environment

### 1.2.2.1 *Alpine plant life conditions and controlling factors*

In this complex geomorphological and sediment reworking context, the alpine vegetation develops and faces challenging conditions to survive and spread.

The term “alpine” refers to the life zone occurring above the natural treeline on mountains worldwide. The treeline is the uppermost limit of the subalpine vegetation belt, naturally dominated by woody plants higher than 50 cm. In European Alps, the lower limit of the alpine belt is located between 2000 (northern Alps) and 2300 m (south Alps). Here the vegetation is dominated by low stature or prostrate woody shrubs, grasses and sedges, herbaceous perennials, cushion plants and sporadic annual plants. The upper limit of the alpine zone is represented by the occurrence of permanent snow cover. Here the plant cover is fragmented and mostly concentrated in favorable rocky places. This transition is observable between 2700 and 3000 m (northern and southern Alps, respectively) and determines the lower boundary of the nival zone (Körner, 2003; Ozenda, 1985; Theurillat et al., 1998 - Figure 1.4).

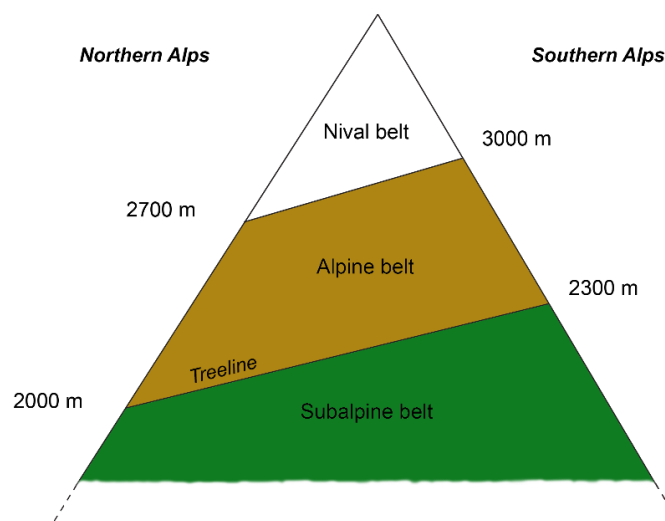


**Figure 1.4** - Representation of the three upper vegetation belts in European Alps.

Life conditions for the plants at alpine elevations are extremely and often considered “hostile”. Low atmospheric pressure, cold temperatures, intense solar radiation, abundant snowfall and long snow cover lead the plant to develop specific evolutionary adaptation, genetic modification or reversible acclimation (Körner, 2003). Slope angle, aspect and topography influence wind, snow patterns and solar radiation and consequently change the micro-climate. At ground level, the micro-climate produces micro-habitat, allowing the existence of a mosaic of plant communities in a relatively small, area within the same elevation range (Scherrer and Körner, 2011). The species themselves develop strategies to survive to these micro-climate extreme conditions, such as prostrated, rosette, or cushion life forms. Indeed, leaf arrangements, stature, surface roughness of

the plant canopy and height above ground exert strong impact on decoupling their climate from the ambient (Huber, 1956).

In addition to the climate, soil and water availability are controlling factor for plant development. Alpine plants acquire mineral resources and water from substrates, which can differ on very short distance, giving place to a large variety of soil types (Körner, 2003). Erosion of parent rock, cryogenic processes, gravity on slopes and sedimentation by water, snow, and wind are among the principal sources of local accumulation of fine material substrate. The parent material influences not only the pH, but also the grain size distribution: siliceous rocks generate coarser and acidic initial grain structure than calcareous rocks, which are essentially alkaline (Ozenda, 1985). Thermal conditions and moisture availability play an important role also for physical and chemical weathering of parent material and organic matter decomposition, which are important drivers for soil formation (Egli et al., 2006). Alpine plants are affected by soil type (Buri et al., 2017; Cianfrani et al., 2018) but, at the same time, they have effect on soil and organic matter properties, through substance production from root and decomposition of root themselves (Jobbágy and Jackson, 2000).

Alpine vegetation starts to colonize the environments free of ice cover some years after the glacier retreat (Matthews, 1992) and this process is called “primary plant succession” because it is developed on lifeless area (Walker and del Moral, 2011). Primary plant succession is driven principally by abiotic processes and influencing factors such as time since deglaciation, soil water content and grain size, topography, snowmelt and disturbance (Anderson et al., 2000; Burga et al., 2010; Matthews and Whittaker, 1987). Instead, biotic processes (e.g. species interactions, reproductive abilities and mycorrhiza development) gain more importance later in the meanwhile of the succession (Erschbamer et al., 2008).

At this stage of primary succession, the linkage between geomorphic processes and alpine vegetation has been studied by some authors and their results suggest that geomorphological factors have a deep importance on the plant development dynamics. Between the abiotic factors mentioned above, the grain size is highly significant for the soil-forming processing, which starts with alteration of the parent material, follows with formation of weathering products and then accumulation of organic matter (Egli et al., 2006). Generally, sediments constituted by large material (e.g. blocks) are colonized by plants very slow (Ellenberg, 1996; Lüdi, 1958), instead, where fine materials are present, the plant development is encouraging thanks to greater and more established water availability (Jochimsen, 1962; Nagl and Erschbamer, 2010). Furthermore, the grain size can operate directly on microtopography, especially in case of depression with fine material. In this case, the grain size constitutes a safe site for seedling germination and establishment, enhancing the fine-scale vegetation patterns (Cooper et al., 2004; Eichel, 2019; Raffl et al., 2006). Consequently it is important to have spatial-distributed data about grain size in order to better understand the possible evolution of the vegetation cover.

### ***1.2.2.2 Disturbance factors and their involvement on plant models***

Disturbances related to geomorphic processes and landform type are as well fundamental on plant community development. They are classified as “environmental fluctuations and destructive events” (Picket and White, 1985) and they have been investigated in many research about artic-alpine environments (Gentili et al., 2013; le Roux and Luoto, 2014; Virtanen et al., 2010). The

geomorphic processes not only modify microhabitat conditions and control species distribution, species richness and community composition, but they are also key dispersal vectors (Gentili et al., 2010) and enhance the colonisation of plant species adapted to the disturbance (Corenblit et al., 2011). Among the earth surface processes (ESPs), defined as the geomorphic processes involving the ground surface, soil frost processes, wind-driven erosion, nivation, runoff water, fluvial processes, solifluction, debris flow, avalanches, and rock/debris falls are the most common in alpine environment (e.g. Baroni et al., 2007, 2013; Gentili et al., 2010, 2013; le Roux and Luoto, 2014). This influence of geomorphic processes on plant communities is not only unidirectional. Indeed, recent studies pointed out also interactions between ecosystem engineering species and sediment reworking on LIA moraines (Eichel et al., 2016, 2017) and between floristic diversity and subalpine alluvial fans (Lane et al., 2016). An ecosystem engineering species promotes decrease of geomorphic activities (e.g. solifluction, frost creep, gully erosion) thanks to its morphology and creates habitat for other species acting as a nurse plant (Jones, 2012).

These studies belong to the biogeomorphology field, defined as the study of interactions between geomorphologic processes and structures and living organisms – plants, animals and microorganisms (Butler, 1995; Gorbushina, 2007; Knox, 1972; Naylor et al., 2002). Indeed, in recent year, the scientific community understood that the vegetation plays an important role into influencing the geomorphic processes and that bi-directional and interconnected relationships exist between them (Osterkamp et al., 2012; Stallins, 2006). This increases the complexity of the Earth system and consequently of the models employed to simulate potential species distribution in a context of global warming.

Called Species Distribution Modelling (SDM), they are among the most widespread models to examine the impact of various threats to biodiversity and to support related political decisions apt to the conservation (Guisan et al., 2013). In the most part of SDMs the variables employed to make predictions are temperature, water and topography related, neglecting several other ecophysiological relevant aspects (e.g. soil, radiation and/or biotic interactions, natural disturbance and land use – Mod et al., 2016). In particular, the rare disturbance variables included in the SDMs are highly environment-specific and include essentially frost-related disturbances in arctic-alpine areas (e.g. le Roux et al., 2013; le Roux and Luoto, 2014) and fire in drier areas (e.g. Tucker et al., 2012). However, in a context of a changing climate, as explained in the previous paragraphs, it becomes more and more important to use predictors related to natural disturbances and geomorphic processes especially at high altitude in SDMs. Indeed, changes in the intensity of these processes, associated with climatic changes, could lead to radical changes in landform morphogenesis and development and consequently on vegetation evolution patterns (Mod et al., 2016).

Climate change effects on alpine vegetation are well documented in bibliography, especially the increase in species richness during the last century (e.g. Cannone et al., 2007; Stöckli et al., 2011) and the upward shift of plant species (Walther et al., 2005; Wipf et al., 2013). Generally, the newly arrived species are lower altitude species able to grow at higher elevations because of shorter snow cover (Matteodo, 2018). Because of warmer summer temperatures, also the vegetation in proglacial areas is subject to an acceleration on colonization velocity (Cannone et al., 2008). Nevertheless, thanks to the individualistic nature of species, differences on responses to environmental warming are highlighted (Erschbamer, 2007). At lower elevations, a shift of the treeline to higher elevation and latitude is observed on European mountains and also in the Swiss Alps (Garamvoelgyi and Hufnagel, 2013). However, the decrease of seasonal grazing and pastures highly contributed to upward forest expansion (Gehrig-Fasel et al., 2007).

### 1.2.2.3 Plant – geomorphological system: joint conceptualization

The sediment fluxes explained in the section “1.2.1.3 Climate change acting on sediment fluxes” are not isolated physical processes reworking the sediments but they can be considered at larger scale as part of the landscape continuum model (Seastedt et al., 2004). In complex topographic ecosystems such as the alpine environments, wind, water, landslide and avalanche act as transport agents not only of sediments but also of nutrient, especially inorganic and organic nitrogen. The transfer from the mountain tops to downslope areas is mainly driven by the gravity. Furthermore, strong winds augment the redeposition on mineral and organic materials. Aeolian deposits of mineral and organic matter are common in mountain regions and their source is generally outside the region of interest (Litaor, 1987; Sievering, 2001) and depends on sediments reworked during Quaternary glaciations (Martignier et al., 2013). In addition to water and wind as external inputs, the freeze-thaw cycles are also responsible of downhill transport of parent material. This shows how the geomorphic processes are directly connected to sediment fluxes since they are part of their cause. Solifluction and frost creep are between the most important phenomena involved on sediment transport and soil formation, enriching the lower zones. Indeed, the soil formation in alpine environments is driven by complex set of transport and deposit at local scale, causing considerable heterogeneity depending on the microtopography.

Vegetation can act as retention mechanism of materials, especially at the tree line, where trees constitute a barrier which collects nutrients, particulates and snow and breaks the wind. Above the treeline, the topography assumes a determinant role to control soil and vegetation communities' development and the landforms play a sink or a source role for their development based on microtopography. Actual studies suggest that in the future, due to anthropogenic emissions in atmosphere, forest production will be maximized and the tree line will experiment nitrogen saturation because of the amplification effects of transport processes (Seastedt et al., 2004; Williams and Tonnessen, 2000).

The connections between plant and geomorphological system can be investigated with different tools based on aim and characteristics of the research project. Plant surveys on plots along a transect or on larger surfaces are the first and fundamental approach to characterise the vegetation communities (e.g. Burga et al., 2004; Cannone and Gerdol, 2003; Eichel et al., 2016, 2017; Gentili et al., 2013; le Roux and Luoto, 2014; Steinbauer et al., 2018; Virtanen et al., 2010). The plot surface changes based on vegetation types, from few meters square for debris vegetation and grasslands to hundred of meters square for forests (Bouizillé, 2007). The identification of species individual, the assessment of species cover and species richness and the phytosociological approach are the main techniques to evaluate the community composition. Cover-abundance value can be assigned to every species to evaluate the floristic dominance. According to the phytosociology (Braun-Blanquet, 1932), the combination of plant taxa, called *association*, characterises univocally the vegetation units, allowing their identification and the interpretation of the ecosystem dynamics.

Unmanned Aerial Vehicles (UAVs), aerial and satellite image and Digital Elevation Models can help to cartography the vegetated surfaces, to reconstruct eventual changes on plant coverage and also to observe, map and quantify landforms and geomorphic processes on large scale (e.g. Lane et al., 2015; NüTTYEN and Luoto, 2018; Riihimäki et al., 2017). As well geophysical surveys, ground surface temperature monitoring, infra-red thermometry, soil moisture analysis and soil profiles inventories help to understand the plant community development and the plant-geomorphic

relationships, as reported in several studies (e.g. Eichel et al., 2016; Gobbi et al., 2014; Scherrer and Körner, 2011).

While the relationships between vegetation composition and soil-topo-climatic variables have been yet highlighted at high resolution and local scale, more specific aspects of the vegetation-geomorphic processes relationships remained unclear, in particular at high elevations. Therefore, face with the ongoing climate change, how does the vegetation react to modifications on geomorphic processes and how to better understand the interactions at different scales? In which way modern science can improve the existing models, facing to the lack of information concerning the natural disturbances, the geomorphic processes and the soil? Being able to predict changes in both biotic and abiotic components of ecosystems is the key challenge to anticipate changes in the ecosystem services (Grêt-Regamey et al., 2008) the most useful for human society.

In this context the interdisciplinary project IntegrAlp was conceived and, inside it, the present thesis was developed.

### 1.3 The IntegrAlp project

Supported by the Swiss National Science Foundation, the interdisciplinary project IntegrAlp aims to take on the above mentioned challenge and to generate new sets of spatially-distributed data for vegetation, soil, geomorphology and hydrology to be able to predict future potential changes of two key ecosystem services: landscape scenic value and water provision.

The project is organized in 6 modules: a first named “GeoDataHub” to collect remote sensing and environmental data and provide methodological support to spatialization procedures, four core thematic modules for the four investigated fields (GeoVeg, GeoSoil, GeoHydro, GeoMorpho) and a sixth module for assessing the effect of climate change on two ecosystem services, the landscape aesthetic value and the water provision/regulation (Figure 1.5). The study area is constituted by the entire Alps of the Vaud Canton (Western Swiss Alps, ca. 720 km<sup>2</sup>), ranging from 400 m to 3200 m a.s.l. but local focus sites have been chosen to carry out detailed field studies.

The **GeoVeg** integrates in the vegetation models the environmental predictors developed in the other modules, to better describe the ecophysiological requirements of the plant species. Furthermore, it develops a method to derive 3D views of current and future vegetated landscapes for the evaluation of scenic value as ecosystem service. The main objective of the **GeoSoil** module is to set soil’s physic-chemical property map for the whole region and for the local areas. These maps can be used in the vegetation and hydrological models. As demonstrated by Buri et al. (2017 and in review), using very high resolution topo-climatic predictors increases slight the power of the SDMs, whereas adding new soil variables (such as soil pH and carbon stable isotope composition) improves them considerably. The **GeoHydro** module developed a 3D geological model and simulation of snow accumulation to evaluate potential water resource on the focus sites (Thornton et al., 2018, 2019) and to produce a surface-subsurface flow model, trying reproduce the hydrological functioning of the catchment over recent years. The topic of **GeoMorpho** module is treated in the framework of the present thesis. The aims are to understand the effects of geomorphic factors on the alpine vegetation through field measurements and to provide

geomorphological spatially-distributed data to the main project. The objectives are discussed deeply in the following sections.

Scale issue is fundamental to develop approaches in optimal way. For this reason, in the present thesis the term ‘fine/local scale’ is used to define a small area, the term ‘large/coarse scale’ to define extended regional areas (Austin and Van Niel, 2011). Collected data in local focus sites allow elaborating models applicable on regional scale. For this reason, the project selected the Vallon de Nant (46°13’44” N, 7°05’59” E) and its surroundings as local site where observe and investigate vegetation, soil, hydrology and geomorphology (Figure 1.6). The Vallon de Nant is a nature reserve, begins at Pont de Nant (1253 m a.s.l.) and climbs up to Dents de Morcles (2969 m a.s.l.) and Gran Muveran (3051 m a.s.l.). It is characterized by great vegetation heterogeneity and geomorphological diversity and it is an ideal natural laboratory to collect data and elaborate later models above the entire Vaud Alps and potentially other alpine areas.

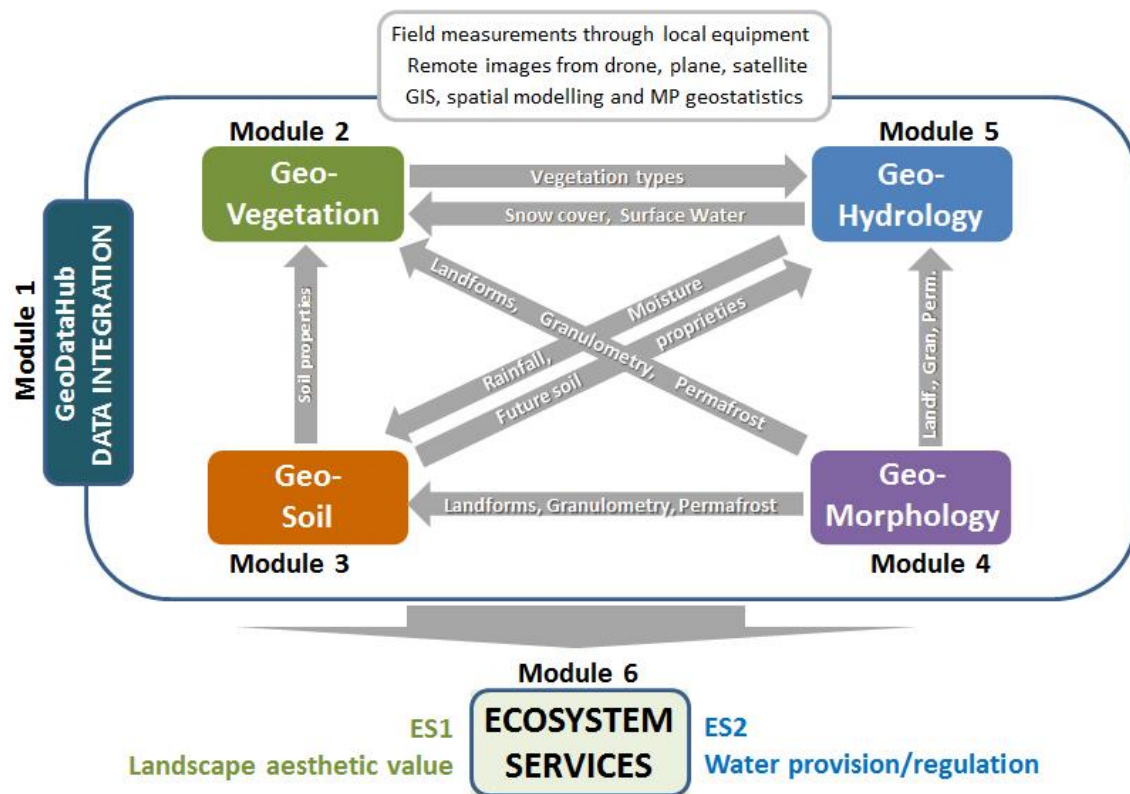


**Figure 1.5** - Structure of the IntegrAlp project, with the four thematic modules, their interactions and the module about data integration. The output model aims assessing the mountain ecosystem services, the landscape aesthetic value and the water provision/regulation.

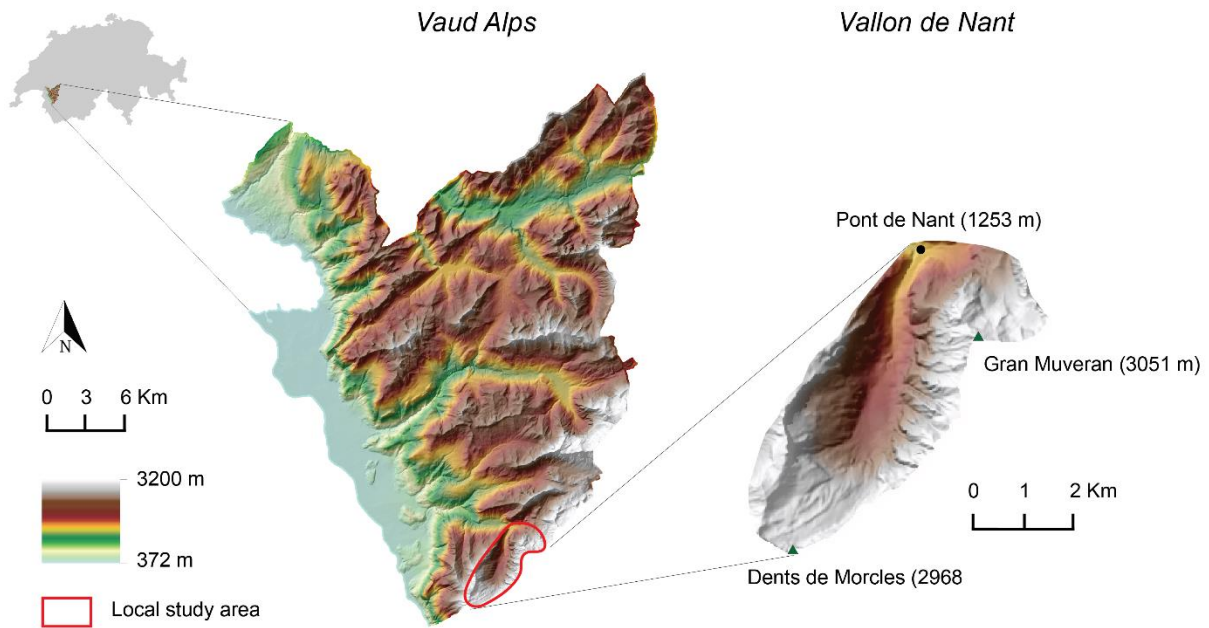


**Figure 1.6** - Location of the regional study area (Vaud Alps, left) and the local study area (Vallon de Nant, right).

## 1.4 Objectives of the thesis

Considering the ongoing climate change and its effects on vegetation communities, it is more and more important to develop models to better understand the interactions between alpine vegetation and geomorphological characteristics also at different scales. Indeed, starting from local observations in focus sites, where it is possible to deep in knowledge directly from collected data, modelling on large scale is useful to obtain an overview of the studied natural phenomena. The present thesis aims to provide additional knowledge in this context of relationships between different natural domains. The purpose is to investigate how geomorphic processes and landforms influence alpine vegetation communities and thus provide geomorphic predictors for SDMs. To meet this purpose, statistical and quantitative approaches coupled with data analysis were developed. The main goal is articulated in three sub-objectives:

- 1) The first sub-objective is the study of the fine scale effects of geomorphic processes on vegetation communities in alpine environment, answering also to the research questions of the IntegrAlp project. As affirmed in the previous sections, geomorphic and disturbance variables are needed to better simulate vegetation evolution in the future (Mod et al., 2016). Indeed, not only water, climate and soil properties influence plant species but also the geomorphic processes which act on the surface also as disturbance (e.g. le Roux and Luoto, 2014). At this aim, in-situ measurements are carried out in prior selected focus sites to investigate the relation between vegetation and geomorphic processes at local scale.

- 2) The second sub-objective is the development of a methodology to map the debris size on extended surfaces and perform a debris size distribution (DSD) map. As asserted before, the debris size is an important factor influencing the type of plant communities in alpine environments (Eichel, 2019) and also the ground thermal regime, controlling the distribution and characteristics of mountain permafrost (Haeberli, 1975, 2000). In addition, the debris size varies based on landforms and it is influenced by geomorphic processes acting on ground surface. Therefore, it is important to perform DSD maps in order to obtain a new predictor able to give information on the possible future evolution of vegetation. The realisation of the debris size distribution map was achieved with the intention to provide an additional large scale variable usable for successive employment in SDMs.
- 3) Considering the ESPs, the debris size and the complex history of an alpine catchment, it is clear that landforms are characterized by specific evolution and also by a specific vegetation cover. This cover depends on many factors and, in some cases, can be related to the dynamics of the landform itself. It is the case, for example, of the active/inactive and relict rock glaciers. As asessed by Burga et al. (2004) and Cannone and Gerdol (2003), vegetation shows greater richness and cover on relict rock glaciers compared to the active or inactive ones. As well, in frost-related landforms, such as patterned grounds, particular plant compositions exist and differ from surrounding area (Béguin et al., 2009). In addition, plant colonization depend also on surface stability especially on landforms subjected to high dynamics like the alluvial fans (Baroni et al., 2007; Gentili et al., 2013). Thus, it is evident that being able to identify correctly the type of landform can provide additional information about the possible type of plant communities living there and on how they could evolve. However, the realisation of a classical geomorphological map is time-consuming, includes fieldworks and features mapping on GIS and it is only suitable for mapping relative limited area. Consequently, automatic procedures are needed but, to be efficient, they need to be driven by geomorphological expertise. Based on these preconditions, the third sub-objective is to implement semi-automated methods to perform a semi-automated geomorphological map. At this aim, two different geostatistical approaches were applied, with the final intention to provide additional variables for the SDMs at regional scale.

## 1.5 Thesis outline

Based on the aforementioned sub-objectives, the thesis is organized in six main sections. Following the actual introduction chapter, three chapters constituted by papers, one for each sub-aim, are presented. Then a chapter where outcomes at larger temporal and spatial scale, not included in the previous papers, are exposed, and finally the conclusion chapter.

The first paper is entitled “Influence of microclimate and geomorphological factors on alpine vegetation in the Western Swiss Alps” and it has been published in the *Earth Surface Processes and Landforms* journal (2019, DOI: 10.1002/esp.4715). It discusses about the influence of environmental parameters on alpine vegetation on three focus sites of the Western Swiss Alps (Les Martinets, Col des Perris Blancs and Les Outans). 72 vegetation plots were carried out and, for



each plot, ground surface temperature was measured with iButtons data loggers. The main results show that landform morphodynamics (the totality of the processes that occur on a landform, including also the possible movement of the landform itself) and soil temperatures are key parameters for plant communities.

“Large scale debris size mapping in alpine environment using UAVs imagery” is the title of the second paper. It was submitted to *Geomorphology* journal. It deals with the debris size mapping using optical high-resolution images acquired by Unmanned Aerial Vehicles (UAVs). Starting from algorithms that identify the debris size, a methodology was developed to obtain a map representing the debris size distribution in alpine and not vegetated environments. This map may be used as predictor variable on the SDMs. The map was generated for two of the before-mentioned three focus sites, where UAVs images were available (Les Martinets and Les Outans). The validation between the algorithm results and the effective grain size showed strong correlation, increasing the suitability of the methodology.

The last paper is entitled “Semi-automated geomorphological map in mountain environment”. It aims to elaborate a geomorphological map starting from automatic procedure that are guided by geomorphological expertise. It will be submitted to *Computer and Geosciences* journal. Two geostatistical methodologies (the Direct Sampling and the Random Forest) were applied and the results were compared between them. In this way, geomorphological mapping can be expanded on large area and employed as variable for vegetation models. In this case, the methodologies were applied in one other alpine valley in the Western Swiss Alps (the Arolla valley), where a traditional geomorphological map already exists and it can be used as validation.

The fifth chapter presents the results coming from complementary analysis not comprised in the main papers. The first chapter section reports the data derived by the microclimate monitoring in the focus sites. The second section illustrates the implementation of a map about permafrost distribution in the Vaud Alps. The third sections is the natural follow-up of the third paper, because the most performing methodology (the Direct Sampling) was applied on the Vaud Alps to simulate a semi-automated geomorphological map above 1500 m a.s.l. and to meet with the IntegrAlp objectives.

Finally, the synthesis and conclusion chapter summarizes the main assessments from the three papers and the previous chapter about additional outcomes, together with future perspectives.

Each section provides answers to the main thesis aim, helps on understanding of mechanisms which cooperate in alpine environments, and produces new predictors for the SDMs to simulate the future evolution of the vegetation, acting on different scales. Indeed, the comprehension of processes acting between different natural domains starts from the in-situ analysis of ground processes and moves to regional scale models, in order to extend the processes to larger areas. To summarize the research question and the three main sections of the thesis, a conceptual figure is here presented, helping the reading to obtain an overall view of my research (Figure 1.7).

## RESEARCH QUESTION

How do geomorphic processes and landforms influence alpine vegetation communities?

## OBJECTIVES

- 1) Study of the fine scale effects of geomorphic processes on vegetation communities
- 2) Development of a methodology to map the debris size on extended surfaces
- 3) Implementation of semi-automated methods to perform a semi-automated geomorphological map

## OUTCOMES

- New theoretical knowledges about geomorphic influence
- Predictors for SDMs

## DATA-INPUT

- 1) Vegetation, ground temperature and environmental factors
- 2) High-resolution drone images
- 3) Geomorphological map and DEM-related variables

## METHODS

- 1) Field observations, novel ordination techniques and multivariate regression
- 2) Basegrain algorithm and computationally codification
- 3) Direct Sampling and Random Forest

Figure 1.7- Conceptual figure summarizing the research questions, the used data sets and the main methods.

## CHAPTER 2

# 2. Influence of microclimate and geomorphological factors on alpine vegetation in the Western Swiss Alps

Giaccone Elisa<sup>1</sup>, Miska Luoto<sup>2</sup>, Pascal Vittoz<sup>1</sup>, Antoine Guisan<sup>1,3</sup>, Grégoire Mariéthoz<sup>1</sup>, Christophe Lambiel<sup>1</sup>

<sup>1</sup> *Institute of Earth Surface Dynamics, University of Lausanne, Lausanne, Switzerland*

<sup>2</sup> *Department of Geosciences and Geography, University of Helsinki, Helsinki, Finland*

<sup>3</sup> *Department of Ecology and Evolution, University of Lausanne, Lausanne, Switzerland*

Earth Surface Processes and Landforms, 2019, DOI: 10.1002/esp.4715

**Personal contribution.** I designed this research with my supervisor C. Lambiel for the geomorphological part and with A. Guisan and P. Vittoz for the vegetation part. I organized and conducted field investigations and data analysis, prepared figures and wrote the manuscript. Data analysis was remarkably improved by support of M. Luoto. Constructive comments and corrections of the co-authors increased considerably the paper quality.

## **Abstract**

Among the numerous environmental factors affecting plant communities in alpine ecosystems, the influence of geomorphic processes and landforms has been minimally investigated. Subjected to persistent climate warming, it is vital to understand how these factors affect vegetation properties. Here, we studied 72 vegetation plots across three sites located in the Western Swiss Alps, characterized by high geomorphological variability and plant diversity. For each plot, vascular plant species were inventoried and ground surface temperature, soil moisture, topographic variables, earth surface processes (ESPs) and landform morphodynamics were assessed. The relationships between plant communities and environmental variables were analysed using non-metric multi-dimensional scaling (NMDS) and multivariate regression techniques (generalized linear model, GLM, and generalized additive model, GAM). Landform morphodynamics, growing degree days (sum of degree days above 5 °C) and mean ground surface temperature were the most important explanatory variables of plant community composition. Furthermore, the regression models for species cover and species richness were significantly improved by adding a morphodynamics variable. This study provides complementary support that landform morphodynamics is a key factor, combined with growing degree days, to explain alpine plant distribution and community composition.

## **Keywords**

Alpine environment; geomorphology; earth surface processes; vegetation community.

## 2.1 Introduction

Understanding the impacts of climate change on earth surface processes and biota is a key challenge for both geomorphological and ecological studies. This is particularly important for alpine environments, where geomorphological processes drive landscape evolution and ecosystem dynamics subjected to climate change (Gobiet et al., 2014; Haeberli and Beniston, 1998). During the last century, the minimum air temperatures increased by as much as to 2°C in these systems, whereas the maximum temperatures exhibited a more modest but measurable rise (Acquaotta et al., 2015; Beniston, 2005). This warming was twice the average temperature change in the Northern Hemisphere, causing an acceleration of snow and ice melt, an upshift of the snowline and changes in water resources availability (Auer et al., 2007; Beniston et al., 2018).

Alpine ecosystems, and especially vegetation, are impacted by ongoing climate change (Füssler et al., 2017). The upward shift of plants is observed in many studies in Europe (Dullinger et al., 2012; Gottfried et al., 2012; Steinbauer et al., 2018). Furthermore, following glacial retreats, new surfaces are exposed to atmospheric conditions. Within a few years, paraglacial adjustments rework the sediments (Ballantyne, 2002) and vegetation begins to colonize the free environments (Matthews, 1992). Primary plant succession is proven to be predominantly driven by time since deglaciation, soil grain size and water content (Burga et al., 2010), but other complex factors such as snowmelt, topography and disturbance also control vegetation development (Anderson et al., 2000; Matthews and Whittaker, 1987).

Several studies have demonstrated the importance of geomorphic processes on alpine ecosystems. Investigations on the effects of earth surface processes (ESPs) on alpine vegetation offer evidence that plant communities are affected by physical disturbances related to geomorphological processes (Gentili et al., 2013; le Roux and Luoto, 2014; Virtanen et al., 2010). The latter can modify microhabitat conditions and therefore control species richness, composition and distribution patterns of plant communities (le Roux et al., 2013; Vonlanthen et al., 2006a). In addition, geomorphic processes not only disturb plant communities, but they are also important dispersal vectors (e.g., Gentili et al., 2010) and promote the colonization of plant species adapted to the disturbance (Corenblit et al., 2011).

Several authors have investigated the linkage between vegetation and geomorphic dynamics in alpine environments. In the permafrost-affected areas, and more broadly in the periglacial domain, vegetation exhibits different patterns between active rock glaciers (low vascular plant cover) and inactive-relict rock glaciers (high cover – Burga et al., 2004; Cannone and Gerdol, 2003), even if quality of substrate, surface deformation and microtopography remain critical factors for plant distribution (Burga et al., 2004; Colombo et al., 2016). This was also demonstrated for frost-related landforms, such as polygonal soils, where only particular plant compositions exist (Béguin et al., 2009). However, in the Alps, permanently frozen ground has rarely a direct interference with plant growth because of the thickness of the surficial layer above permafrost which thaws during summer (called “active layer” – Körner, 2003; van Tatenhove and Dikau, 1990). The latter has for instance values around 3 to 5 m depth in the Swiss Alps (PERMOS, 2019). Besides, arctic-alpine communities exhibit strong responses to different ESPs, such as cryoturbation, deflation, fluvial processes, nivation and solifluction (le Roux and Luoto, 2014), and they are also influenced by other geomorphological processes such as rock/debris falls, debris flow, avalanches and running water (Gentili et al., 2013). Furthermore, in addition to water, nutrients availability and the

microclimate, plant colonization also depends on surface stability (Baroni et al., 2007, 2013; Gentili et al., 2010). Such a two-way linkage was confirmed by other authors studying the interactions between subalpine alluvial fans and floristic diversity (Lane et al., 2016) and between sediment reworking on a lateral Little Ice Age (LIA) moraine and bioengineering species (Eichel et al., 2016, 2017).

While the relationships between plant composition and soil-topo-climatic variables have been yet highlighted at high resolution especially on lowland and montane regions (e.g. Dubuis et al., 2013; Pradervand et al., 2014), more specific aspects of the plant-geomorphic processes relationships remained unclear, in particular at high elevations. This would allow answering questions such as: how do ESPs influence plant communities? How do geomorphological heterogeneity and landform morphodynamics affect vegetation distribution? Among the geomorphic processes, which types control alpine community composition? Moreover, in the context of climate change, which mechanisms operate between alpine plant distribution and landform stabilization (Alatalo et al., 2016; Eichel et al., 2017; Virtanen et al., 2010)? In the present study, the term ESP indicates different processes that involve the ground surface. With landform morphodynamics, however, we refer to the entire processes that can occur on a specific landform, including the possible movement of the landform itself. For geomorphological heterogeneity, we refer to the variability of landforms in a catchment.

The objective of this study is to understand the joint influence of geomorphology, topography and microclimatology on alpine vegetation. More specifically, we aim to assess how landform morphodynamics, ESPs (solifluction, rill erosion, nivation and frost weathering), topography (elevation, slope, aspect) and other environmental variables such as ground temperature and soil moisture drive alpine plant distribution, species richness and community composition. The study was conducted in three high-elevation sites in the Western Swiss Alps, characterized by different age deposits and high geomorphological variability and biodiversity. Based on the theory and findings reported previously (and elsewhere, e.g., in Körner, 2003; Ozenda, 1985), we expect microtopography, microclimate, snow cover, soil moisture and ESPs to be among the most important explanatory factors of community composition and species richness.

## **2.2 Material and methods**

### **2.2.1 Study area**

Our study area is located in the Vaud Alps (Western Swiss Alps). All three sites are situated in or near the Vallon de Nant (46°13'44" N, 7°05'59" E), a tight valley surrounded by high rock walls (max. elevation 3051 m a.s.l.) and oriented SW-NE, which has been extensively studied in geomorphological and biological fields (e.g. Lambiel et al., 2009; Lane et al., 2016; Thornton et al., 2018; Vittoz et al., 2009).

Due to its location on the northwest side of the Alps and because most of the climatic perturbations come from the west, the region receives abundant annual precipitation (1800 mm/y in Pont de

Nant, 1253 m a.s.l.) and winter snow-fall. The mean annual temperatures are 7°C in Pont de Nant and -3°C on the summits. This cold and wet climate, associated with the shadow of the high rock walls, supports the presence of small glaciers (Les Martinets and Plan Névé glaciers).

Geologically, the region is located on the inverse flank of the Morcles nappe and it consists primarily of limestone and some siliceous rocks deposited between the Middle Jurassic and the Eocene (Badoux, 1991). The geomorphological diversity of the region is high, with various landforms, such as Holocene moraines, rock glaciers and talus slopes. According to the Alpine Permafrost Index Map (Boeckli et al., 2012) and geomorphological interpretation (Lambiel et al., 2009; Perret and Martin, 2015), permafrost is expected to be present above 2400 m a.s.l. in the north-exposed slopes.

Three focus sites situated at elevations ranging between 1950 and 2550 m a.s.l. were selected based on geomorphological variability and biodiversity: Les Martinets, Col des Perris Blancs and Les Outans (Figure 2.1). The landscape of *Les Martinets* (Figure 2.1b, d) is dominated by the Glacier des Martinets (ca. 2200-2680 m a.s.l.), with its numerous moraines dating back to the LIA and to older Holocene or Late Glacial periods. A large and thick rock glacier is located on the western part of the catchment, at elevations between 2240 and 2440 m a.s.l. This rock glacier consists of two different lobes corresponding to two different generations. Orthoimage analyses suggest very low activity for the upper lobe, whereas the lower one seems to be inactive. The geomorphological characteristics (steep front, bulging surface) suggest the presence of permafrost conditions in the rock glacier despite the relatively low elevation (Lambiel et al., 2009). It was confirmed by an electrical resistivity tomography profile (Giaccone et al., 2016 – see Supplementary material Figure 2.6). Finally, talus slopes crossed by several debris flow channels and a large area of rock fall/avalanche deposits are present on the northwest side.

The *Col des Perris Blancs* site (Figure 2.1b, e) is located on the northwest side of the Martinets catchment, at elevations between 2400 and 2544 m a.s.l. It corresponds to a north-exposed slope, with outcrops generating frost weathering deposits and some areas covered by alpine grasslands. The high quantity of debris derived from outcrops formed a debris slope with small lobes, which suggests frost creep, and originated a protalus rampart.

*Les Outans* site (Figure 2.1c, f) is characterized by steep slopes exposed to the north, with elevations between ca. 1950 and 2300 m a.s.l. The main landforms are LIA moraines created by the Glacier de Plan Névé, located in the southeast section (ca. 2400-2680 m a.s.l.), and, in the western part, an unnamed small debris-covered glacier that erected voluminous moraines (ca. 2100-2300 m a.s.l.). The remaining surface is constituted by an extended debris slope made of gravitative (talus slope) and torrential deposits.

The vegetation in Vallon de Nant was studied by Dutoit (1983) and summarized in Vittoz and Gmür (2009) and Vittoz et al. (2009). Beech, fir and spruce forests (*Abieti-Fagenion* according to Delarze et al., 2015) dominate the lowest part of the region (1200-1400 m a.s.l.), replaced locally by pasturelands (*Cynosurion*) grazed by cows in summer. Spruce and larch forests (*Vaccinio-Piceion*) dominate the subalpine belt (1400-1900 m a.s.l.), replaced by maple forests (*Lunario-Acerion*) on steep, unstable slopes, green alder bushes (*Alnenion viridis*) on avalanche paths, pasturelands (*Poion alpinae*, *Nardion*) on the flat, exploited areas and heathlands (*Rhododendron-Vaccinion*) when grazing is abandoned. The alpine belt (1900-2800 m a.s.l.) is a mixture of calcareous alpine grasslands (*Seslerion*, *Caricion ferrugineae*, *Arabidion caeruleae*) and rocky areas (moraines, rock glaciers, cliffs). The subalpine and alpine belts are severely intersected by long talus slopes and alluvial/colluvial fans



colonized by communities of the *Thlaspion rotundifolii*, *Epilobion fleischeri* or *Petasition paradoxici* according to the dynamics, stone size and humidity.

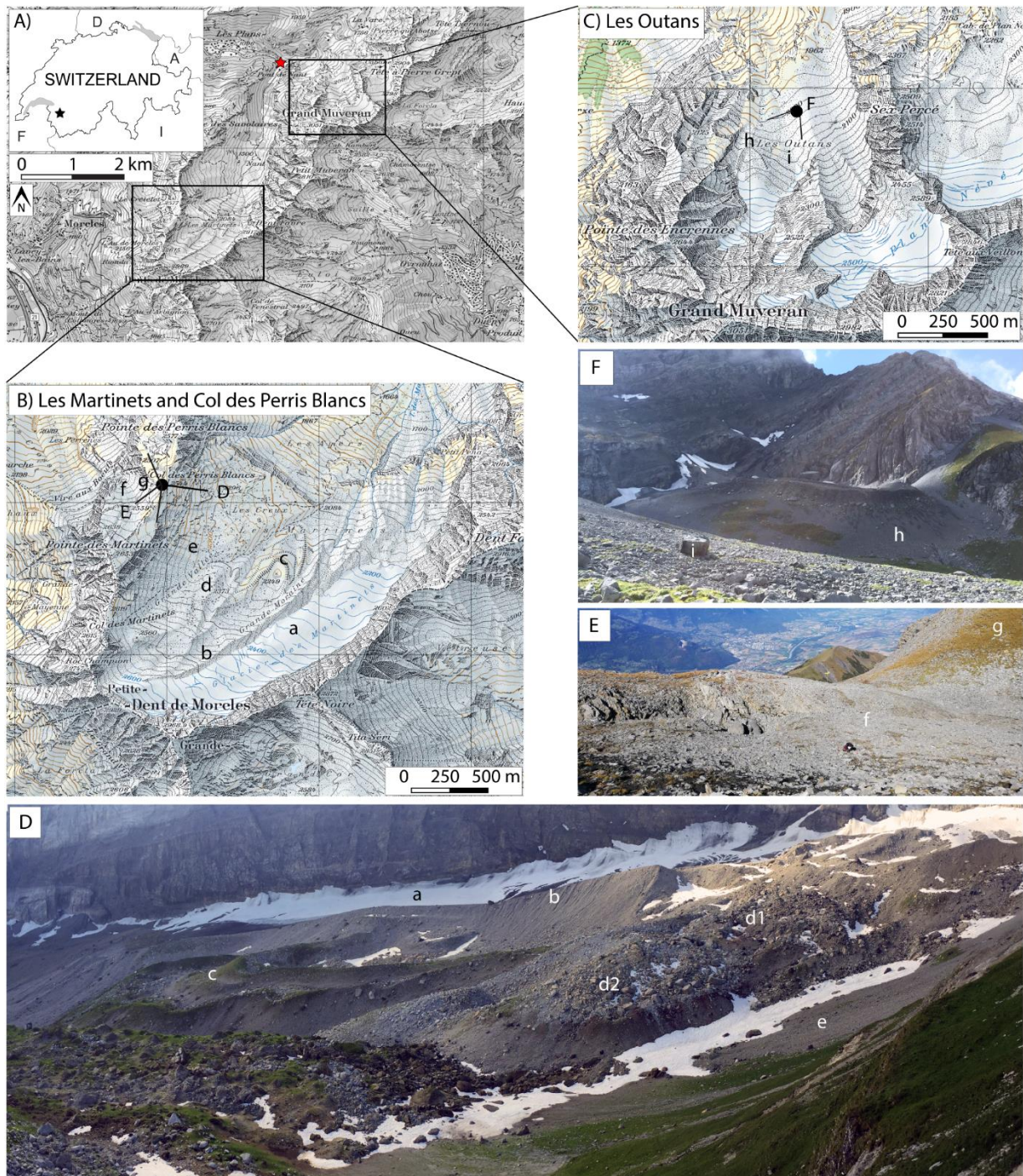


**Figure 2.1** - A) Locations of the three selected sites. The red star indicates the location of Pont de Nant (1253 m a.s.l.) B) Topographic map of Les Martinets and Col des Perris Blancs. C) Topographic map of Les Outans. D) Detailed picture of Les Martinets, seen from the Col des Perris Blancs (August 2016); a: The Glacier des Martinets; b: LIA moraine; c: Holocene moraines; d1: rock glacier, upper lobe; d2: rock glacier, lower lobe; e: talus slope. E) Detailed picture of Col des Perris Blancs, seen from the namesake alpine pass (September 2018); f: debris slope; g: alpine grassland. F) Detailed picture of Les Outans; h: steep latero-frontal moraines of the debris-covered glacier; i: debris slope (September 2018). SwissMapRaster © swisstopo (DV084371).



## 2.2.2 Vegetation plot surveys

During the summers of 2016 and 2017, vegetation surveys were conducted in 72 plots of 2 x 2 m each, scattered in the three study sites. The innovative aspect of our study was that the location of the plots, selected in an ad-hoc stratified way before fieldwork in order to ensure that samples represented each geomorphological feature (e.g., LIA and pre-LIA moraines, talus slope, rock glacier, rock fall/avalanche deposit, debris-covered glacier, glacial surface accumulation, periglacial deposit) with all types of vegetation cover, from pioneer plants with low percentage cover on debris to stable grasslands with high cover. The topographical information and type of landforms for each plot are reported in Supplementary material Table 2.7, along with species cover and species richness. Each vascular plant species in the plot was listed (nomenclature following Lauber et al., 2012) and a cover-abundance value was assigned to every species (Table 2.1), in accordance to the Braun-Blanquet scale (Braun-Blanquet, 1932). The total vascular plant cover (here species cover) was estimated in the field. The central point of each plot was registered by GNSS (using a Garmin Montana® 610). For each survey, species richness (number of species per plot) and evenness (biodiversity index measuring the dominance of one species above the others in the same survey) were calculated to characterize the biodiversity within the plots.

For each vegetation plot, a morphodynamics index, ranging from 0 to 9, was defined according to the landform morphodynamics: 0 corresponds to a plot location on a stable landform and 9 on a landform affected by high activity. The details for the attribution of each value are given in Table 2.2. The index is composed of three criteria: frequency of disturbances that affect the deposit (i.e., debris flow, avalanche), movement of the surface and soil development. For each criterion, a value ranging from 0 and 4 is assigned based on intensity of phenomenon and then summed to obtain the final index for each plot. This index is adapted from the methodology reported in Randin et al. (2009).

**Table 2.1** - Braun-Blanquet scale (Braun-Blanquet, 1932) and its transformations used in the analyses.

<b>Range of species cover (%)</b>	<b>Braun-Blanquet scale</b>	<b>Mean cover (mod. from Wildi 2013)</b>	<b>Numerical dominance</b>
Absent	Absent	0	0
1-2 individuals	r	0.05	0.1
<5, few individuals	+	0.5	0.5
<5	1	3	1
5-25	2	15	2
25-50	3	37.5	3
50-75	4	62.5	4
75-100	5	87.5	5

The frequency of disturbances and the surface movement were evaluated using orthophotos of the study area from 1980 to 2016, obtained from the Swiss Office of Topography (<https://map.geo.admin.ch>), and through geomorphological interpretation; soil development was evaluated in the field.

To define the type of external disturbance in each site, the presence of the four selected ESPs - solifluction, rill erosion, nivation and frost weathering - were reported using a value from 0 to 4 to inform on the intensity of the phenomenon (0: phenomenon absent, 4: phenomenon very intense), following the methodology reported in Gentili et al. (2013). If no ESP evidence was found, the plot was assigned to the “No ESP” category. To limit any potential human bias, the same observer performed all surveys.

Furthermore, in September 2018, after a particularly dry period, soil moisture was measured as volumetric water content (VWC %) with a hand-held reflectometry sensor (FieldScout, TDR150; Spectrum Technologies). Short rods (3.8 cm) were adopted. For each plot, 5 measurements at 5 points (corners and centre), for a total of 25 measurements, were averaged (Kemppinen et al., 2018). However, for most of the plots it was impossible to measure the soil moisture due to the extremely low proportion of fine soil material. Therefore, as an alternative, we used the triangle method of Sandholt et al. (2002) to compute the temperature vegetation dryness index as:

$$TVDI = (T_s - T_{smin}) / [(a + b \cdot NDVI) - T_{smin}]$$

where  $T_s$  is the observed surface temperature at a given pixel,  $T_{smin}$  is the minimum surface temperature,  $a$  and  $b$  are parameters defining the dry edge modelled as a linear fit to the data and  $NDVI$  is the observed normalized difference vegetation index. The term  $a + b \cdot NDVI$ , also known as  $T_{smax}$ , is the maximum surface temperature observation for a given NDVI. To measure the temperature, iButton temperature data were employed (see chapter 2.2.3). Considering the high soil moisture variability,  $T_{smin}$  and  $T_{smax}$  were, respectively, the minimum and maximum daily temperatures recorded during July and August 2017 between all the iButtons and  $T_s$  the mean daily temperatures of the same months. NDVI was calculated at a resolution of 25 cm, using the infrared and red bands of the false-color infrared orthophoto mosaic obtained from the Swiss Office of Topography for the year 2013. Then the value corresponding to the plot center was selected for the calculation.

Finally, topographic variables (elevation, orientation, slope angle) were computed for each plot location, based on the SwissAlti3D DEM (resolution grid 2 m, Swiss Office of Topography).

**Table 2.2** - Guidelines to assign the morphodynamics index to each plot (based on Randin et al., 2009).

	<b>Morphodynamics index</b>				
	<b>0</b>	<b>1</b>	<b>2</b>	<b>3</b>	<b>4</b>
<b>Frequency of disturbances</b>	Absence of disturbances	Return time of disturbances > 10 years	Return time of disturbances < 10 years	Annual disturbances	Several time in one year
<b>Surface movement</b>	No movement	Movement (cm-dm/year)	-	-	-
<b>Soil</b>	Developed soil, dominated by fine material	Developed fine soil material with rock texture	Sparse fine soil material and rock texture	Rock texture with poor fine material	Absence of fine material

### 2.2.3 Ground surface temperature monitoring

To investigate the microclimate of the ground surface, snow duration and occurrence of permafrost at each vegetation plot, continuous monitoring of the ground surface temperature (GST) was performed using iButton® DS1922L miniature temperature loggers (accuracy  $\pm 0.5$  °C, resolution 0.0625 °C – Gubler et al., 2011; Ishikawa, 2003). In total, 72 loggers were buried at 5 cm depth from 1 of October 2016 to 30 September 2018 with a measurement interval of 3 hours. Because the iButtons are not entirely impermeable, they were placed inside small waterproof containers sealed with tape.

To study the ground thermal regime, different temperature indices were calculated based on the two-year data average:

- i) Mean ground surface temperature (MGST), minimum ( $T_{min}$ ) and maximum ( $T_{max}$ ) temperatures;
- ii) Basal-ripening date (RD): time when a frozen ground surface is warmed to 0°C by percolating melt-water or by strong rain-on-snow events (Schmid et al., 2012; Westermann et al., 2011);
- iii) Melt-out date (MD): time when the snow cover is completely melted and thus when the ground can warm above 0°C (Schmid et al., 2012);
- iv) Freezing degree day (FDD): sum of degree days below 0°C;
- v) Growing degree day (GDD): sum of degree days above 5°C (Scherrer and Körner, 2011);
- vi) Growing season length (GSL): number of days between MD and the first day of September with ground temperatures below 3.2 °C (Körner and Paulsen, 2004).

In addition, the bottom temperature of the winter snow cover (BTS) method was employed to define the areas where permafrost is possible (Haeberli, 1973; Hoelzle et al., 1993; Ikeda and Matsuoka, 2002; Lambiel and Pieracci, 2008). The method is based on the fact that heat exchanges between atmosphere and ground surface are strongly reduced during late winter below a snow cover thicker than  $\sim 80$  cm, which maintains stable temperatures (Staub et al., 2015). Therefore, the temperature measured at the snow/ground interface reflect the ground thermal state and can be used as an indirect indicator of permafrost conditions (Hoelzle et al., 1999; Ishikawa, 2003). Temperature below -2 °C during late winter are usually considered as an indicator for the possible presence of permafrost (Haeberli, 1973; Ishikawa, 2003).

### 2.2.4 Statistical analysis

All statistical analyses and models were conducted using R v. 3.2.3 (R Core Team, 2015).

Spearman's rank correlation coefficient was performed to assess the relationship between species cover, species richness and evenness variables. A Mantel's test (Mantel, 1967) was achieved with the *mantel.rtest* function of the *ade4* package (v. 1.7-13) to test for spatial autocorrelation in the

species cover and species richness variables across plots. Null hypothesis affirmed that matrices were not correlated.

The plant covers determined using the Braun-Blanquet scale were transformed according to the mean cover of Wildi (2013) for subsequent analyses (see Table 1). The Bray-Curtis dissimilarity index (Bray and Curtis, 1957) was calculated between plots. The resulting dissimilarity matrix was employed as an input for a non-metric multi-dimensional scaling (NMDS) ordination method, performed with the *metaMDS* function of the *vegan* package (v. 2.4-0) and which visualizes plots according to their floristic similarities (Oksanen et al., 2007). NMDS allows the ordering relationships among objects in two main axes to be represented, using rank orders and minimizing the ordination stress (i.e., disagreement between the 2D configuration and similarity matrix) with multiple iterations. Two dimensions were calculated for NMDS. Then, we incorporated the environmental factors (MGST, maximum temperature, minimum temperature, FDD, GDD, GSL, elevation, aspect, slope, morphodynamics, TVDI, solifluction, rill erosion, nivation and frost weathering) into the NMDS analysis with the *emfit* function using a permutation approach (999 permutations), to test the relations between the ordered plant communities and environmental factors. The linear fit for each variable along the NMDS axis was determined and its significance tested. Non-parametric smoothed surfaces were calculated for each environmental factor and reproduced on the ordination plot by using the *ordisurf* function to investigate the non-linearity of the relationships.

Cluster analysis was also performed to classify the plots according to their floristic similarity. For this analysis, individual species cover was transformed following the numerical dominance reported in Table 2.1. The Bray-Curtis dissimilarity index was used to build the dendrogram using the *hclust* function (Ward's method) of the *stats* package. Based on fieldwork observations, five groups were retained to classify the plant communities and the mean temperature and environmental factor values were specified for each.

The influence of predictor variables on species cover and species richness was examined using generalized linear models (GLMs) and generalized additive models (GAMs) as applied in previous studies (e.g., le Roux and Luoto, 2014). GLMs and GAMs are generalized regression methods. A GAM is a semi-parametric equivalent of parametric GLM that uses smoothers to estimate the relationship between predictor and response variables (Franklin, 2010; Guisan et al., 2002; Yee and Mitchell, 1991). More specifically, GLMs and GAMs were used to examine the relationships between response variables (species cover and species richness) and baseline explanatory variables (elevation, slope, aspect, MGST, Tmax, Tmin, FDD, GDD, GSL, TVDI). Then, environmental factors (morphodynamics index and ESPs) were added to the baseline model to test their additional effect in an advanced model. The Spearman correlation coefficient was set to  $|\rho| > 0.7$  as criterion to limit collinearity between the explanatory variables (Dormann et al., 2013). For pairs of variables with correlation above this threshold, we selected the one with the highest value of correlation in the NMDS analysis. GLMs were fitted using the *stats* package. An ANOVA *F*-test was applied to analyse the variance. To model species cover, four types of models were tested to identify the most appropriate setting. The first trial included linear terms of explanatory variables and the family argument “quasipoisson”; the second included quadratic terms of the explanatory variables and the “quasipoisson” family; the third included linear terms and the “quasibinomial” family; and the final trial included quadratic terms and the “quasibinomial” family. When the family argument “quasibinomial” was used, species cover values were transformed to a proportion scale (0-1). To model species richness, the family argument was defined as “quasipoisson” due to over-dispersion in the data (Crawley, 2007). GAMs were fitted using the *mgcv* package (v. 1.8.22). The family was

defined as “quasipoisson” for the same reason as for GLMs. The initial degree of smoothness was set to 3 for each variable (Wood, 2017). Once again, we first developed a baseline model and then added the additional environmental factors tested in this study.

## 2.3 Results

### 2.3.1 Plant communities

The location of the plots is illustrated in the next section (Figure 2.2). The identified communities belong to the alliances described in Table 2.3 (Delarze et al., 2015).

**Table 2.3** - Alliances (Delarze et al., 2015) to which the plots belong and their characteristics.

<b>Alliance name</b>	<b>Characteristics</b>
<i>Thlaspion rotundifolii</i>	calcareous screes of alpine belt
<i>Drabion hoppeanae</i>	calcschist screes of alpine belt
<i>Petasion paradoxii</i>	wet calcareous screes
<i>Androsacion alpinae</i>	siliceous screes of alpine belt
<i>Elymion</i>	grasslands on windy ridge
<i>Seslerion</i>	dry calcareous grasslands
<i>Caricion firmae</i>	rocky calcareous grasslands of alpine belt
<i>Caricion curvulae</i>	acidophilous grasslands of alpine belt
<i>Poion alpinae</i>	pastures of the subalpine and lower alpine belts
<i>Arabidion caeruleae</i>	calcareous snow beds
<i>Salicion herbaceae</i>	acidophilous snow beds
<i>Rhododendro-Vaccinion</i>	subalpine heaths on acidic soil

In total, 128 species were identified. In plot n° 11 no species was present. A large portion of plots was unaffected by ESPs (27 plots). Rill erosion affected mainly 21 plots, frost weathering 11, nivation 7 and solifluction 5, but most of the plots were affected by more than one ESP. Values of species cover and species richness were lower in the plots characterized by ESPs, compared to the category “No ESP”. Instead, values of evenness were higher. Details are provided in Table 2.4. Equally, plots characterized by high morphodynamics index presented lower species cover and species richness.

Species cover differed strongly between debris plots (0-40 %) and grassland plots (75-100 %). Species richness increased progressively but not linearly from debris locations (minimum 0 species in plot n° 11, Les Martinets) to grasslands (maximum 26 species in plot n° 6, Les Martinets). In some cases, microtopographic factors induced a higher species richness in debris areas (e.g., 20 species in plot n° 16 located on the lower lobe of the Martinets rock glacier).

**Table 2.4** - Number of plots and community characteristics observed in the different ESP categories (absence of ESP, solifluction, rill erosion, nivation and frost weathering). Mean values and standard deviation are reported. Species cover: percentage of vascular plant cover [%]. Species richness: number of species per plot. Evenness: biodiversity index measuring the dominance of one species above the others in the same survey.

ESPs	Number of plots	Sp. cover	Sp. richness	Evenness
No ESP	27	52 ± 38	15 ± 5	0.31 ± 0.13
Solifluction	5	11 ± 4	8 ± 7	0.44 ± 0.19
Rill erosion	21	25 ± 23	11 ± 4	0.43 ± 0.19
Nivation	7	20 ± 20	11 ± 5	0.45 ± 0.15
Frost weathering	11	31 ± 24	12 ± 4	0.48 ± 0.21

The mean evenness was low ( $< 0.5$ ), indicating a general prevalence of a low number of species (see Supplementary material Figure 2.7 for images). Species cover and species richness were highly correlated (Spearman's correlation  $\rho = 0.82$ ). Evenness was negatively correlated with both species cover ( $\rho = -0.78$ ) and species richness ( $\rho = -0.71$ ). The Mantel test revealed no spatial autocorrelation in the two response variables (species cover and species richness).

According to the clustering of the 71 plant surveys in five groups (the empty plot is not considered here – Figure 4), the first group comprised pre-LIA sites, characterized by late-successional species belonging to *Poion alpinae*, *Rhododendro-Vaccinion*, *Elynion*, *Seslerion*, *Caricion firmae* and *Caricion curvulae* (according to Delarze et al., 2015). In the second group, debris plots with *Salix* sp. (snowbeds of *Arabidion caeruleae* or *Salicion herbaceae*) and the debris characterized by high water availability (due to percolation or late melting of snow patches – named hereafter “wet debris”; *Petasidion paradoxii*) were grouped. The plots located on the older debris belonging to pre-LIA periods (*Thlaspion rotundifolii* and *Drabion hoppeanae*, with some species belonging to *Cystopteridion* and *Potentillion* - shady and sunny calcareous cliffs with vascular vegetation) were found in the third cluster. In contrast, vegetation on moraines and dynamics debris more recent than LIA (*Thlaspion rotundifolii*, *Drabion hoppeanae*) constituted the fourth group. Plots in the last group were characterized by species adapted to low temperatures; thus, the plots belonged to *Androsacion alpinae* and *Thlaspion rotundifolii*. The ecological and environmental characteristics of the five groups are reported in Table 2.5.

The pre-LIA moraines, as well as the surfaces not covered by ice during the LIA and those not affected by ESPs, were colonized by late successional stage species (plots of group 1). In Les Outans, grasslands were only present in the lower elevation areas (1960-2030 m a.s.l.) or on bedrock outcrops. The wet calcareous screes as well as the debris-covered glacier were colonized by pioneer species belonging to *Petasidion paradoxii*, *Thlaspion rotundifolii* and *Drabion hoppeanae* (groups 2, 4 and 5). In the Col des Perris Blancs, acidophilous species such as *Ranunculus glacialis* (*Androsacion alpinae*) were identified next to basiphilous species belonging to *Thlaspion rotundifolii* (group 5). Pioneer species were present in the front of the creeping lobes (*Thlaspion rotundifolii*, groups 5 and 2), whereas windy (*Elynion*) and dry (*Seslerion*) calcareous grasslands colonized the highest elevation of the pass (group 1). The highest plant diversity was found in Les Martinets because this site presents the highest geomorphological diversity and all types of ESPs. The vegetation plots there belonged to all five groups.

**Table 2.5** - Environmental characteristics of the five vegetation groups. Mean values and standard deviations are reported. Species richness: number of species per plot. Evenness: biodiversity index measuring the dominance of one species above the others in the same plot. Elevation: [meters]. Aspect: North (-1) South (+1) gradient. Slope: [degrees]. MGST: Mean Ground Surface Temperature [°C]. Tmax: mean maximum temperature [°C]. Tmin: mean minimum temperature [°C]. FDD: Freezing Degree Day [degree day]. GDD: Growing Degree Day [degree day]. GSL: Growing Season Length [day].

Groups	Number of plots	Species richness	Evenness	Elevation	Aspect	Slope
1	19	17 ± 4	0.25 ± 0.08	2281 ± 185	-0.33 ± 0.69	20 ± 9
2	14	11 ± 5	0.50 ± 0.20	2269 ± 158	-0.52 ± 0.56	21 ± 6
3	16	13 ± 4	0.35 ± 0.11	2315 ± 48	-0.39 ± 0.71	24 ± 11
4	9	8 ± 3	0.61 ± 0.19	2355 ± 94	-0.24 ± 0.79	21 ± 12
5	13	9 ± 3	0.40 ± 0.10	2353 ± 194	-0.54 ± 0.41	24 ± 8
Groups	MGST	Tmax	Tmin	FDD	GDD	GSL
1	3.6 ± 0.5	4.9 ± 0.6	1.1 ± 0.5	85 ± 88	1429 ± 144	109 ± 9
2	3.1 ± 0.7	4.5 ± 1.0	0.8 ± 0.7	82 ± 153	1151 ± 305	105 ± 48
3	2.5 ± 0.6	3.6 ± 1.1	0.7 ± 0.3	47 ± 61	965 ± 255	84 ± 14
4	2.5 ± 0.5	3.6 ± 0.8	0.6 ± 0.5	87 ± 94	922 ± 182	80 ± 14
5	2.6 ± 0.8	4.1 ± 0.9	-0.2 ± 1.6	233 ± 239	1176 ± 217	100 ± 14

### 2.3.2 Ground Surface Temperatures

The temperature distribution within two years of GST monitoring (01.10.2016 - 30.09.2018) is presented in Supplementary material Figure 2.8. During the study period, the snow arrived late in the 2016-2017 winter season and the snow cover thickness remained below average. Then, early snow melt coupled with warm air temperatures during early summer led to high ground surface temperatures during the snow free period (Meteoswiss, 2018). Instead, winter 2017-2018 had thicker and longer snow cover and mild air temperatures, which maintained GSTs around 0 °C in most of the site. Air temperatures of the 2018 summer in Switzerland were among the highest ever recorded, overstepping the 1981-2010 mean (Meteoswiss, 2019). Consequently, the ground in the study area warmed more than the year before. Therefore, high variability was observed: the minimum winter temperatures were -13.1 °C on 2017 (Col des Perris Blancs, plot n° 44 on 24 January) and -8.9 °C on 2018 (Col des Perris Blancs, plot n° 44 on 2 March) and maximum summer temperatures were 21.9 °C on 2017 (Les Outans, plot n° 52 on 24 June) and 23.3 °C on 2018 (Les Martinets, plot n° 1 on 1 July).

The vegetation plots corresponding to groups 1 and 2 (see Table 2.5) had the highest MGST (3.6 and 3.1 °C, respectively) and Tmax (4.9 and 4.5 °C, respectively) and the longest GSL (109 and 105 days, respectively). The plots of groups 3 and 4 had the lowest MGST (2.5°C) and Tmax (3.6°C) but the group 3 had also the lowest FDD index (47 degree days), whereas the plots in group 4 had the lowest GDD (922 degree days) and GSL (80 days). The plots in group 5 had the lowest Tmin (-0.2 °C) and the highest FDD index (233 degree days), even if MGST and Tmax were in average.

The basal-ripening date (RD) was not present for all data loggers due to a lack of ground freezing in some cases. As a result, it was calculated for only 40 plots in 2017 and for 9 in 2018. The earliest date when the ground temperature reached 0 °C was 1 February 2017 (plot n° 53), whereas the latest date was 31 May 2017 (plot n° 30). In 2018, the RDs were between April and May. The melt-

out date was detected for all data loggers. The snowmelt started earlier in 2017 than in 2018. In 2017, the snow disappeared first at the plot n° 44 on 22 May and lastly at the plot n° 11 on 21 July. In 2018, it disappeared first at the plot n° 18 on 30 June and lastly at the plot n° 27 on 2 August. Examples of two typical curves of temperature evolution are reported in Supplementary material Figure 2.9.

The FDD index points out the coldest areas: these were located on the debris-covered glacier in Les Outans (plots n° 47 and 52), at the Col des Perris Blancs, especially on the protalus rampart (plots n° 43, 44, 62, 63), and in the upper part of the Martinets rock glacier and in the lateral morainic deposit (plots n° 19, 20 and 30 – Figure 2.2). On the same locations, daily temperatures below -2 °C were recorded on late winter, before the RD. During 2016-2017 winter, temperatures below -3 °C were recorded at the plots n° 19, 43, 44, 47, 62, 63, 64 and 69; during 2017-2018 winter, at the plots n° 43, 44 and 62. These data indicate a possible presence of permafrost.

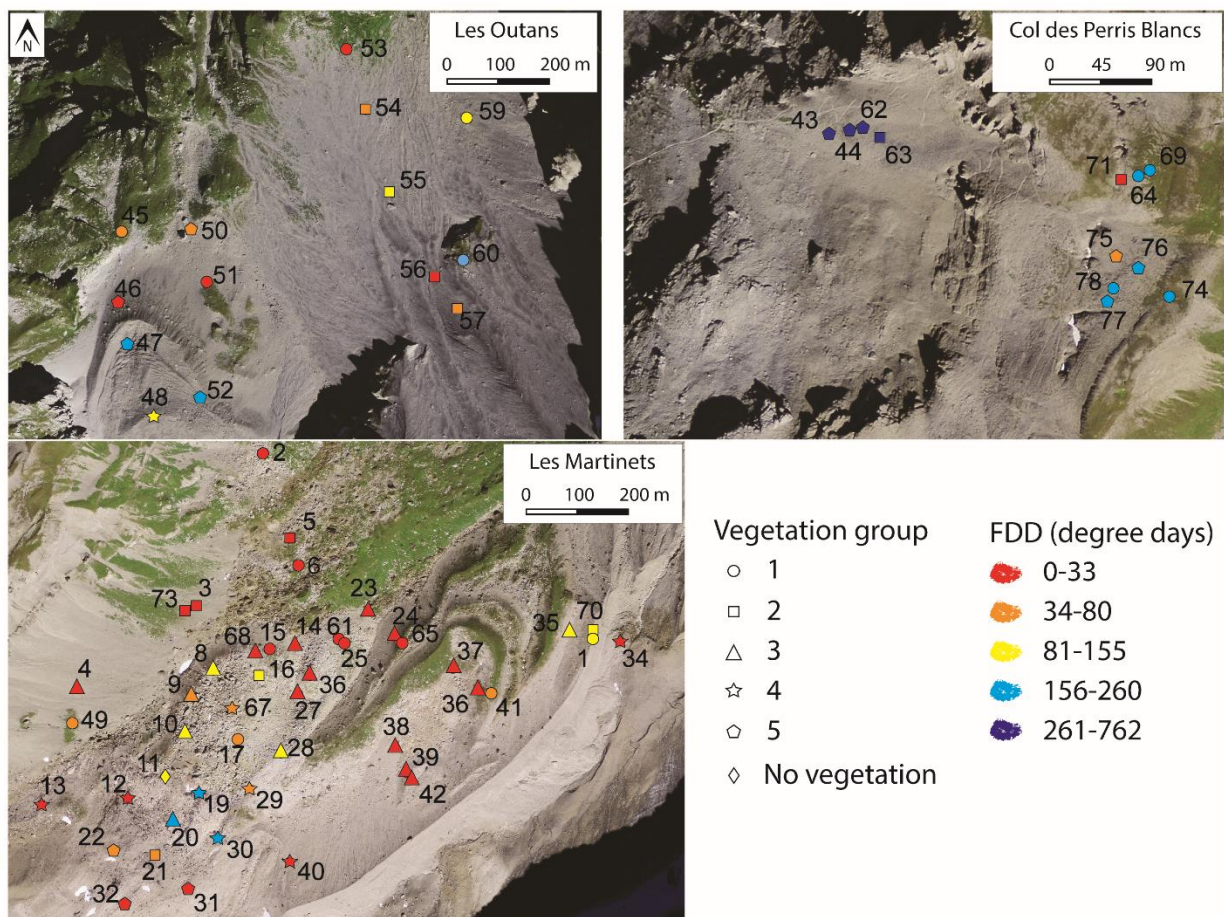


**Figure 2.2** - Location of vegetation plots, grouped based on cluster analysis. Colors indicate the value of the Freezing degree days index (01.10.2016 - 30.09.2018) for Les Outans, Col des Perris Blancs and Les Martinets. SwissImage © swisstopo (DV084371).



### 2.3.3 Vegetation–environment relationships

The NMDS offers a graphical visualization of the vegetation plots distributed according to plant composition. Their disposition reflects the previous clustering in five groups, although the elements in group 2 are scattered. The ordination stress was 0.22 (Figure 2.3). Among the environmental factors added with the *envfit* function to test for the correlation with plant communities, morphodynamics was the most explicative variable with the highest value of linear fit ( $R^2 = 57\%$ ), followed by GDD ( $R^2 = 50\%$ ), MGST and Tmax ( $R^2 = 32\%$ ), rill erosion and FDD ( $R^2 = 23\%$ ), GSL ( $R^2 = 20\%$ ), Tmin ( $R^2 = 19\%$ ) and solifluction ( $R^2 = 17\%$ ), all with  $p$ -value  $< 0.001$  (linear correlation). Frost weathering, TVDI and nivation influenced less the vegetation composition ( $R^2 \leq 12\%$ ;  $p$ -value  $< 0.05$ ) and slope had the lowest influence ( $R^2 = 9\%$ ;  $p$ -value  $< 0.1$ ). Elevation and aspect were not significantly correlated. More details are reported in Table 2.6. The linear and smoothed surface fits indicate clear gradients in surface activity corresponding to community structure (Figure 2.4).

Based on the results of the Spearman correlation, MGST, Tmin and Tmax were all correlated and GDD was correlated with MGST, Tmax and GSL (values  $> |0.7|$ ; see Supplementary material Figure 2.10). Then, to calculate the GLMs and GAMs, only GDD plus the other variables were added.

The significant baseline variables used to model species cover with the GLM were FDD, GDD and elevation, whereas GDD and elevation were used with the GAM because their inclusion in the models was significant ( $p$ -value  $< 0.1$ ). To model species richness, the baseline variables of the GLM and GAM were FDD, GDD and slope ( $p$ -value  $< 0.05$ ).

The best GLM prediction of species cover was achieved using quadratic terms and family argument “quasipoisson”. The explained deviance was 45.7% for the baseline model and 71.9% for the advanced model. In the other case, it was lower (41-45.7% and 64.1-67.1%). The details of all trials with quadratic terms and the family argument “quasibinomial” are presented in Supplementary material Figure 2.11-2.18. The predictions of species cover and species richness were significantly improved by the addition of the morphodynamics variable ( $p$ -value  $< 0.001$ ). For species cover, the explained deviance improved from 43.3% to 70.8% using the GAM. For species richness, the explained deviance in the GLM changed from 31.2% to 52.6%, and in the GAM from 32.7% to 55.4%. According to the GLM results, species richness increased as GDD ( $p$ -value  $< 0.05$ ) increased and decreased as morphodynamics ( $p$ -value  $< 0.001$ ), FDD ( $p$  value  $< 0.05$ ) and slope increased ( $p$  value  $< 0.1$ ). As long as the models are linear, no Figures are shown. From the GAM results, the species cover increased as GDD ( $p$ -value  $< 0.001$ ) and elevation (but  $p$ -value not significant) increased (Figure 2.5a and b), whereas it decreased significantly ( $p$ -value  $< 0.001$ ) with an increase in morphodynamics (Figure 2.5c). Species richness increased as GDD increased ( $p$ -value not significant – Figure 2.5d) and decreased as FDD ( $p$ -value  $< 0.01$ ), slope (not significant) and morphodynamics ( $p$ -value  $< 0.001$ ) increased (Figure 2.5e and f).

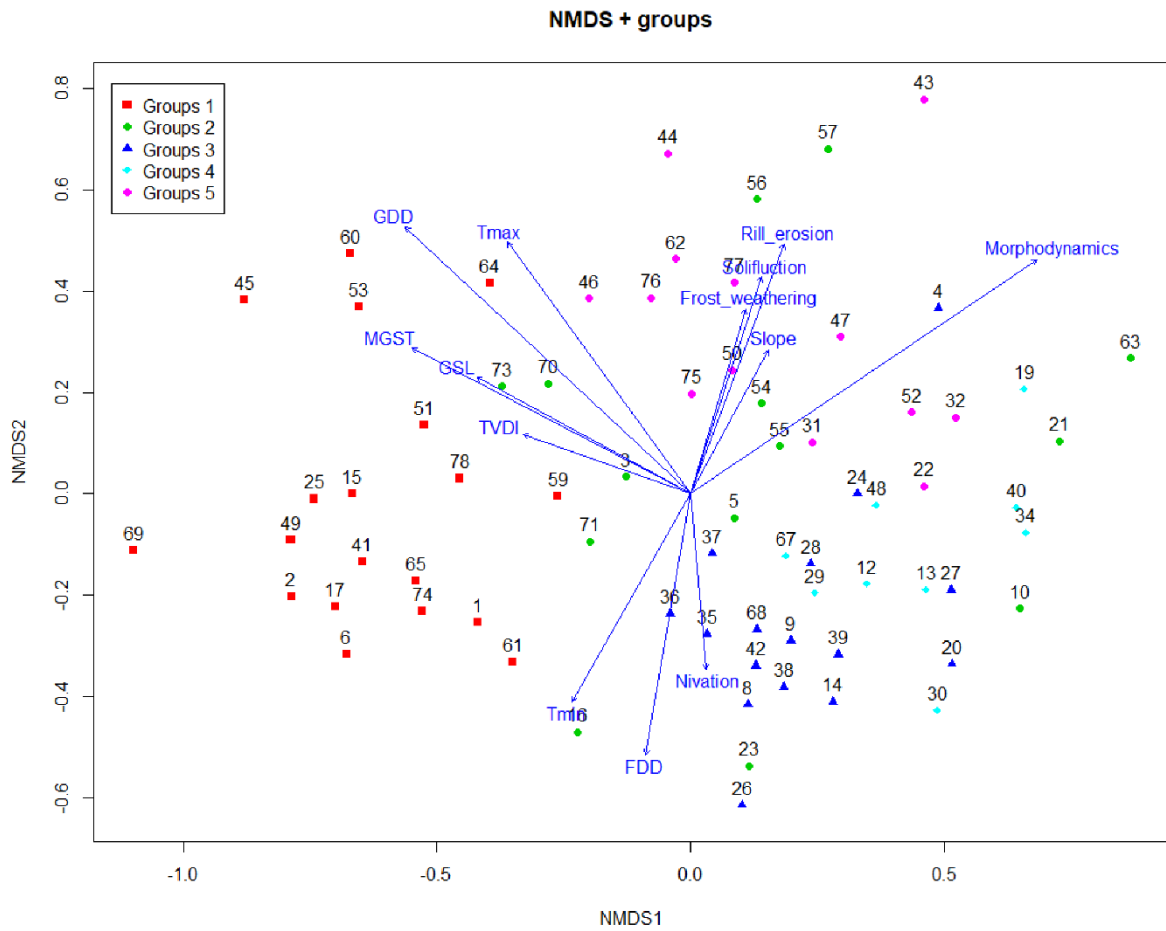


**Figure 2.3** - NMDS biplot of the vegetation plots, based on the Bray–Curtis dissimilarity matrix, with fitted vectors of all environmental factors. The plot data are regrouped in 5 groups. Ordination stress = 0.22. GSL = Growing Season Length; GDD = Growing Degree Day; FDD = Freezing Degree Day; MGST = Mean Annual Ground Surface Temperature; TVDI = Temperature Vegetation Dryness Index.

**Table 2.6** - Correlations between NMDS axes and explained variables. NMDS1 and NMDS2 are the axis scores about the 2D ordination space.  $R^2$  = linear fit of correlation. Signif.: indicate the *p-value*. \*\*\*  $\leq 0.001$ ; \*\*  $\leq 0.01$ ; \*  $\leq 0.05$ ; .  $\leq 0.1$ ; ns = not significant. GSL = Growing Season Length; GDD = Growing Degree Day; FDD = Freezing Degree Day; TVDI = Temperature Vegetation Dryness Index; MGST = Mean Ground Surface Temperature; Tmax and Tmin = maximum and minimum temperature.

	NMDS1	NMDS2	$R^2$	Signif.
Morphodynamics	0.83	0.56	0.57	***
GDD	-0.73	0.68	0.50	***
MGST	-0.89	0.46	0.32	***
Tmax	-0.59	0.81	0.32	***
Rill_erosion	0.35	0.94	0.23	***
FDD	-0.17	-0.99	0.23	***
GSL	-0.88	0.48	0.20	***
Tmin	-0.50	-0.87	0.19	***
Solifluction	0.31	0.95	0.17	***
Frost_weathering	0.28	0.96	0.12	*
TVDI	-0.94	0.34	0.10	*
Nivation	0.09	-1.00	0.10	*
Slope	0.48	0.88	0.09	.
Elevation	0.55	-0.84	0.04	ns
Aspect	-0.33	-0.94	0.04	ns

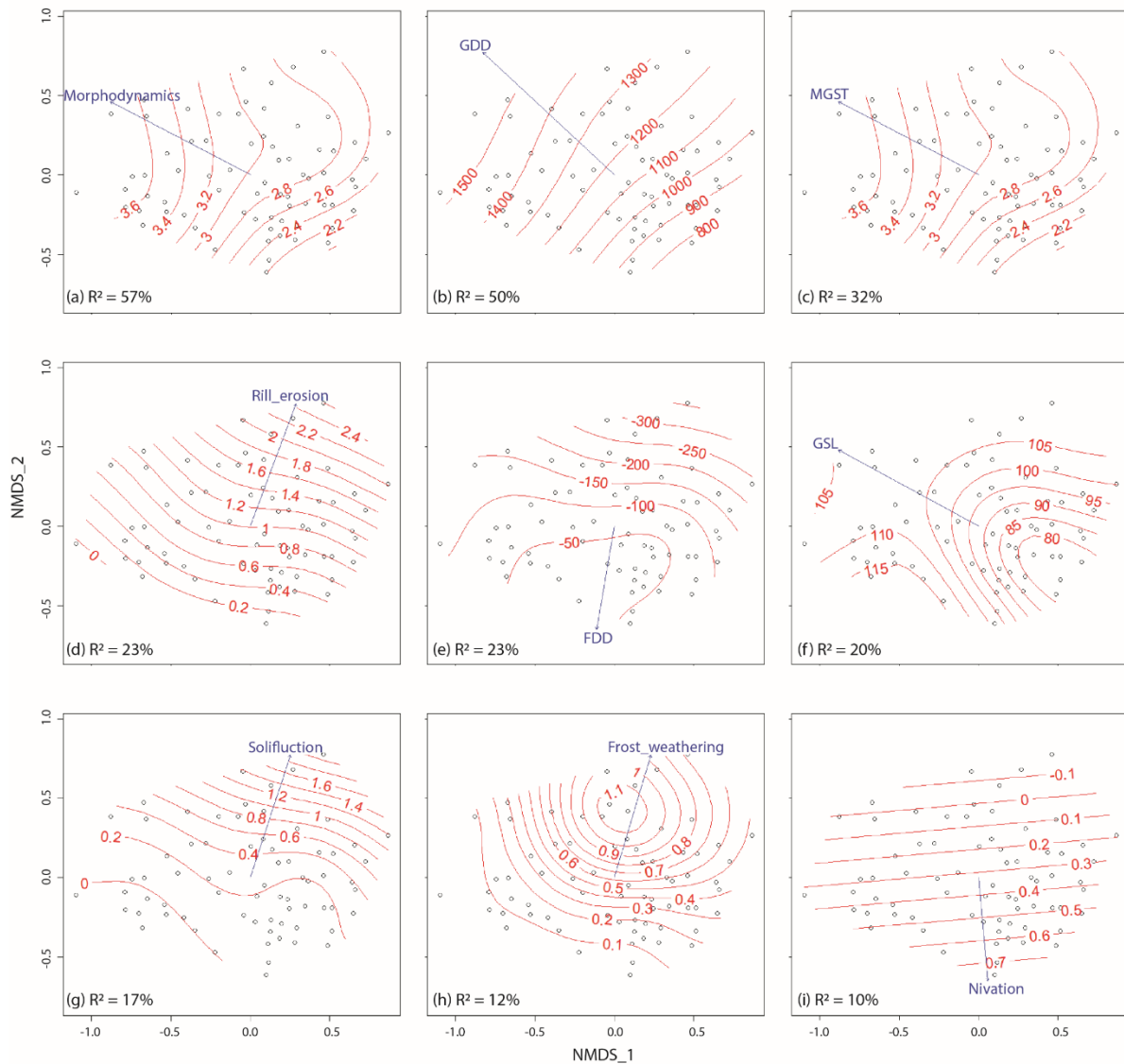


**Figure 2.4** - Relationship between the plant community (black points; ordination conducted using NMDS) and the environmental variables that are the most significant. The blue vectors indicate the direction of maximum linear correlation (ordination score reported in percentage). The red smoothed surface fits represent the change of the variable between the plots. The *p*-value of vectors is < 0.001 for (a)-(g) and < 0.05 for (h)-(i). GSL = Growing Season Length; GDD = Growing Degree Day; FDD = Freezing Degree Day; TVDI = Temperature Vegetation Dryness Index.

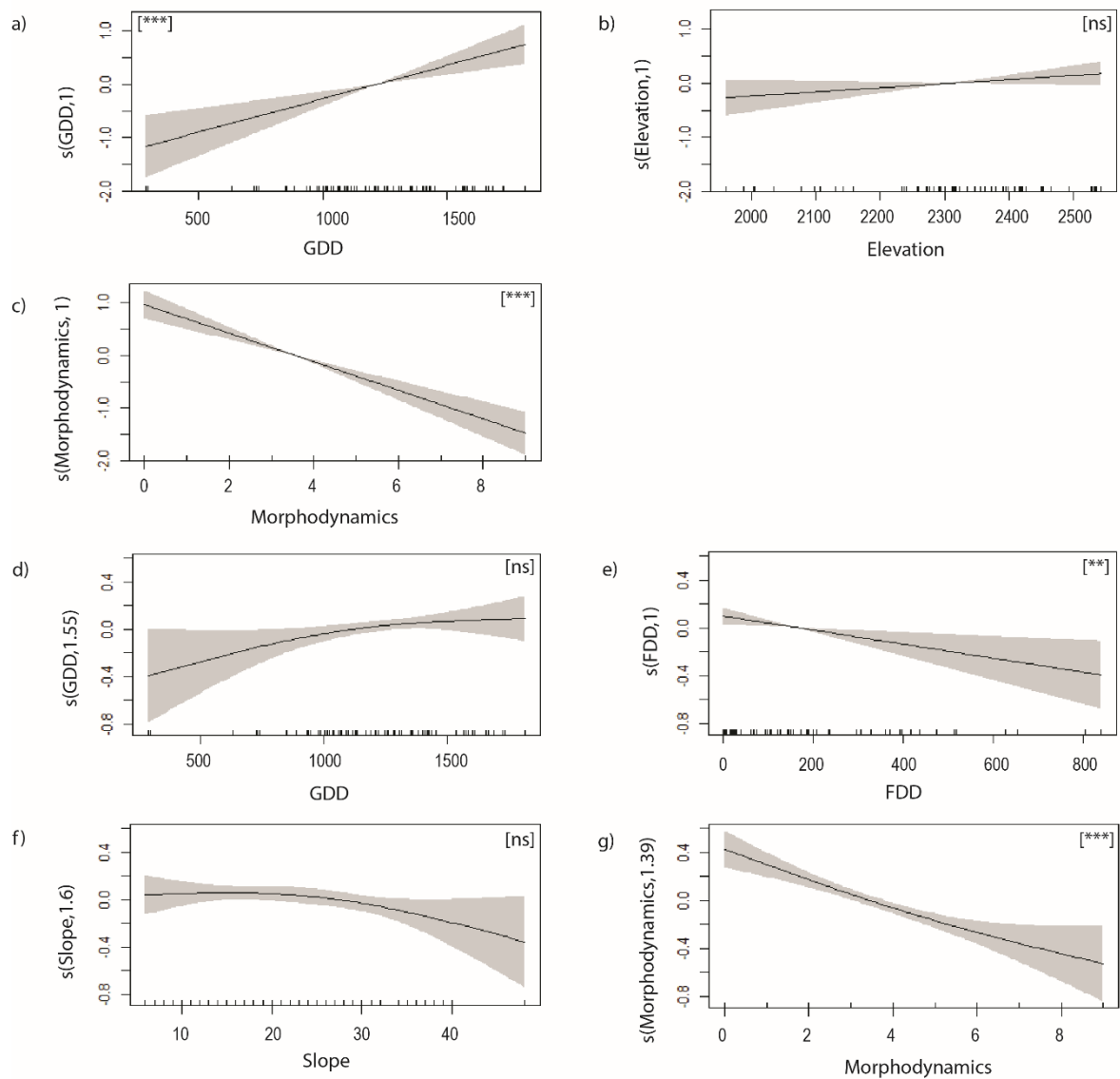


**Figure 2.5** - Species cover (a-c) and species richness (d-g) models conducted using GAMs. (a-b) and (d-f) represent the baseline explanatory variables, (c) and (g) the environmental variables added to improve models. The x-axis represents the environmental variables and the y-axis the smoothed factor of the variable with estimated degrees of freedom. Shaded area represents the confidence interval. GDD = Growing Degree Day. FDD = Freezing Degree Day. Symbols between [ ] indicate statistical significance. [\*\*\*] = p-value < 0.001; [\*] = p-value < 0.05; [.] = p-values < 0.1; [ns] = not significant.

## 2.4 Discussion

In the present study, we investigated the influence of environmental variables, especially geomorphic processes, on the composition of plant communities in the Western Swiss Alps. The innovative aspect of this research is that we have worked on sites characterized by a high degree of heterogeneity regarding ages, landforms and plant communities, using a large data-set including vegetation and temperature. Indeed, to enhance plant species distribution model, not only improving the resolution of topographic data is important but also conducting thorough field measurements (Pradervand et al., 2014), as in our case. We expected microtopography, microclimate, soil moisture, snow cover and ESPs to be the most important environmental factors for plant communities. However, the initial expectations were only partly confirmed. Our results highlighted that landform morphodynamics (which acts on microtopography), growing degree days and mean ground surface temperature were the most explicative environmental variables for community composition and species richness. Indeed, different geomorphological characteristics support different plant communities, depending on age, soil development, frequency of disturbances and landforms dynamics, confirming previous studies (e.g., Gentili et al., 2013; Le Roux & Luoto, 2014). However, the ESPs and the temperature vegetation dryness index (TVDI) exhibited low statistical significance in our analysis, even if the TVDI is likely directly correlated to vegetation properties because it includes the NDVI.

Considerable heterogeneity not affected by spatial autocorrelation was observed among the plant communities in all three focus sites. Indeed, due to the heterogeneity of landforms, characterized by different ages and stability, we found a high diversity of plant communities from pioneer, typical of young moraine deposits, to stable communities, typical of alpine grasslands. As expected, species cover and species richness were positively correlated with each other and negatively correlated with evenness (Stirling and Wilsey, 2001). Furthermore, their values were lower in the plots characterized by ESPs. The composition of the different plant communities is constrained by the respective adaptations of the species to environmental conditions. In Les Outans, superficial processes (rill erosion, debris flow, rock falls) affecting wet calcareous screes and subsidence due to ice melt on the debris-covered glacier resulted in the survival of only pioneer species. Indeed, the superficial processes maintain pioneer vegetation groups (Moreau et al., 2008). In the Col des Perris Blancs, pioneer species were present on poorly developed soils and solifluction areas. In contrast, windy and dry alpine grasslands were identified in areas not modified by the LIA glacier, which were characterized by well-developed organic soil. Les Martinets site showed the highest plant community diversity. Indeed, the complex history of this catchment (Perret and Martin, 2015) results in the establishment of a large variety of successional stages, from pioneer species in the recently deglaciated areas (observed in the plots belonging to *Thlaspion rotundifolii* and *Drabion hoppeanae*) to late successional grasslands in the stable surfaces of the Holocene period (*Elymion*, *Seslerion*, *Caricion ferrugineae* and *Caricion curvulae*).

Monitoring of ground surface temperatures was helpful in documenting the microclimatology of the study area and evaluating the possible presence of permafrost. During the monitoring period (October 2016 – September 2018), the thin snowpack at the beginning of winter 2016/2017 induced a low insulation and, consequently, a strong overcooling of the winter GST, which was the lowest recorded in the Swiss Alps over the last ten years (PERMOS, 2019). In contrast, winter 2017/2018 was characterized by a thicker and longer snow cover that, together with warmer air temperatures, maintained GST higher than in 2017. The FDD analysis and the negative daily

temperatures highlighted where the coolest sites were located in the study areas. According to the BTS method (Haeberli, 1973; Hoelzle et al., 1993; Ikeda and Matsuoka, 2006; Ishikawa, 2003), permafrost is present around the Col des Perris Blancs area and in the upper part of the rock glacier in Les Martinets above 2400 m a.s.l. because winter temperatures below thick snow were lower than -2 °C (and locally -3 °C). This was also confirmed by an electrical resistivity tomography profile (Giaccone et al., 2016). Negative BTS were also reported for Les Outans debris-covered glacier, due to the presence of glacier ice close to the surface. The warmer temperatures measured on the lower part of the Martinets rock glacier does not exclude permafrost conditions. They can indeed be explained by a thick active layer that prevents the detection of cold ground conditions by the BTS method. Eventually, the outlining of these cold sectors fit well with the Alpine Permafrost Index Map (Boeckli et al., 2012) and with previous geomorphological analyses (Lambiel et al., 2009; Perret and Martin, 2015). However, temperature was less correlated to the NMDS axes than GDD and, due to the high correlation between these variables (~0.8 with T<sub>min</sub> and MGST), only GDD was finally used in vegetation models.

While the rock glacier in Les Martinets suggests the presence of permafrost in the upper part, landform dynamics and related topography were more important to explain the distribution of vegetation types (e.g., Colombo et al., 2016; Gobbi et al., 2014). Besides, the active layer thickness prevents any influence of permafrost on plant life (Körner, 2003; van Tatenhove and Dikau, 1990). In Les Martinets, the lower part of the rock glacier had vegetation patches of late-successional stages (grassland), whereas the upper part was colonized exclusively by pioneer species. In most cases, grass species were found in *Salix retusa* and *S. serpillifolia* mats. This was because dwarf *Salix* species, due to their creeping growth and abundant root development, promote debris stabilization, the accumulation of fine sediments, biomass and humus thus facilitating the colonization of other species (Reisigl and Keller, 1987). These elements, together with morphological indices, suggest that the lower part of the rock glacier is older than the upper part. Furthermore, no evident signs of movements were visible in the frontal part of the lower lobe, in contrast to the upper part where the front is less stable. Thus, the vegetation allows us to discern between active and inactive rock glaciers, as also shown by Cannone and Gerdol (2003) and Burga et al. (2004).

Microtopography controls soil moisture patterns and nutrient availability (Kemppinen et al., 2018), playing a major role in the development of vegetation types and plant community succession (Riihimäki et al., 2017; Stewart et al., 2014), and generates habitats with heterogeneous snow distribution (Aalto et al., 2018; Hülber et al., 2010), which also influences plant communities. For example, places where the snow disappears later in summer, as in the Col des Perris Blancs and Les Martinets sites, were mainly colonized by snowbed species (e.g. *Arabis caerulea*, *Salix herbacea*). Based on correlations between vegetation plots and environmental variables, the growing degree days and the growing season length appeared to be between the most explicative variables, confirming how snow persistence influences vegetation communities (Braun, 1913; Nüttynen and Luoto, 2018).

NMDS analysis was decisive in identifying the influence of environmental parameters on alpine plant communities, even if the ordination stress was high (Clarke, 1993), which could cause misinterpretation. Nevertheless, a relatively low number of dimensions was needed to obtain the best fit (Hair Jr et al., 2014). Including the landform morphodynamics variable in the NMDS was crucial to explaining plant communities, as this variable exhibited the highest value of linear fit ( $R^2 = 57\%$ ). Furthermore, it significantly improved the species cover and species richness predictions with both the GLMs and GAMs. It was, indeed, the only significant variable ( $p$ -value < 0.001) among those added to the baseline GLM and GAM that augmented the explained deviance in both

models. We demonstrated that higher landform morphodynamics cause a decrease in species cover and species richness. Examples are the plots n° 11, 12, 43 and 44, the first two of which were located at the front of the higher lobe of the rock glacier in Les Martinets, and the latter two were located in the protalus rampart in the Col des Perris Blancs. These plots are characterized by a maximum morphodynamics index and low level of species cover (0-10 %) and species richness (max 8 species).

However, contrary to our initial expectations, solifluction, rill erosion and nivation were not significant in the species cover and species richness models, although ESPs were shown to be influential on plant communities in previous studies (Malanson et al., 2012; le Roux et al., 2013). The reason for this difference may result from an insufficient sample size to fit the GLMs and GAMs, as evidences of ESPs were only found in a limited number of plots. The plots most affected by rill erosion, solifluction and frost weathering are included in groups 2 and 5. In these groups, the species belong to *Petasidion paradoxici*, *Thlaspion rotundifolii* and *Drabion hoppeanae*, all being markers of calcareous screes (Delarze et al., 2015), with high rates of geomorphic processes. The plots characterized by nivation were found in groups 2 and 3 (composed of species belonging to *Arabidion caeruleae*, *Salicion herbaceae*, *Thlaspion rotundifolii* and *Drabion hoppeanae*) and were located in small areas, where the local topography supports longer snow persistence and, consequently, the growth of snowbed species (Björk and Molau, 2007). The plots not affected by ESPs were composed of late successional species and pioneer species.

The choice to include the morphodynamics index in our analysis was fundamental even if it has some limitations. Indeed, the relationships between species composition and landform morphodynamics derive from the effect of landform changes (e.g. Cannone & Gerdol, 2003; Gentili et al., 2013; le Roux & Luoto, 2014) and direct disturbance impact on species, but also from other factors which were not integrated in our index. Within the morphodynamics index, we took into consideration the soil texture and development (fine material or rock texture) but not pH, nutrients, quantitative soil organic matter and other soil properties, which are also known to be essential for plant species development, for example ions concentration, water content and soil respiration (Buri et al., 2017; Cianfrani et al., 2018; Gobat et al., 2010; Grand et al., 2016; Matteodo et al., 2018). Furthermore, soil properties are particularly difficult to include in the models due to their high spatial variability, which depends on bedrock, climate and topographical factors, but also on the activity of microorganisms (e.g. Yashiro et al., 2018). A further complication is that they are tightly associated to vegetation, and vice versa (Guisan et al., 1998; Lavelle et al., 1995).

Our results confirmed also the importance of the thermal indices for plant species. Climatic factors are in fact between the most important factors shaping plant distributions and especially the temperature is a key parameter influencing plant life cycles. Under ongoing climate warming, several studies have pointed out that phenology is accelerated and growth enhanced (Chen et al., 2015; Hollister et al., 2005) but freezing and heat stress still played decisive roles for alpine plants life (Körner, 2003).



## 2.5 Conclusion

In this study, we investigated three alpine sites in the Western Swiss Alps (1950-2550 m a.s.l.) that exhibited high geomorphological variability and habitat diversity. We demonstrated that landform morphodynamics, growing degree days and mean ground surface temperature are the most explicative environmental variables of plant communities in such heterogeneous environments. Specifically, the morphodynamics index proved fundamental as it provided important information concerning landform stability, frequency of disturbances, age of deposits and soil development. Moreover, vegetation shows to be critically relevant to identify the different degrees of activity in the rock glacier.

The morphodynamics index significantly improved the models of species cover and species richness. The earth surface processes (rill erosion, solifluction, frost weathering and nivation) are also known to influence vegetation types (le Roux & Luoto, 2014; Virtanen et al., 2010) but were less significant in our study. However, in the plots characterized by earth surface processes (ESPs), vascular plant cover and species richness had lower values compared to the “No ESP” category, indicating that an increase in geomorphological disturbance causes a reduction in the number of species and their cover percentage. Furthermore, high species richness values were generally associated with low morphodynamics index. Therefore, our results do not support the intermediate disturbance hypothesis (Connell, 1978), which asserts that maximum species richness should be reached at intermediate intensities of disturbance. Nevertheless, in alpine environments, this hypothesis should not be evaluated as the only explanation because other important abiotic factors, such as temperature, length of growing season and soil pH, are more actively involved (Vonlanthen et al., 2006b). Part of these factors induce probably too stressful conditions to allow competitive species to dominate the communities and to exclude stress tolerant species, as observed in lowlands with forests.

The results of this study contribute to a better understanding of the environmental factors influencing the type and distribution of alpine plant communities. Subjected to persistent atmospheric warming, changes in ground surface temperatures, snow cover and correlated earth surface processes may directly modify plant communities and soil properties. Future research should investigate the effects of soil texture, nutrient and pH, as done by Dubuis et al. (2013), and couple these results with geomorphological assessment in high alpine sites, as those presented here. Additionally, it would be important to work with longer ground surface temperature series, to obtain a more complete overview of the factors affecting vegetation in alpine ecosystems, and to take in consideration a biogeomorphic approach, because plant communities and geomorphic disturbance regime could be co-dependent as demonstrated by some authors (e.g., Corenblit and Steiger, 2009; Eichel et al., 2016, 2017; Lane et al., 2016).

## 2.6 Acknowledgements

This research is part of the project “Integrating spatial predictions of vegetation, soils, geomorphology and hydrology for improved assessment of ecosystem services under climate change”, supported by the Swiss National Science Foundation (project N° CR23I2\_162754). The Vaud Alps, where this research is carried out, are a priority research area for the University of Lausanne (<http://rechalp.unil.ch>).

## 2.7 Supplementary material

Figure 2.6

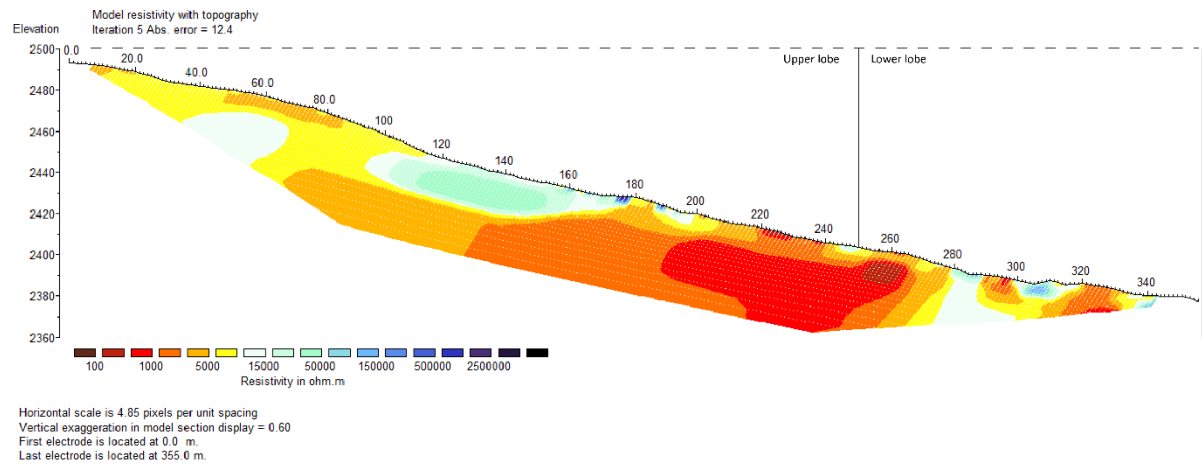


**Figure 2.6** - Longitudinal electrical resistivity tomography (ERT) profile realized the 16<sup>th</sup> August 2016 on Les Martinets rock glacier. The x-axis represents the longitudinal distance in meters from the profile starting point and the y-axis the elevation (m a.s.l.). The ERT profile was carried out with 48 electrodes and an inter-electrode spacing of 5 m from the upper lobe (UL) to the half part of the lower lobe (LL). The apparent resistivity were measured with the Syscal Pro Switch 96 (Iris Instruments). Salt-water saturated sponges were used to improve the contact between the electrodes and the ground because the surface was characterized by plurimetric blocks. Collected data were analysed with the Prosys II software, in which the surface topography measured with dGPS was inserted. The inversion was carried out with the RES2DINV software. We choose least-square inversion and robust parameters, providing a good visualization of high resistivity contrasts (for further details in the methodology see (Bosson et al., 2015; Marescot, 2006). A high resistivity body (30 k $\Omega$ m on average with maximum of 300-500 k $\Omega$ m) is present in the upper part of the UL up to a depth of 30 m. This can be interpreted as a permafrost layer. In the lower part of the UL, no permafrost is detected, considering low resistivity values (< 5 k $\Omega$ m). In the LL, small patches of very high resistivities (300-500 k $\Omega$ m) are interpreted as permafrost lenses. However, care have to be taken in the interpretation because of the relatively high error value (12.4%).

**Table 2.7**

**Table 2.7** - List of plots with topographic information (elevation [meters], aspect [North (-1) South (+1) gradient] and slope [degrees]), landforms type, species cover (percentage of vascular plant cover - %), and species richness (number of species per plot).

<b>Plot</b>	<b>Elevation</b>	<b>Aspect</b>	<b>Slope</b>	<b>Landforms</b>	<b>Sp_cover</b>	<b>Sp_richness</b>
1	2259	1	21	LIA moraine	70	18
2	2300	0.26	13	Avalanche-rockfall deposit	85	19
3	2311	0.15	18	Alluvial fan	20	18
4	2392	0	28	Talus slope	15	10
5	2292	-0.88	14	Avalanche-rockfall deposit	15	14
6	2292	0.92	6	Avalanche-rockfall deposit	100	26
8	2335	1	10	Lower rock glacier	15	17
9	2346	-0.94	12	Lower rock glacier	10	15
10	2362	-0.97	24	Lower rock glacier	10	7
11	2389	-0.97	48	Higher rock glacier	0	0
12	2416	1	13	Higher rock glacier	15	11
13	2451	1	34	Higher rock glacier	10	7
14	2291	-0.98	35	Lower rock glacier	25	12
15	2315	-0.71	32	Lower rock glacier	100	18
16	2335	-0.91	17	Lower rock glacier	20	20
17	2373	0.89	10	Lower rock glacier	85	15
19	2395	-0.9	34	Higher rock glacier	5	6
20	2418	-0.44	27	Higher rock glacier	25	9
21	2449	-0.99	34	Higher rock glacier	5	5
22	2465	-0.97	32	Higher rock glacier	25	9
23	2240	0.68	26	Lower rock glacier	5	8
24	2271	-0.61	39	Holocene moraine	10	10
25	2283	-0.89	23	Lower rock glacier	85	17
26	2312	-0.96	11	Lower rock glacier	5	5
27	2300	0.89	14	Lower rock glacier	5	7
28	2355	-0.81	35	Holocene moraine	25	13
29	2379	-0.28	14	Holocene moraine	20	13
30	2399	0.15	30	Holocene moraine	10	6
31	2453	-0.38	21	LIA moraine	40	10
32	2493	-0.59	8	LIA moraine	10	8
34	2237	-0.42	10	Post LIA moraine	5	6
35	2234	-0.86	9	LIA moraine	20	14
36	2277	-0.46	40	Holocene moraine	30	13
37	2257	0.98	28	Holocene moraine	50	15
38	2294	-0.91	29	Holocene moraine	30	11
39	2310	-0.73	32	Protalus rampart	25	15
40	2392	-0.99	35	LIA moraine	10	6
41	2290	-0.96	14	Holocene moraine	100	17

42	2318	-0.54	14	Protalus rampart	30	17
43	2408	0	34	Protalus rampart	5	4
44	2417	-0.19	30	Protalus rampart	10	8
45	2034	-0.4	37	Glacial accumulation surface	95	20
46	2078	-1	36	LIA moraine	5	8
47	2107	-0.97	12	Debris-covered glacier	5	7
48	2159	-0.89	8	Debris-covered glacier	5	9
49	2391	0.33	38	Vegetation-covered talus slope	100	15
50	2006	-0.93	24	Talus slope	40	11
51	2034	-0.98	16	LIA moraine	70	19
52	2143	0.24	27	LIA moraine	5	7
53	1961	-0.94	12	Vegetation-covered talus slope	80	15
54	1988	-0.97	18	Talus slope	10	10
55	2034	-0.86	20	Talus slope	15	12
56	2098	-0.8	23	Talus slope	10	9
57	2131	-0.83	31	Talus slope	5	7
59	2004	-0.77	27	Talus slope	60	18
60	2107	-0.57	30	Soil developed on rock	90	18
61	2283	-0.94	23	Lower rock glacier	30	13
62	2420	-0.18	19	Protalus rampart	10	12
63	2426	-0.42	21	Protalus rampart	5	2
64	2532	-0.12	18	Frost weathering deposit	45	10
65	2273	-0.99	17	Holocene moraine	95	24
67	2363	-0.8	12	Lower rock glacier	35	12
68	2322	-0.85	22	Lower rock glacier	20	17
69	2534	-0.35	12	Soil developed on rock	100	15
70	2259	-0.63	15	LIA moraine	10	8
71	2529	-0.2	12	Frost weathering deposit	50	13
73	2316	0.4	19	Vegetation-covered talus slope	40	14
74	2543	-0.61	12	Soil developed on rock	60	20
75	2526	-0.7	22	Frost weathering deposit	50	17
76	2535	-0.64	25	Frost weathering deposit	40	12
77	2533	-0.76	25	Frost weathering deposit	10	9
78	2533	-0.47	24	Soil developed on rock	75	15

Figure 2.7

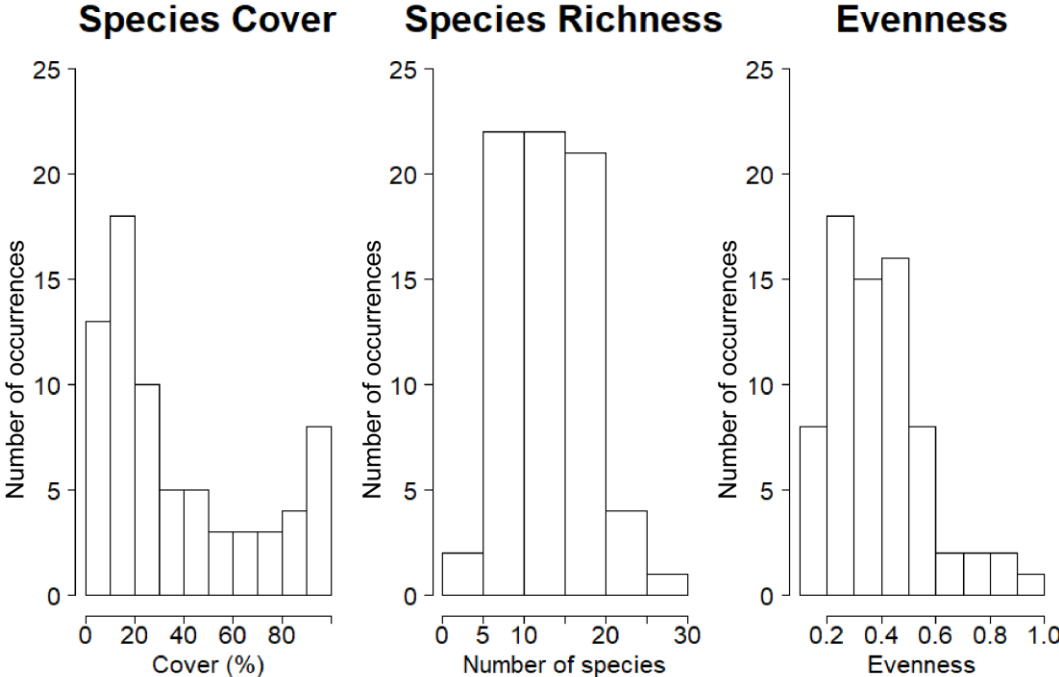


Figure 2.7 - Left. Frequency of species cover [%]. Center. Frequency of species richness [ $n^\circ$ ]. Right. Frequency of evenness.

Figure 2.8

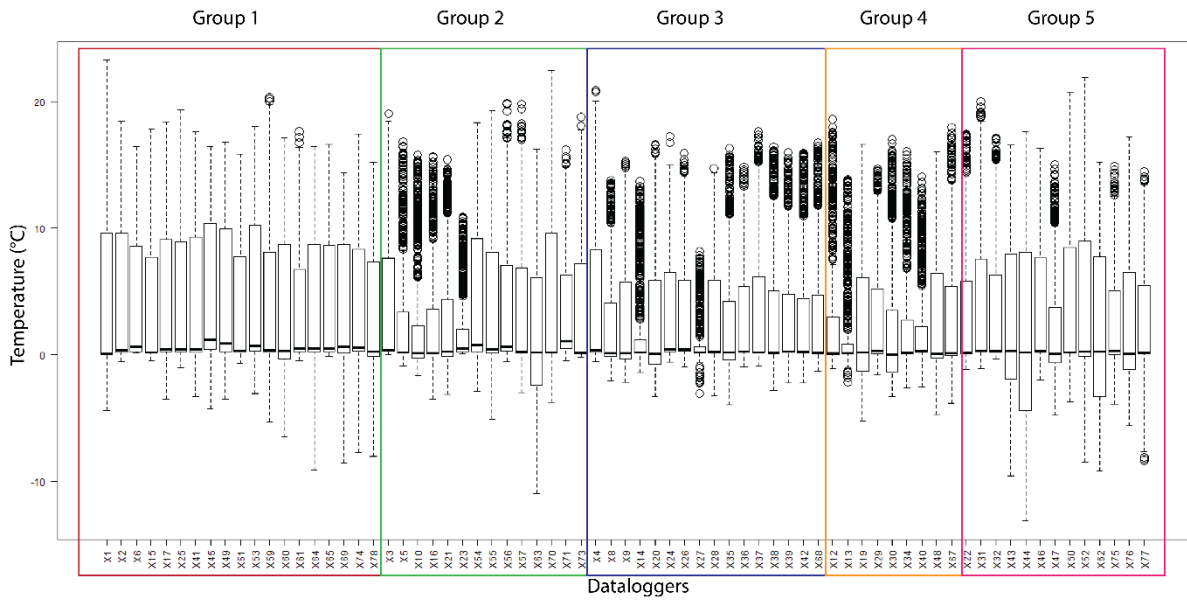
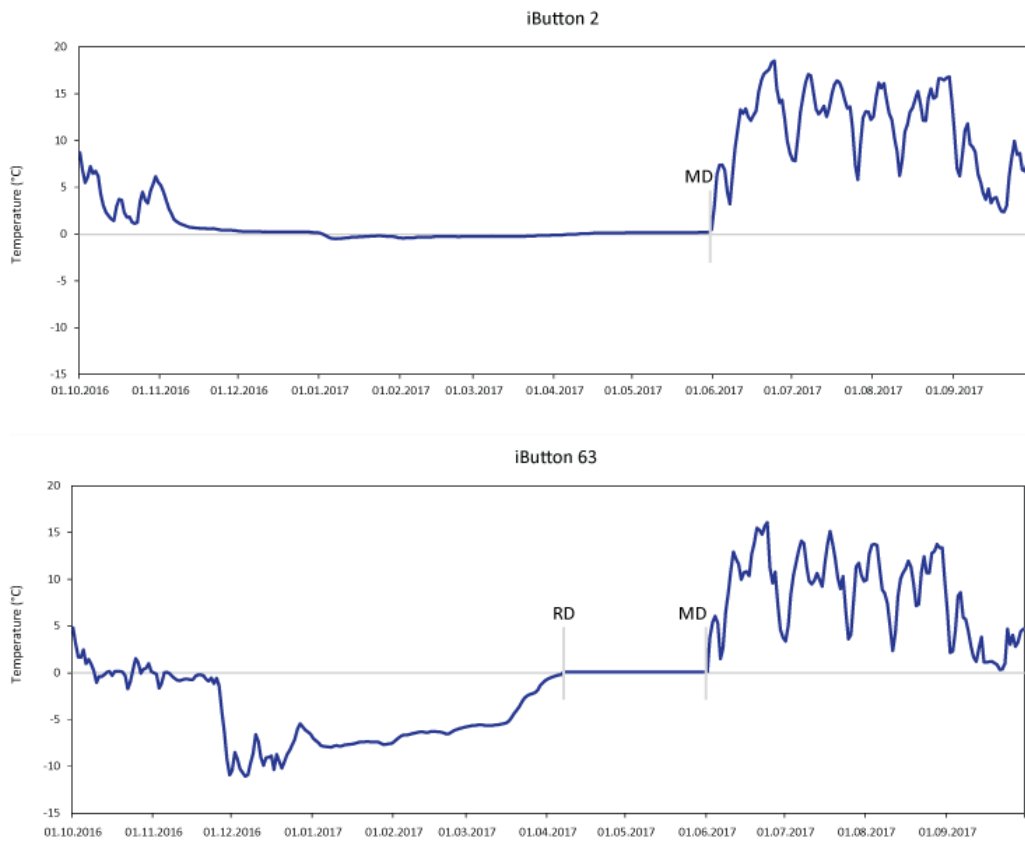


Figure 2.8 - Temperature distributions (period from 1<sup>st</sup> October 2016 to 30<sup>th</sup> September 2018) of iButtons, grouped according to plant composition. The box-plot delimit the 1<sup>st</sup> and the 3<sup>rd</sup> quartiles and the median (bold segment). The dotted line indicates the extremes and the small circle the outliers.

**Figure 2.9**



**Figure 2.9** - Examples of temperature evolution during one year. RD = basal-ripening data; MD = melt-out date. iButton n°2 is located at 2300 m a.s.l. in Les Martinets, in a debris area composed of ancient rock fall deposit and avalanche deposit. It does not have RD because of lack of ground freezing during the winter. iButton n°63 is situated in the upper part of the creeping talus slope in Col des Perris Blancs site, at 2426 m of elevation. In this case, both RD and MD were detected.



Figure 2.10

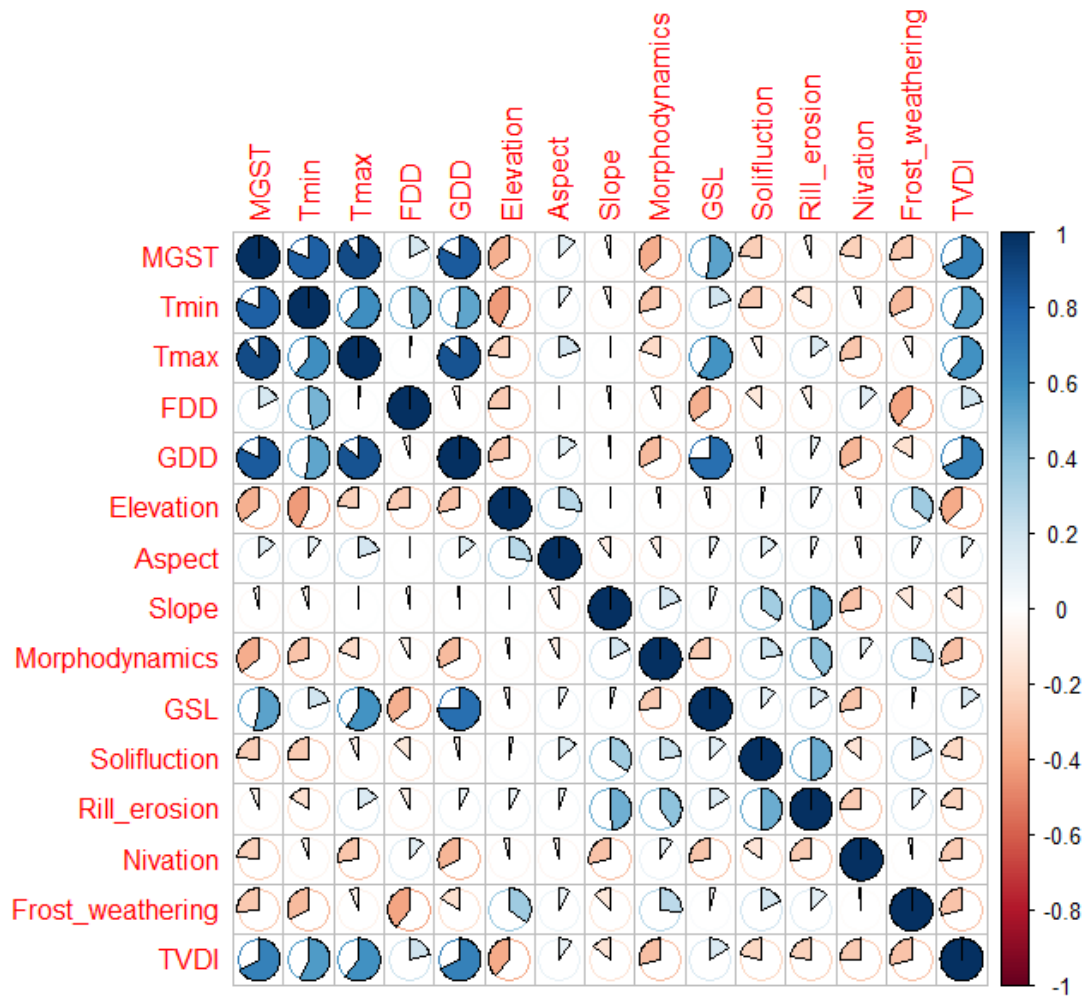


Figure 2.10 - Correlation matrix between explanatory variables based on Spearman's rank correlation coefficient. Spearman correlation coefficient was set to  $|r| > 0.7$  as criterion to limit collinearity between the variables. MGST = Mean Annual Ground Surface Temperature; Tmin = minimum temperature; Tmax = maximum temperature; FDD = Freezing Degree Day; GDD = Growing Degree Day; GSL = Growing season length; TVDI = Temperature Vegetation Dryness Index.

Figure 2.11

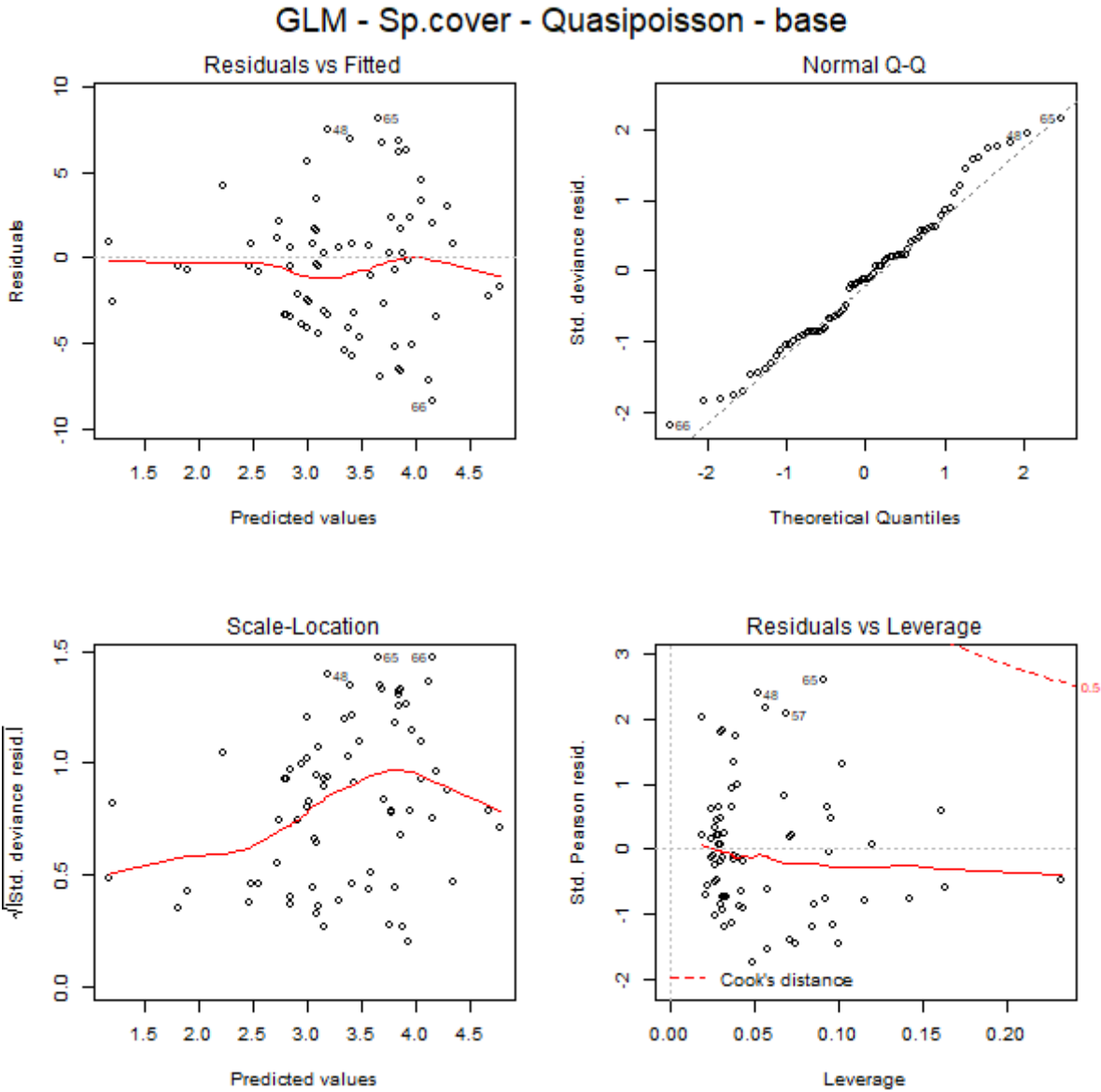


Figure 2.11 - Baseline GLM of species cover, with normal explanatory variables, family argument “Quasipoisson”. Residuals vs Fitted, Normal Q-Q, Scale-Location and Residuals vs Leverage plots are shown.

Figure 2.12

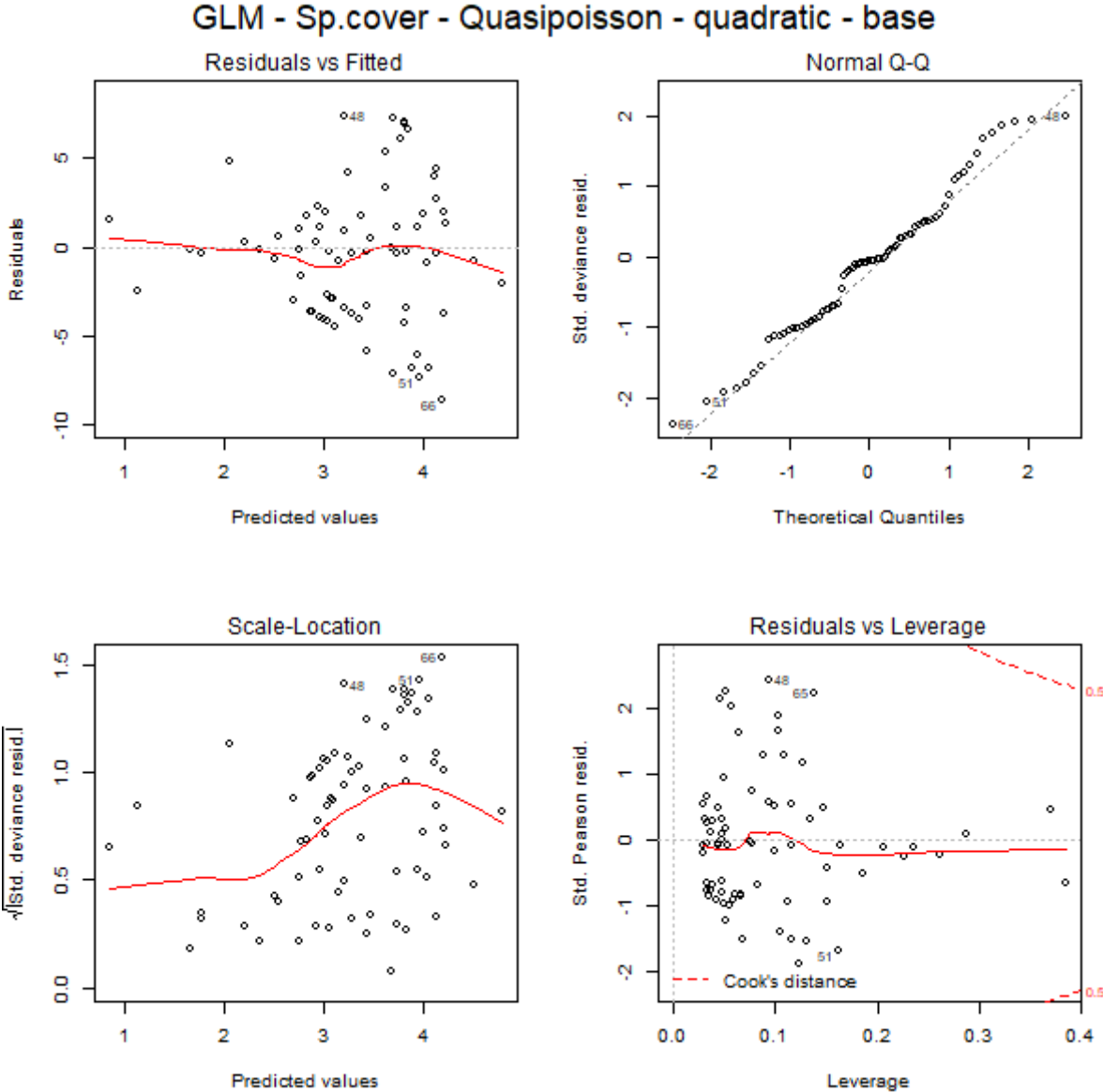


Figure 2.12 - Baseline GLM of species cover, with quadratic explanatory variables, family argument “Quasipoisson”. Residuals vs Fitted, Normal Q-Q, Scale-Location and Residuals vs Leverage plots are shown.

Figure 2.13

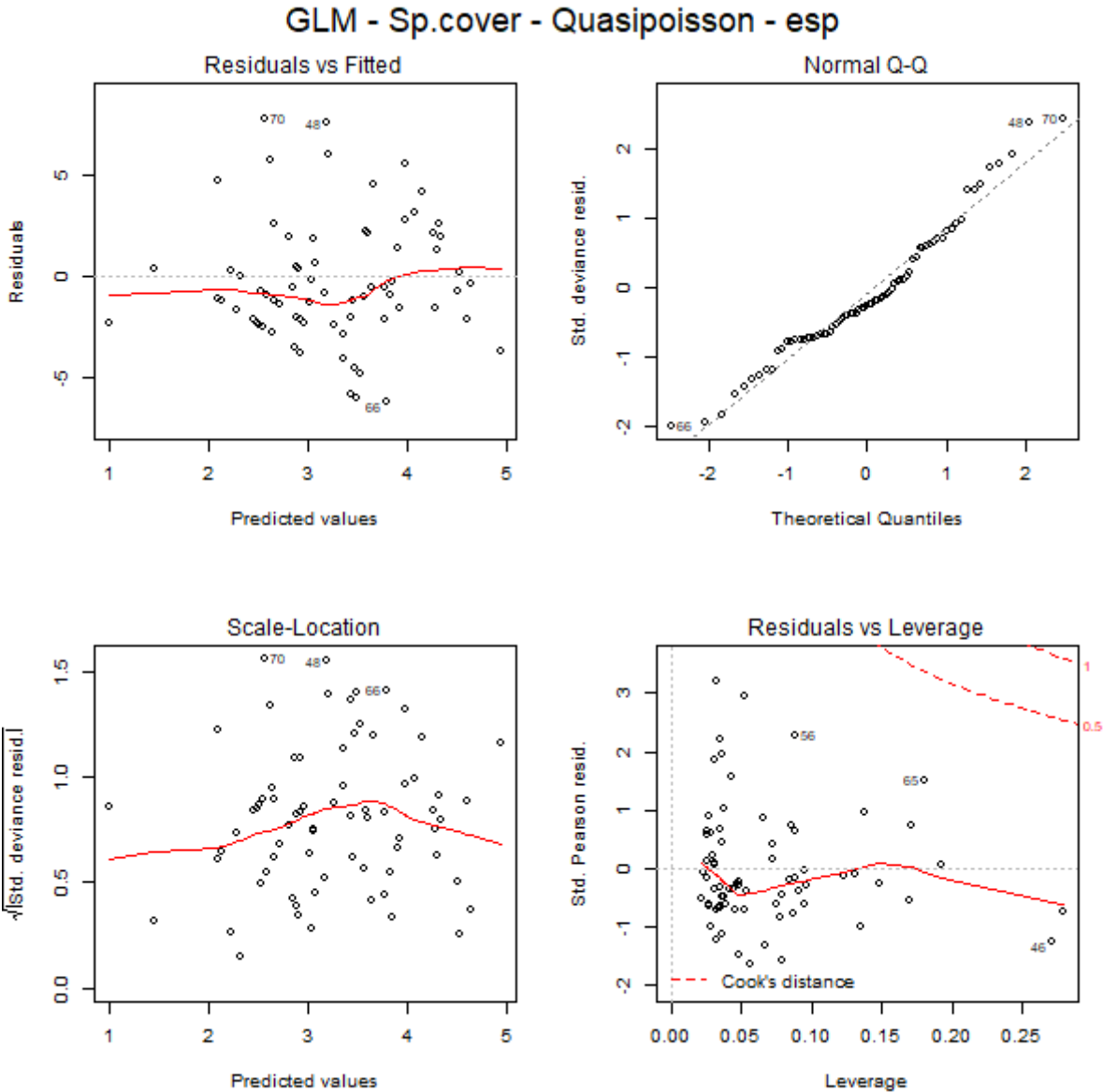


Figure 2.13 - Advanced GLM of species cover, with normal explanatory variables, family argument “Quasipoisson”. Residuals vs Fitted, Normal Q-Q, Scale-Location and Residuals vs Leverage plots are shown.

Figure 2.14

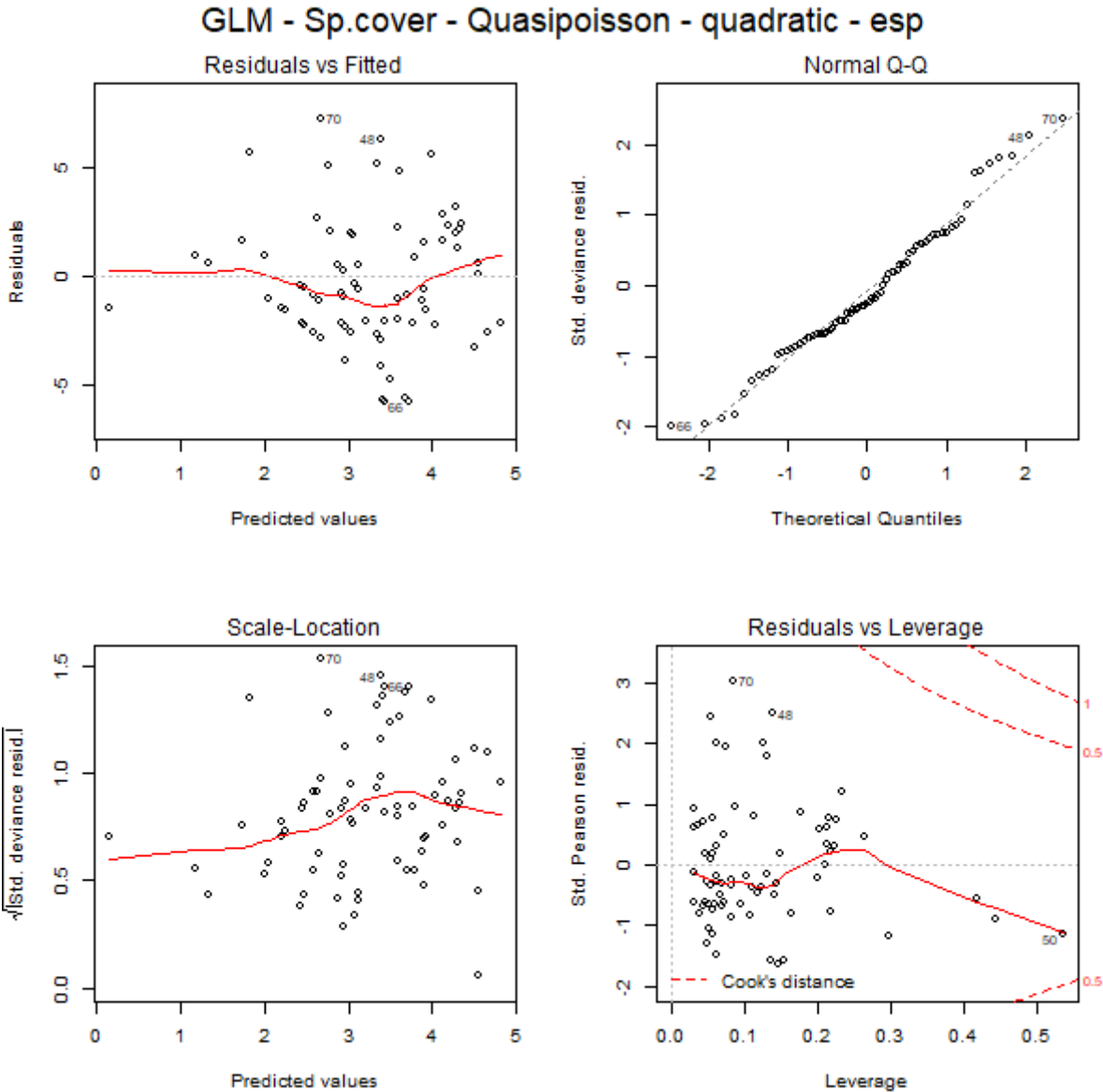
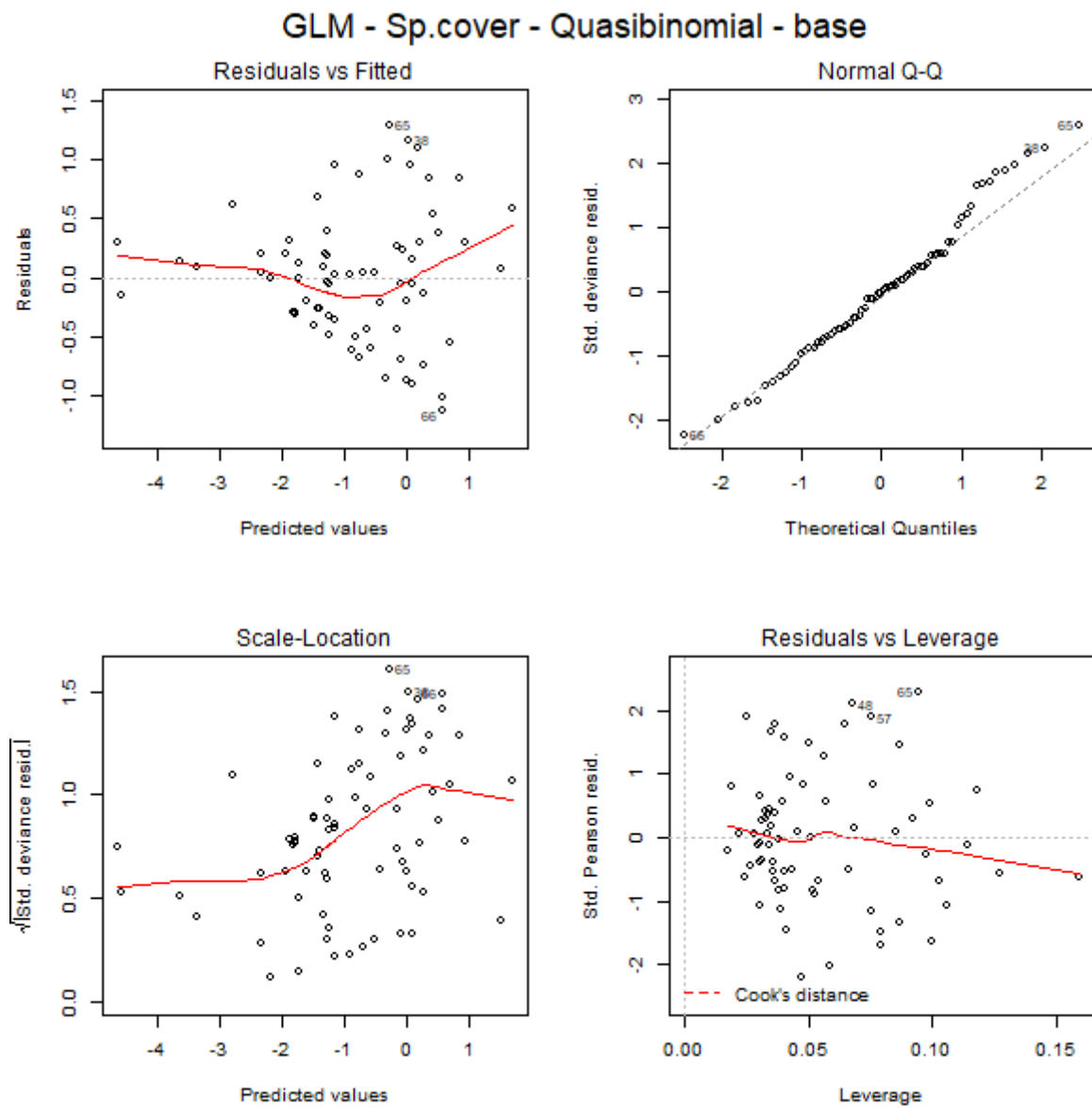


Figure 2.14 - Advanced GLM of species cover, with quadratic explanatory variables, family argument “Quasipoisson”. Residuals vs Fitted, Normal Q-Q, Scale-Location and Residuals vs Leverage plots are shown.

Figure 2.15



**Figure 2.15** - Baseline GLM of species cover, with normal explanatory variables, family argument “Quasibinomial”. Residuals vs Fitted, Normal Q-Q, Scale-Location and Residuals vs Leverage plots are shown.

Figure 2.16

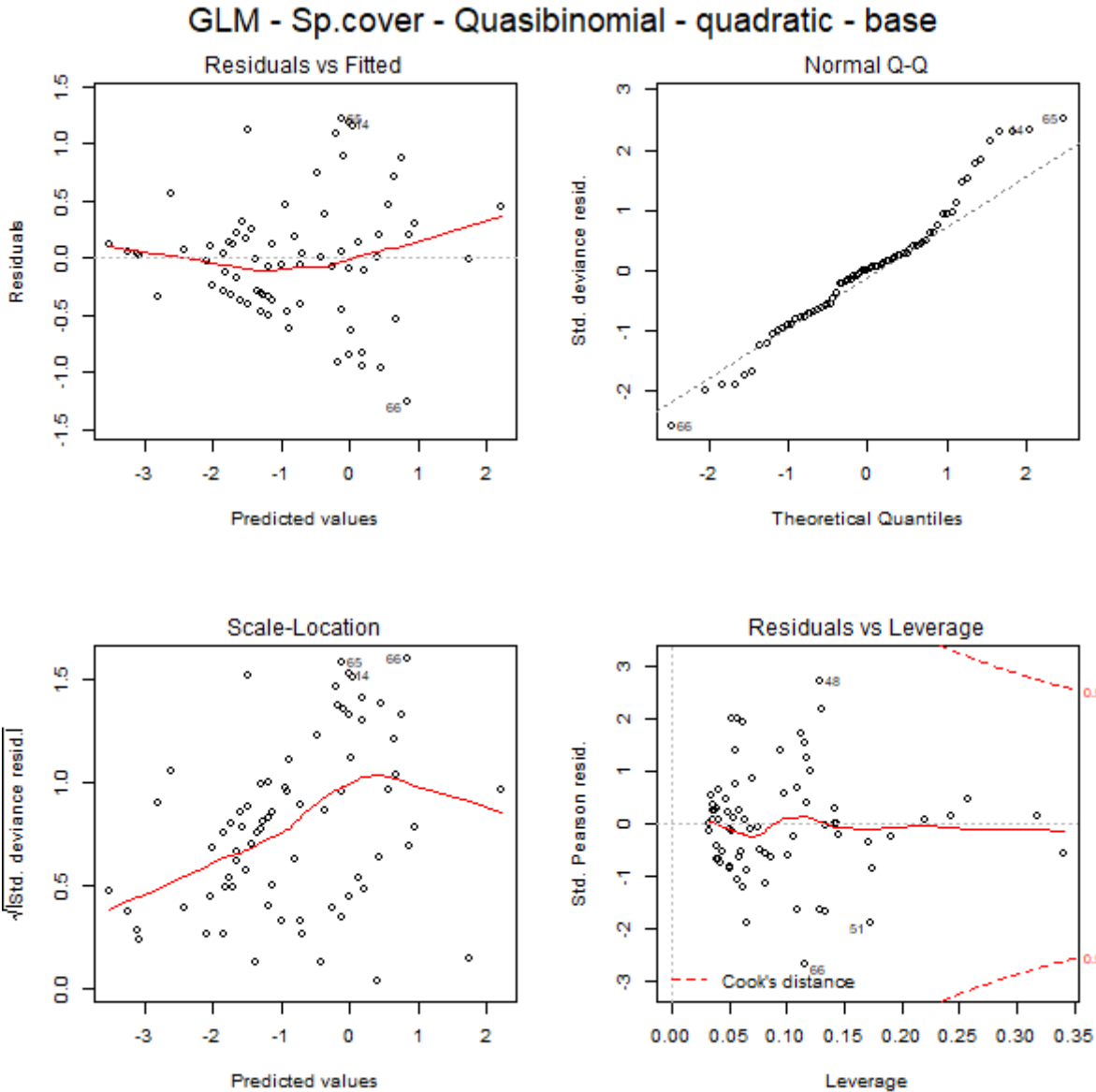


Figure 2.16 - Baseline GLM of species cover, with quadratic explanatory variables, family argument “Quasibinomial”. Residuals vs Fitted, Normal Q-Q, Scale-Location and Residuals vs Leverage plots are shown.

Figure 2.17

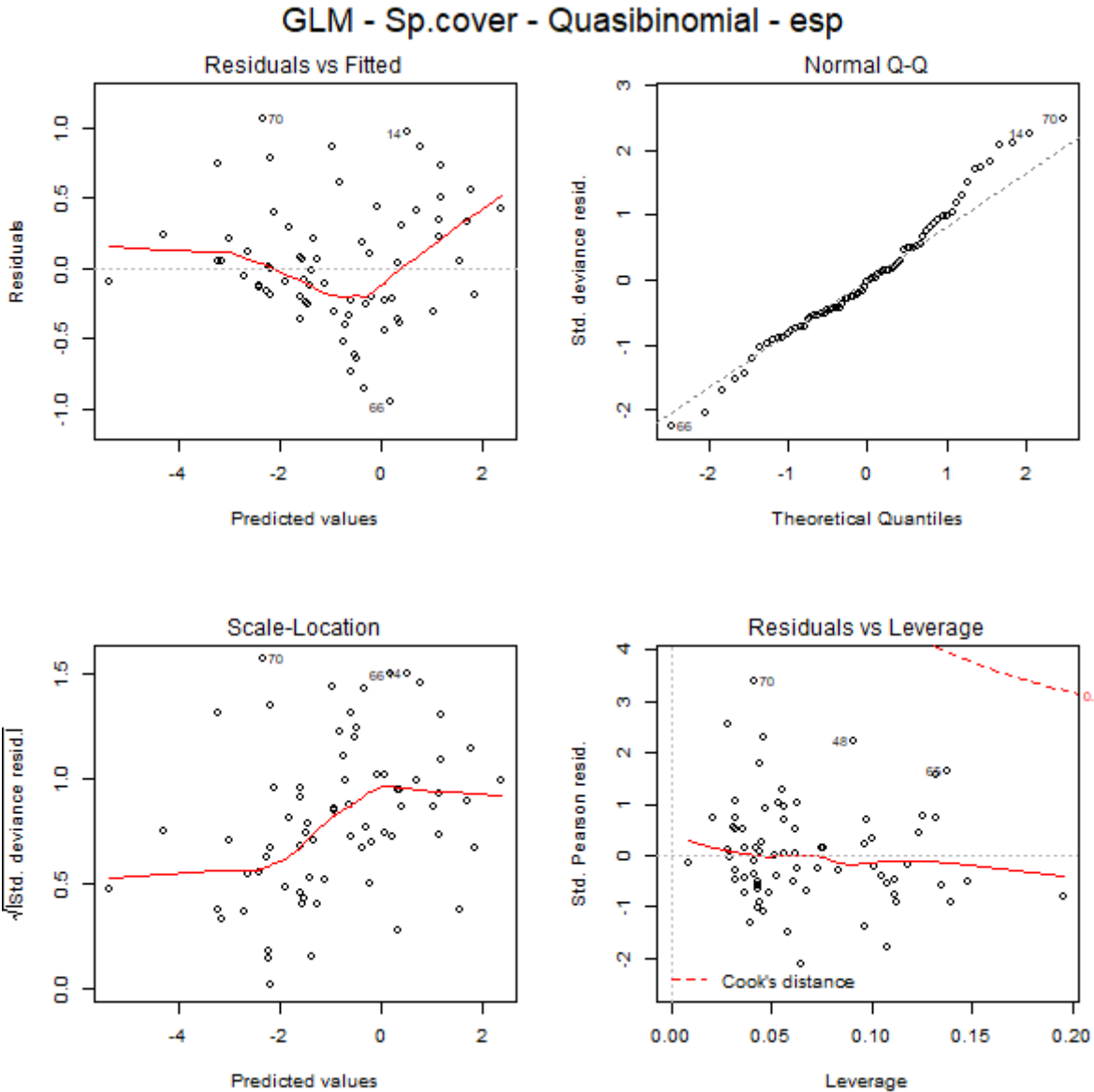


Figure 2.17 - Advanced GLM of species cover, with normal explanatory variables, family argument “Quasibinomial”. Residuals vs Fitted, Normal Q-Q, Scale-Location and Residuals vs Leverage plots are shown.



Figure 2.18

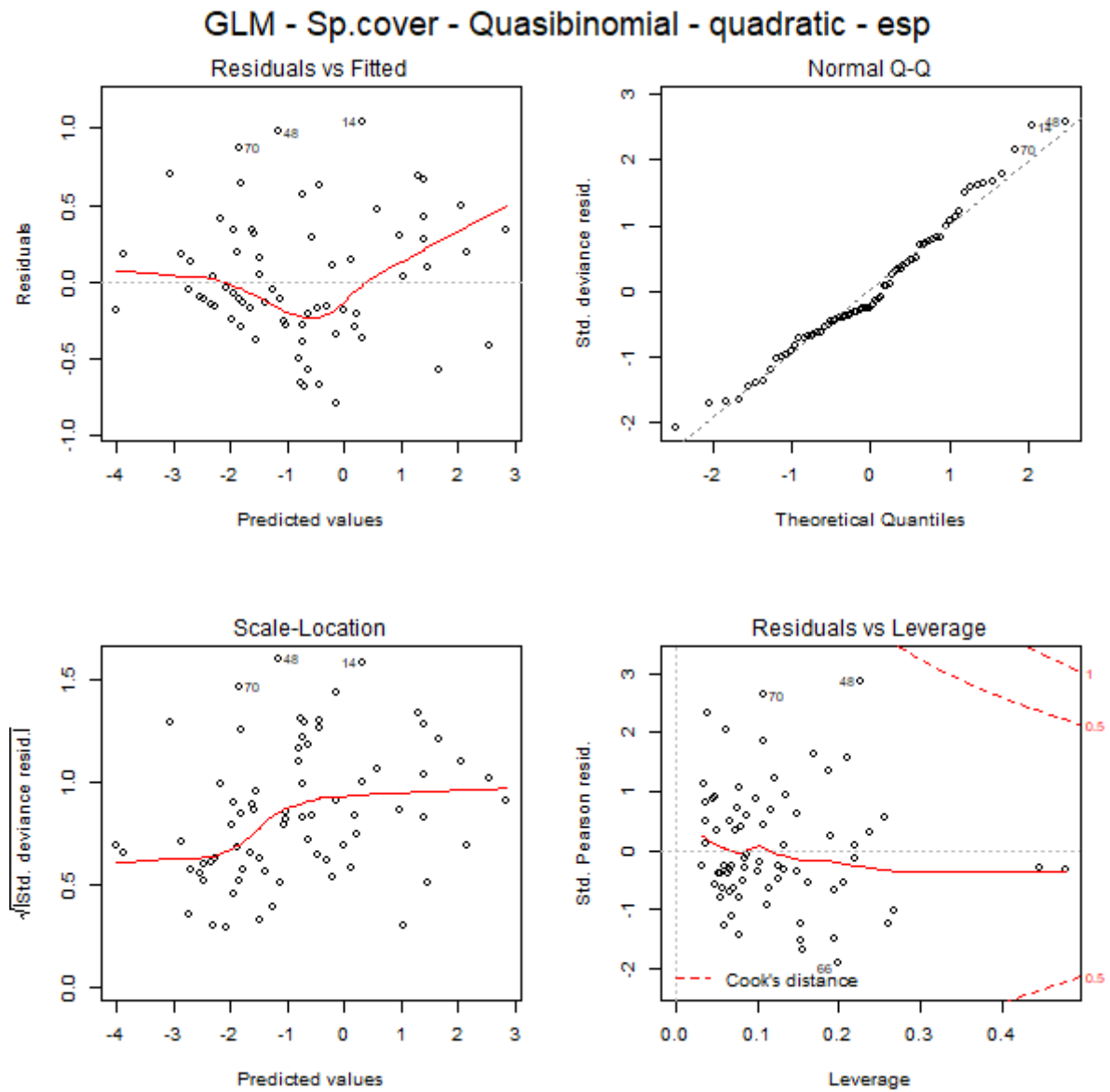


Figure 2.18 - Advanced GLM of species cover, with quadratic explanatory variables, family argument “Quasibinomial”. Residuals vs Fitted, Normal Q-Q, Scale-Location and Residuals vs Leverage plots are shown.

## CHAPTER 3

### 3. Large scale debris size mapping in alpine environment using UAVs imagery

Elisa Giaccone<sup>1</sup>, Christophe Lambiel<sup>1</sup>, Grégoire Mariéthoz<sup>1</sup>

*<sup>1</sup>University of Lausanne, Institute of Earth Surface Dynamics, Lausanne, Switzerland*

**Personal contribution.** I designed this research with my supervisors C. Lambiel and G. Mariéthoz. I made method implementation with the support of G. Mariéthoz, prepared figures and wrote the manuscript. Constructive comments and corrections of both co-authors increased considerably the paper quality.

## **Abstract**

The study of debris size in alpine environments can inform a range of processes such as ground thermal regimes or the mechanisms behind plant colonisation. Here we developed a new methodological approach based on optical high-resolution imagery on a large scale, such as acquired by Unmanned Aerial Vehicles (UAVs), to map the debris size distribution (DSD). The orthomosaics acquired by UAVs are processed with algorithms that were initially designed to analyse close-up images of fluvial gravel beds. Direct application of these methods to large scale imagery generates artefacts related to the presence of e.g. shadows, vegetation, or snow. For this reason, we propose here a processing workflow that addresses these issues and produces maps of DSD that are validated with strong correlation against individual debris measured manually. Our goal is to offer a methodology able to exploit UAVs image covering other landforms where debris are visible, such as talus slopes, rock glaciers or moraine deposits, as well as other environments like deserts or river beds.

## **Keywords**

Debris size classification; alpine environment; high-resolution images; Unmanned Aerial Vehicles; data processing.

### 3.1 Introduction

In alpine environments, debris size depends mainly on geology and on the geomorphological processes at the origin of the deposit (Ikeda and Matsuoka, 2006; Stoffel et al., 2013). The weathering of rocks and the transport of the sediments, thus obtained by gravity, water and ice action, influence the sediment size (Selby, 1982). Depending on surface material dimensions, the sediments can be successively remobilized during intense rain events causing debris flows and a further modifications on debris size (Berger et al., 2011; Gilli et al., 2013; Major et al., 2005). The debris size controls microtopography, heat exchange processes between air and surface and consequently ground temperatures (Rödder and Kneisel, 2012; Zhang, 2005). Several authors discussed the cooling effect of coarse blocks on ground temperatures (e.g. Delaloye and Lambiel, 2005; Gruber and Hoelzle, 2008; Harris and Pedersen, 1998). Indeed, high porosity and low thermal conductivity contribute significantly to differences in subsurface thermal regime between coarse blocs and fine-grained surface material (Otto et al., 2012). For instance, the chimney effect is a well-known process that overcools the ground in the lower part of porous talus slopes (Delaloye and Lambiel, 2005; Morard et al., 2008). Also the Balch effect (cold air tends to stay low due to high density) leads to ground cooling especially in slopes characterized by a seasonal circulation pattern (Harris and Pedersen, 1998; Wakonigg, 1996). As a result, the debris size indirectly controls the distribution and characteristics of mountain permafrost (Haeberli, 2000, 1975).

Debris size is also significant for the colonization of glacier forelands by plants and for the development of later successional stages on alpine slopes. Indeed, grain size controls soil-forming processes by sourcing parent material, formation of weathering products and accumulation of organic matter (Egli et al., 2006). It is well recognized that fine material enhances plant establishment, providing stable water supply due to high water retention capacity (Jochimsen, 1962; Nagl and Erschbamer, 2010). On the contrary, blocky material is colonized very slow (Ellenberg, 1996; Lüdi, 1958). Furthermore, the debris size acts directly on microtopography and consequently on fine-scale vegetation patterns (Eichel, 2019). Depressions with fine material can operate as safe sites for seedling germination and establishment, because physical conditions are more favorable than elsewhere (Cooper et al., 2004; Nagl and Erschbamer, 2010; Raffl et al., 2006), for example, due to higher moisture availability, slower surface water flow and lower wind velocities (Jumpponen et al., 1999).

Under the ongoing climate change (Beniston et al., 2018), it is important to understand how alpine ecosystem could evolve through field studies and models developed with the aim to adopt strategies focused on risk mitigation and prevention. To this end, studies about geomorphological factors (e.g. Colombo et al., 2016; Gentili et al., 2013; Giaccone et al., 2019), soil properties (e.g. Buri et al., in review; Matteodo et al., 2018), glacial retreat (e.g. Cannone et al., 2008; Moreau et al., 2008), sediment transport (e.g. Lane et al., 2017) are the base for a better knowledge of the alpine system. Successively, these data can be used to implement models and make regional predictions useful not only to the scientific communities but also to the policy makers (Guisan et al., 2013).

The present work is integrated in this context with the aim to provide a useful and innovative tool for the debris size analysis, which could be employed successively in predicting models for ground thermal regime, permafrost distribution assessment, or vegetation colonisation, or other application not connected to the mountain environment.

Generally, to estimate the debris size distribution in alpine environments, accurate punctual measurements of the two or three axis of debris typically have to be carried out (e.g. Ikeda and Matsuoka, 2006). However, on large surfaces, manual data acquisition is time-consuming. An efficient method is the analysis of high-resolution Digital Elevation Models (DEMs) from which information regarding surface roughness is extracted. According to Grohmann et al. (2011), in the context of geomorphometry, the surface roughness is the variability of a topographic surface at a given scale. The surface roughness can be quantified using area ratio method (Hobson, 1967), vector dispersion or orientation (McKean and Roering, 2004), standard deviation of elevation, slope and profile curvature (see Grohmann et al. 2011 for a detailed review), and standard deviation of residual topography (Cavalli et al., 2008; Cavalli and Marchi, 2008; Otto et al., 2012). The residual topography is obtained from the difference between the original and a smoothed DEM (Grohmann et al., 2011; Haneberg et al., 2005; Raseria et al., 2019). Another solution for retrieving grain size over large areas is terrestrial or airborne laser scanning, however the associated cost often makes it inaccessible for large-scale environmental studies (Blasone et al., 2014; Imaizumi et al., 2016; Schürch et al., 2011).

The aim of this study is to develop a new and easily applicable methodology to determine the debris size distribution (DSD) in alpine environments. The novelty resides in the use of optical high-resolution images, such as those acquired by Unmanned Aerial Vehicles (UAVs), associated with algorithms created for the identification of the grain size. Nowadays UAVs are easily available at reasonable costs and they are successfully used for many purposes, such as civil engineering (e.g. Uyanik and Wesley, 2019), landslide monitoring (e.g. Bilaşco et al., 2019; Cignetti et al., 2019), rock glacier studies (Dall’Asta et al., 2017; Vivero and Lambiel, 2019) or glacier evolution (e.g. Benoit et al., 2019; Fugazza et al., 2018; Jouvét et al., 2017). Our approach produces maps identifying areas with boulder, cobble or finer debris, and it could be employed in a range of geomorphological applications. It is demonstrated using two different UAVs technologies in two sites located in the Western Swiss Alps, but it can be employed with other UAV platforms. The methodology is composed of 4 steps: 1) image acquisition using UAV technology and processing to produce a high-resolution orthomosaic; 2) debris size detection using the Basegrain algorithm (Detert and Weitbrecht, 2012; Detert and Weitbrecht, 2013); 3) data validation and calibration; 4) debris size classification and map production. In the remainder of this paper, section 3.2 describes the method, the section 3.3 presents practical applications and discusses the results, and section 3.4 presents conclusions.

## 3.2 Methods

The methodology proposed here is composed of four main phases, which are summarized in Figure 3.1. The first one is the study area selection and data acquisition. The second consists in grain size detection through an existing algorithm that allows having a detailed list of all detected grains. This list is used in the third phase for the validation and potentially for the calibration. Finally, the fourth phase creates a density map and subsequent debris size map. Details are explained in the subsections below.

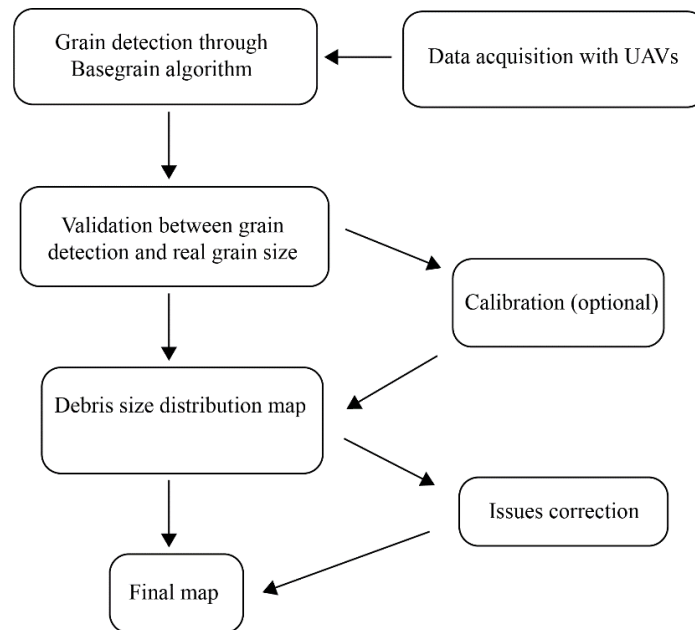


**Figure 3.1** - Flowchart showing the developed methodology. UAVs: Unmanned Aerial Vehicles.

### 3.2.1 Study area and data acquisition

The methodology is tested and validated on two sites in the Western Swiss Alps (Figure 3.2): Les Martinets and Les Outans areas. Both sites are located in or near the Vallon de Nant, a small valley surrounded by high rock walls and with an elevation comprised between 1950 and 2700 m a.s.l.

Les Martinets site has a high importance from a geomorphological point of view because of the high diversity of landforms, characterized by different origin, age, debris size and vegetation cover. It is notable by the nearby presence of the Martinets glacier (ca. 2200-2700 m a.s.l.) and its numerous moraines dating back to the Little Ice Age (LIA) and to older Holocene or Late Glacial stages. On the western side of the moraines, a rock glacier, made of two different lobes, is located (ca. 2240-2560 m a.s.l.). On the north-west side, a large area of rock avalanche/rock fall deposits and a talus slope crossed by several debris flow channels are present. This site was chosen due to its heterogeneity that is suited to test our methodology. The region is constituted primarily by limestone and some siliceous rocks deposited between the Middle Jurassic and the Eocene (Badoux, 1991).

Les Outans site is characterized by steep slopes exposed to the north, with elevation ranging between ca. 1950 and 2300 m a.s.l. The main landforms are an unnamed small debris-covered glacier, which erected large moraines in the western part (ca. 2100-2300 m a.s.l.), and an extended debris slope made of torrential and gravitative deposits in the eastern part. Here the geology is constituted by limestone of the same age as the first site.

The images on Les Martinets are acquired using an eBee RTK, UAV made by Sensefly (Lausanne, Switzerland - Vallet et al., 2011) through a flight on 2016/10/04. The imagery at Les Outans is acquired on 2016/09/28 using a DJI Phantom 3 professional UAV. After acquisition, the images are processed through mosaicking in the Pix4D Mapper software to produce high-resolution orthomosaics and Digital Surface Models (DSMs).



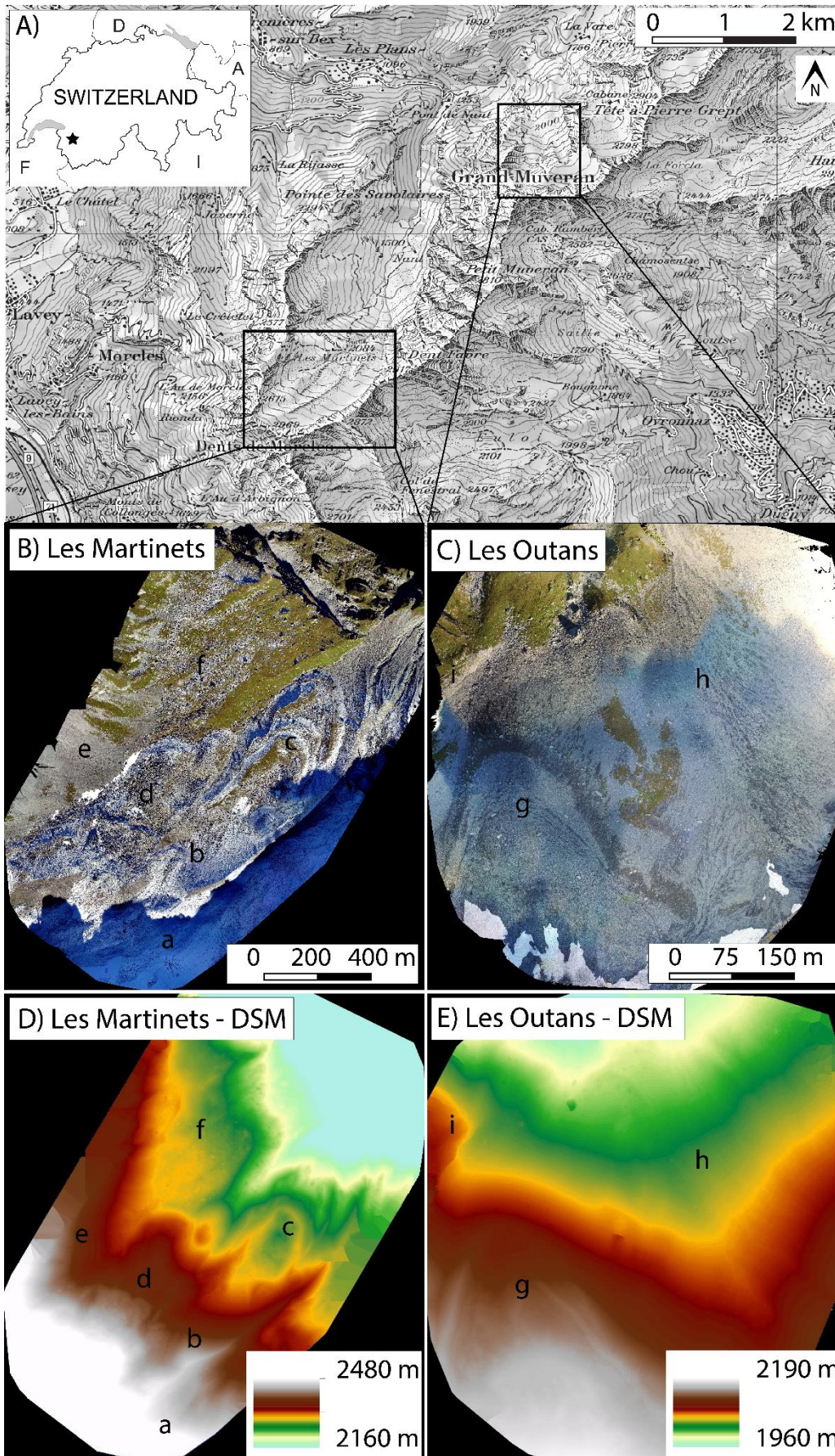


**Figure 3.2 -**  
 A) Location of the study area. B) Orthomosaic of Les Martinets (eBee RTK UAV, October 2016); a: Les Martinets glacier; b: LIA moraine; c: Holocene moraines; d: rock glacier; e: talus slope; f: rock falls / avalanche deposits. C) Orthomosaic of les Outans (Phantom 3 professional UAV, September 2016); g: debris-covered glacier; h: debris slope; i: bedrock outcrop. D) Digital Surface Model of Les Martinets. E) Digital Surface Model of Les Outans.

On Les Martinets area, the eBee RTK acquired 384 RGB pictures covering an area of 1.6 km<sup>2</sup> and the Pix4D Mapper processing produced orthomosaic and DSM of 5.75 cm/pixel of resolution. For Les Outans site, the Phantom 3 shot 998 RGB pictures covering an area of 0.2 km<sup>2</sup>. The orthomosaic and the DSM have a resolution of 3 cm/pixel.

### 3.2.2 Grain detection

In the last decade, several automatic approaches were developed to analyse the debris size. Carbonneau et al. (2004), Heritage and Milan (2009) and Buscombe et al. (2010) focused on achieving one single characteristic grain size parameter. Weichert et al. (2004), Graham et al. (2005b, 2005a) and Strom et al. (2010) used image processing techniques to measure each grain area and its related properties through digital top-view photographs. In 2005, Graham and co-workers created the Digital Gravelometer software to measure gravel sediments but the software was not updated later. In more recent years, Detert & Weitbrecht (2012, 2013) elaborated new approaches based on algorithm combination of mathematical morphology (Serra and Soille, 1994) that allowed the development of the Basegrain software, a MATLAB-based automatic tool.

To meet the proposed aim of the present study, we decided to work with the methodology presented by Detert & Weitbrecht (2012, 2013) as it is implemented in the Basegrain software (v. 2.2.0.4). Basegrain was originally designed to estimate the granulometry of fluvial non-cohesive gravel beds from digital top-view photographs, with photographs taken perpendicularly to the bed and in cloudy weather cast to minimize shadows. UAV-based imagery does not correspond to these characteristics, and this paper explores how to address the associated challenges.

The Basegrain algorithm identifies individual grains based on a grayscale gridded image. It proceeds in five steps:

1. Interstices between grains are detected using Otsu's thresholding (Otsu, 1979), which minimizes the intra-class variance.
2. A morphological bottom-hat filtering is performed to determine further interstices on the grayscale image. The confirmed interstices are then smoothed by applying a morphological closing.
3. The Canny and the Sobel methods are applied to detect edges. The Canny method allows edge identification by applying a Gaussian filter to the grayscale image and finding local maxima of the filter derivative. The Sobel method uses the Sobel approximation applied to the derivative of the grayscale image to find edges.
4. The watershed algorithm (Beucher, 1979) is used to separate single grain areas.
5. Each identified grain is represented as an ellipse and its properties are defined (major and minor axes, area, center coordinates and grain orientation). The final output consists in a list of all the detected grains and their properties.

The innovative aspect of our work is that we use the Basegrain approach to analyse drone images covering wide surfaces in an alpine environment, with high geomorphological diversity and without optimal conditions (i.e. not corresponding to the recommended setting for top-view photographs of gravel beds). Because the input to the above algorithm is a grayscale image, among the three



bands composing the orthomosaic derived from drone acquisition, we choose the blue band, which presents the best visibility. The parts of the orthomosaic presenting blurry areas, for example at the margins, are discarded. The remaining part of the orthomosaic is split into overlapping tiles that are processed separately to reduce the computational burden associated to very large images. Each tile results in a list of detected grains, then all lists are merged to form a single list of all grains in the area of interest.

### **3.2.3 Validation and calibration**

For the validation of our methodology, a sample of 200 individual debris of different sizes covering all the size distribution is selected in a random stratified way after the grain detection on Basegrain and their area is measured in the orthomosaics using the measuring tools in the ArcGIS software. This step is repeated for each site because of the different resolution and acquisition platforms. The match between manually measured and automatically detected grain sizes is assessed qualitatively through scatter-plots and quantitatively by using the Spearman's rank correlation coefficient. If the estimated and measured grain sizes do not correspond, a calibration phase is carried out, correcting the data issue from Basegrain algorithm according to the regression line before continuing to computing the DSD map.

### **3.2.4 Debris size distribution map**

The Basegrain processing results in a list with the position and area of each grain. This list can consist in a very large number of detected objects, and is not necessarily appropriate for producing a DSD map. Here we convert this list of objects into an object density map. This is accomplished by first defining a regular grid, encompassing the area of interest. Each image tile is assembled to reconstruct a mosaic of the same dimensions of the original orthomosaic. One pixel of the tile has the same resolution than in the orthomosaic. Then for each grid cell we compute the median grain area within a radius of  $R$  pixels, as well as the standard deviation of the grain area within the same radius  $R$ . The median grain size is computed on a coarser grid than the original orthophoto. We define  $C$  as the coarsening factor, meaning that the median grain size is calculated on a grid where size of pixels is  $C$  times larger in each direction than the pixels of the orthophoto. Adjusting  $C$  can be useful to reduce the computational cost of the operation by computing the DSD on a coarser grid. The radius  $R$  controls the number of debris that will be accounted for when computing the median and standard deviation. Larger  $R$  values result in DSD maps that are more statistically representative because each pixel is based on a large number of grains, but at the same time more smooth.

In our tests, we set values of  $R = 30$  pixels and  $C = 30$  pixels. These values can be adapted depending on the resolution of the initial orthoimage. The resulting DSD is transformed in meters to obtain a resolution of 1 m/pixel.

### 3.2.5 Innovative aspects

Using UAVs images instead of top view photographs on Basegrain, the interstice and edge detection in some areas does not correspond to the reality because of the ground complexity, the presence of shadows, snow patches, and grassland and, in some cases, blurry parts of the image. It is the case for example of some large blocks, which are segmented in many small boulders, or areas with particular small debris, which are recognized as large dimension blocks. In the same way, snow patches and vegetation cover can be considered as debris. These issues are solved applying masks on the final DSD map.

The areas composed of small debris not individually detectable, which are identified as large debris after the Basegrain estimation, are corrected through roughness index defining the surface irregularity. The roughness index is calculated for both focus sites starting from the DSM, obtained by the Pix4D mapper processing with the same resolution as the orthomosaics. We use the roughness index implementation present in the TopoToolbox (Schwanghart and Kuhn, 2010; Schwanghart and Scherler, 2014), which is calculated as the largest inter-cell difference of a central pixel and its surrounding cells. To identify the areas with low surface irregularity, we define a threshold of  $< 0.025$  and  $< 0.012$  respectively for Les Martinets and Les Outans, and apply the mask at the end of the DSD map computing.

The masks used to cover vegetated areas are performed based on the observed normalized difference vegetation index (NDVI). NDVI is calculated using the red and infrared bands of the false-color infrared orthophoto mosaic obtained from the Swiss Office of Topography for the year 2013 at a resolution of 25 cm. For our region, we selected a threshold  $> 0.25$  for Les Martinets and  $> 0.16$  for Les Outans to accentuate grassland, since forests are not present.

Regarding the snow patches, we used the raster calculator ArcGIS tool to extract from the blue band image pixels with value  $> 220$ . A Focal Statistic filter based on a circle with a radius of 5 pixels is applied subsequently to smooth and homogenize snow pixels, and to remove the isolated pixels. Finally, to cover the Martinets glacier, we applied directly a mask contouring the glacier extension in the final output.

## 3.3 Results and discussion

### 3.3.1 Validation test and calibration

The validation scatter plots (Figure 3.3) show a strong correlation between the manually measured and automatically estimated grain sizes with Basegrain algorithm. In Les Martinets area, in case of small debris ( $< 5 \text{ m}^2$ ), the point dispersion around the curve is minimum. It augments with large boulders because they are segmented in smaller blocks. Spearman's rank correlation is 0.9, *p-value*  $< 0.001$  (Figure 3.3, left side). In Les Outans site, the validation curve is similar to that of Les

Martinets, with solid correlation for debris  $< 3.5 \text{ m}^2$ , but the Spearman's rank correlation is higher (0.96,  $p$ -value  $< 0.001$ ) (Figure 3.3, right side).

Because the slope of the regression line is not equal to 1 between the two axes, especially for large debris, we decided to calibrate data above a correction minimal threshold. This threshold is evaluated qualitatively and quantitatively using the line equations of the two focus sites and it is  $>$  of  $5 \text{ m}^2$  for Les Martinets and  $> 3.5 \text{ m}^2$  for Les Outans. Thereafter, we proceed to compute the DSD map.

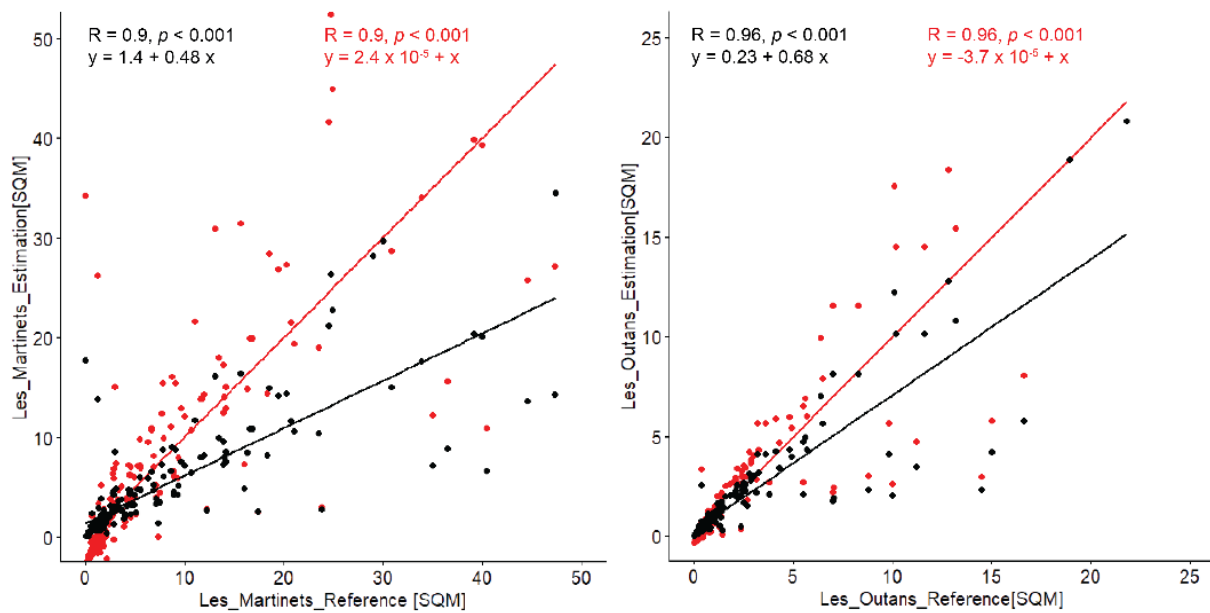


**Figure 3.3** – Validation and calibration curves for Les Martinets (left side) and Les Outans (right side) images. The y-axis represents the ellipse size estimated in Basegrain (square meters SQM), the x-axis the real size (square meters SQM) of debris measured manually in ArcGIS. The equation of the curves is shown in the top part in black and it was employed to calibrate data before proceeding with the computing of the median area.  $R$  = Spearman's rank correlation;  $p$  =  $p$ -value. In red, the equation after the calibration. The 200 black dots are the grain size values before calibration, the 200 red dots the values after calibration.

### 3.3.2 Debris size map results

In terms of computing time, each tile is analysed in about 7 minutes by the Basegrain algorithm on a laptop computer and using a non-optimized Matlab code. Computing the tile assemblage and the following DSD map computation take up to 1hr. The DSD maps with median and standard deviation values, compared with the original orthoimages for both study areas, are shown in Figure 3.4. The main geomorphological features are highlighted by changes on granulometry and the heterogeneity on debris size is marked by high values of standard deviation.

Regarding the focus sites where the methodology is applied, the technical data about number and size of tiles obtained from the division of the blue band of the orthomosaic, overlapping of tiles,

minimum and maximum detected grain size, after Basegrain estimation, and final surface of the images are exposed in Table 3.1.

**Table 3.1** - Technical data about tiles characteristics, overlapping, minimum and maximum debris size and final area investigated for both focus sites.

Technical data	Les Martinets	Les Outans
Tile (n°)	30 (5 horizontal, 6 vertical)	4 (2 horizontal, 2 vertical)
Tile (pixel)	5000 x 5000	5000 x 5000
Overlapping (pixel)	300	300
Min grain size (m <sup>2</sup> )	0.10	0.10
Max grain size (m <sup>2</sup> )	143	46
Surface (m)	1325 x 1553	289 x 289

Globally, the Basegrain algorithm can recognize most cobbles and boulders. The mobile median points out large blocks and the mobile standard deviation highlights where high variability is present. The areas characterized by large boulders are preserved with still high area values despite Basegrain having segmented some large blocks. This can be observed in Figure 3.5, where a comparison between Basegrain computation, median and standard deviation values is carried out.

Despite the accuracy shown in the Figure 3.4 and 3.5, the interstice and edge detection in some areas does not correspond to the reality because of ground heterogeneities and limited image resolution. In some cases it could not avoid errors caused by shadows, covering debris deposits (yellow circles in Figure 3.6a, b). Only in few conditions, the shadows did not prevent the grain identification. In case of some large boulders, Basegrain segments the large blocks in many small boulders, probably due to the presence of discontinuities, cracks and irregularities in the block surface (red circles in Figure 3.6a, b). In areas where the image has blurry portions and where the observation of debris is difficult also for human eyes due to small dimensions (<10 cm), Basegrain algorithm recognizes debris of larger dimensions instead of the real small ones (orange circle in Figure 3.6c, d).

Where snowfields are consistent and present white color without interference, the algorithm does not identify any edge or interstices, leaving these portions debris-free (blue area in Figure 3.6c). Conversely, in case of snowfields presenting a patterned surface, some debris are identified (red circle in Figure 3.6c, d). The problems on the debris identification appears especially in the grassland. Since the ground presents irregularities due to both microtopography and plant presence, at the end of the processing, debris can be wrongly identified (e.g. red circle in Figure 3.6e, f). This is the reason why we applied masks to cover small debris areas, snowfields and grasslands in the final DSD maps, as shown in Figure 3.7.

For Les Martinets site, it is possible to recognize the geomorphology from the DSD map (Figure 3.4). From the top to the bottom of the Figure, we can observe between the large grassland patches the area of rock falls / avalanche deposits, where large blocks (> 5 m<sup>2</sup>) are present. On the left side of the central part, the talus slope is composed by fine debris (< 1 m<sup>2</sup>), while large debris are concentrated at its foot next to the snow patches (in white). In the center, the rock glacier is easily recognizable thanks to its shape: the frontal part is characterized by small debris (< 1 m<sup>2</sup>), whereas on the top the biggest blocks (up to 20 m<sup>2</sup>) are visible. Generally, indeed, the rock glaciers are characterized by coarse rock fragments on their surfaces and finer sediments at their frontal and

lateral sides (Barsch, 1996). Instead, talus slopes are composed of sorted sediments due to gravity, finer materials in upper zones and coarser sediments at their foot. Moraine deposits are not-sorted sediments constituted by matrix and rock fragments.

Based on the obtained data we observe that the rock glacier is constituted both by boulders and cobbles. The granulometry is larger on the rock glacier surface (average value  $0.7 \text{ m}^2$ , maximum value  $37 \text{ m}^2$ ), as highlighted by the elevated median and standard deviation values in Figure 3.5, and lower in the frontal and lateral parts (average value  $0.34 \text{ m}^2$ , maximum value  $10.3 \text{ m}^2$ ). To the right, the partially vegetated moraines dating back to the LIA or to older Holocene periods are marked by finer granulometry excepted in the internal part, where large blocks (up to  $30 \text{ m}^2$ ) are identifiable. In the bottom part of the Figure, the morphology is more difficult to identify but globally the granulometry is smaller, except for some large blocks present on the surface. This area is constituted by LIA moraine deposits. On the extreme bottom and right part of the Figure, we applied the white mask to cover the areas occupied by the Martinets glacier (see Figure 3.7). Instead in some areas the algorithms do not manage to identify the debris size correctly. It is the case, for example, of the upper part of the image, where an extended area is classified as large blocks but it is constituted by grasslands. Or of the lower part of the image, where the glacier is located.

For Les Outans site, the main visible morphology is the debris-covered glacier characterized by fine debris ( $< 0.5 \text{ m}^2$ ) in the frontal part and on the top of its moraine and large blocks (up to  $9 \text{ m}^2$ ) in the central part and on the lateral moraine. In the top part of the Figure, a bedrock outcrop is visible between the debris-covered glacier and the grassland, characterized by large debris sizes. On the right side, the extended debris slope is composed of diverse small debris and sparse large blocks ( $2\text{-}4 \text{ m}^2$ ). Also in this case, some areas are identified with the wrong debris size, for example the top-left part of the image where grassland is identified as large blocks.

### 3.3.3 Limitations

The presented methodology produces a more detailed representation of the DSD than previous techniques based on covariates such as surface roughness (e.g. Grohmann et al., 2011). However, we can also identify some limitations. The images have to be clean and must contain low percentage of shadow, so that the interstices and the edge detection steps can be performed optimally in all the image extension. To this end, it is preferable to carry out the drone flights around noon to minimize shadow presence or under cloud-covered sky.

The dimensions of the overlapping images before the Basegrain estimation have to be adapted case by case based on the orthomosaic size and its resolution, as well the radius and the coarsening, in order to obtain the best results emphasizing the debris size differences. We suggest to keep the overlap between 5 and 10% of the tile pixels and radius and coarsening comprised both between 0.5 and 0.10% of the tile pixels to obtain a correct smoothness degree without loosening of data. Equally, the validation and the calibration phases have to be adapted at each case study, evaluating qualitatively and quantitatively the degree of correlation before validation.

The Basegrain algorithm itself shows some critical points because it cannot identify correctly all the debris size in the UAV tiles, but, how explained before, this is due to limited image resolution and ground heterogeneities in some portions of the images. This is the case especially of vegetation

covered areas, snowfields, debris of small dimensions. However, applying masks help us to increase the precision of our methodology.

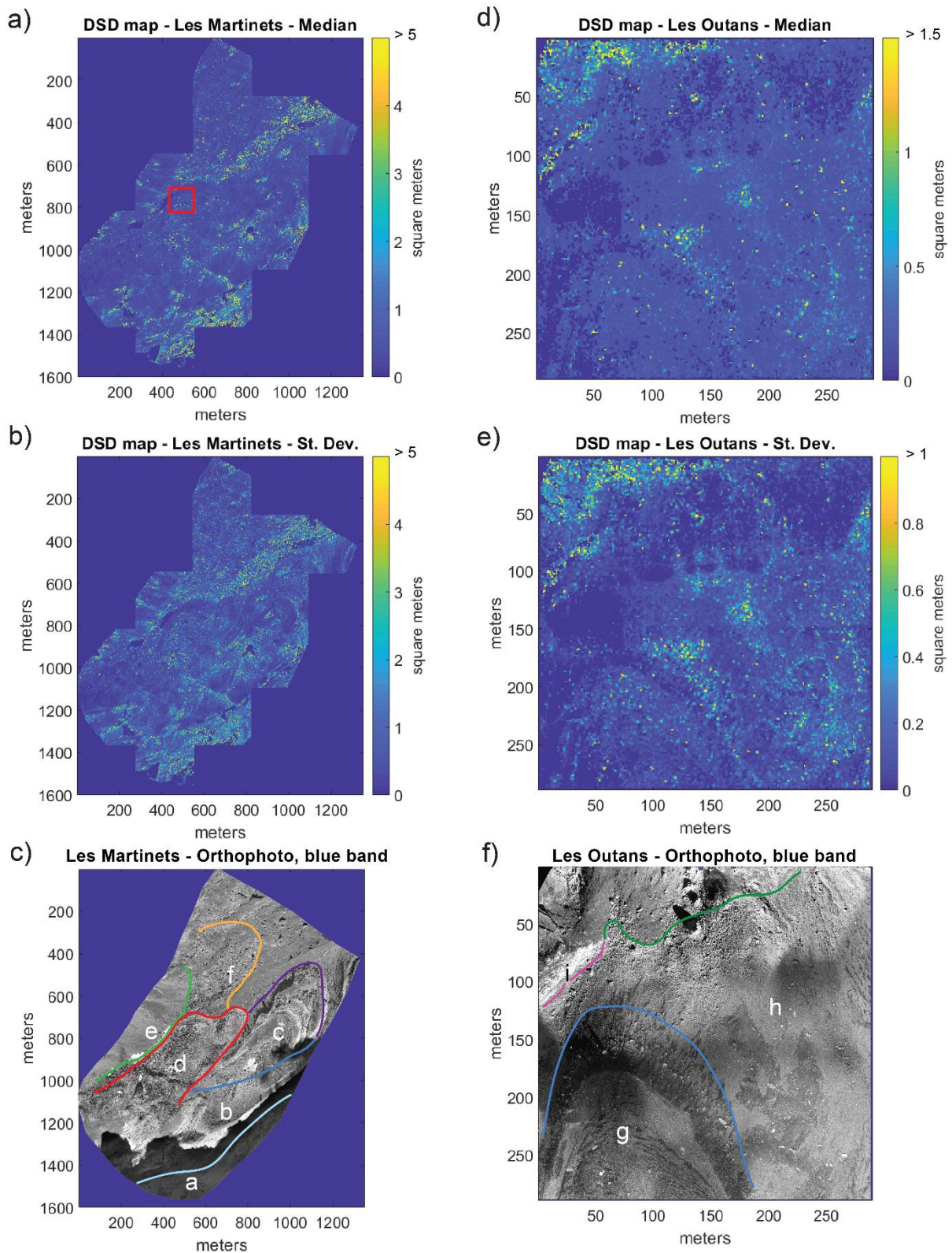


**Figure 3.4** - DSD map with median values (a and d on the top), standard deviation values (b and e in the middle) and the original orthophoto with the main landforms delimited by colored contours (c and f on



the bottom) for Les Martinets and Les Outans focus sites. The red square in a indicates the zoom reported in Figure 3.6. Landforms explanation in c) and f): a: Les Martinets glacier; b: LIA moraine; c: Holocene moraines; d: rock glacier; e: talus slope; f: rock falls / avalanche deposits; g: debris-covered glacier; h: debris slope; i: bedrock outcrop.

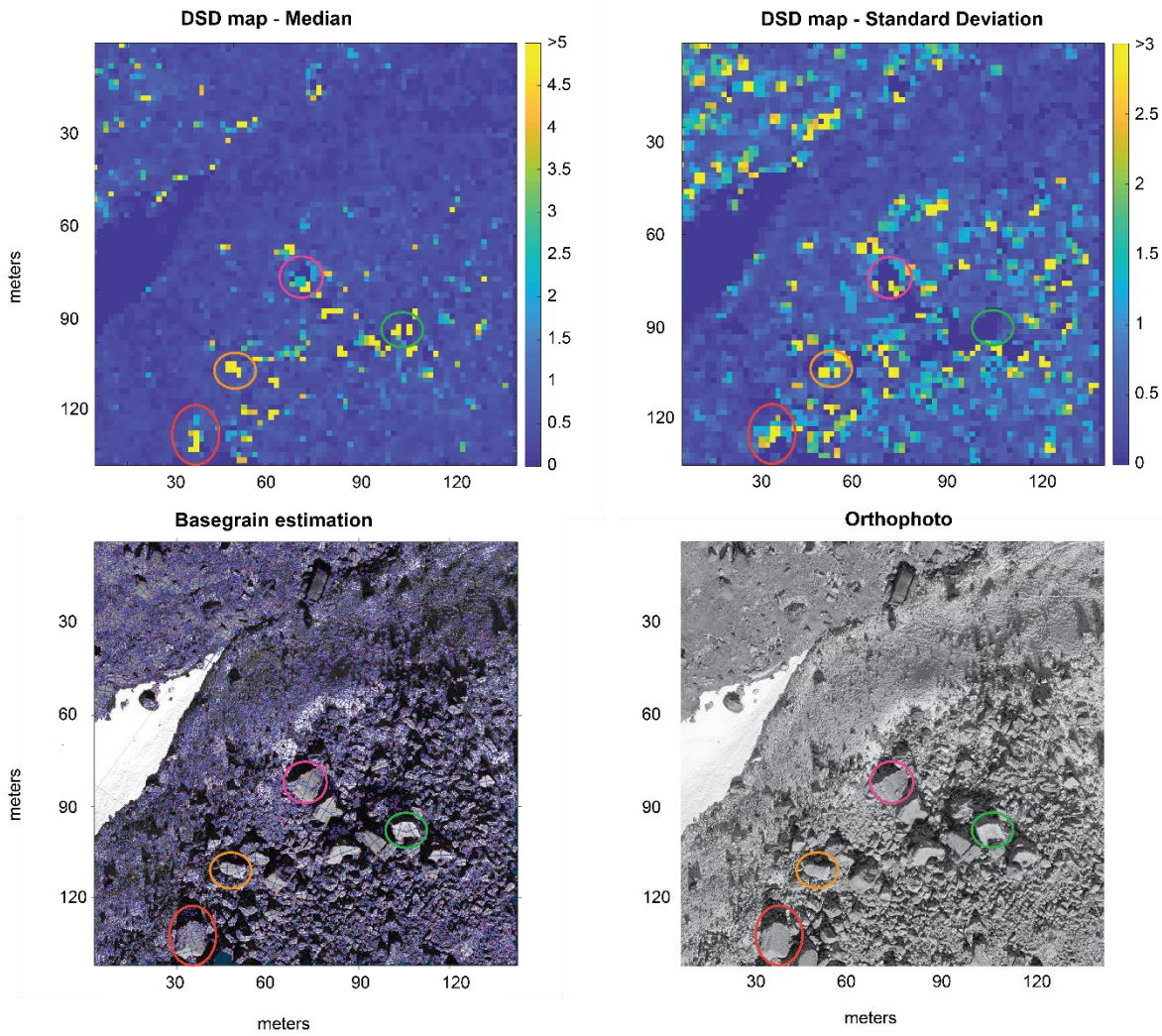


**Figure 3.5** - Zoom of Figure 3.4, DSD map - Les Martinets - Median. Examples of large boulders divided in smaller blocks (circles red, orange, fuchsia and green). DSD map - Median: mobile mean values (sqm) developed starting from the density map of the debris size values. DSD map – Standard Deviation: mobile standard deviation values (sqm) developed starting from the density map of the debris size values. Basegrain estimation: processed tile with delineated ellipses in correspondence to the debris. Orthophoto: original part of the tile from UAV campaign.



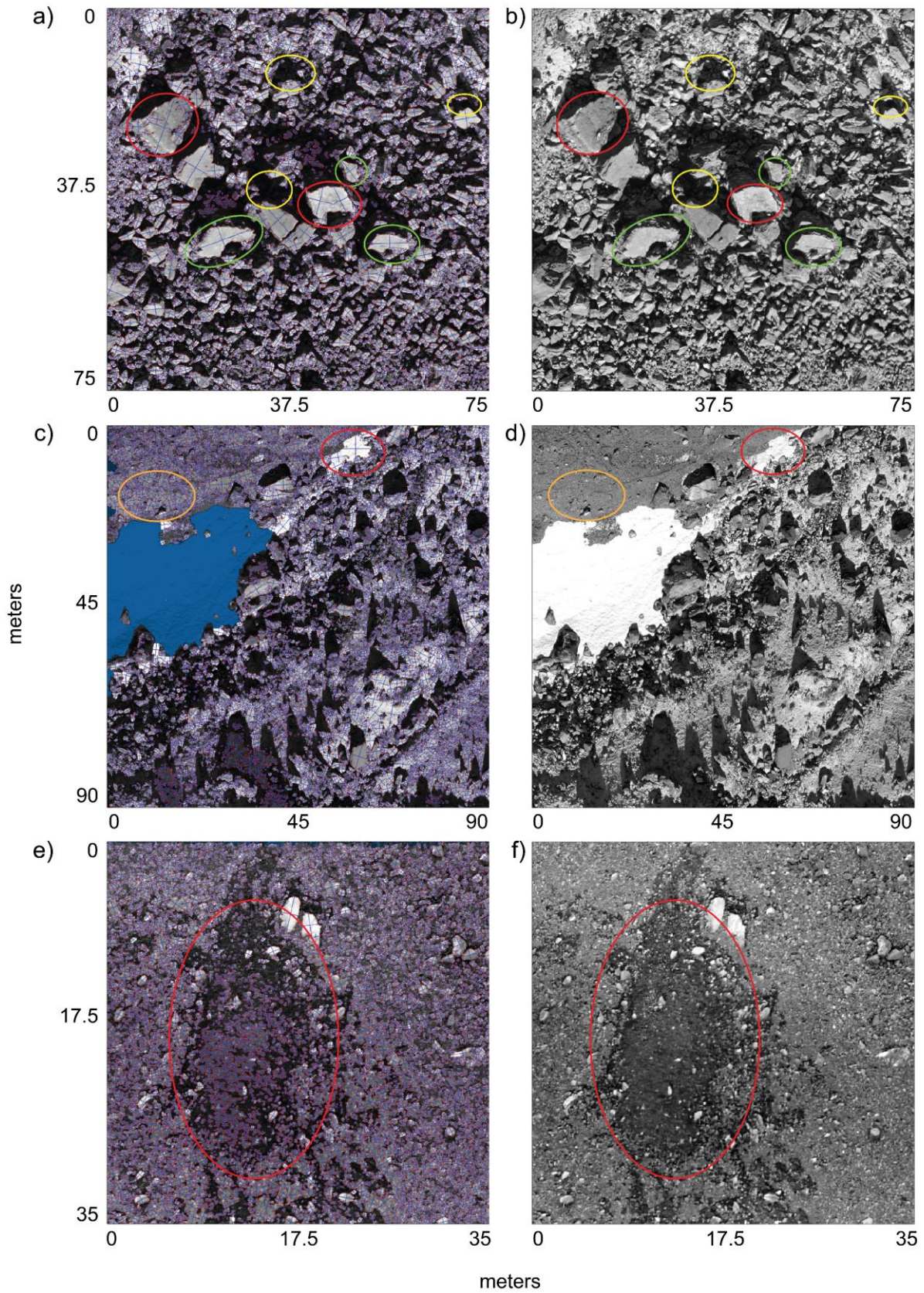


**Figure 3.6** - Example of Basegrain results (a, c and e) and original images (b, d and f). The scale is represented in pixel. In a-d 1 px = 5.75 cm; in e-f 1 px = 3 cm. In a and b, the red ovals indicate incorrect grain identification, the green ones a correct identification and the yellow ones the areas where no grain was detected. In c and d, the red oval indicates a snowfield identified as debris and the yellow one a portion



with small granulometry. In e and f, the red oval underlines a grassland patches, where debris were wrongly recognized.

### 3.4 Data and code availability

All the data presented in this paper are available in the following repository: <https://github.com/GAIA-UNIL/DSDmap>. The results of the mosaicking processes (i.e. the orthomosaics and the DSMs), the variables employed to create the masks and the MATLAB code written by the authors and used to elaborate the DSD map are available in the same repository.

### 3.5 Conclusions

In this study, we developed a new methodology to generate a debris size distribution map, which can be employed successively in other application such as predictive model for vegetation evolution, for sediment transport during intense rain or for determining the heat exchange processes and consequently the likelihood of the presence of permafrost. The method is composed of four phases: image acquisition through UAV technology and mosaicking processing to produce a high-resolution orthomosaic, debris size detection using the Basegrain algorithm, validation and eventually calibration, and, finally, debris size classification and map production.

Our methodology is an innovative application of grain detection algorithms that were originally designed to analyse grain size in river beds. It includes adaptations that allow deriving grain size maps based on imagery acquired in high mountain environments, which contain important areas not constituted of debris areas that have to be removed. As we demonstrated in our tests, it is particularly suited to UAVs images, which are becoming increasingly available.

We applied the developed methodology in two focus sites in the Western Swiss Alps, characterized by high geomorphological variability and consequently different debris size. The DSD maps emphasised the fine and large material areas, even if some limitations were highlighted and solved with mask applications.

The developed procedure indicates that the Basegrain algorithm is a useful and powerful instrument to detect the grain size not only in river beds, reason for which it was originally created, but also in other applications such as using drone images in high mountain environments. Nevertheless, some expedients are adopted where the algorithm is not performant, allowing a correct representation of the debris size distribution.

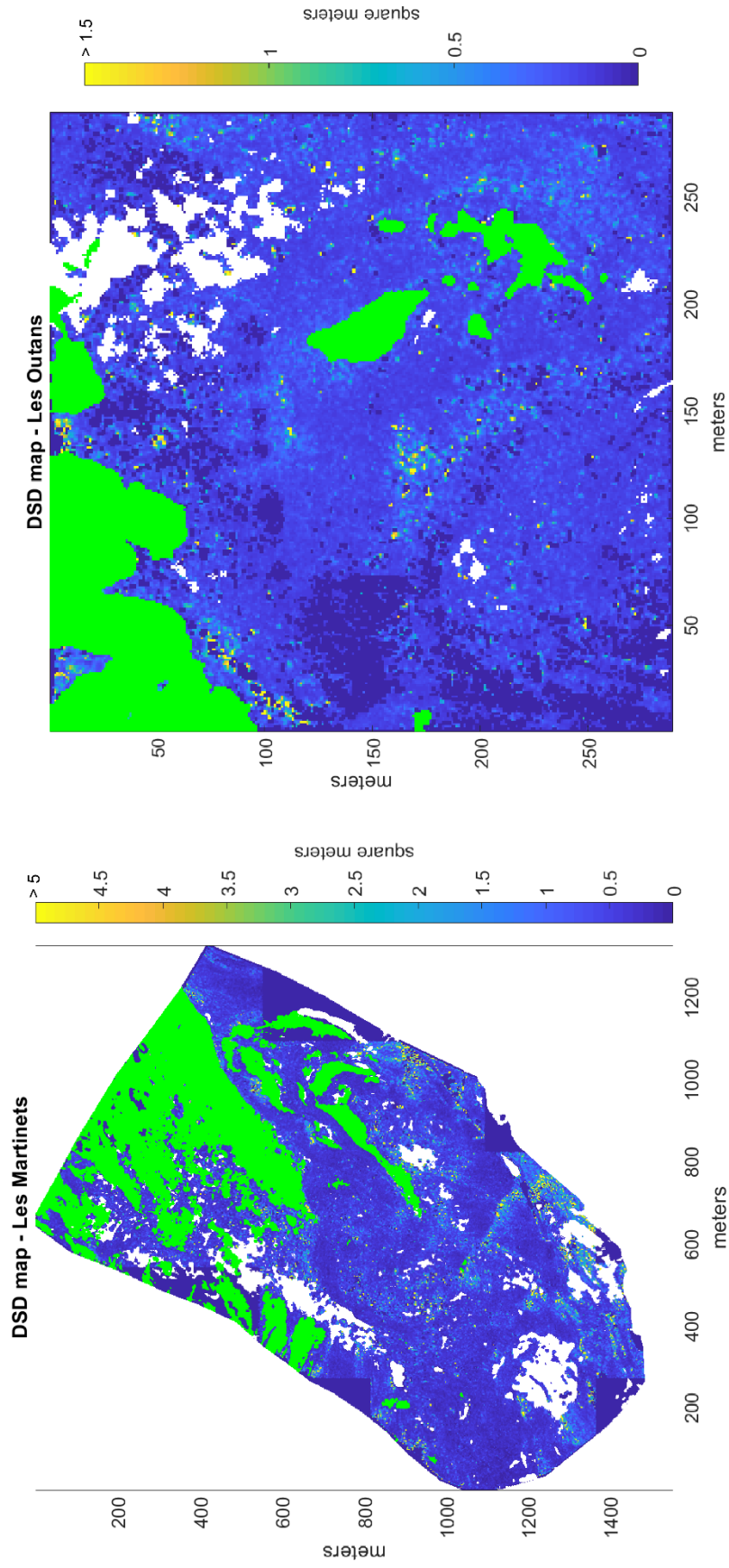


**Figure 3.7** - Final map with mask application for Les Martinets (left side) and Les Outans (right side). The vegetation mask is colored in green, the snow mask and/or the area with low roughness and/or the glacier in white.

## 3.6 Acknowledgments

This research was developed in the framework of the project “Integrating spatial predictions of vegetation, soils, geomorphology and hydrology for improved assessment of ecosystem services under climate change”, supported by the Swiss National Science Foundation (project N° CR23I2\_162754 / 1). The authors would like to acknowledge Lionel Benoit and Mathieu Gravey for their support for the development of the MATLAB codes.

## CHAPTER 4

### 4. Semi-automated geomorphological mapping in mountain environment

Elisa Giaccone<sup>1</sup>, Christophe Lambiel<sup>1</sup>, Marj Tonini<sup>1</sup>, Fabio Oriani<sup>1</sup>, Grégoire Mariéthoz<sup>1</sup>

<sup>1</sup>*University of Lausanne, Institute of Earth Surface Dynamics, Lausanne, Switzerland*

**Personal contribution.** I designed this research with my supervisors C. Lambiel and G. Mariéthoz. I made method implementation with the support of all the co-authors, prepared figures and wrote the manuscript. Constructive comments and corrections of the co-authors increased considerably the paper quality.

## **Abstract**

In the last decades, the availability of high-resolution imagery and innovative algorithms enabled the automatic classification of land use and land cover. These automatic procedures can potentially be used in other disciplines. In this paper, we compare the results from two data-driven algorithms applied to supervised classification: Direct Sampling (DS) and Random Forest (RF). Both approaches are tested for the geomorphological mapping of an alpine valley, with 12 predictor variables for the geomorphological classification. Results are compared with a geomorphological map based on field data acquisition and considered as ground truth. Both methods present a similar accuracy (0.54 for DS and 0.55 for RF), and a Cohen's Kappa of 0.44 for both approaches. Late Glacial deposits, glaciers, rock outcrops, and rock walls are identified with higher precision, while alluvial fans and alluvial plains show the highest misclassification error. The results suggest that DS and RF are both suitable techniques to simulate semi-automated geomorphological maps in alpine environments and on regional scale.

## **Keywords**

Alpine environments; geomorphological mapping; supervised classification; direct sampling; random forest.

## 4.1 Introduction

Classical geomorphological maps are usually realised by manual mapping and digitisation of features on the field or from topographic data, orthoimages and remote sensing imagery (Batten, 2001; Bocco et al., 2001; Dent and Young, 1981; Mantovani et al., 1996; Pain, 1985; Reddy, 2018). These approaches are time-consuming, particularly for large areas with limited accessibility and they are therefore only applicable to small areas (Adediran et al., 2004; Schneevoigt et al., 2008). In the last decades, different supervised and unsupervised numerical approaches, were proposed to automatically classify key landforms (Smith et al., 2011). In the case of supervised methods, training areas selected with geomorphological expertise are employed (Brown et al., 1998). For unsupervised approaches, algorithms used to identify the land surface parameters through combinations of predictor variables (Pike, 1988). Generally, predictors are morphometric factors derived from digital elevation models (DEMs), such as slope and aspect, and non-morphometric variables, which inform on vegetation, land cover, lithology and soil (e.g. Adediran et al., 2004; Gharari et al., 2011; Irvin et al., 1997). These techniques do not usually consider the spatial relations among the variables and may generate misclassifications on terrain discontinuities (Minár and Evans, 2008; van Niekerk, 2010).

In the recent years, more advanced mapping techniques, based on machine learning and geostatistics were developed. They showed improved classifications, relying on the analysis of the increasingly available high-resolution terrestrial images. In addition, they allowed incorporating spatial information between multiple locations (Evans, 2012; Vannamettee et al., 2014).

To test the potential of latest-generation supervised classification techniques on geomorphological mapping, we provide here a comparative study of two recent classification methods based on the use of training datasets (Brenning, 2005; Brenning et al., 2007; Brown et al., 1998; Marmion et al., 2008; Veronesi and Hurni, 2014). The aim is to perform semi-automated geomorphological mapping (SAGM) of an area guided by an already classified map from an analogue area.

Developing automatic procedures for geomorphological mapping is relevant in several domains of geomorphological modelling. It is the case, for example, of the plant ecology. Notably under the effect of global warming (Beniston et al., 2018), it is of primary importance to produce small-scale species distribution models which take into account all variables that influence vegetation. Indeed, plant development and their potential distribution depend on indirect variables (e.g. geology, topography, climate), on direct variables (e.g. nutrients, soil, temperature controls and photosynthetically active radiation), on biotic interactions and disturbances and on land use (Guisan and Zimmermann, 2000; Mod et al., 2016). Using a geomorphological dataset, with detailed information about processes and landforms, as well as physical disturbances, can improve the predictions of species distribution in mountain environment. Indeed it has been shown that landform morphodynamics is an important factor for alpine plant distribution (Cannone and Gerdol, 2003; Giaccone et al., 2019; le Roux and Luoto, 2014).

The first classification method considered is Direct Sampling (DS). The DS has been employed in different domains, such as generating stochastic sand channels for aquifer modeling (Huang et al., 2013), gap-filling of daily streamflow time series (Dembélé et al., 2019), simulating rainfall time-series (Oriani et al., 2018), colorizing grayscale or multispectral images (Gravey et al., 2019), or resource estimation of mineral deposits (Dagasan et al., 2019). However, its applicability for

geomorphological classification has never been investigated before, despite its potential to account for spatial dependence of the classes.

The second approach tested here is Random Forest (RF - Breiman, 2001). It is widely used in the scientific community for different domains, such as ecology (e.g. Cutler et al., 2007; Prasad et al., 2006), permafrost modeling (Deluigi et al., 2017), susceptibility mapping (e.g. Catani et al., 2013; Leuenberger et al., 2018; Stumpf and Kerle, 2011a), remote sensing (e.g. Belgiu and Drăguț, 2016; Chan and Paelinckx, 2008) and geomorphological classification (e.g. Marmion et al., 2008; Stumpf and Kerle, 2011; Veronesi and Hurni, 2014).

In those previous geomorphological applications, the classification was limited to specific landforms belonging to the same morphogenetic class (e.g. periglacial landforms, landslides or shaded relief landforms), without testing on contiguous areas. Moreover, the realisation of a classical geomorphological map with multiple classes is still lacking.

In this paper, our approach seeks to provide solutions for the semi-automatic classification, comparing DS and RF on the realisation of a multi-class SAGM. To reach this aim, we tested both techniques in an alpine area, where a classical geomorphological map already exists.

## 4.2 Material and Methods

### 4.2.1 Direct Sampling

The DS is part of the multiple-point geostatistics (MPS) family of techniques (Mariethoz and Caers, 2014), that simulate a random variable at unknown locations by generating similar data patterns to the ones observed in a given training image (TI - Caers and Zhang, 2004; de Vries et al., 2008; Strebelle, 2002; Vannamettee et al., 2014). A TI can be a real dataset or a conceptual image of the expected spatial heterogeneity based on prior information (Meerschman et al., 2013). In their pioneer study, Vannamettee et al. (2014) showed the applicability of MPS to map eight landform classes in the French Alps. With respect to previous MPS algorithms, DS, developed by Mariethoz et al. (2010), has the capability of simulating continuous and categorical variables at the same time, which makes it suited for generating classes based on continuous predictors.

The DS algorithm generates a random variable on the simulation grid (SG) representing the study zone, by resampling the TI under pattern-matching constraints. In the present case, a categorical variable denoting geomorphological classes is the target variable and it is manually defined for the TI by geomorphological expertise. A series of morphometric, physical, and remote-sensing variables can be given as predictors of the geomorphological classes. These are defined for both the TI and SG. The algorithm identifies correspondences between patterns of these variables, then sequentially import in the SG the target-variable values associated to the most similar patterns found in the TI.

Since DS is a geostatistical simulation algorithm, it does not produce a unique classification, but a (possibly infinite) number of possible scenarios of classes, called realisations. The most probable

estimation of the classes can be estimated by computing the mode of the realisations, i.e. the most frequent class across all realisations. In addition, the variability between realisations can be analysed to quantify the classification uncertainty.

The DS parameters are defined as follows: 1) maximum fraction of the TI to scan  $F \in (0, 1)$ ; 2) neighborhood distance, i.e. the maximum search distance as number of cells; 3) threshold position  $T \in (0, 1)$ , used to stop or continue the sampling processes if a data event is found in the TI; 4) number of realisations; 5) weight of conditioning data  $W \in (0, 1)$ . In our case, we decided to completely scan the TI ( $F = 1$ ) to have access to all the patterns in the TI, with a maximum search window of 50 x 50 cells and with rotation possibility, to increase the matching possibilities. The threshold position  $T$  was set to 0.01 in agreement with Meerschman et al. (2013), 100 realisations were carried out and all the variables were considered with the same weight ( $W = 1$ ).

DS is run in a computer provided with two processors of 2.30 GHz and a 64 GB RAM.

## 4.2.2 Random Forest

RF is an ensemble-learning algorithm for classification and regression based on decision trees. As a common characteristic of machine learning based approaches, RF is capable of learning from and make predictions on data, modeling the hidden relationships between a set of input and output variables (Breiman, 2001). Computationally, it is based on decision trees (*ntree*). Decision trees are supervised classifiers providing decisions at multiple levels and they are constituted by a root node and child node. At each node, decisions are performed based on training predictor values. The number of generated *ntree* and the number of variables randomly sampled as candidates at each split (*mtry*) are the parameters that need to be specified. The algorithm generates *ntree* subsets of the training dataset (counting about one-third of the observations) by bootstrapping (i.e. random sampling with replacement). For each subset, a decision tree is generated by iterating the following rules up to the maximum level, when each node contains less than a fixed number of data points: at each split, the algorithm select randomly *mtry* variables and computes the Gini index to select the best variable. The prediction of a new data point is finally computed by taking the average value of all decision trees for regression and the maximum voting for classification. The parameters of the model are optimized by evaluating the prediction-error on those observations that were not used in the training subsets (called “out-of-bag”). Finally, the Simulation Grid, containing data that has never been used in the training step, was considered as simulation/testing dataset: this way allowed to compare RF with DS results.

RF is run in a computer provided with a processor of 2.60 GHz and a 12 GB RAM.

## 4.2.3 Test design and dataset

To run both algorithms, we selected a rectangular area of 70 km<sup>2</sup> within the Arolla valley, located in the Western Swiss Alps (46° 01' N, 7° 28' E). We chose this valley because a classical geomorphological map already exists and can be used for validation (Lambiel et al., 2016). The map was elaborated with the legend of the University of Lausanne (Schoeneich and Reynard, 1993),



which highlights the process categories, the morphogenesis of landforms and their activity rate (Figure 4.1).

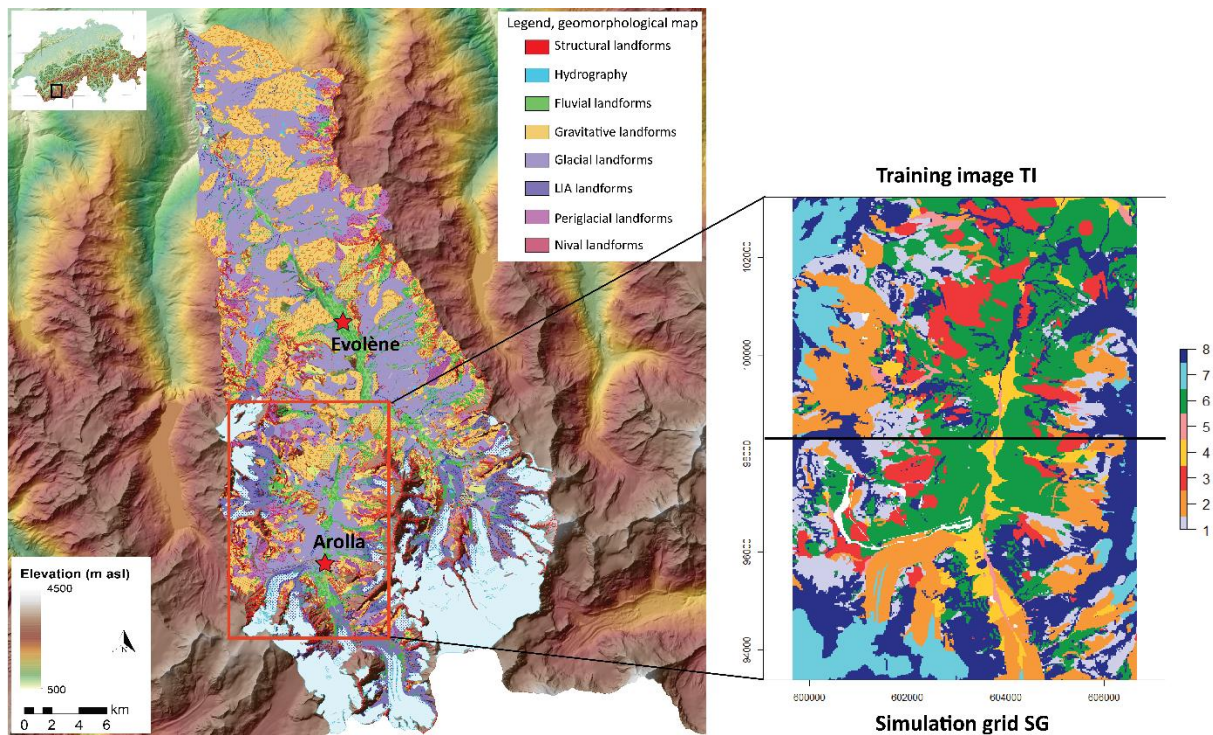


**Figure 4.1** - Focus site where the traditional geomorphological map was elaborated realized by Lambiel et al. (2016) (left side). On the right side, the area selected for calibrating and running the algorithms to produce the SAGM. The area was divided in two part, the training image (upper part) and the simulation grid (lower part). Legend of the selected area: 1) talus slope; 2) active-inactive rock glacier, debris-covered glacier, Little Ice Age moraine deposit; 3) rockslide, landslide, relict rock glacier; 4) alluvial fan; 5) alluvial plain; 6) Late Glacial deposit; 7) glacier and permanent snow; 8) rock outcrop, rock wall. White zones are excluded from all the calculations.

The Arolla valley is located in the upper part of the Hérens valley, a south-north catchment on the left side of the Rhone River, ranging from 470 to 4357 m a.s.l. (Dent Blanche). Geologically, the Arolla valley is constituted of oceanic sediments and orthogneisses, metagabbros and breccias (Steck et al., 2001). The climate of the valley is dry, with a mean annual precipitation of 736 mm recorded at the Evolène-Villa climatic station (1825 m a.s.l.) for the norm period 1981-2010. The 0°C isotherm is around 2600 m a.s.l. The valley is characterized by several glaciers in retreat since the end of the Little Ice Age (19th century), large moraines, periglacial landforms (e.g. active and inactive rock glaciers, solifluction lobes), talus slopes, debris flows associated landforms (gullies, fans).

The selected area was divided in two equal parts, the TI for training and the SG for simulation/testing, composed both of the same dataset. The dataset is composed of 13 variables (Table 4.1): the geomorphological classification as target variable and 12 predictor variables, defined on a regular grid with a spatial resolution of 20 m. The aerial orthophoto mosaics, the FCIR and the DEM are obtained from the Swiss Office of Topography. In the TI, the geomorphological categories are informed. Conversely, in the SG the target variable is uninformed

and simulated by the classification algorithms (Figure 4.2). All the variables were built in ArcGIS (ESRI), except for flow accumulation and roughness that were computed with the Matlab TopoToolbox (Schwanghart and Kuhn, 2010; Schwanghart and Scherler, 2014). The aspect was transformed from degrees to sine (aspect\_sin) and cosine (aspect\_cos) to highlight all the cardinal points. More information about the geomorphological classification are found at the section “4.2.4 Landform classification”.

**Table 4.1** - Dataset composition.

<b>Variable</b>	<b>Name into dataset</b>	<b>Source</b>
Geomorphology	Geomorphology	Lambiel et al., 2016
R band	Ortho1	aerial orthophoto mosaic (year 2013)
G band	Ortho2	aerial orthophoto mosaic (year 2013)
B band	Ortho3	aerial orthophoto mosaic (year 2013)
Slope	Slope	Alti3D DEM (year 2016)
Sine aspect	Aspect_sin	Alti3D DEM (year 2016)
Cosine aspect	Aspect_cos	Alti3D DEM (year 2016)
Normal curvature	Curvature	Alti3D DEM (year 2016)
Plan curvature	Plan_curv	Alti3D DEM (year 2016)
Profile curvature	Prof_curv	Alti3D DEM (year 2016)
Solar radiation	Solradiation	Alti3D DEM (year 2016)
Flow accumulation	Flow_accumulation	Alti3D DEM (year 2016)
Roughness	Roughness	Alti3D DEM (year 2016)

#### **4.2.4 Landform classification**

The geomorphological legend of the University of Lausanne is organized in 11 main classes, which regroup more than 100 landforms (Table 4.2).

To allow a feasible automatic classification of the complex landform distribution, the numerous geomorphological classes are grouped in 8 main process-based classes. This simplification is in part dictated by the limited size of the TI, as it most likely occurs in real applications. In the TI not all the original classes are present with a sufficient number of pixels to be detected with geostatistical or machine learning algorithms, especially the karstic, lacustrine and organic classes. The anthropic class was excluded from the elaboration. The selected classes are listed in Table 4.3. This classification was chosen based on geomorphological interpretation of the authors.

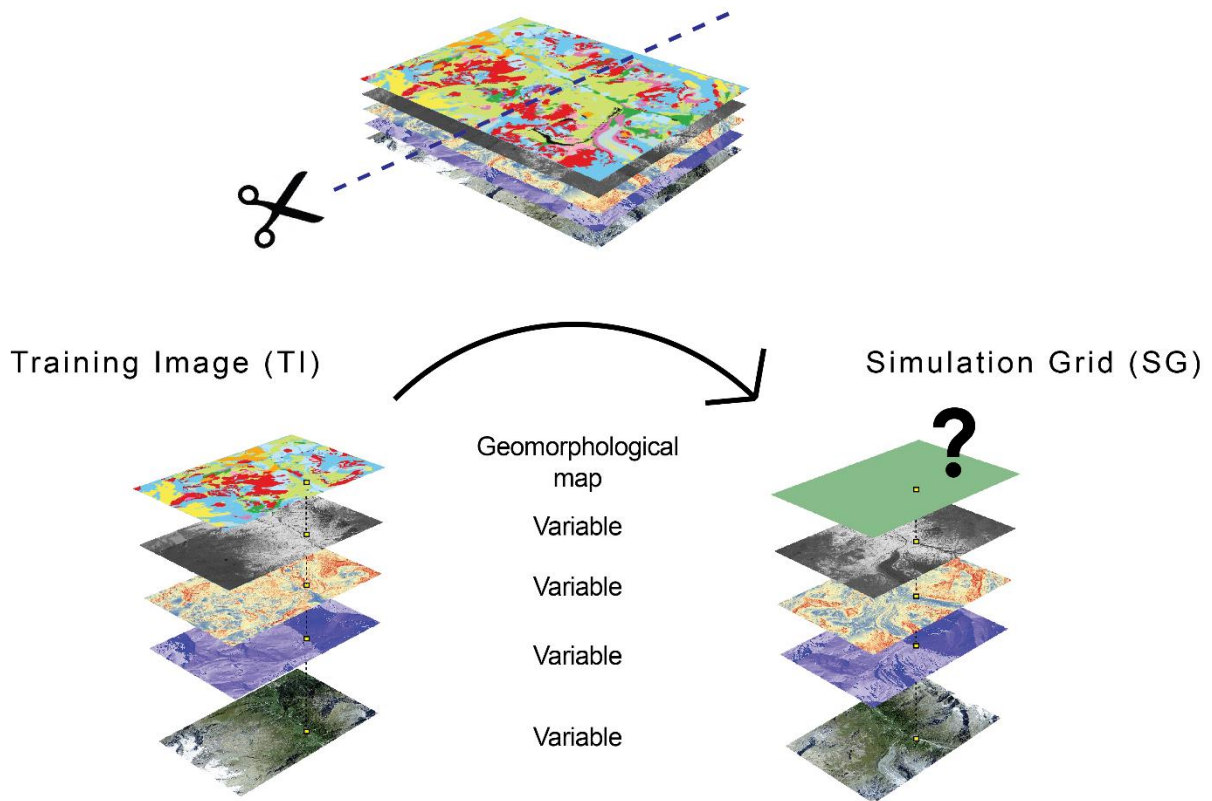


**Figure 4.2** - Conceptual model of the test design. The study area is split in two parts, the training image (TI) and the Simulation Grid (SG). Both are composed of the same number of variables with equal resolution grid. In the TI the geomorphological classification is represented because it serves to train the model, in the SG it is absent because it is the variable to simulate.

**Table 4.2** - Main classes of the geomorphological map of the University of Lausanne and example of typical landforms.

Class	Landform example
Structural	Fault, rock scarp, rock step, fault escarpment
Hydrological	River, spring, lake, marsh, glacier, debris-covered glacier, permanent snow
Fluvial	Gorge, debris flow channel, alluvial fan, fluvial accumulation area
Gravitative	Scar, rockslide, landslide, talus slope, rockfall deposit
Glacial	Moraine deposit, glacial basin, kame terrace, glacial accumulation area
Periglacial	Rock glacier, push moraine, solifluction lobe, patterned ground
Nival	Nival accumulation area, avalanche deposit area, snow moraine
Karstic	Gypsum karst, doline, ouvala, polje, karstic accumulation area
Lacustrine	Lacustrine terrace, delta, lacustrine accumulation area
Anthropic	Slope excavated, ski run, irrigation channel, avalanche protection, mine
Organic	Soil developed on rocks, vegetation-derived accumulation

**Table 4.3** - Geomorphological classification selected for testing in DS and RF algorithms.

Class	Landform
1	Talus slope
2	Active-inactive rock glacier, debris-covered glacier, Little Ice Age moraine deposit
3	Rockslide, landslide, relict rock glacier
4	Alluvial fan
5	Alluvial plain
6	Late Glacial deposit
7	Glaciers, permanent snow
8	Rock outcrop, rock wall

### 4.2.5 Model validation

The final results from both algorithms were compared with the original geomorphological map through a confusion matrix. This allows the calculation of the accuracy and the Kappa value (Cohen, 1960). Accuracy is the percentage of correctly classified data events, representing the overall quality of the model. Kappa is a measure of agreement normalized at the baseline of random chance on the dataset:

$$k = \frac{p_o - p_e}{1 - p_e}$$

where  $p_o$  is the relative observed agreement among raters and  $p_e$  is the hypothetical probability of chance agreement. The Kappa value ranges from 0 (lack of agreement) to 1 (perfect agreement – Viera and Garrett, 2005).

Moreover, the performance of the algorithms are evaluated as confusion matrix as follows:

		Predicted	
		Event	No event
Reference	Event	True Positive (TP)	False Negative (FN)
	No event	False Positive (FP)	True Negative (TN)

The following statistics for each class have also been calculated:

$$Sensitivity = TP / (TP + FN)$$

$$Specificity = TN / (TN + FP)$$

*Positive Predicted Value PPV or Precision* =  $TP / (TP + FP)$

The sensitivity informs about the probability that the result shows a prediction of a geomorphological class when that class is effectively present. The specificity is the probability that the absence of a geomorphological class is predicted when that class is absent. The Positive Predicted Value is the probability that the geomorphological class is present when the reference is positive.

In the result section, the DS data with one realisation and the mode of 100 realisations are shown to highlight how the mode computing improves the results also from a visual point of view. Furthermore, the probability for each class within the 100 realisations is calculated to quantify the uncertainty. Equally, the RF data are shown as categorical values and as probabilities.

## 4.3 Results

### 4.3.1 Direct Sampling

The SAGMs obtained with one DS realisation and with the mode of the 100 DS realisations are reported in Figure 4.3b and 4.3c and compared with the reference map (Figure 4.3a) and the orthophoto (Figure 4.3g). The one-realisation results scattered comparing to the mode result, but the main patterns are simulated. Consequently, it is possible to observe main landforms such as talus slopes (class n° 1), active-inactive rock glaciers, debris-covered glaciers and Little Ice Age moraine deposits (n° 2), Late Glacial deposits (n° 6), glaciers (n° 7), and rock outcrops (n° 8), even if their shape is more delineated in the mode result. Instead, the class n° 3 (rockslide, landslide, relict rock glacier) presents a structure not coincident with the ground truth. This is also the case for the classes n° 4 (alluvial fans) and 5 (alluvial plains), which do not present a defined pattern. Instead, their simulation is improved with 100 realisations. Regarding the computation time of the 100 realisations, it was higher than 6 hours.

The uncertainty map (Figure 4.3d) highlights the areas that are better predicted (light and dark blue pixels probabilities > 0.7) and these areas match mainly with the classes n° 1, 2, 6, 7 and 8. In particular, the Late Glacial deposits in the top-center part, the glaciers in the left-bottom part and the debris-covered glacier and its Little Ice Age moraines in the left side of the image are easily identifiable, as well as the rock outcrops.

The data of the confusion matrices confirm the visual interpretation. Respectively for one-realisation and for the mode computing, the overall accuracy is 0.45 and 0.54, confidence interval 95% for both, and Kappa 0.34 and 0.44. Details about confusion matrix and statistics by class are reported in Tables 4.4 and 4.5. Concerning the one-realisation, the best predicted classes are the Late Glacial deposits (class n° 6), the glaciers (n° 7) and the rock outcrops (n° 8): they have PPVs higher than 0.53. As well, they report greater values of sensitivity (> 0.52). Specificity is elevated for all the classes (> 0.83).

Regarding the 100 realisations, the classes with the best predictions area are the active-inactive rock glaciers, the debris-covered glaciers and the Little Ice Age moraine deposits (class n° 2), the Late Glacial deposits (n° 6), the glaciers (n° 7) and the rock outcrops (n° 8). Sensitivity index is 0.49 for classes n° 2 and 6 and  $> 0.87$  for classes n° 7 and 8. As well, the PPVs are higher for the before-mentioned classes and for class n° 1 ( $> 0.45$ ). Specificity is high for all the classes like in the one-realisation ( $> 0.85$ ).

### 4.3.2 Random Forest

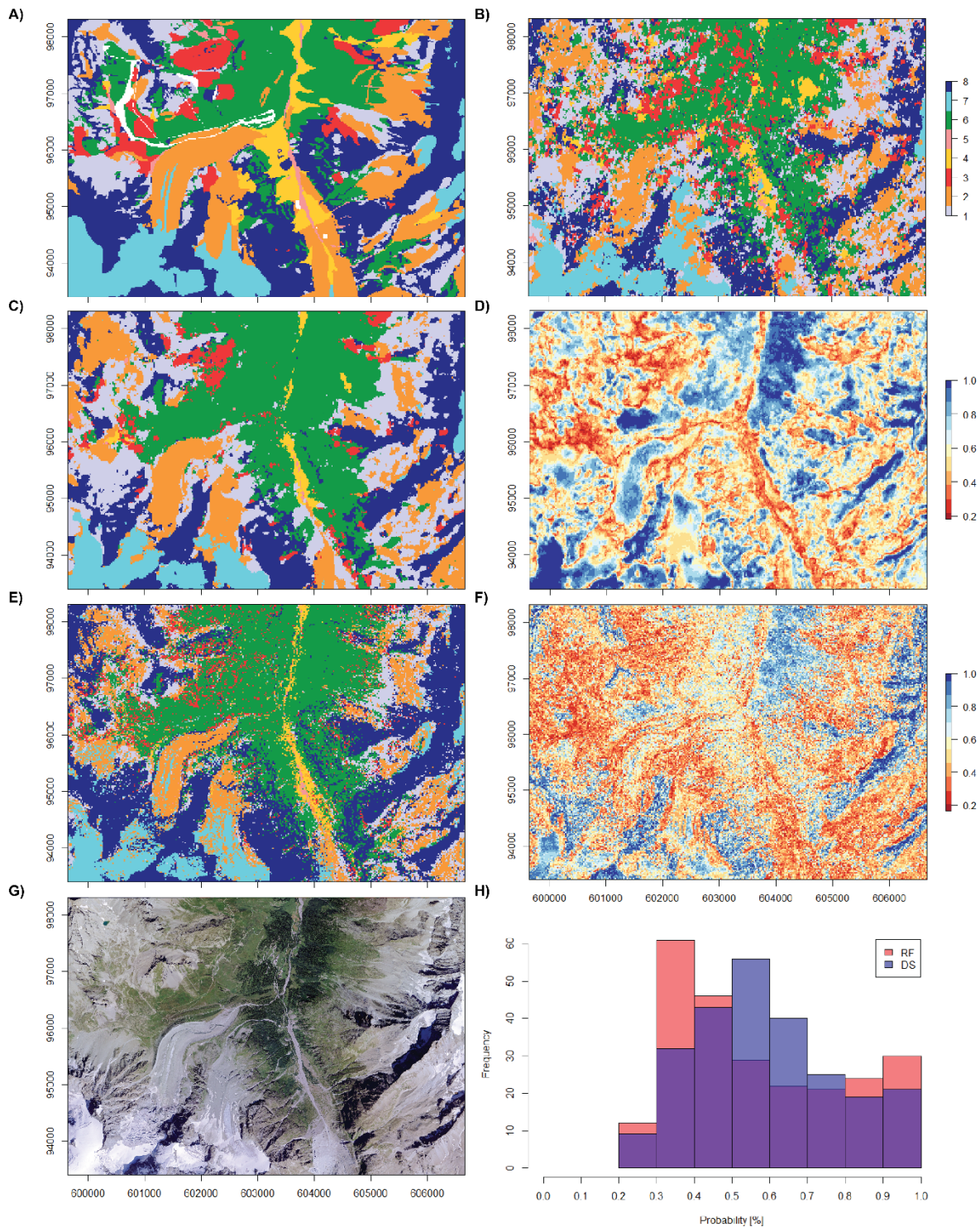
Following the OOB decrease (Figure 4.4), the *mtree* is set to 500 and 4 variables were sampled randomly at each split. The final OOB error is 35.77% and the error for each class is shown in Table 4.6. According to the mean decrease in Gini index (Figure 4.5), blue band, slope, roughness and solar radiation are key predictor variables to decrease the node purity. Regarding other variables, they offer moderate improvement, excepted in the case of flow accumulation, which results negligible. The computation time to train and test the models was less than 1 hour.

Figure 4.3e shows the classification resulting of the RF model and the Figure 4.3f the uncertainty map. Both images are scattered and landform outlines are less defined. The uncertainty map presents high probability values (light-dark blue,  $> 0.7$ ) only in few areas, such as some rock outcrops in the right and in the left-bottom side of the image, as well as the glaciers. In the top-central side, the high probability patch indicates a portion of Late Glacial deposit.

Even if polygons are scattered, the class n° 2 (active-inactive rock glaciers, debris-covered glaciers, Little Ice Age moraine deposits) is simulated in detail: in the left-bottom area, for example, two debris cover glaciers with their Little Ice Age moraines are located. They still present elongated portions of free-debris ice that are detected efficiently by the algorithms. As well in the right part, glaciers in the rock outcrops / rock walls area are identified.

According to the results of the confusion matrix, the accuracy is 0.55, confidence interval 95% and Kappa 0.44. Confusion matrix and statistics calculated for each class are shown in Tables 4.4 and 4.5. Also in this case, the classes with the best predictions are the active-inactive rock glaciers, the debris-covered glaciers and the Little Ice Age moraine deposits (class n° 2), the Late Glacial deposits (n° 6), the glaciers (n° 7) and the rock outcrops (n° 8). Sensitivity index confirms the assessment with values  $> 0.40$  for the classes n° 2 and 6 and values  $> 0.70$  for the classes n° 7 and 8. Equally, the PPVs are higher for the before-mentioned classes and for the class n° 1, the talus slopes (0.29). Instead, they are  $< 0.13$  for rockslide, landslide, relict rock glacier (n° 3), alluvial fan (n° 4) and alluvial plain (n° 5). Rather, specificity has elevated values for all the classes ( $> 0.87$ ).





**Figure 4.3** - A) Reference geomorphological map for the selected study area. In white the areas not considered for classification. B) Semi-automated geomorphological map obtained from one DS realisation. C) Semi-automated geomorphological map obtained from the mode of 100 DS realisations. D) Probability map of the 100 DS realisations, showing the frequency of detection of the class corresponding to the mode. The higher is the probability, the more certain is the estimation. E) Semi-automated geomorphological map obtained through RF. F) Probability map of the RF result. G) Aerial orthophoto mosaic SwissMapRaster © swisstopo (DV084371). H) Histograms of the uncertainty maps. Legend: 1) talus slope; 2) active-inactive rock glacier, debris-covered glacier, Little Ice Age moraine deposit; 3) rockslide, landslide, relict rock glacier; 4) alluvial fan; 5) alluvial plain; 6) Late Glacial deposit; 7) glacier and permanent snow; 8) rock outcrop, rock wall.

**Table 4.4** - Confusion matrices about DS and RF data.

<b>DS 1 simulation</b>		<b>PREDICTED</b>								
<b>Class</b>	1	2	3	4	5	6	7	8	Sum	
<b>REFERENCE</b>	1	4277	2785	562	132	91	1015	108	1104	10074
	2	5063	5055	943	237	220	2040	1112	619	15289
	3	1328	560	1007	153	103	1368	55	313	4887
	4	877	348	486	551	152	1707	65	89	4275
	5	138	74	51	169	90	292	20	41	875
	6	1833	1131	1999	677	157	10576	102	611	17086
	7	1230	1737	34	9	58	59	4999	405	8531
	8	4086	1938	1499	100	100	3263	589	12956	24531
	Sum	18832	13628	6581	2028	971	20320	7050	16138	85548
<b>DS 100 simulations</b>										
<b>REFERENCE</b>	1	5440	2401	246	20	19	997	1	950	10074
	2	4897	6922	404	109	8	2549	188	212	15289
	3	1041	620	635	56	66	2342	0	127	4887
	4	956	366	106	498	23	2317	0	9	4275
	5	98	102	7	269	43	349	0	7	875
	6	1708	1228	416	108	37	13259	0	330	17086
	7	1207	1323	3	0	6	174	5330	488	8531
	8	3479	1072	356	42	6	5311	273	13992	24531
	Sum	18826	14034	2173	1102	208	27298	5792	16115	85548
<b>RF</b>										
<b>REFERENCE</b>	1	2884	3585	311	31	21	920	313	2009	10074
	2	2560	6253	510	339	58	2625	1485	1459	15289
	3	536	978	655	20	8	2058	24	608	4887
	4	325	768	64	570	53	2228	100	167	4275
	5	19	145	26	259	100	292	1	33	875
	6	905	1592	1260	112	22	11892	101	1202	17086
	7	416	1278	23	17	5	129	5530	1133	8531
	8	991	909	345	52	2	2992	353	18887	24531
	Sum	8636	15508	3194	1400	269	23136	7907	25498	85548



**Table 4.5** - Quality indexes showing the DS and the RF performance for each modeled class. PPV: positive predicted value.

	<b>Class</b>							
<b>DS 1 realisation</b>	<b>1</b>	<b>2</b>	<b>3</b>	<b>4</b>	<b>5</b>	<b>6</b>	<b>7</b>	<b>8</b>
Sensitivity	0.23	0.37	0.15	0.27	0.09	0.52	0.71	0.80
Specificity	0.91	0.86	0.95	0.96	0.99	0.90	0.96	0.83
PPV	0.42	0.33	0.21	0.13	0.10	0.62	0.59	0.53
<b>DS 100 realisations</b>								
Sensitivity	0.29	0.49	0.29	0.45	0.21	0.49	0.92	0.87
Specificity	0.93	0.88	0.95	0.96	0.99	0.93	0.96	0.85
PPV	0.54	0.45	0.13	0.12	0.05	0.78	0.62	0.57
<b>RF</b>								
Sensitivity	0.33	0.40	0.21	0.41	0.37	0.51	0.70	0.74
Specificity	0.91	0.87	0.95	0.96	0.99	0.92	0.96	0.91
PPV	0.29	0.41	0.13	0.13	0.11	0.70	0.65	0.77

**Table 4.6** - Error for each simulated class, obtained from RF model training on the TI.

<b>Class</b>	<b>Class error</b>
1	0.52
2	0.33
3	0.68
4	0.63
5	0.75
6	0.22
7	0.24
8	0.31

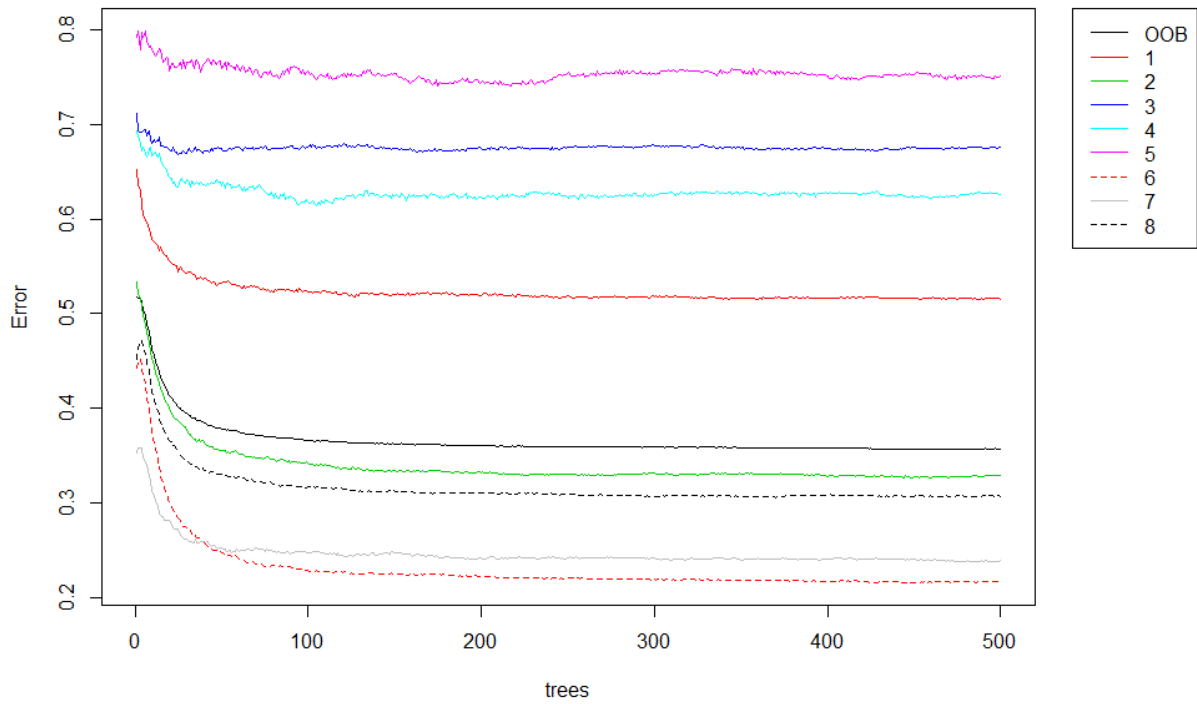


**Figure 4.4** - Error evolution of RF model trained on the TI, through 500 trees. OOB indicates out of bag error. Numbers from 1 to 8 correspond to geomorphological classes listed in Table 4.3.

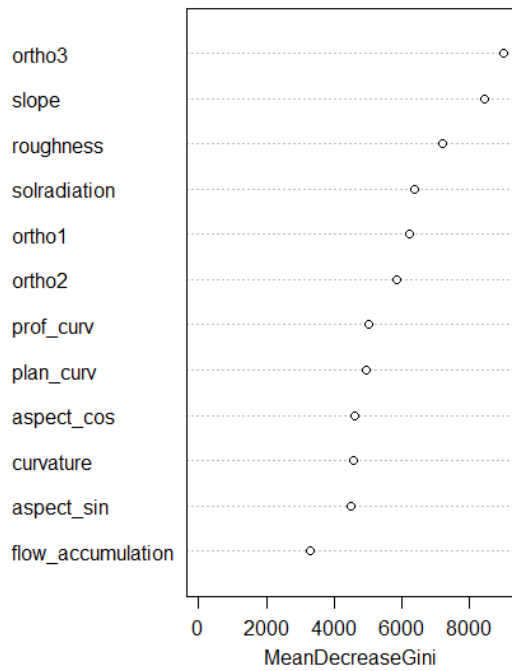


**Figure 4.5** - Importance of the 12 predictor variables expressed with mean decrease of Gini index.

## 4.4 Discussion

The first challenge we met in this study was the selection of the right number of geomorphological classes. Indeed, trying to simulate the geomorphological diversity of the landscape is challenging, despite the actual progresses on machine learning and geostatistical techniques. Many approaches were attempted before identifying key geomorphic features. Whereas Marmion et al. (2008) focused on periglacial landforms in Finland and Stumpf and Kerle (2011) worked on landslides, we aimed at simulating the heterogeneity of alpine landforms selecting 8 main classes, trying to preserve, as much as possible, the dominant process, the shape, and the age of the landforms. In this sense, we were inspired by the classification of Vannamettee et al. (2014) and Veronesi and Hurni (2014) classifying screes, alluvial fans and rock outcrops, periglacial-glacial active deposits (active-inactive rock glacier, debris-covered glacier, Little Ice Age moraine deposit), gravitative and/or inactive deposits (rockslide, landslide, relict rock glacier), fluvial deposits, Late Glacial deposits and glaciers. Moreover, increasing the number of classes is not appropriate because it reduces the number of cell occurrences for each class and consequently the simulation results weakened (Vannamettee et al., 2014).

As shown in the results, the mode calculation on 100 realisations improves the DS results, compared to a single realisation. In this sense, we recommend multiple realisations and a subsequent mode computing.

Globally, the Direct Sampling and the Random Forest give similar results. Indeed, the overall accuracy has only one point percentage of difference (0.54 for DS and 0.55 for RF) and the Kappa value is the same for both algorithms (0.44). According to the literature, a Kappa value comprised between 0.41 and 0.6 indicates moderate agreement between reference and simulation (Viera and Garrett, 2005), normalizing the overall accuracy (Allouche et al., 2006).

Graphically, the DS is a more efficient method because, after the mode calculation, defined polygons representing geomorphological features are better delineated. Furthermore, because it takes into account the spatial correlation between neighborhood attributes, the landform map results less noisy (Vannamettee et al., 2014). Nevertheless, the computation time is longer than the RF. Instead, the RF produces scattered simulations since the model does not include spatial correlation. Since on geomorphological mapping isolated pixels are to avoid, having compacted polygons represent better the reality. Nevertheless, RF provides more information on the predictive power of the conditioning variables, making more effortless the variable choice. While the DS requires more testing.

Late Glacial deposits (class n° 6), glaciers (n° 7) and rock outcrops (n° 8) are the classes with the best positive predicted values ( $> 0.61$ ) and their characteristics play probably a central role into the simulation. Indeed, Late Glacial deposits are generally vegetated. In this case, NDVI is fundamental for the detection of this class. RGB bands of the aerial orthophotos are key factors for glaciers simulations. Instead, slope angle is decisive for rock outcrops / rock walls. The RF is particularly efficient in the simulation of classes n° 7 and 8, with PPVs higher than in the DS (respectively 0.62 and 0.57 in DS, 0.65 and 0.77 in RF). Conversely, the PPV of class n° 6 is higher with DS (0.78 vs 0.70).

Moderate PPVs are calculated for talus slopes (class n° 1) and for active-inactive rock glaciers, debris-covered glaciers and Little Ice Age moraine deposits (n° 2), but in both cases the DS has

better performances compared to the RF (respectively 0.54 and 0.45 in DS, 0.29 and 0.41 in RF). The moderate simulation performance of these two classes can be due to their morphology. Talus slopes are constituted by debris with a slope angle of 33-40° (Chandler, 1973; Francou and Manté, 1990). Due to grain size sorting, the size of debris increases towards the bottom of the slope. Instead, active-inactive rock glaciers, debris-covered glaciers and Little Ice Age moraine deposits are constituted by multi-dimensional debris and they present a large intra-variability on size, slope and shape. Despite these differences, both algorithms confuse the two classes, presenting zones of more difficult interpretation, probably because the predictor variables are not informative enough to make a clear distinction.

The lowest PPVs (< 0.13) are found for rockslides, landslides and relict rock glaciers (class n° 3), alluvial fans (n° 4) and alluvial plains (n° 5). The challenging simulation of alluvial fans is already shown by Veronesi and Hurni (2014). Indeed, the slope angle of this type of landform can vary naturally, but it also follows the land use change, especially at the bottom part of the valleys that are under anthropic influence. This is valid also for alluvial plains, which are subjected to changes on water flow, sediment contribution, and human activities (Gabbud et al., 2019). Consequently, they have highly variable morphology in time and space.

Regarding class n° 3, its intrinsic heterogeneity could be responsible of the low PPVs. Indeed, rockslides and landslides are characterized by chaotic deposits, with rock fragments, soil, and vegetated portions. Instead, relict rock glaciers have a more structured form, generally colonized by vegetation.

The second issue we faced is the selection of predictor variables. As shown by the mean decrease of the Gini index, the estimation is highly sensitive to the NDVI, slope, and the blue band. Roughness provided also additional information because some landforms have marked surface irregularities. This is the case of rock walls, which present high roughness values, compared to other more homogeneous landforms such as the glaciers. Conversely, flow accumulation has poor results. It was not expected because, defining the number of upstream cells based on a flow direction, this variable helps into identifying fluvial landforms such as alluvial fan and fluvial deposits.

The choice of the training location is also fundamental to obtain valid results. In fact, even if there are no strict guidelines on the size of the TI, it should contain a sufficient variety of spatial patterns and a representative distribution of landform classes in order to avoid sampling biases (Caers and Zhang, 2004). This requirement is important especially for DS that tends to underestimate rarely detected classes (Vannamettee et al., 2014). Finally, the spatial resolution must be high enough to correctly represent the spatial distribution of the patches for all classes, without incurring into overly long computational time, which can easily increase for DS.

## 4.5 Conclusion

In this research, we compared two semi-automatic classification methods, the first based on the Direct Sampling (DS) algorithm and the second on Random Forest (RF). The aim was to realize a Semi-Automated Geomorphological Map (SAGM) at the regional scale, using a pre-classified map to train the methods (training image, TI) and a study zone where the methods were tested (simulation grid, SG). To our knowledge, it was the first DS application to SAGM generation and the first RF application to simulate a multi-class variables for SAGM. Indeed, the categorical variable was organized on eight different morphogenetic classes.

Together with the geomorphological classification, we selected 13 environmental predictor variables in an alpine area located in the Western Swiss Alps. In this area, a classical geomorphological map was already available and was employed for validation. The selected TI was representative for the occurrence of all the geomorphological classes and the SG was chosen based on similarities with the TI.

Both methods gave similar results in accuracy, resulting appropriate techniques to map SAGMs. However, the map estimated using RF presented noisier spatial distribution of the classes, but the algorithm was more efficient in terms of computation time compared to DS. On the other hand, DS simulated more defined polygons but required more computational efforts. Some classes, such as the Late Glacial deposits, the glaciers and the rock outcrop areas, obtained high sensitivity and positive predictive values, highlighting the suitability of the employed methods for the realisation of geomorphological maps in alpine environment. Nonetheless, other classes as alluvial fans and alluvial plains were weakly detected, assessing that not all the landforms are appropriate to be classified with the proposed strategies and algorithm setup.

These results suggest that DS and RF are fairly accurate techniques to map SAGMs on regional scale. Despite the uncertainty related to some classes, which are not well represented on the TI, they can be successfully employed to elaborate SAGMs in analogue areas, and can provide detailed geomorphological maps for vegetation models or other applications. Nevertheless, the geomorphological classification employed in the current analysis should be improved in the future to enhance the model performance.

## 4.6 Acknowledgments

This research is developed in the framework of the project “Integrating spatial predictions of vegetation, soils, geomorphology and hydrology for improved assessment of ecosystem services under climate change”, supported by the Swiss National Science Foundation (project N° CR23I2\_162754).

## CHAPTER 5

### 5. Outcomes at larger temporal and spatial scale

#### 5.1 Microclimate monitoring

The monitoring of the ground surface temperature (GST), started on the summer of 2016 with the iButtons installed in many locations in the three focus sites, continued for an additional year until the end of the summer 2019. It was performed with the aim to obtain supplementary data to investigate the inter-annual variability of the microclimate and deepen the knowledge not only for plant life but also potentially for other environmental factors such as permafrost distribution.

The data from 1<sup>st</sup> of October 2018 to 30<sup>th</sup> of September 2019 in the 72 analysed plots are presented in Appendix 3, preceded by 2016-2017 (Appendix 1) and 2017-2018 (Appendix 2) data. In Table 5.1, the 2018-2019 data are regrouped following the cluster analysis on 5 groups, which identify the plots according to their floristic similarity. The empty plot n° 11 is not considered in the group classification.

**Table 5.1** - Environmental characteristics of the five vegetation groups (2018-2019 year). Mean values and standard deviations are reported. MGST: Mean Ground Surface Temperature [°C]; Tmax: mean maximum temperature [°C]; Tmin: mean minimum temperature [°C]; FDD: Freezing Degree Day [degree day]; GDD: Growing Degree Day [degree day]; GSL: Growing Season Length [day].

Group	MGST	Tmax	Tmin	FDD	GDD	GSL
1	3.4 ± 5.3	5.0 ± 7.7	2.3 ± 3.8	31 ± 39	1141 ± 138	85 ± 16
2	2.5 ± 4.8	3.9 ± 7.0	1.6 ± 3.3	84 ± 199	888 ± 307	63 ± 17
3	2.3 ± 4.2	3.4 ± 6.2	1.5 ± 2.9	25 ± 37	725 ± 215	57 ± 11
4	1.9 ± 4.3	3.1 ± 6.6	1.1 ± 2.8	69 ± 97	683 ± 121	50 ± 12
5	2.0 ± 4.9	3.7 ± 7.6	0.9 ± 3.3	219 ± 264	844 ± 230	68 ± 10

Six data loggers were lost or presented errors in the memory system and they could not be analysed (n° 40, 48, 49, 50, 56 and 59). Compared to the previous years, the data loggers recorded lower MGST and maximum temperatures (excepted for the group n° 1), but higher minimum temperature. Also Freezing Degree Day (FDD), Growing Degree Days (GDD) and Growing Season Length (GSL) globally had lower values, indicating a decrease in cold periods and a shorter growing season for vegetation. Autumn 2018 was generally warmer and drier compared to the 1981-2010 mean. Winter 2018-2019 had temperatures in average with the 1981-2010 mean, but more copious snow falls especially in December and January. Spring 2019 was in average with the 30-years mean during the first months, instead May was colder and with abundant precipitation, liquid in plains and solid in mountains. It allowed a longer permanence of snow cover and consequently a reduction of the GDDs and the GSL. Summer 2019 was hotter than the 30-years mean (data from Meteoswiss website).

During the monitored period, the minimum winter temperature was -10.19 °C (recorded on 20.11.2018, plot n° 63) and the maximum summer temperature was 24.44 °C (recorded on 24.07.2019, plot n° 80). Also for this year, the basal-Ripening Date (RD) was not measured for all data loggers because of lack of ground freezing period in some cases. Consequently, it was calculated only for 33 plots. In some plots, there was a short negative temperature period, followed by a rapid increasing to 0 °C in early winter (RD in December 2018 for plots n° 29, 46, 53, 54, 55 and 57); in the most part of the cases, RD was in spring, the latest on 26 June (plot n° 11). Melt-out Date was detected for all the data loggers: snow melt started in June (plot n° 52) and finished in August (plot n° 11), confirming that the snow season was longer during 2019.

The coldest areas pointed out with the FDD index are the same as reported in the previous years: on the rock glacier and on lateral morainic deposit on Les Martinets (plots n° 19 and 30), on the debris-covered glacier on Les Outans (plot n° 52) and at the Col des Perris Blancs, especially on the protalus rampart (plots n° 43, 44, 62, 63 and 76). At the plots n° 43, 44, 62 and 63, late winter temperatures below -3 °C were recorded attesting a possible presence of permafrost (Haeberli, 1973; Hoelzle et al., 1993; Ikeda and Matsuoka, 2006; Ishikawa, 2003).

The vegetation plots corresponding to groups 1 (pre-LIA sites characterized by late-successional species, belonging to *Poion alpinae*, *Rhododendro-Vaccinion*, *Elynion*, *Seslerion*, *Caricion firmae* and *Caricion curvulae*, according to Delarze et al., 2015) and 2 (debris plots with *Salix* sp. and characterized by high water availability) had the highest MGST (3.4 and 2.5 °C, respectively) and Tmax (5.0 and 3.9 °C, respectively) as in the previous years. The plots in the group 1 prove to be characterized by the warmest temperature, the lowest FDD and the longest GSL. The plots of groups 3 (debris plots of pre-LIA periods, with species belonging to *Thlaspion rotundifolii*, *Drabion hoppeanae*, *Cystopteridion* and *Potentillion*) and 4 (debris plots of post-LIA periods composed by species belonging to *Thlaspion rotundifolii* and *Drabion hoppeanae*) had the lowest FDD (25 and 69 degree days, respectively) and the shortest GSL (57 and 50 days, respectively), confirming partially the data of the Chapter 2. The plots in group 5 (plots characterized by species adapted to low temperature, belonging to *Androsacion alpinae* and *Thlaspion rotundifolii*) had the lowest Tmin (0.9 °C) and the highest FDD index (219 degree days), as in the 2016-2018 period. These data are compared to the data of the previous years 2016-2017 and 2017-2018 in Figure 5.1.

The 2018-2019 data confirms, therefore, the previous analysis reported in the Chapter 2, indicating how ground temperature is a fundamental factor for the alpine plant species.

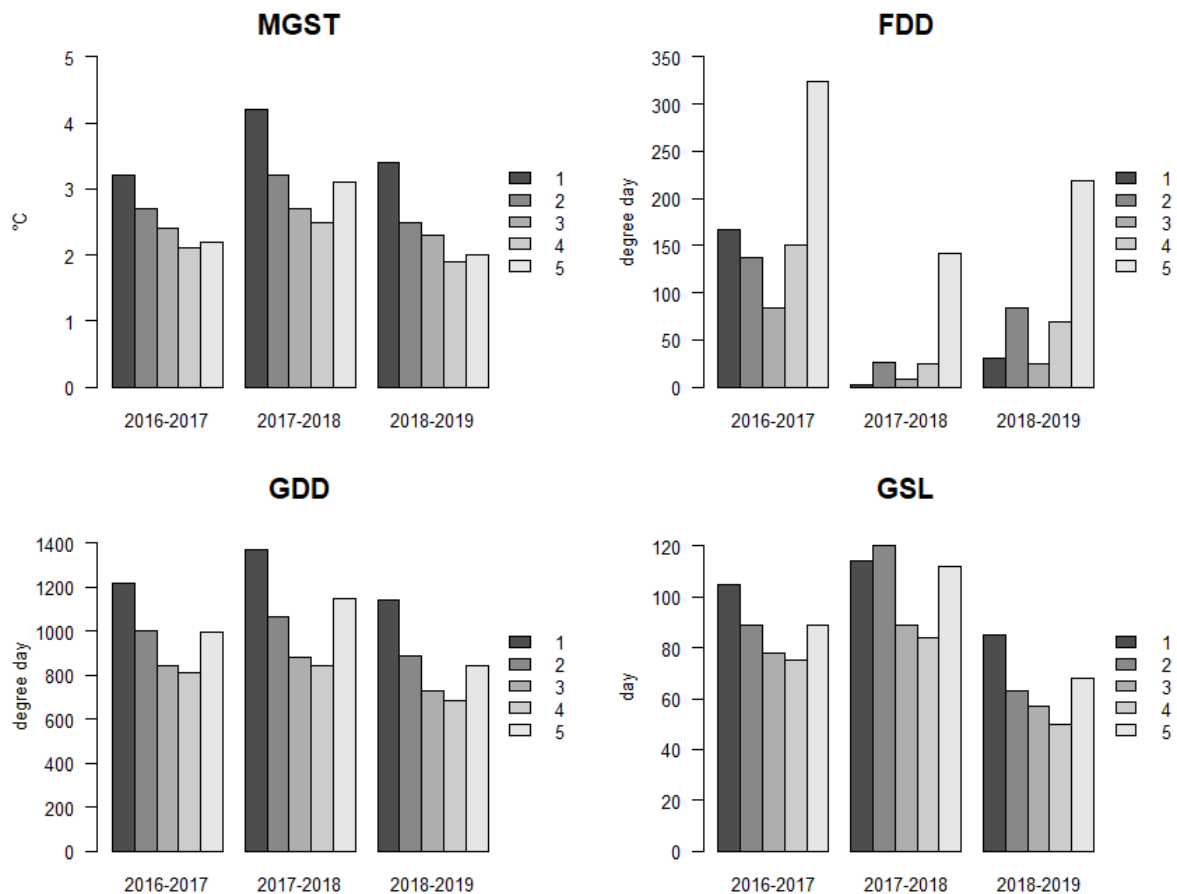


**Figure 5.1** - Comparison between the vegetation plots classified in 5 groups based on cluster analysis and the 3 years of ground thermal monitoring. MGST: Mean Ground Surface Temperature [°C]; FDD: Freezing Degree Day [degree day]; GDD: Growing Degree Day [degree day]; GSL: Growing Season Length [day].

## 5.2 Permafrost distribution in the Vaud Alps

Temperature data together with electrical resistivity tomography profiles and landform classification are important empirical elements to validate outputs coming from permafrost distribution models. In the framework of the present thesis and the IntegrAlp project, a permafrost model was applied in the Vaud Alps to identify the locations where permafrost could be possible and to employ it afterwards as predictor variable in SDMs. To this aim, the PERmafrost modelling with Machine Learning (PERMAL - Deluigi, 2018; Deluigi et al., 2017; Deluigi and Lambiel, 2012) was performed in collaboration with dr. Nicola Deluigi through Random Forest (RF) technique (Breiman, 2001) and the results are shown in Figure 5.2.



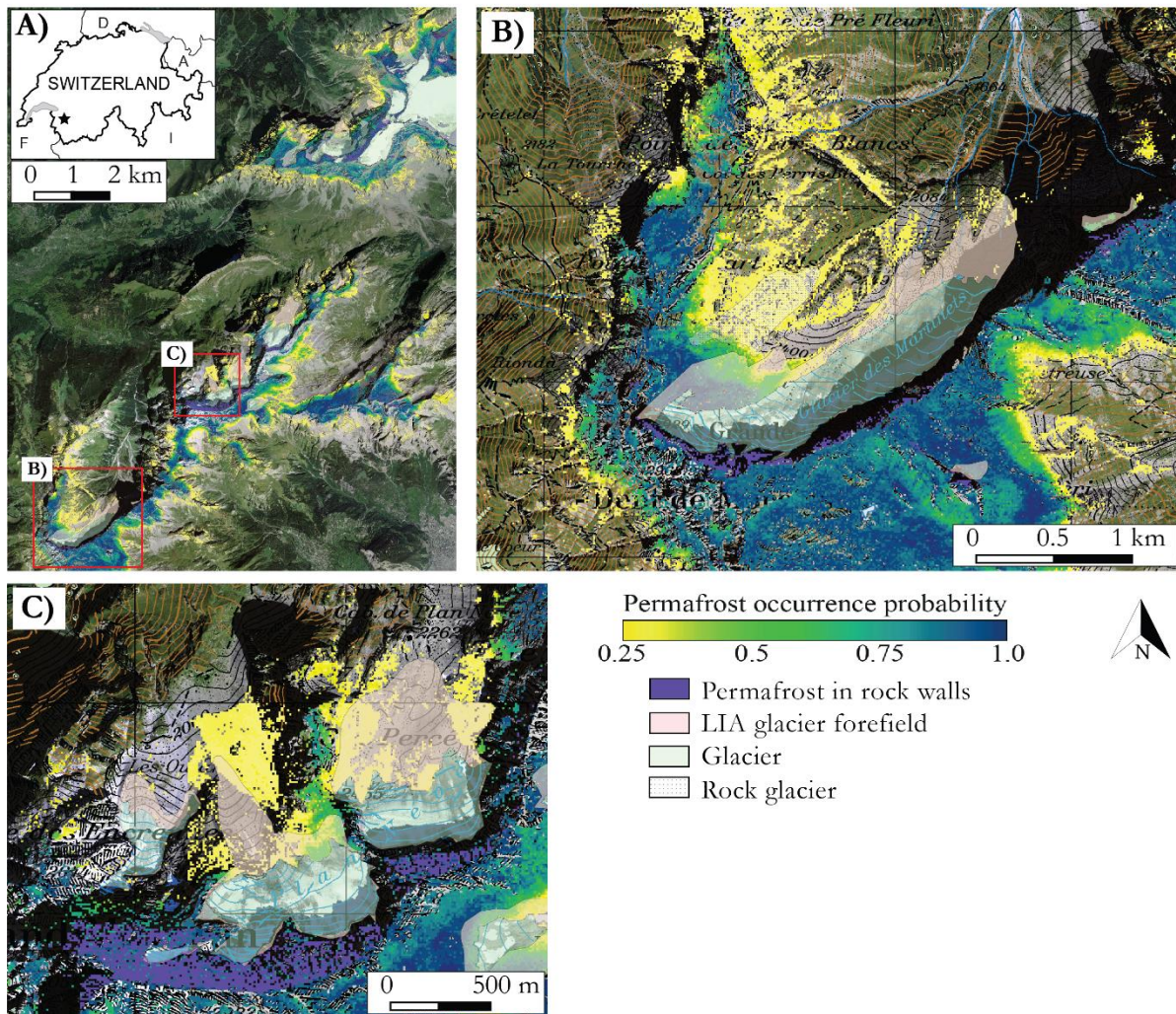


**Figure 5.2** - PERMAL probability of permafrost occurrence map elaborated through Random Forest classification for the Vaud Alps (A). Detailed focus on Les Martinets – Col des Perris Blancs (B) and Les Outans (C) sites.

PERMAL is a potential permafrost occurrence model showing permafrost probability on debris. The RF was trained with evidences of permafrost presence and absence coming from rock glacier inventories as well as geoelectrical and thermal data in the Western Valais Alps. These data were collected by the Universities of Lausanne and Fribourg since the mid-1990s and they constitute a large set of good-quality data. Furthermore, rock glacier inventory from the Vaud Alps was added to have representative data of the study region. Altitude, mean annual air temperature, aspect, terrain slope angle, potential incoming solar radiation, NDVI and planar, profile and combined terrain curvature indices were the environmental predictor variables used in the model (Figure 5.3). The spatial resolution of the dataset was set to a regular grid of 10 x 10 m. The RF model was replicated 10 times, setting  $n_{tree} = 300$  and  $m_{try} = 4$ . Mean OOB error of 10 repetitions was  $7.6 \pm 0.7 \%$  and Kappa was  $0.83 \pm 0.02$ , showing the robustness of the model. The PERMAL results in the mean of the repetitions. For more details see Deluigi (2018) and Deluigi et al. (2017). The permafrost occurrence in rock walls was added to the final permafrost map using the mean annual rock surface temperatures for the region of interest (Magnin et al., 2015).

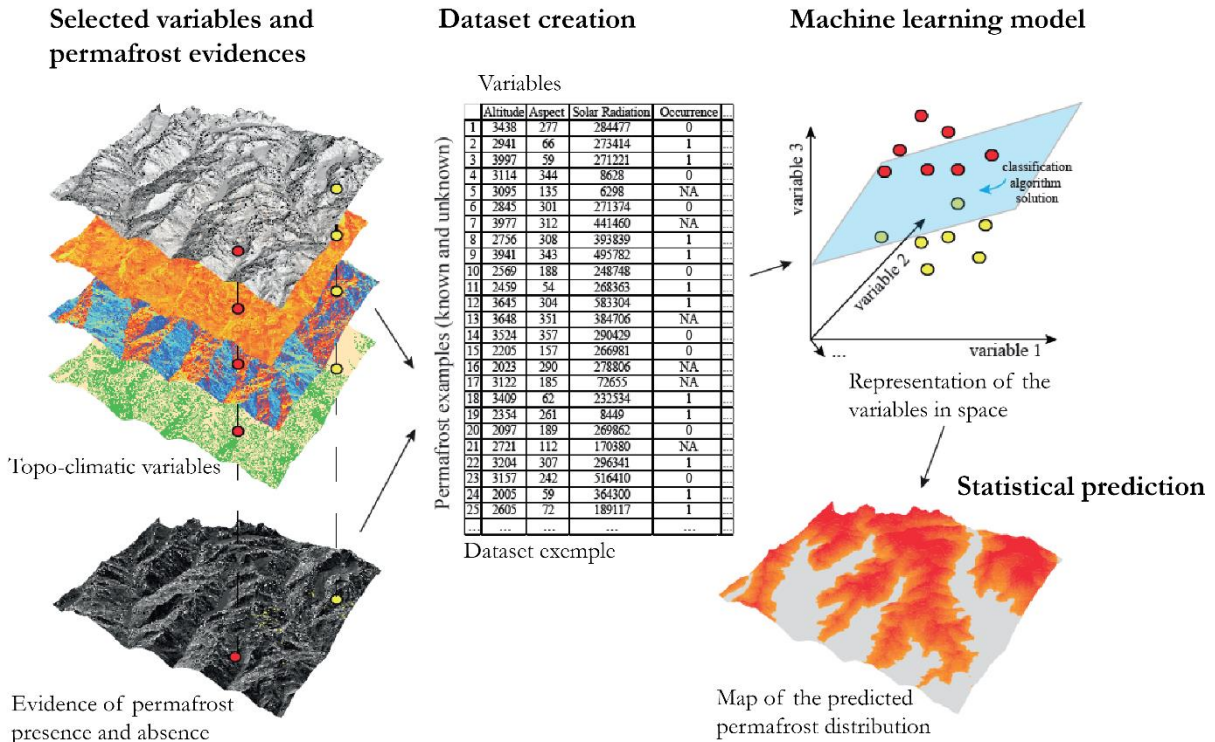


**Figure 5.3** - Workflow of the PERMAL modelling, from data collection to permafrost prediction. Modified from Deluigi (2018).

According to PERMAL, in the study area the permafrost is possible above 2000 m a.s.l. Regarding the local sites, on Les Martinets the permafrost is possible on the rock walls above the Martinets glacier, it presents low probabilities (0.25-0.5) below 2400 m a.s.l. and high probabilities (0.5-1) above 2400 m. In the area occupied by the rock glacier, probabilities are low, but they augment in the upper lobe of the rock glacier. This result is in accordance with the electrical resistivity tomography profile carried out in 2016 (see Chapter “2.8 Supplementary material”, Figure S1) and the negative winter temperatures (below  $-2^{\circ}\text{C}$ ) recorded during the monitoring period. PERMAL predicted high permafrost probabilities on the morainic deposit on the top of the catchment and in the area of the Col des Perris Blancs. Also these model results are in accordance with the recorded temperatures. In Les Outans focus site, permafrost is absent in the most part of the catchment, because of the low elevation, the presence of the debris-covered glacier and of Little Ice Age glacier deposits. Indeed, generally glacier ice excludes permafrost presence (French, 2007) and in the LIA glacier forefields, located in the periglacial belt, large portions of deposits are generally unfrozen (Bosson et al., 2015; Harris and Murton, 2005; Kneisel and Kääb, 2007).

Only in the eastern part of the debris slope, PERMAL indicates low probabilities (0.25-0.35) but the iButton temperatures did not record negative temperature during late winter, excluding consequently a possible presence of permafrost (Haeberli, 1973; Ishikawa, 2003). In this focus site, iButton temperatures present negative temperature only on the debris-covered glacier, where they can be directly influenced by the glacier ice presence. Instead, in the rock walls above the debris-

covered glacier and above the Plan N ev e glacier, model probabilities are higher, nonetheless physical data are not available to confirm the simulation.

### 5.3 Semi-automated geomorphological map in the Vaud Alps

The semi-automated techniques, employed to develop a Semi-automated Geomorphological Map (SAGM) on large scale in the Arolla valley (cf. Chapter 4), were applied afterwards in the study area of the IntegrAlp project. The purpose was to achieve a SAGM over the Vaud Alps and meet in this way the project deals. Among Direct Sampling (DS) and Random Forest (RF), the DS was selected as method for the simulation because it performs defined polygons compared to the RF, thanks to the spatial correlation between the attributes which are taken into account (Vannamettee et al., 2014). An elevation limit of 1500 m a.s.l. was fixed because the present thesis is focused on alpine environment.

The dataset composition and the approach design are based on the methodology reported in Chapter 4. The TI was kept in the Arolla valley, because the alpine landforms there present are representative of the new study area. The SG was composed with the same number of variables (cf. Table 4.1), defined on a regular grid with a spatial resolution of 20 m. The same approach with 100 realisations and the following mode calculation was performed. The resulting map is presented in Figure 5.4. Late Glacial deposits (class n o 6) cover extended areas, especially the zones at lower elevation, with extended forests and pasturelands (Figure 5.4a, c, and d). These areas have the highest probability values (Figure 5.4b). In the high elevation areas, the rock outcrops / rock walls (n o 8) and the glaciers (n o 7) are correctly simulated and present high probability values (0.7-1), except for the Martinets glacier (on the bottom-left part of the Figure 5.4a), which is confused with Late Glacial deposits in some portions. The classes n o 1 (talus slopes) and 2 (active-inactive rock glaciers, debris-covered glaciers and LIA moraine deposits) are extensively simulated around glaciers and rock walls, even if their uncertainty is high (probability values 0.2-0.6). The classes n o 3 (rockslides, landslides, relict rock glaciers), 4 (alluvial fans) and 5 (alluvial plains) are, instead, less represented spatially in the study area.

To provide a visual comparison between the SAGM and the ground reality, a zoom on the three focus sites (Les Martinets, Col des Perris Blancs and Les Outans) was carried out and the results are reported in Figure 5.5. A classical geomorphological map for the focus sites, carried out during the present thesis, was added to the figure to help in the comparison of the results. The geomorphological legend is organized in 8 classes, following the SAGM classification. According to SAGM results, in the Col des Perris Blancs area (Figure 5.5a, b and c) talus slopes and rock outcrops are the main detected landforms and they correspond to the landforms observed *in situ*. Some polygons of Late Glacial deposits are equally simulated in areas occupied by alpine grasslands. Instead, small polygons belonging to the class n o 2 (active-inactive rock glaciers, debris-covered glaciers and LIA moraine deposits) are delineated even if their occurrence is not detected. In the same way, an extended polygon belonging to the class n o 3 (rockslides, landslides, relict rock glaciers) is simulated, but in the reality only small portions of this area are constituted by rock falls/avalanche deposits; the others portions are grasslands, rock outcrop and alluvial fans. The



SAGM of Les Martinets (Figure 5.5a, b and c) is dominated by talus slopes, Late Glacial deposits, by limited portions of active-inactive rock glaciers, debris-covered glaciers and Little Ice Age moraine deposits, and by the glacier surrounded by high rock walls. Nevertheless, as described in the section “2.2.1 Study area” and as shown in Figure 5.5, the geomorphology appears more complex. Indeed the catchment is constituted by numerous morainic deposits dating back to the LIA and to older Holocene or Late Glacial periods, by a two-lobe rock glacier, by talus slopes and by a large area of rock fall/avalanche deposits, partially vegetated. The model uncertainty (see Figure 5.4b) could be connected to the fact that in this geographical limited area the geomorphological diversity is elevated and the topography is characterized by abrupt slope changes and heterogeneous roughness. Consequently, it results more challenging for the DS to identify landforms constituted by debris with different slopes, such as talus slopes or active-inactive rock glaciers and LIA moraine deposits. This problem was observed first in the SAGM for the Arolla Valley (see section “4.4 Discussion”). Furthermore, the high rock walls on Les Martinets create shadows in the underlying areas, the glacier in this case, causing color differences in the RGB bands that are interpreted as Late Glacial deposits by the DS.

The SAGM for Les Outans focus site (Figure 5.5d, e and f) presents mostly rock outcrops / rock walls that are correspondent to the reality, as well the Plan Nivé glacier, its moraines, and some portions of talus slopes. However, instead of the debris-covered glacier, the DS simulated erroneously a glacier in the upper section and Late Glacial deposit in the lower section. The last category is simulated as well as in some rock outcrop area to the left of the debris-covered glacier. These results are barely interpretable, probably they are due to variable's setting and to extremely restricted geographic area. The debris-covered glacier presents snow patches visibles also in the Figure 5.5f in its upper part that are interpreted as glacier, therefore the simulated Late Glacial deposits in the lower part are scarcely interpretable.

At lower elevation in Figure 5.5a and c, Late Glacial deposits are simulated correctly by the DS. Nevertheless, as highlighted in the previous paragraphs, the use of semi-automated technique, in this case the DS, resulted challenging to map geomorphological classes in such alpine environments and probably it requires to be refined.

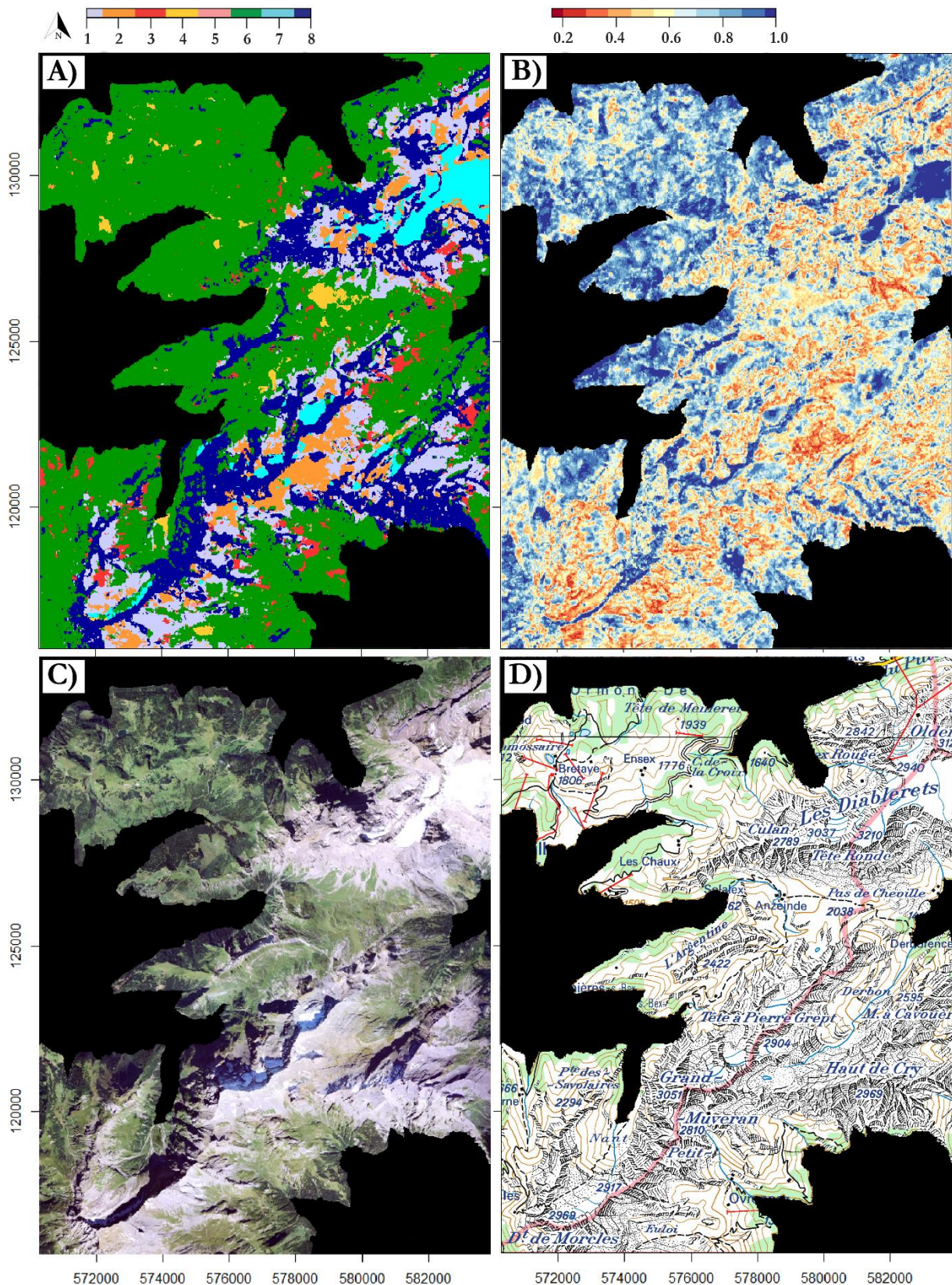
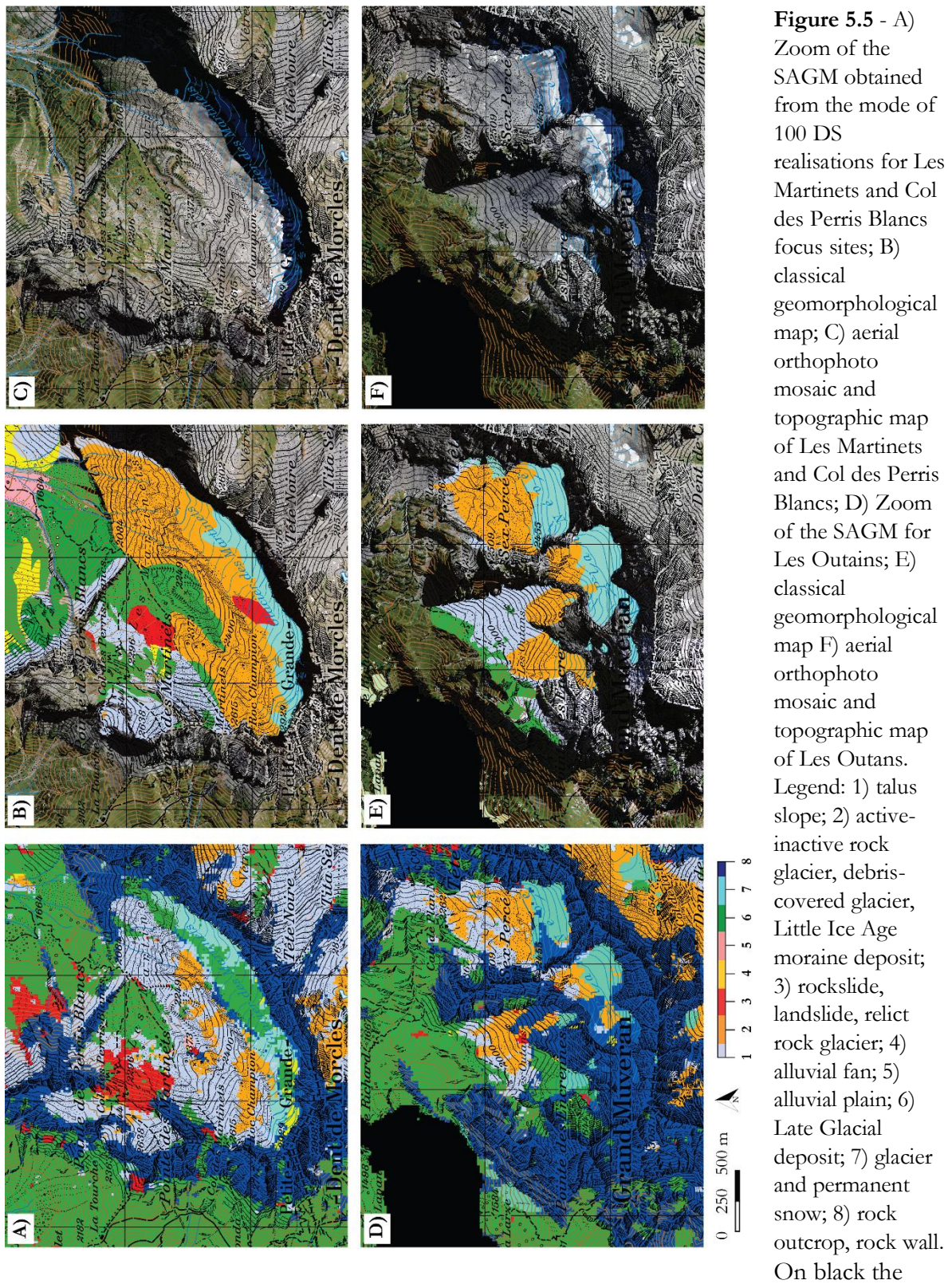


**Figure 5.4** - A) Semi-automated geomorphological map obtained from the mode of 100 DS realisations. Legend: 1) talus slope; 2) active-inactive rock glacier, debris-covered glacier, Little Ice Age moraine deposit; 3) rockslide, landslide, relict rock glacier; 4) alluvial fan; 5) alluvial plain; 6) Late Glacial deposit; 7) glacier and permanent snow; 8) rock outcrop, rock wall. On black the areas lower than 1500 m; B) uncertainty map



showing the frequency of detection of the class corresponding to the mode; C) aerial orthophoto mosaic; D) topographic map, SwissMapRaster © swisstopo (DV084371).



# CHAPTER 6

## 6. Synthesis and conclusions

### 6.1 General discussion

The alpine environments are subjected to heterogeneous processes that modify and shape the landscape, the ecosystem resources and the biota. Among the biota components, vegetation is highly susceptible to modifications under the ongoing climate change. Alpine vegetation has already exhibited the signals of the temperature warming especially on high altitude, with a consequent increase in species richness during the last century (e.g. Cannone et al., 2007; Stöckli et al., 2011) and an upward shift of plant species (Walther et al., 2005; Wipf et al., 2013). Consequently, especially under the actual climatic conditions, it becomes necessary to understand the relations between the vegetation and the other natural domains. The current instruments to study, monitor and predict these changes include investigations at local scale and generalization at regional scale, through Species Distribution Models (SDMs). These models need specific predictors which take into account the capacity to evaluate the relations between different domains.

In this perspective, the present thesis provided complementary knowledge about the influence of geomorphological processes on alpine vegetation at local scale, confirming previous studies (e.g., Gentili et al., 2013; Le Roux and Luoto, 2014) but also introducing novelties about dataset heterogeneity and the importance of the morphodynamics variable. In addition, new methodologies to provide geomorphic spatially-distributed data for the SDMs were developed, achieving the initial goals and supplying to the scientific community new instruments for the analysis of geomorphic-related variables. Furthermore, these results answered also to the research purposes of the IntegrAlp project. A synthesis figure of the main results is illustrated in Figure 6.1.



## RESEARCH QUESTION

How do geomorphic processes and landforms influence alpine vegetation communities?

## OBJECTIVES

- 1) Study of the fine scale effects of geomorphic processes on vegetation communities
- 2) Development of a methodology to map the debris size on extended surfaces
- 3) Implementation of semi-automated methods to perform a semi-automated geomorphological map

## RESULTS 1

Morphodynamics index and temperature indexes are key environmental factors for plant communities

## RESULTS 2

Using drone images and an existent debris size identification algorithm, the debris size distribution map is elaborated

## RESULTS 3

The Semi-Automated Geomorphological Map is performed with geostatistical and machine learning techniques

## OUTCOMES

- Morphodynamics index and geomorphic processes are important factors for vegetation development
- Grain size and geomorphological map as new geomorphic-predictors for SDMs

**Figure 6.1** - Conceptualization figure about the main outcomes of the present thesis in relation to the research objectives.

The first sub-objective was the study at local scale of the effects of geomorphic processes on alpine vegetation communities. Many studies discussed the relationships between plant composition and soil-topo-climatic variables on lowland in the Arctic or in mountain regions (e.g. Eichel et al., 2017; Gentili et al., 2013; le Roux and Luoto, 2014). Nonetheless, at high elevation few investigated the directly influence of Earth Surface Processes (ESPs), geomorphological heterogeneity and landform morphodynamics on plant communities. The Chapter 2 presented and discussed the data obtained from the 72 vegetation plots in Les Martinets, Les Outans and the Col des Perris Blancs sites, located in the Vaud Alps (1950-2550 m a.s.l.). The innovative aspect of this study was the selection of the plots, in order to ensure the representativeness of each geomorphological feature with all the types of vegetation cover, from pioneer plants with low percentage cover on debris to stable grasslands with high cover. The data about identified plant species in each vegetation plot are reported in Appendix 4. This research found out that the morphodynamics index, defining the frequency of disturbances, the surface movement and the soil structure of a surface, and the temperature indexes are key environmental factors for plant communities. In particular, the morphodynamics index provided important information about frequency of disturbances, landform stability, soil development and age of deposit. Among the temperature indexes, Growing



Degree Days (GDD) and Mean Ground Surface Temperature (MGST) were the most explicative predictors for species richness and species cover, confirming how temperature is an important control factor for vegetation development (Körner, 2003). This thesis section confirmed that the microclimate monitoring is essential not only to better understand the climatic parameters affecting the vegetation but also, as demonstrated in the section “5.1 Microclimate monitoring”, to analyse ground thermal conditions and infer permafrost presence. Such type of data together with geoelectrical surveys are suitable to validate permafrost models (see section “5.2 Permafrost distribution in the Vaud Alps”), developing an integrated approach and allowing reaching a deepened knowledge of alpine system.

Since the debris size is a significant factor influencing the growth of plant species (Eichel, 2019) and the ground thermal regime (Haebeli 1975, 2000), the development of a new methodological approach based on analysis of optical high-resolution imagery to map the debris size was essential. The methodology presented in the Chapter 3 is composed of four phases: 1) acquisition of high-resolution images through Unmanned Aerial Vehicle (UAV) survey and processing to obtain an orthomosaic, 2) debris size detection using the Basegrain algorithm (Detert and Weitbrecht, 2013; Detert and Weitbrecht, 2012), 3) validation and calibration of detected grains, and 4) Debris Size Distribution (DSD) map production starting from an object density map. The DSD map answers to the second sub-objective of the present thesis, allowing the identification of surfaces with small or large debris and providing a new predictor for SDMs. Indeed, the inclusion on the SDMs of predictor connected to geomorphological factors, disturbance factors and sediment size is lacking. The omission of similar predictors can be connected to data unavailability, due to the complexity to obtain this kind of data above extended surfaces (Mod et al., 2016). With the developed methodology, coupled with UAV technology, it is now possible to achieve a DSD map with accuracy and time efficiency and use it for models. Calibration showed strong correlation between the manually measured and automatically estimated grain size, encouraging the proposed approach. Furthermore, the proposed method can be exploited not only on mountain environments, but also on other environments where debris are visible and detectable by UAVs technology, such as deserts or river beds. This thesis section introduced a novelty in this research domain because the employed algorithm was originally designed to analyse grain size in river beds. With appropriate adaptations, now the implemented method allows deriving grain size map starting from images acquired in high mountain environment using UAVs. Furthermore, the UAVs are now easily accessible and their employment also in scientific disciplines is increasing, allowing more accurate and precise analysis through image acquisition.

The alpine vegetation is influenced by different factors, such as microclimatology, topography, ESPs, debris size, soil and nutrients (e.g. Buri et al., 2017; Körner, 2003; le Roux and Luoto, 2014), as highlighted in the previous chapters. Besides, the landform morphodynamic provides further informations about the type of vegetation cover (Cannone and Gerdol, 2003) and improves the performance of the Generalized Linear Models and the Generalized Additive Models for the species cover and species richness (see Chapter 2). Therefore, the landforms play a fundamental role in the study of plant communities. For this reason, the third sub-objective of the thesis was the development of a methodology with semi-automated techniques to elaborate a geomorphological map. As explained in the Chapter 4, classical geomorphological maps are time-consuming approaches, particularly for large areas. For this reason, automatic techniques are needed. However, to be efficient, they have to be guided by geomorphological expertise and, for this reason, they are called semi-automated. In this framework, two techniques based on geostatistics (the Direct Sampling – DS – Mariethoz et al., 2010) and on machine learning (the RF) were employed to achieve a Semi-Automated Geomorphological Map (SAGM). 12 environmental

predictor variables were selected to simulate the SAGM composed of 8 geomorphological classes. Both DS and RF provided similar results (model accuracy respectively 0.55 and 0.56), with some geomorphological classes correctly simulated and few ones (alluvial fans and alluvial plains) with weakly correspondence. Nevertheless, the methods proved to be fairly accurate to map SAGMs on mountain area at regional scale, because some classes present high uncertainty. In this research, for the first time the DS was employed in a simulation of a multi-class categorical variable and the RF, as well for the first time, was used to simulate eight different morphogenetic geomorphological classes, improving the current classifications (e.g. Veronesi and Hurni, 2014). The innovative developed methodology was afterwards applied in the Vaud Alps, to deal with the IntegrAlp project. To this aim, the DS was selected to simulate the SAGM in the study area because it provided a better visual performance, even if some misclassification are simulated in the results.

## 6.2 Conclusions and perspectives

The present thesis provided new results about the influence of the geomorphic characteristics on alpine vegetation and developed new methodologies to obtain regional scale geomorphic data. In particular the attention was focused on the implementation of techniques to elaborate debris size distribution and geomorphological maps, two significant variables for plant community investigations. First, the thesis demonstrated that landform morphodynamics and ground temperature indexes are the most explicative environmental variables of plant communities in alpine environments. Second, it developed a new methodology to generate a large scale debris size distribution map starting from UAV images. This methodology can be applied not only on alpine region but also in other environments where debris are easily detectable by UAVs. And third, it compared two semi-automatic classification methods, the geostatistical algorithm Direct Sampling and the machine learning algorithm Random Forest, to achieve a semi-automated geomorphological map, based on eight different morphogenetic classes, on large scale. These spatially-distributed data together with the morphodynamics index can be used as geomorphic predictors for successive employment in Species Distribution Models (SDMs) in order to improve the actual models and perform more accurate simulations about the future evolution of the vegetation. Indeed, it is an actual and important challenge to develop models that take into account not only soil-topo-climatic variables but also geomorphic-disturbance related variables, because of the ongoing climate change and its proclaimed effects on alpine vegetation communities.

The present work demonstrated also how it is crucial to carry out multidisciplinary researches, showing the relationships between the different natural domains. Nevertheless, other aspects, for example the biointeractions (micro and macrobiota), still need to be investigated more deeply to reach a more complete vision of the natural interactions. Consequently, in the context of climate change, it becomes relevant to investigate the bilateral interconnections between vegetation and environmental factors, as some biogeomorphological researches highlighted (Eichel et al., 2017; Osterkamp et al., 2012; Stallins, 2006). In this sense, it would be suitable to combine the physical approach adopted in the present thesis with studies focused on how vegetation acts actively on geomorphic dynamics, e.g. slope stabilisation, frost weathering action or nivation. The extension of the altitudinal range, to include also the nival belt and the sub-alpine and mountain vegetation,

with shrubs and trees, will allow having a global perception of the interconnections between plants and geomorphic processes and how these relationships change with elevation.

Being able to quantify and generalise over extended areas the impact of geomorphic dynamics on plant life will enable their selection as predictor variables in SDMs. The inclusion in the SDMs of the debris size distribution and the geomorphological classes as further predictor variables will solve some issues connected to the absence of “disturbance variables”, as illustrated by Mod et al. (2016). Furthermore, incorporating the results coming from the other modules of the IntegrAlp project will provide the right instruments to quantify and evaluate the effects of climate change on the ecosystem services. Thus, this project permitted to highlight how it is decisive to adopt a multidisciplinary approach, which acts on different research domains to collect a complete vision about all the natural elements interconnected between them.

The present thesis was just a single piece in the large puzzle of the environmental sciences. Researches about natural environments, such as the alpine areas, and about relationships between the numerous elements, which compose them (e.g. flora, fauna, hydric resources, atmosphere, cryosphere, soil, bedrock), are the keys to understand the Earth surface system. Indeed, these researches will allow us adopting the necessary strategies to contrast the effects of the ongoing climate change and preserving (or trying to preserve) the life system as we know it.

## 7. Bibliography

- Aalto J, Scherrer D, Lenoir J, Guisan A, Luoto M. 2018. Biogeophysical controls on soil-atmosphere thermal differences: implications on warming Arctic ecosystems. *Environmental Research Letters* 13 : 74003.
- Acquaotta F, Fratianni S, Garzena D. 2015. Temperature changes in the North-Western Italian Alps from 1961 to 2010. *Theoretical and Applied Climatology* 122 : 619–634.
- Adediran AO, Parcharidis I, Poscolieri M, Pavlopoulos K. 2004. Computer-assisted discrimination of morphological units on north-central Crete (Greece) by applying multivariate statistics to local relief gradients. *Geomorphology* 58 : 357–370.
- Alatalo JM, Jägerbrand AK, Molau U. 2016. Impacts of different climate change regimes and extreme climatic events on an alpine meadow community. *Scientific Reports* 6 : 21720.
- Allouche O, Tsoar A, Kadmon R. 2006. Assessing the accuracy of species distribution models: prevalence, kappa and the true skill statistic (TSS). *Journal of Applied Ecology* 43 : 1223–1232.
- Anderson R, Anderson S. 2010. *Geomorphology: The Mechanics and Chemistry of Landscapes*. Cambridge University Press: Cambridge
- Anderson SP, Drever JI, Frost CD, Holden P. 2000. Chemical weathering in the foreland of a retreating glacier. *Geochimica et Cosmochimica Acta* 64 : 1173–1189.
- Arenson L, Hoelzle M, Springman S. 2002. Borehole deformation measurements and internal structure of some rock glaciers in Switzerland. *Permafrost and Periglacial Processes* 13 : 117–135.
- Auer I et al. 2007. HISTALP—historical instrumental climatological surface time series of the Greater Alpine Region. *International journal of climatology* 27 : 17–46.
- Austin MP, Van Niel KP. 2011. Improving species distribution models for climate change studies: variable selection and scale. *Journal of Biogeography* 38 : 1–8.
- Badoux H. 1991. Aperçu géologique du Vallon de Nant. In *La Thomasia. Jardin alpin de Pont de Nant 1891-1991*. Musées et jardins botaniques cantonaux: Lausanne; 37–43.
- Ballantyne C, Harris C. 1994. *The Periglaciation of Great Britain*. Cambridge University Press
- Ballantyne CK. 2002. Paraglacial geomorphology. *Quaternary Science Reviews* 21 : 1935–2017.

- Baroni C, Armiraglio S, Gentili R, Carton A. 2007. Landform–vegetation units for investigating the dynamics and geomorphologic evolution of alpine composite debris cones (Valle dell’Avio, Adamello Group, Italy). *Geomorphology* 84 : 59–79.
- Baroni C, Gentili R, Armiraglio S. 2013. Vegetation Analysis on Composite Debris Cones. In *Dating Torrential Processes on Fans and Cones: Methods and Their Application for Hazard and Risk Assessment*, Schneuwly-Bollscheider Michelle, and Stoffel M, and Rudolf-Miklau Florian (eds). Springer Netherlands: Dordrecht; 187–201.
- Barsch D. 1996. Rock glaciers. Indicators for the Present and Former Geoecology in High Mountain Environments. Springer, Berlin.
- Barsch D. 2012. Rockglaciers: indicators for the present and former geoecology in high mountain environments. Springer Science & Business Media.
- Batten P. 2001. A new approach for landscape mapping, in: *Proceedings of the 6th International Conference on Geocomputation*. University of Queensland, Brisbane, Australia.
- Béguin C, Progin Sonney M, Vonlanthen M. 2009. Le cortège floristique des sols polygonaux dans les Alpes valaisannes. *Bulletin de la Murithienne* 126 : 47–51.
- Belgiu M, Drăguț L. 2016. Random forest in remote sensing: A review of applications and future directions. *ISPRS Journal of Photogrammetry and Remote Sensing* 114 : 24–31.
- Beniston M et al. 2018. The European mountain cryosphere: a review of its current state, trends, and future challenges. *The Cryosphere* 12 : 759–794.
- Beniston M. 2005. Mountain climates and climatic change: an overview of processes focusing on the European Alps. *Pure and Applied Geophysics* 162 : 1587–1606.
- Benoit L, Gourdon A, Vallat R, Irrazaval I, Gravey M, Lehmann B, Prasicek G, Gräff D, Herman F, Mariethoz G. 2019. A high-resolution image time series of the Gorner Glacier – Swiss Alps – derived from repeated unmanned aerial vehicle surveys. *Earth Syst. Sci. Data* 11 : 579–588.
- Berger C, McArdell BW, Schlunegger F. 2011. Sediment transfer patterns at the Illgraben catchment, Switzerland: Implications for the time scales of debris flow activities. *Geomorphology* 125 : 421–432.
- Beucher S. 1979. Use of watersheds in contour detection, in: *Proceedings of the International Workshop on Image Processing*. CCETT.
- Bilașco Ș, Roșca S, Petrea D, Vescan I, Fodorean I, Filip S. 2019. 3D Reconstruction of Landslides for the Acquisition of Digital Databases and Monitoring Spatiotemporal Dynamics of Landslides Based on GIS Spatial Analysis and UAV Techniques. *Spatial Modeling in GIS and R for Earth and Environmental Sciences* : 451–465.
- Björk RG, Molau U. 2007. Ecology of alpine snowbeds and the impact of global change. *Arctic, Antarctic, and Alpine Research* 39 : 34–43.
- Blasone G, Cavalli M, Marchi L, Cazorzi F. 2014. Monitoring sediment source areas in a debris-flow catchment using terrestrial laser scanning. *CATENA* 123 : 23–36.
- Bocco G, Mendoza M, Velázquez A. 2001. Remote sensing and GIS-based regional geomorphological mapping - a tool for land use planning in developing countries. *Geomorphology* 39 : 211–219.
- Boeckli L, Brenning A, Gruber S, Noetzli J. 2012. Permafrost distribution in the European Alps: calculation and evaluation of an index map and summary statistics. *The Cryosphere* 6 : 807–820.

- Bosson J-B, Deline P, Bodin X, Schoeneich P, Baron L, Gardent M, Lambiel C. 2015. The influence of ground ice distribution on geomorphic dynamics since the Little Ice Age in proglacial areas of two cirque glacier systems. *Earth Surface Processes and Landforms* 40 : 666–680.
- Bouzillé J-B. 2007. *Gestion des habitats naturels et biodiversité. Concepts, méthodes et démarches.* Tec & Doc Lavoisier: Paris
- Braun J. 1913. Die Vegetationsverhältnisse der Schneestufe in den Rätisch-Lepontischen Alpen. Ein Bild des Pflanzenlebens an seinen äussersten Grenzen. *Neue Denkschriften der Schweizerischen Naturforschenden Gesellschaft* 48 : 1–347.
- Braun-Blanquet J. 1932. *Plant sociology; the study of plant communities.* McGraw-Hill: New York and London
- Bray R, Curtis J. 1957. An ordination of the upland forest communities of southern Wisconsin. *Ecological Monographs* 27 : 325–349.
- Breiman L. 2001. Random Forests. *Machine Learning* 45 : 5–32.
- Brenning A, Grasser M, Friend DA. 2007. Statistical estimation and generalized additive modeling of rock glacier distribution in the San Juan Mountains, Colorado, United States. *Journal of Geophysical Research: Earth Surface* 112
- Brenning A. 2005. Spatial prediction models for landslide hazards: review, comparison and evaluation. *Nat. Hazards Earth Syst. Sci.* 5 : 853–862.
- Brown DG, Lusch DP, Duda KA. 1998. Supervised classification of types of glaciated landscapes using digital elevation data. *Geomorphology* 21 : 233–250.
- Burga CA, Frauenfelder R, Ruffet J, Hoelzle M, Käab A. 2004. Vegetation on Alpine rock glacier surfaces: a contribution to abundance and dynamics on extreme plant habitats. *Flora - Morphology, Distribution, Functional Ecology of Plants* 199 : 505–515.
- Burga CA, Krüsi B, Egli M, Wernli M, Elsener S, Ziefle M, Fischer T, Mavris C. 2010. Plant succession and soil development on the foreland of the Morteratsch glacier (Pontresina, Switzerland): Straight forward or chaotic? *Flora - Morphology, Distribution, Functional Ecology of Plants* 205 : 561–576.
- Buri A, Cianfrani C, Pinto-Figueroa E, Yashiro E, Spangenberg JE, Adatte T, Verrecchia E, Guisan A, Pradervand J-N. 2017. Soil factors improve predictions of plant species distribution in a mountain environment. *Progress in Physical Geography: Earth and Environment* 41 : 703–722.
- Buri A, Grand S, Yashiro E, Adatte T, Spangenberg J, Pinto-Pigueroa E, Verrecchia E, Guisan A. 2020. What are the most crucial soil variables for predicting the distribution of mountain plant species? A comprehensive study in the Swiss Alps. *Journal of Biogeography*, in press.
- Buscombe D, Rubin DM, Warrick JA. 2010. A universal approximation of grain size from images of noncohesive sediment. *Journal of Geophysical Research: Earth Surface* 115
- Butler DR. 1995. *Zoogeomorphology: animals as geomorphic agents.* Cambridge University Press
- Caers J, Zhang T. 2004. Multiple-point geostatistics: a quantitative vehicle for integrating geologic analogs into multiple reservoir models. In *Integration of Outcrop and Modern Analogs in Reservoir Modeling*, Gramer M, Harris P, and Eberli G (eds). Association of Petroleum Geologist Memoir; 383–394.
- Cannone N, Diolaiuti G, Guglielmin M, Smiraglia C. 2008. Accelerating climate change impacts on alpine glacier forefield ecosystems in the European Alps. *Ecological Applications* 18 : 637–648.

- Cannone N, Gerdol R. 2003. Vegetation as an ecological indicator of surface instability in rock glaciers. *Arctic, Antarctic, and Alpine Research* 35 : 384–390.
- Cannone N, Sgorbati S, Guglielmin M. 2007. Unexpected impacts of climate change on alpine vegetation. *Frontiers in Ecology and the Environment* 5 : 360–364.
- Carbonneau PE, Lane SN, Bergeron NE. 2004. Catchment-scale mapping of surface grain size in gravel bed rivers using airborne digital imagery. *Water resources research* 40
- Carrivick JL, Chase SE. 2011. Spatial and temporal variability of annual glacier equilibrium line altitudes in the Southern Alps, New Zealand. *New Zealand Journal of Geology and Geophysics* 54 : 415–429.
- Carrivick JL, Geilhausen M, Warburton J, Dickson NE, Carver SJ, Evans AJ, Brown LE. 2013. Contemporary geomorphological activity throughout the proglacial area of an alpine catchment. *Geomorphology* 188 : 83–95.
- Catani F, Lagomarsino D, Segoni S, Tofani V. 2013. Landslide susceptibility estimation by random forests technique: sensitivity and scaling issues. *Nat. Hazards Earth Syst. Sci.* 13 : 2815–2831.
- Cavalli M, Marchi L. 2008. Characterisation of the surface morphology of an alpine alluvial fan using airborne LiDAR. *Nat. Hazards Earth Syst. Sci.* 8 : 323–333.
- Cavalli M, Tarolli P, Marchi L, Dalla Fontana G. 2008. The effectiveness of airborne LiDAR data in the recognition of channel-bed morphology. *CATENA* 73 : 249–260.
- Chan JC-W, Paelinckx D. 2008. Evaluation of Random Forest and Adaboost tree-based ensemble classification and spectral band selection for ecotope mapping using airborne hyperspectral imagery. *Remote Sensing of Environment* 112 : 2999–3011.
- Chandler RJ. 1973. The Inclination of Talus, Arctic Talus Terraces, and Other Slopes Composed of Granular Materials. *The Journal of Geology* 81 : 1–14.
- Chen X, An S, Inouye DW, Schwartz MD. 2015. Temperature and snowfall trigger alpine vegetation green-up on the world's roof. *Global Change Biology* 21 : 3635–3646.
- Christiansen HH. 1998. Nivation forms and processes in unconsolidated sediments, NE Greenland. *Earth Surface Processes and Landforms: The Journal of the British Geomorphological Group* 23 : 751–760.
- Church M, Ryder J. 1972. Paraglacial Sedimentation: A Consideration of Fluvial Processes Conditioned by Glaciation. *GSA Bulletin* 83 : 3059–3072.
- Cianfrani C, Buri A, Verrecchia E, Guisan A. 2018. Generalizing soil properties in geographic space: Approaches used and ways forward. *Minasny B (ed). PLOS ONE* 13 : e0208823.
- Cignetti M, Godone D, Wrzesniak A, Giordan D. 2019. Structure from Motion Multisource Application for Landslide Characterization and Monitoring: The Champlas du Col Case Study, Sestriere, North-Western Italy. *Sensors* 19
- Clarke K. 1993. Non-parametric multivariate analyses of changes in community structure. *Australian Journal of Ecology* 18 : 117–143.
- Cohen J. 1960. A Coefficient of Agreement for Nominal Scales. *Educational and Psychological Measurement* 20 : 37–46.
- Colombo N, Giaccone E, Paro L, Buffa G, Fratianni S. 2016. The recent transition from glacial to periglacial environment in a high altitude alpine basin (Sabbione basin, north-western Italian Alps).

- Preliminary outcomes from a multidisciplinary approach. *Geografia Fisica e Dinamica Quaternaria* 39 : 21–36.
- Connell JH. 1978. Diversity in tropical rain forests and coral reefs. *Science* 199 : 1302–1310.
- Cooper EJ, Alsos IG, Hagen D, Smith FM, Coulson SJ, Hodkinson ID. 2004. Plant recruitment in the High Arctic: Seed bank and seedling emergence on Svalbard. *Journal of Vegetation Science* 15 : 115–124.
- Corenblit D, Baas ACW, Bornette G, Darrozes J, Delmotte S, Francis RA, Gurnell AM, Julien F, Naiman RJ, Steiger J. 2011. Feedbacks between geomorphology and biota controlling Earth surface processes and landforms: A review of foundation concepts and current understandings. *Earth-Science Reviews* 106 : 307–331.
- Corenblit D, Steiger J. 2009. Vegetation as a major conductor of geomorphic changes on the Earth surface: toward evolutionary geomorphology. *Earth Surface Processes and Landforms* 34 : 891–896.
- Cossart E. 2014. Des sources sédimentaires à l'exutoire: un problème de connectivité? Université Blaise Pascal-Clermont 2
- Crawley MJ. 2007. Generalized linear models. *The R book* : 511–526.
- Cutler DR, Edwards Jr. TC, Beard KH, Cutler A, Hess KT, Gibson J, Lawler JJ. 2007. Random Forests for Classification in Ecology. *Ecology* 88 : 2783–2792.
- Dagasan Y, Erten O, Renard P, Straubhaar J, Topal E. 2019. Multiple-point statistical simulation of the ore boundaries for a lateritic bauxite deposit. *Stochastic Environmental Research and Risk Assessment* 33 : 865–878.
- Dall'Asta E, Forlani G, Roncella R, Santise M, Diotri F, di Cella UM. 2017. Unmanned Aerial Systems and DSM matching for rock glacier monitoring. *ISPRS Journal of Photogrammetry and Remote Sensing* 127 : 102–114.
- de Vries LM, Carrera J, Falivene O, Gratacós O, Slooten LJ. 2008. Application of Multiple Point Geostatistics to Non-stationary Images. *Mathematical Geosciences* 41 : 29.
- Delaloye R, Lambiel C. 2005. Evidence of winter ascending air circulation throughout talus slopes and rock glaciers situated in the lower belt of alpine discontinuous permafrost (Swiss Alps). *Norsk Geografisk Tidsskrift - Norwegian Journal of Geography* 59 : 194–203.
- Delarze R, Gonseth Y, Eggenberg S, Vust M. 2015. Guide des milieux naturels de Suisse. Ecologie, menaces, espèces caractéristiques . 3rd ed. Rossolis: Bussigny
- Deluigi N, Lambiel C, Kanevski M. 2017. Data-driven mapping of the potential mountain permafrost distribution. *Science of The Total Environment* 590–591 : 370–380.
- Deluigi N, Lambiel C. 2012. PERMAL: a machine learning approach for alpine permafrost distribution modeling. Graf C (ed). *Mattertal - ein tal in bewegung. Jahrestagung der schweizerischen geomorphologischen gesellschaft* 4 : 47–62.
- Deluigi N. 2018. Data-driven analysis and mapping of the potential distribution of mountain permafrost, University of Lausanne
- Dembélé M, Oriani F, Tumbulto J, Mariéthoz G, Schaepli B. 2019. Gap-filling of daily streamflow time series using Direct Sampling in various hydroclimatic settings. *Journal of Hydrology* 569 : 573–586.



- Dent D, Young A. 1981. Soil survey and land evaluation. . George Allen & Unwin: London
- Detert M, Weitbrecht V. 2012. Automatic object detection to analyse the geometry of gravel grains – a free stand-alone tool. In *River Flow*, Murillo (ed). Taylor & Francis Group: London; 595–600.
- Detert M, Weitbrecht V. 2013. User guide to gravelometric image analysis by BASEGRAIN. In *Advances in River Sediment Research*, Fukuoka et al (ed). Taylor & Francis Group: London; 1789–1796.
- Dormann CF et al. 2013. Collinearity: a review of methods to deal with it and a simulation study evaluating their performance. *Ecography* 36 : 27–46.
- Dubuis A, Giovanettina S, Pellissier L, Pottier J, Vittoz P, Guisan A. 2013. Improving the prediction of plant species distribution and community composition by adding edaphic to topoclimatic variables. *Journal of Vegetation Science* 24 : 593–606.
- Dullinger S et al. 2012. Extinction debt of high-mountain plants under twenty-first-century climate change. *Nature Climate Change* 2 : 619.
- Dutoit A. 1983. La végétation de l'étage subalpin du vallon de Nant. Section protection de la nature et des sites et conservation de la faune du Canton de Vaud: Lausanne
- Egli M, Mirabella A, Sartori G, Zanelli R, Bischof S. 2006. Effect of north and south exposure on weathering rates and clay mineral formation in Alpine soils. *CATENA* 67 : 155–174.
- Eichel J, Corenblit D, Dikau R. 2016. Conditions for feedbacks between geomorphic and vegetation dynamics on lateral moraine slopes: a biogeomorphic feedback window. *Earth Surface Processes and Landforms* 41 : 406–419.
- Eichel J, Draebing D, Klingbeil L, Wieland M, Eling C, Schmidlein S, Kuhlmann H, Dikau R. 2017. Solifluction meets vegetation: the role of biogeomorphic feedbacks for turf-banked solifluction lobe development. *Earth Surface Processes and Landforms* 42 : 1623–1635.
- Eichel J. 2019. Vegetation Succession and Biogeomorphic Interactions in Glacier Forelands. In *Geomorphology of Proglacial Systems: Landform and Sediment Dynamics in Recently Deglaciated Alpine Landscapes*, Heckmann T and Morche D (eds). Springer International Publishing: Cham; 327–349.
- Ellenberg H. 1996. *Vegetation Mitteleuropas mit den Alpen: in ökologischer, dynamischer und historischer Sicht*. UTB: Stuttgart
- Erschbamer B, Niederfringer Schlag R, Winkler E. 2008. Colonization processes on a central Alpine glacier foreland. *Journal of Vegetation Science* 19 : 855–862.
- Erschbamer B. 2007. Winners and losers of climate change in a central alpine glacier foreland. *Arctic, Antarctic, and Alpine Research* 39 : 237–244.
- Evans IS. 2012. Geomorphometry and landform mapping: What is a landform? *Geomorphology* 137 : 94–106.
- Francou B, Manté C. 1990. Analysis of the segmentation in the profile of alpine talus slopes. *Permafrost and Periglacial Processes* 1 : 53–60.
- Franklin J. 2010. *Mapping species distributions: spatial inference and prediction*. Cambridge University Press
- French HM. 2007. *The periglacial environment*. 3rd ed. John Wiley & Sons: Chichester

- Fugazza D, Scaioni M, Corti M, D'Agata C, Azzoni RS, Cernuschi M, Smiraglia C, Diolaiuti GA. 2018. Combination of UAV and terrestrial photogrammetry to assess rapid glacier evolution and map glacier hazards. *Nat. Hazards Earth Syst. Sci.* 18 : 1055–1071.
- Füssel H-M et al. 2017. Climate change, impacts and vulnerability in Europe 2016-An indicator-based report. European Environment Agency (EEA) Report No 1.
- Gabbud C, Robinson C, Lane S. 2019. Sub-basin and temporal variability of macroinvertebrate assemblages in Alpine streams: when and where to sample? *Hydrobiologia* 830 : 179–200.
- Garamvoelgyi A, Hufnagel L. 2013. Impacts of climate change on vegetation distribution no. 1 climate change induced vegetation shifts in the palearctic region. *Appl. Ecol. Environ. Res* 11 : 79–122.
- Gehrig-Fasel J, Guisan A, Zimmermann NE. 2007. Tree line shifts in the Swiss Alps: Climate change or land abandonment? *Journal of Vegetation Science* 18 : 571–582.
- Gentili R, Armiraglio S, Rossi G, Sgorbati S, Baroni C. 2010. Floristic patterns, ecological gradients and biodiversity in the composite channels (Central Alps, Italy). *Flora - Morphology, Distribution, Functional Ecology of Plants* 205 : 388–398.
- Gentili R, Armiraglio S, Sgorbati S, Baroni C. 2013. Geomorphological disturbance affects ecological driving forces and plant turnover along an altitudinal stress gradient on alpine slopes. *Plant Ecology* 214 : 571–586.
- Gharari S, Hrachowitz M, Fenicia F, Savenije HHG. 2011. Hydrological landscape classification: investigating the performance of HAND based landscape classifications in a central European meso-scale catchment. *Hydrol. Earth Syst. Sci.* 15 : 3275–3291.
- Giaccone E, Luoto M, Vittoz P, Guisan A, Mariéthoz G, Lambiel C. 2019. Influence of microclimate and geomorphological factors on alpine vegetation in the Western Swiss Alps. *Earth Surface Processes and Landforms* 44 : 3093–3107.
- Giaccone E, Mariéthoz G, Lambiel C. 2016. Interactions between geomorphology and vegetation in the Vaud Alps: first investigations. *Abstract Volume 14th Swiss Geoscience Meeting*, 10 : 369–370.
- Gilbert G. 1877. Report on the Geology of the Henry Mountains. US Government Printing Office: Washington, DC
- Gilli A, Anselmetti FS, Glur L, Wirth SB. 2013. Lake Sediments as Archives of Recurrence Rates and Intensities of Past Flood Events. In *Dating Torrential Processes on Fans and Cones: Methods and Their Application for Hazard and Risk Assessment*, Schneuwly-Bollschweiler M, Stoffel M, and Rudolf-Miklau F (eds). Springer Netherlands: Dordrecht; 225–242.
- Gobat J-M, Aragno M, Matthey W. 2010. *Le sol vivant. Bases de pédologie - Biologie des sols*. 3rd ed. Presses polytechniques et universitaires romandes: Lausanne
- Gobbi M, Ballarin F, Compostella C, Lencioni V, Seppi R, Tampucci D, Caccianiga M. 2014. Physical and biological features of an active rock glacier in the Italian Alps. *The Holocene* 24 : 1624–1631.
- Gobiet A, Kotlarski S, Beniston M, Heinrich G, Rajczak J, Stoffel M. 2014. 21st century climate change in the European Alps—A review. *Science of The Total Environment* 493 : 1138–1151.
- Gorbushina AA. 2007. Life on the rocks. *Environmental microbiology* 9 : 1613–1631.

- Gottfried M et al. 2012. Continent-wide response of mountain vegetation to climate change. *Nature Climate Change* 2 : 111.
- Graham DJ, Reid I, Rice SP. 2005a. Automated sizing of coarse-grained sediments: image-processing procedures. *Mathematical Geology* 37 : 1–28.
- Graham DJ, Rice SP, Reid I. 2005b. A transferable method for the automated grain sizing of river gravels. *Water Resources Research* 41 : W07020.
- Grand S, Rubin A, Verrecchia EP, Vittoz P. 2016. Variation in Soil Respiration across Soil and Vegetation Types in an Alpine Valley. Araujo WL (ed). *PLOS ONE* 11 : e0163968.
- Gravey M, Rasera LG, Mariethoz G. 2019. Analogue-based colorization of remote sensing images using textural information. *ISPRS Journal of Photogrammetry and Remote Sensing* 147 : 242–254.
- Grêt-Regamey A, Walz A, Bebi P. 2008. Valuing ecosystem services for sustainable landscape planning in Alpine regions. *Mountain Research and Development* 28 : 156–166.
- Grohmann CH, Smith MJ, Riccomini C. 2011. Multiscale Analysis of Topographic Surface Roughness in the Midland Valley, Scotland. *IEEE Transactions on Geoscience and Remote Sensing* 49 : 1200–1213.
- Gruber S, Hoelzle M. 2008. The cooling effect of coarse blocks revisited: a modeling study of a purely conductive mechanism. 557–5611 pp.
- Gubler S, Fiddes J, Keller M, Gruber S. 2011. Scale-dependent measurement and analysis of ground surface temperature variability in alpine terrain. *The Cryosphere* 5 : 431–443.
- Guisan A et al. 2013. Predicting species distributions for conservation decisions. *Ecology Letters* 16 : 1424–1435.
- Guisan A, Edwards TC, Hastie T. 2002. Generalized linear and generalized additive models in studies of species distributions: setting the scene. *Ecological Modelling* 157 : 89–100.
- Guisan A, Theurillat J-P, Kienast F. 1998. Predicting the Potential Distribution of Plant Species in an Alpine Environment. *Journal of Vegetation Science* 9 : 65–74.
- Guisan A, Zimmermann NE. 2000. Predictive habitat distribution models in ecology. *Ecological Modelling* 135 : 147–186.
- Haerberli W, Beniston M. 1998. Climate change and its impacts on glaciers and permafrost in the Alps. *Ambio*: 258–265.
- Haerberli W. 1973. Die Basis-Temperatur der winterlichen Schneedecke als möglicher Indikator für die Verbreitung von Permafrost in den Alpen. *Zeitschrift für Gletscherkunde und Glazialgeologie* 9 : 221–227.
- Haerberli W. 1975. Untersuchungen zur Verbreitung von Permafrost zwischen Flüelapass and Piz Grialetsch (Graubünden). *Mitteilungen der Versuchsanstalt für Wasserbau, Hydrologie und Glaziologie, Eidgenössische Technische Hochschule*
- Haerberli W. 1985. Creep of mountain permafrost: internal structure and flow of alpine rock glaciers. *Mitteilungen der Versuchsanstalt für Wasserbau, Hydrologie und Glaziologie an der ETH Zurich* 77
- Haerberli W. 2000. Modern Research Perspectives Relating to Permafrost Creep and Rock Glaciers: A Discussion. *Permafrost and Periglacial Processes* 11 : 290–293.

- Hair Jr J, Black W, Babin B, Anderson R. 2014. *Multivariate Data Analysis*. Pearson New International Edition
- Haneberg W, Creighton A, Medley E, Jonas D. 2005. Use of LiDAR to assess slope hazards at the Lihir gold mine, Papua New Guinea
- Harris C, Arenson LU, Christiansen HH, Etzelmüller B, Frauenfelder R, Gruber S, Haeberli W, Hauck C, Hoelzle M, Humlum O. 2009. Permafrost and climate in Europe: Monitoring and modelling thermal, geomorphological and geotechnical responses. *Earth-Science Reviews* 92 : 117–171.
- Harris C, Murton JB. 2005. Interactions between glaciers and permafrost: an introduction. Geological Society, London, Special Publications 242 : 1–9.
- Harris SA, Pedersen DE. 1998. Thermal regimes beneath coarse blocky materials. *Permafrost and Periglacial Processes* 9 : 107–120.
- Harvey A. 2013. Processes of sediment supply to alluvial fans and debris cones. In *Dating Torrential Processes on Fans and Cones*. Springer; 15–32.
- Hauck C, Kneisel C. 2008. *Applied geophysics in periglacial environments*. . Cambridge University Press: Cambridge
- Heritage GL, Milan DJ. 2009. Terrestrial laser scanning of grain roughness in a gravel-bed river. *Geomorphology* 113 : 4–11.
- Hobson RD. 1967. FORTRAN IV programs to determine the surface roughness in topography for the CDC 3400 computer. *Comput. Contrib. State Geol. Surv. Kansas* 14 : 1–28.
- Hoelzle M, Haeberli W, Keller F. 1993. Application of BTS-measurements for modelling mountain permafrost distribution. 272–277 pp.
- Hoelzle M, Wegmann M, Krummenacher B. 1999. Miniature temperature dataloggers for mapping and monitoring of permafrost in high mountain areas: first experience from the Swiss Alps. *Permafrost and Periglacial Processes* 10 : 113–124.
- Hollister RD, Webber PJ, Bay C. 2005. Plant Response to Temperature in Northern Alaska: Implications for Predicting Vegetation Change. *Ecology* 86 : 1562–1570.
- Huang T, Li X, Zhang T, Lu D-T. 2013. GPU-accelerated Direct Sampling method for multiple-point statistical simulation. *Computers & Geosciences* 57 : 13–23.
- Huber B. 1956. Die Temperatur pflanzlicher Oberflächen. In *Pflanze und Wasser/Water Relations of Plants*. Springer; 285–292.
- Hülber K, Winkler M, Grabherr G. 2010. Intraseasonal climate and habitat-specific variability controls the flowering phenology of high alpine plant species. *Functional Ecology* 24 : 245–252.
- Ikeda A, Matsuoka N. 2002. Degradation of talus-derived rock glaciers in the Upper Engadin, Swiss Alps. *Permafrost and Periglacial Processes* 13 : 145–161.
- Ikeda A, Matsuoka N. 2006. Pebbly versus bouldery rock glaciers: Morphology, structure and processes. *Geomorphology* 73 : 279–296.
- Imaizumi F, Trappmann D, Matsuoka N, Tsuchiya S, Ohsaka O. 2016. Biographical sketch of a giant: Deciphering recent debris-flow dynamics from the Ohya landslide body (Japanese Alps). *Geomorphology* 272 : 102–114.

- IPCC. 2018. Global warming of 1.5°C. An IPCC Special Report on the impacts of global warming of 1.5°C above pre-industrial levels and related global greenhouse gas emission pathways, in the context of strengthening the global response to the threat of climate change, sustainable development, and efforts to eradicate poverty . Geneva, Switzerland
- Irvin BJ, Ventura SJ, Slater BK. 1997. Fuzzy and isodata classification of landform elements from digital terrain data in Pleasant Valley, Wisconsin. *Geoderma* 77 : 137–154.
- Ishikawa M. 2003. Thermal regimes at the snow–ground interface and their implications for permafrost investigation. *Geomorphology* 52 : 105–120.
- Iverson NR. 2002. Processes of glacial erosion. *Modern and Past Glacial Environments*: 131–145.
- Jobbágy EG, Jackson RB. 2000. The vertical distribution of soil organic carbon and its relation to climate and vegetation. *Ecological applications* 10 : 423–436.
- Jochimsen M. 1962. Das Gletschervorfeld - keine Wüste. *Jahrb Österr Alpenvereins* 87 : 135–142.
- Jones CG. 2012. Ecosystem engineers and geomorphological signatures in landscapes. *Geomorphology* 157–158 : 75–87.
- Jouvet G, Weidmann Y, Seguinot J, Funk M, Abe T, Sakakibara D, Seddik H, Sugiyama S. 2017. Initiation of a major calving event on the Bowdoin Glacier captured by UAV photogrammetry. *The Cryosphere* 11 : 911–921.
- Jumpponen A, Väre H, Mattson KG, Ohtonen R, Trappe JM. 1999. Characterization of ‘safe sites’ for pioneers in primary succession on recently deglaciated terrain. *Journal of Ecology* 87 : 98–105.
- Keiler M, Knight J, Harrison S. 2010. Climate change and geomorphological hazards in the eastern European Alps. *Philosophical Transactions of the Royal Society A: Mathematical, Physical and Engineering Sciences* 368 : 2461–2479.
- Kemppinen J, Niittynen P, Riihimäki H, Luoto M. 2018. Modelling soil moisture in a high-latitude landscape using LiDAR and soil data. *Earth Surface Processes and Landforms* 43 : 1019–1031.
- Klein G, Vitasse Y, Rixen C, Marty C, Rebetez M. 2016. Shorter snow cover duration since 1970 in the Swiss Alps due to earlier snowmelt more than to later snow onset. *Climatic Change* 139 : 637–649.
- Kneisel C, Kääb A. 2007. Mountain permafrost dynamics within a recently exposed glacier forefield inferred by a combined geomorphological, geophysical and photogrammetrical approach. *Earth Surface Processes and Landforms* 32 : 1797–1810.
- Knox JC. 1972. Valley Alluviation In Southwestern Wisconsin. *Annals of the Association of American Geographers* 62 : 401–410.
- Körner C, Paulsen J. 2004. A world-wide study of high altitude treeline temperatures. *Journal of Biogeography* 31 : 713–732.
- Körner C. 2003. *Alpine plant life: functional plant ecology of high mountain ecosystems*. 2nd ed. Springer-Verlag Berlin Heidelberg
- Lambiel C, Bardou E, Delaloye R, Schuetz P, Schoeneich P. 2009. Extension spatiale du pergélisol dans les Alpes vaudoises; implication pour la dynamique sédimentaire locale. *Bulletin de la Société vaudoise des sciences naturelles* 91 : 407–424.
- Lambiel C, Maillard B, Kummert M, Reynard E. 2016. Geomorphology of the Hérens valley (Swiss Alps). *Journal of Maps* 12 : 160–172.

- Lambiel C, Pieracci K. 2008. Permafrost distribution in talus slopes located within the alpine periglacial belt, Swiss Alps. *Permafrost and Periglacial Processes* 19 : 293–304.
- Lane SN, Bakker M, Gabbud C, Micheletti N, Saugy J-N. 2017. Sediment export, transient landscape response and catchment-scale connectivity following rapid climate warming and Alpine glacier recession. *Geomorphology* 277 : 210–227.
- Lane SN, Borgeaud L, Vittoz P. 2016. Emergent geomorphic–vegetation interactions on a subalpine alluvial fan. *Earth Surface Processes and Landforms* 41 : 72–86.
- Lauber K, Wagner G, Gygax A. 2012. *Flora Helvetica: flore illustrée de Suisse*. Haupt
- Lavelle P, Lattaud C, Trigo D, Barois I. 1995. Mutualism and biodiversity in soils. In *The Significance and Regulation of Soil Biodiversity*, Collins H, Robertson G, and Klug M (eds). Springer: Dordrecht;
- le Roux PC, Luoto M. 2014. Earth surface processes drive the richness, composition and occurrence of plant species in an arctic–alpine environment. *Journal of Vegetation Science* 25 : 45–54.
- le Roux PC, Virtanen R, Luoto M. 2013. Geomorphological disturbance is necessary for predicting fine-scale species distributions. *Ecography* 36 : 800–808.
- Lee EM. 2001. *Geomorphological mapping*. Geological Society, London, Engineering Geology Special Publications 18 : 53–56.
- Leopold LB, Wolman MG, Miller JP. 2012. *Fluvial processes in geomorphology*. Courier Corporation
- Leuenberger M, Parente J, Tonini M, Pereira MG, Kanevski M. 2018. Wildfire susceptibility mapping: Deterministic vs. stochastic approaches. *Environmental Modelling & Software* 101 : 194–203.
- Litaor MI. 1987. The influence of eolian dust on the genesis of alpine soils in the Front Range, Colorado. *Soil Science Society of America Journal* 51 : 142–147.
- Lozinski W. 1909. Über die mechanische Verwitterung der Sandsteine im gemässigten Klima.– *Academie des Sciences Cracovie. Bulletin Internationale Classe des Sciences Mathematiques et Naturelles* 1 : 1–25.
- Lüdi W. 1958. Beobachtungen über die Besiedlung von Gletschervorfeldern in den Schweizeralpen. *Flora oder Allgemeine Botanische Zeitung* 146 : 386–407.
- Magnin F, Brenning A, Bodin X, Deline P, Ravel L. 2015. Statistical modelling of rock wall permafrost distribution: application to the Mont Blanc massif. *Geomorphologie: relief, processus, environnement* 21 : 145-162
- Major JJ, Pierson TC, Scott KM. 2005. Debris flows at Mount St. Helens, Washington, USA. In *Debris-flow Hazards and Related Phenomena*, Jakob M and Hungr O (eds). Springer Berlin Heidelberg: Berlin, Heidelberg; 685–731.
- Malanson GP, Bengtson LE, Fagre DB. 2012. Geomorphic Determinants of Species Composition of Alpine Tundra, Glacier National Park, U.S.A. *Arctic, Antarctic, and Alpine Research* 44 : 197–209.
- Mantel N. 1967. The detection of disease clustering and a generalized regression approach. *Cancer Research* 27 : 209–220.

- Mantovani F, Soeters R, Van Westen CJ. 1996. Remote sensing techniques for landslide studies and hazard zonation in Europe. *Geomorphology* 15 : 213–225.
- Marescot L. 2006. Introduction à l'imagerie électrique du sous-sol. *Bulletins des séances de la Société vaudoise des sciences naturelles* 90 : 23–40.
- Mariethoz G, Caers J. 2014. *Multiple-point geostatistics: stochastic modelling with training images*. John Wiley & Sons
- Mariethoz G, Renard P, Straubhaar J. 2010. The Direct Sampling method to perform multiple-point geostatistical simulations. *Water Resources Research* 46
- Marmion M, Hjort J, Thuiller W, Luoto M. 2008. A comparison of predictive methods in modelling the distribution of periglacial landforms in Finnish Lapland. *Earth Surface Processes and Landforms* 33 : 2241–2254.
- Martignier L, Adatte T, Verrecchia EP. 2013. Bedrock versus superficial deposits in the Swiss Jura Mountains: what is the legitimate soil parent material? *Earth Surface Processes and Landforms* 38 : 331–345.
- Matsuoka N, Murton J. 2008. Frost weathering: recent advances and future directions. *Permafrost and Periglacial Processes* 19 : 195–210.
- Matteodo M, Grand S, Sebag D, Rowley MC, Vittoz P, Verrecchia EP. 2018. Decoupling of topsoil and subsoil controls on organic matter dynamics in the Swiss Alps. *Geoderma* 330 : 41–51.
- Matteodo M. 2018. Response of Swiss subalpine-alpine vegetation to recent climate changes and consequences on soil organic matter dynamics, Thèse de doctorat. Thèse de doctorat, Université de Lausanne
- Matthews JA, Whittaker RJ. 1987. Vegetation Succession on the Storbreven Glacier Foreland, Jotunheimen, Norway: A Review. *Arctic and Alpine Research* 19 : 385–395.
- Matthews JA. 1992. *The ecology of recently-deglaciated terrain: a geoecological approach to glacier forelands*. Cambridge University Press
- McKean J, Roering J. 2004. Objective landslide detection and surface morphology mapping using high-resolution airborne laser altimetry. *Geomorphology* 57 : 331–351.
- Meerschman E, Pirot G, Mariethoz G, Straubhaar J, Van Meirvenne M, Renard P. 2013. A practical guide to performing multiple-point statistical simulations with the Direct Sampling algorithm. *Computers & Geosciences* 52 : 307–324.
- Meteoswiss. 2018. *Bulletin climatologique année 2017*. Geneva
- Meteoswiss. 2019. *Bulletin climatologique année 2018*. Geneva
- Minár J, Evans IS. 2008. Elementary forms for land surface segmentation: The theoretical basis of terrain analysis and geomorphological mapping. *Geomorphology* 95 : 236–259.
- Mod HK, Scherrer D, Luoto M, Guisan A. 2016. What we use is not what we know: environmental predictors in plant distribution models. *Journal of Vegetation Science* 27 : 1308–1322.
- Morard S, Delaloye R, Dorthe J. 2008. Seasonal thermal regime of a mid-latitude ventilated debris accumulation. 1233–1238 pp.
- Moreau M, Mercier D, Laffly D, Roussel E. 2008. Impacts of recent paraglacial dynamics on plant colonization: A case study on Midtre Lovénbreen foreland, Spitsbergen (79°N). *Geomorphology* 95 : 48–60.

- Nagl F, Erschbamer B. 2010. Kapitel 6. Pflanzliche Sukzessionen im Gletschervorfeld. Vegetation und Besiedlungsstrategien. In *Glaziale und periglaziale Lebensräume im Raum Obergurgl*, Erschbamer B and Koch E (eds). Innsbruck University press: Innsbruck; 121–142.
- Naylor LA, Viles HA, Carter NEA. 2002. Biogeomorphology revisited: looking towards the future. *Geomorphology* 47 : 3–14.
- Niittynen P, Luoto M. 2018. The importance of snow in species distribution models of arctic vegetation. *Ecography* 41 : 1024–1037.
- Oksanen J, Kindt R, Legendre P, O'Hara B, Stevens MHH, Oksanen MJ, Suggests M. 2007. The vegan package. *Community ecology package* 10 : 631–637.
- Oriani F, Mehrotra R, Mariéthoz G, Straubhaar J, Sharma A, Renard P. 2018. Simulating rainfall time-series: how to account for statistical variability at multiple scales? *Stochastic Environmental Research and Risk Assessment* 32 : 321–340.
- Osterkamp WR, Hupp CR, Stoffel M. 2012. The interactions between vegetation and erosion: new directions for research at the interface of ecology and geomorphology. *Earth Surface Processes and Landforms* 37 : 23–36.
- Otsu N. 1979. A threshold selection method from gray-level histograms. *IEEE transactions on systems, man, and cybernetics* 9 : 62–66.
- Otto J, Keuschnig M, Götz J, Marbach M, Schrott L. 2012. Detection of mountain permafrost by combining high resolution surface and subsurface information – an example from the glatzbach catchment, Austrian Alps. *Geografiska Annaler: Series A, Physical Geography* 94 : 43–57.
- Otto J-C, Götz J, Schrott L. 2008. Sediment storage in Alpine sedimentary systems--Quantification and scaling issues. *IAHS publication* 325 : 258.
- Ozenda P. 1985. *La végétation de la chaîne alpine dans l'espace montagnard européen*. Masson
- Pain CF. 1985. Mapping of landforms from Landsat imagery: an example from eastern new south wales, Australia. *Remote Sensing of Environment* 17 : 55–65.
- PERMOS. 2019. Permafrost in Switzerland 2014/2015 to 2017/2018. In *Glaciological Report (Permafrost) No. 16-19 of the Cryospheric Commission of the Swiss Academy of Sciences*, Noetzli J, Pellet C, and Staub B (eds). 104.
- Perret A, Martin S. 2015. Carte géomorphologique du vallon de Nant et étude de la marge proglaciaire du glacier des Martinets. *Bulletin de la Murithienne* 132 : 69–82.
- Pickett STA, White PS. 1985. The ecology of natural disturbance and patch dynamics
- Pike RJ. 1988. The geometric signature: quantifying landslide-terrain types from digital elevation models. *Mathematical geology* 20 : 491–511.
- Pradervand J-N, Dubuis A, Pellissier L, Guisan A, Randin C. 2014. Very high resolution environmental predictors in species distribution models: Moving beyond topography? *Progress in Physical Geography: Earth and Environment* 38 : 79–96.
- Prasad AM, Iverson LR, Liaw A. 2006. Newer Classification and Regression Tree Techniques: Bagging and Random Forests for Ecological Prediction. *Ecosystems* 9 : 181–199.
- R Core Team. 2015. *R: A language and environment for statistical computing*. Foundation for Statistical Computing: Vienna.



- Raffl C, Mallaun M, Mayer R, Erschbamer B. 2006. Vegetation Succession Pattern and Diversity Changes in a Glacier Valley, Central Alps, Austria. *Arctic, Antarctic, and Alpine Research* 38 : 421-428–8.
- Randin CF, Vuissoz G, Liston GE, Vittoz P, Guisan A. 2009. Introduction of Snow and Geomorphic Disturbance Variables into Predictive Models of Alpine Plant Distribution in the Western Swiss Alps. *Arctic, Antarctic, and Alpine Research* 41 : 347–361.
- Rasera LG, Gravey M, Lane Stuart N., Mariethoz Gregoire. 2019. Downscaling Images with Trends Using Multiple-Point Statistics Simulation: An Application to Digital Elevation Models. *Mathematical Geosciences*
- Ravanel L, Magnin F, Deline P. 2017. Impacts of the 2003 and 2015 summer heatwaves on permafrost-affected rock-walls in the Mont Blanc massif. *Science of the Total Environment* 609 : 132–143.
- Reddy GPO. 2018. Remote Sensing and GIS for Geomorphological Mapping. In *Geospatial Technologies in Land Resources Mapping, Monitoring and Management*, Reddy GPO and Singh SK (eds). Springer International Publishing: Cham; 223–252.
- Reisigl H, Keller R. 1987. *Alpenpflanzen in Lebensraum: Alpine Rasen Schutt-und Felsvegetation. Vegetationsökologische Informationen für Studien, Exkursionen und Wanderungen.*
- Riihimäki H, Heiskanen J, Luoto M. 2017. The effect of topography on arctic-alpine aboveground biomass and NDVI patterns. *International Journal of Applied Earth Observation and Geoinformation* 56 : 44–53.
- Rödler T, Kneisel C. 2012. Influence of snow cover and grain size on the ground thermal regime in the discontinuous permafrost zone, Swiss Alps. *Geomorphology* 175–176 : 176–189.
- Rose J. 1991. Subaerial modification of glacier bedforms immediately following ice wastage. *Norsk Geografisk Tidsskrift - Norwegian Journal of Geography* 45 : 143–153.
- Rost KT. 2001. Late Holocene loess deposits and dust accumulation in the alpine meadow belt of the Wutai Shan, China. *Quaternary International* 76–77 : 85–92.
- Sandholt I, Rasmussen K, Andersen J. 2002. A simple interpretation of the surface temperature/vegetation index space for assessment of surface moisture status. *Remote Sensing of Environment* 79 : 213–224.
- Scherrer D, Körner C. 2011. Topographically controlled thermal-habitat differentiation buffers alpine plant diversity against climate warming. *Journal of biogeography* 38 : 406–416.
- Schmid M-O, Gubler S, Fiddes J, Gruber S. 2012. Inferring snowpack ripening and melt-out from distributed measurements of near-surface ground temperatures. *The Cryosphere* 6 : 1127–1139.
- Schneevoigt NJ, van der Linden S, Thamm H-P, Schrott L. 2008. Detecting Alpine landforms from remotely sensed imagery. A pilot study in the Bavarian Alps. *Geomorphology* 93 : 104–119.
- Schoeneich P, Reynard E. 1993. *Cartographie géomorphologique-Cartographie des risques. Actes de la réunion annuelle 1992 de la Société suisse de géomorphologie*
- Schürch P, Densmore AL, Rosser NJ, Lim M, McArdeell BW. 2011. Detection of surface change in complex topography using terrestrial laser scanning: application to the Illgraben debris-flow channel. *Earth Surface Processes and Landforms* 36 : 1847–1859.
- Schwanghart W, Kuhn NJ. 2010. TopoToolbox: a set of Matlab functions for topographic analysis. *Environmental Modelling & Software* 25 : 770–781.

- Schwanghart W, Scherler NJ. 2014. TopoToolbox 2 – MATLAB-based software for topographic analysis and modeling in Earth surface sciences. *Earth Surface Dynamics* 2 : 1–7.
- Seastedt TR, Bowman WD, Caine TN, McKnight D, Townsend A, Williams MW. 2004. The landscape continuum: a model for high-elevation ecosystems. *BioScience* 54 : 111–121.
- Seijmonsbergen AC, Hengl T, Anders NS. 2011. Semi-automated identification and extraction of geomorphological features using digital elevation data. *Developments in earth surface processes* 15 : 297–335.
- Selby MJ. 1982. Hillslope materials and processes. Hillslope materials and processes
- Serra J, Soille P. 1994. Mathematical morphology and its applications to image processing. Springer Science & Business Media: Dordrecht
- Sievering H. 2001. Atmospheric chemistry and deposition. In *Structure and Function of an Alpine Ecosystem: Niwot Ridge, Colorado*, Bowman WD, Seastedt TR (eds). New York: Oxford University Press; 32–44.
- Smith MJ, Paron P, Griffiths JS. 2011. Geomorphological mapping: methods and applications. Elsevier
- Stallins JA. 2006. Geomorphology and ecology: unifying themes for complex systems in biogeomorphology. *Geomorphology* 77 : 207–216.
- Staub B, Marmy A, Hauck C, Hilbich C, Delaloye R. 2015. Ground temperature variations in a talus slope influenced by permafrost: a comparison of field observations and model simulations. *Geogr. Helv.* 70 : 45–62.
- Steck A, Eparid J, Escher A, Gouffon Y, Masson H. 2001. Carte tectonique des Alpes de Suisse occidentale. Notice explicative.
- Steinbauer MJ, Grytnes JA, Jurasinski G, Kulonen A, Lenoir J, Pauli H, & Bjorkman A D. 2018. Accelerated increase in plant species richness on mountain summits is linked to warming. *Nature* 556 : 231.
- Stewart KJ, Grogan P, Coxson DS, Siciliano SD. 2014. Topography as a key factor driving atmospheric nitrogen exchanges in arctic terrestrial ecosystems. *Soil Biology and Biochemistry* 70 : 96–112.
- Stirling G, Wilsey B. 2001. Empirical Relationships between Species Richness, Evenness, and Proportional Diversity. *The American Naturalist* 158 : 286–299.
- Stöckli V, Wipf S, Nilsson C, Rixen C. 2011. Using historical plant surveys to track biodiversity on mountain summits. *Plant Ecology & Diversity* 4 : 415–425.
- Stoffel M, Schneuwly-Bollscheweiler M, Rudolf-Miklau F. 2013. Dating Past Events on Fans and Cones – An Introduction. In *Dating Torrential Processes on Fans and Cones: Methods and Their Application for Hazard and Risk Assessment*, Schneuwly-Bollscheweiler M, Stoffel M, and Rudolf-Miklau F (eds). Springer Netherlands: Dordrecht; 1–11.
- Strebelle S. 2002. Conditional Simulation of Complex Geological Structures Using Multiple-Point Statistics. *Mathematical Geology* 34 : 1–21.
- Strom KB, Kuhns RD, Lucas HJ. 2010. Comparison of automated image-based grain sizing to standard pebble-count methods. *Journal of Hydraulic Engineering* 136 : 461–473.

- Stumpf A, Kerle N. 2011. Object-oriented mapping of landslides using Random Forests. *Remote Sensing of Environment* 115 : 2564–2577.
- Terzi S, Torresan S, Schneiderbauer S, Critto A, Zebisch M, Marcomini A. 2019. Multi-risk assessment in mountain regions: A review of modelling approaches for climate change adaptation. *Journal of Environmental Management* 232 : 759–771.
- Theurillat J-P, Felber F, Geissler P, Gobat J-M, Fierz M, Fischlin A, Küpfer P, Schlüssel A, Velluti C, Zhao G-F. 1998. Sensitivity of plant and soil ecosystems of the Alps to climate change. *Views from the Alps: regional perspectives on climate change*, 225–308.
- Thornton JM, Mariethoz G, Brauchli TJ, Brunner P. 2019. Efficient multi-objective calibration and uncertainty analysis of distributed snow simulations in rugged alpine terrain. *The Cryosphere Discuss.* 2019 : 1–48.
- Thornton JM, Mariethoz G, Brunner P. 2018. A 3D geological model of a structurally complex Alpine region as a basis for interdisciplinary research. *Scientific data* 5 : 180238.
- Tucker CM, Rebelo AG, Manne LL. 2012. Contribution of disturbance to distribution and abundance in a fire-adapted system. *Ecography* 35 : 348–355.
- Uyanik I, Wesley A. 2019. Next Generation Gas Emission Monitoring System. SPE-195015-MS PP.
- Vallet J, Panissod F, Strecha C, Tracol M. 2011. Photogrammetric performance of an ultra light weight swinglet UAV. *International Archives of the Photogrammetry, Remote Sensing and Spatial Information Sciences XXXVIII-1* : 253–258.
- van Niekerk A. 2010. A comparison of land unit delineation techniques for land evaluation in the Western Cape, South Africa. *Land Use Policy* 27 : 937–945.
- van Tatenhove F, Dikau R. 1990. Past and Present Permafrost Distribution in the Turtmanntal, Wallis, Swiss Alps. *Arctic and Alpine Research* 22 : 302–316.
- Vannamettee E, Babel LV, Hendriks MR, Schuur J, de Jong SM, Bierkens MFP, Karssenberg D. 2014. Semi-automated mapping of landforms using multiple point geostatistics. *Geomorphology* 221 : 298–319.
- Varnes DJ. 1978. Slope movement types and processes. *Special report 176* : 11–33.
- Veronesi F, Hurni L. 2014. Random Forest with semantic tie points for classifying landforms and creating rigorous shaded relief representations. *Geomorphology* 224 : 152–160.
- Verstappen HT. 2011. Old and new trends in geomorphological and landform mapping. In *Developments in earth surface processes*, 13–38.
- Viera AJ, Garrett JM. 2005. Understanding interobserver agreement: the kappa statistic. *Fam med* 37 : 360–363.
- Virtanen R, Luoto M, Rämä T, Mikkola K, Hjort J, Grytnes J-A, Birks HJB. 2010. Recent vegetation changes at the high-latitude tree line ecotone are controlled by geomorphological disturbance, productivity and diversity. *Global Ecology and Biogeography* 19 : 810–821.
- Vittoz P, Gmür P. 2009. Introduction aux Journées de la biodiversité dans le Vallon de Nant (Bex, Alpes vaudoises). *Mémoire de la Société vaudoise des Sciences naturelles* 23 : 3–20.
- Vittoz P, Randin C, Dutoit A, Bonnet F, Hegg O. 2009. Low impact of climate change on subalpine grasslands in the Swiss Northern Alps. *Global Change Biology* 15 : 209–220.

- Vivero S, Lambiel C. 2019. Monitoring the crisis of a rock glacier with repeated UAV surveys. *Geographica Helvetica* 74 : 59–69.
- Viviroli D, Archer DR, Buytaert W, Fowler HJ, Greenwood G, Hamlet AF, Huang Y, Koboltschnig G, Litaor I, López-Moreno JI. 2011. Climate change and mountain water resources: overview and recommendations for research, management and policy. *Hydrology and Earth System Sciences* 15 : 471–504.
- Vonlanthen CM, Bühler A, Veit H, Kammer PM, Eugster W. 2006a. Alpine Plant Communities: A Statistical Assessment of Their Relation to Microclimatological, Pedological, Geomorphological, and Other Factors. *Physical Geography* 27 : 137–154.
- Vonlanthen CM, Kammer PM, Eugster W, Bühler A, Veit H. 2006b. Alpine vascular plant species richness: the importance of daily maximum temperature and pH. *Plant Ecology* 184 : 13–25.
- Wakonigg H. 1996. Unterkühlte Schutthalden. Arbeiten aus dem Institut für Geographie der Universität Graz, Universität Graz, Austria
- Walker LR, del Moral R. 2011. Primary Succession. In eLS, American Cancer Society.
- Walther G-R, Beißner S, Burga CA. 2005. Trends in the upward shift of alpine plants. *Journal of Vegetation Science* 16 : 541–548.
- Washburn AL. 1980. *Geocryology: a survey of periglacial processes and environments*. Wiley
- Weichert R, Wickenhäuser M, Bezzola GR, Minor HE. 2004. Grain size analysis for coarse river beds using digital imagery processing. *Proc. RF* : 753–760.
- Westermann S, Boike J, Langer M, Schuler T V, Etzelmüller B. 2011. Modeling the impact of wintertime rain events on the thermal regime of permafrost. *The Cryosphere* 5 : 945–959.
- Wildi O. 2013. *Data analysis in vegetation ecology*. 2nd ed. Wiley-Blackwell (ed). Wiley-Blackwell, Chichester: Chichester
- Williams MW, Tonnessen KA. 2000. Critical loads for inorganic nitrogen deposition in the Colorado Front Range, USA. *Ecological Applications* 10 : 1648–1665.
- Wipf S, Stöckli V, Herz K, Rixen C. 2013. The oldest monitoring site of the Alps revisited: accelerated increase in plant species richness on Piz Linard summit since 1835. *Plant Ecology & Diversity* 6 : 447–455.
- Wood S. 2017. *Generalized Additive Models*. New York: Chapman and Hall/CRC,
- Yashiro E, Pinto-Figueroa E, Buri A, Spangenberg JE, Adatte T, Niculita-Hirzel H, Guisan A, van der Meer JR. 2018. Meta-scale mountain grassland observatories uncover commonalities as well as specific interactions among plant and non-rhizosphere soil bacterial communities. *Scientific Reports* 8 : 5758.
- Yee TW, Mitchell ND. 1991. Generalized additive models in plant ecology. *Journal of Vegetation Science* 2 : 587–602.
- Zhang T. 2005. Influence of the seasonal snow cover on the ground thermal regime: An overview. *Reviews of Geophysics* 43–4.

## 8. Appendices

## Appendix 1

**Table 8.1** - iButtons data for the year 01-10-2016/30-09-2017. MGST: Mean Ground Surface Temperature [°C]; Tmax: mean maximum temperature [°C]; Tmin: mean minimum temperature [°C]; RD: basal-Ripening Date; MD: Melt-out Date; FDD: Freezing Degree Day [degree day]; GDD: Growing Degree Day [degree day]; GSL: Growing Season Length [day].

Plot	MGST	Tmax	Tmin	RD	MD	FDD	GDD	GSL
1	3.0	4.1	2.2	04.04.2017	01.06.2017	233	1264	103
2	4.2	5.4	3.3	-	30.05.2017	25	1408	111
3	3.5	5.5	2.2	-	18.06.2017	0	1120	86
4	3.5	5.6	2.0	-	01.06.2017	15	1145	93
5	2.3	3.1	1.5	-	03.07.2017	38	758	62
6	4.0	4.8	3.4	-	04.06.2017	0	1263	104
8	1.7	2.5	1.1	11.04.2017	20.06.2017	187	705	74
9	2.3	3.3	1.5	12.05.2017	22.06.2017	129	856	82
10	2.0	3.0	1.1	19.05.2017	28.06.2017	173	790	76
11	0.5	0.8	0.2	15.05.2017	21.07.2017	237	299	44
12	2.4	3.7	1.4	-	04.07.2017	39	851	70
13	1.8	2.5	1.2	-	03.07.2017	21	603	61
14	1.9	2.4	1.3	-	03.07.2017	19	599	61
15	3.2	4.5	2.3	-	18.06.2017	21	1098	86
16	2.0	3.0	1.2	05.04.2017	19.06.2017	142	803	75
17	3.2	4.4	2.2	23.03.2017	31.05.2017	142	1201	104
19	1.6	2.4	0.8	24.05.2017	02.06.2017	396	874	92
20	1.8	2.9	0.8	12.05.2017	13.06.2017	360	920	81
21	2.0	3.3	1.0	05.05.2017	17.06.2017	151	793	77
22	2.6	4.1	1.5	-	23.06.2017	74	942	81
23	1.8	1.9	1.6	-	08.07.2017	0	438	67
24	3.2	4.4	2.4	-	09.06.2017	3	1027	95
25	3.9	6.4	2.4	-	02.06.2017	22	1321	105
26	2.8	3.2	2.4	-	09.06.2017	5	873	86
27	0.9	1.1	0.7	-	19.07.2017	23	211	45
28	2.0	2.9	1.2	09.04.2017	11.06.2017	200	804	83
29	2.3	3.2	1.7	26.04.2017	18.06.2017	102	824	86
30	1.5	2.7	0.5	31.05.2017	27.06.2017	327	792	67
31	3.3	5.1	2.0	-	13.06.2017	25	1137	81
32	2.9	4.4	1.9	-	20.06.2017	1	957	74
34	2.4	3.7	1.5	-	27.06.2017	30	774	68
35	2.0	3.3	1.1	14.04.2017	23.06.2017	208	862	71
36	2.7	3.6	2.0	-	16.06.2017	13	867	87
37	3.2	4.7	2.2	-	23.06.2017	16	1093	87
38	2.6	3.7	1.8	-	23.06.2017	38	918	81
39	2.6	4.0	1.7	-	17.06.2017	30	881	78
40	2.0	2.6	1.3	-	26.06.2017	15	624	68
41	3.0	3.6	2.5	26.02.2017	12.06.2017	124	1148	95
42	2.5	3.7	1.7	-	20.06.2017	38	873	75
43	1.6	3.2	0.4	17.03.2017	23.05.2017	627	1060	102
44	1.0	3.6	-0.7	22.04.2017	22.05.2017	806	1049	103

45	4.1	5.0	3.3	14.03.2017	23.05.2017	106	1422	121
46	3.0	4.0	2.3	20.03.2017	01.06.2017	67	1049	103
47	1.0	1.7	0.4	29.04.2017	22.06.2017	436	694	72
48	2.1	3.6	1.1	30.04.2017	12.06.2017	295	1012	92
49	3.9	5.1	3.0	18.03.2017	23.05.2017	121	1426	130
50	3.5	5.2	2.2	13.03.2017	09.06.2017	145	1306	98
51	3.3	4.2	2.6	-	10.06.2017	27	1119	97
52	3.0	5.0	1.5	10.03.2017	28.05.2017	371	1343	97
53	4.4	5.3	3.7	01.02.2017	28.05.2017	60	1504	116
54	4.0	5.2	3.0	09.03.2017	27.05.2017	93	1390	114
55	3.6	4.9	2.5	16.03.2017	28.05.2017	190	1368	110
56	3.4	4.4	2.7	-	11.06.2017	6	1105	93
57	3.1	4.6	2.1	07.03.2017	10.06.2017	97	1141	93
59	3.6	5.1	2.5	17.03.2017	02.06.2017	185	1360	105
60	3.0	4.7	1.9	05.04.2017	27.05.2017	306	1301	111
61	3.3	4.2	2.5	-	10.06.2017	1	1052	94
62	1.4	3.4	0.0	04.04.2017	23.05.2017	655	1025	102
63	0.6	2.4	-0.7	03.04.2017	02.06.2017	840	925	92
64	2.0	4.2	0.4	08.04.2017	27.05.2017	515	1082	98
65	3.5	4.4	2.8	-	09.06.2017	1	1144	99
67	2.4	3.8	1.4	-	22.06.2017	121	943	72
68	2.4	3.6	1.4	-	24.06.2017	68	845	70
69	1.9	2.8	1.2	10.04.2017	27.05.2017	473	1025	114
70	3.4	5.3	2.0	23.03.2017	02.06.2017	183	1329	101
71	3.4	5.0	2.5	-	08.06.2017	0	981	114
73	3.2	4.6	2.1	-	23.06.2017	7	1074	82
74	2.3	4.2	0.8	09.04.2017	03.06.2017	392	1080	101
75	1.9	2.9	1.1	08.04.2017	18.06.2017	156	700	76
76	1.6	3.2	0.3	13.04.2017	14.06.2017	329	821	80
77	1.1	2.6	-0.1	11.04.2017	10.06.2017	520	844	84
78	1.6	2.7	0.8	12.04.2017	12.06.2017	417	899	92

## Appendix 2

**Table 8.2** - iButtons data for the year 01-10-2017/30-09-2018. MGST: Mean Ground Surface Temperature [°C]; Tmax: mean maximum temperature [°C]; Tmin: mean minimum temperature [°C]; RD: basal-Ripening Date; MD: Melt-out Date; FDD: Freezing Degree Day [degree day]; GDD: Growing Degree Day [degree day]; GSL: Growing Season Length [day].

Plot	MGST	Tmax	Tmin	RD	MD	FDD	GDD	GSL
1	4.6	6.8	3.1	-	25.05.2018	0	1598	128
2	4.4	5.5	3.3	-	09.06.2018	0	1490	113
3	3.7	5.6	2.2	-	01.07.2018	0	1235	91
4	4.4	6.9	2.4	-	09.06.2018	0	1485	113
5	2.6	3.5	1.7	-	16.07.2018	0	818	76
6	3.9	4.7	3.1	-	25.06.2018	0	1264	97
8	2.5	3.2	2.0	-	30.06.2018	4	800	92
9	2.7	3.7	1.8	-	07.07.2018	22	899	85
10	2.1	2.9	1.4	-	25.07.2018	12	709	67
11	1.5	1.8	1.2	-	15.07.2018	38	464	73
12	2.7	4.0	1.6	-	20.07.2018	0	883	72
13	1.8	2.4	1.3	-	19.07.2018	0	552	68
14	2.0	2.5	1.5	-	15.07.2018	0	584	73
15	3.6	4.6	2.6	-	01.07.2018	0	1207	91
16	2.5	3.5	1.8	-	30.06.2017	0	836	452
17	4.4	5.7	3.2	-	31.05.2018	0	1450	122
19	3.0	4.0	2.0	20.04.2018	04.06.2018	88	1070	115
20	3.0	4.2	1.8	03.05.2018	04.06.2018	78	1095	118
21	2.8	4.0	1.8	-	22.06.2018	3	913	100
22	3.1	4.5	1.9	-	04.07.2018	0	977	88
23	1.9	2.0	1.7	-	20.07.2018	0	463	72
24	3.2	4.4	2.4	-	21.06.2018	0	1005	101
25	4.3	5.9	3.0	-	17.06.2018	0	1379	105
26	3.2	3.6	2.8	-	11.06.2018	0	983	111
27	1.2	1.3	1.1	-	02.08.2018	1	220	55
28	3.1	4.0	2.3	-	08.06.2018	0	1008	114
29	2.8	3.5	2.2	-	29.06.2018	0	852	93
30	2.3	3.7	1.2	06.05.2018	09.07.2018	114	922	83
31	4.0	5.8	2.4	-	15.06.2018	0	1315	107
32	3.5	5.0	2.2	-	26.06.2018	0	1122	96
34	2.0	2.9	1.3	-	30.07.2018	0	629	62
35	2.2	3.3	1.3	-	19.07.2018	44	775	73
36	2.5	3.5	1.8	-	08.07.2018	0	794	84
37	3.0	4.0	2.1	-	23.07.2018	0	982	69
38	2.8	3.8	1.9	-	14.07.2018	0	889	78
39	2.6	3.9	1.8	-	05.07.2018	0	822	87
40	2.0	2.5	1.5	-	06.07.2018	0	555	81
41	4.4	5.3	3.7	-	03.06.2018	0	1474	119
42	2.7	3.6	1.9	-	04.07.2018	0	850	88
43	2.8	4.9	1.3	20.04.2018	28.05.2018	322	1271	125
44	1.7	4.5	0.0	20.04.2018	07.05.2018	718	1268	146



45	4.9	5.5	4.3	-	29.05.2018	0	1534	124
46	3.6	4.8	2.7	-	03.06.2018	0	1170	119
47	1.9	2.5	1.4	-	03.07.2018	86	696	85
48	3.1	4.6	2.0	-	19.06.2018	15	1084	99
49	4.7	6.0	3.6	-	06.06.2018	0	1574	116
50	4.0	5.5	2.8	-	15.06.2018	0	1339	107
51	3.6	4.4	2.8	-	18.06.2018	0	1157	104
52	4.5	6.5	2.8	-	19.05.2018	24	1549	130
53	4.4	5.3	3.7	-	12.06.2018	0	1409	110
54	4.2	5.4	3.4	-	13.06.2018	0	1370	109
55	4.0	5.7	2.8	-	20.06.2018	1	1326	102
56	4.0	6.4	2.7	-	20.06.2018	0	1248	102
57	3.5	5.1	2.5	-	17.06.2018	0	1165	105
59	4.0	6.7	2.5	-	22.06.2018	0	1326	100
60	3.8	5.5	2.7	25.04.2018	04.06.2018	43	1352	118
61	3.6	4.4	2.8	-	20.06.2018	0	1125	102
62	2.1	4.4	0.6	19.04.2018	25.05.2018	489	1140	128
63	2.1	4.0	0.7	05.05.2018	20.06.2018	351	1035	102
64	4.1	6.0	2.6	-	28.05.2018	0	1357	125
65	4.1	5.2	3.2	-	11.06.2018	0	1321	111
67	3.0	4.3	1.9	-	06.07.2018	1	1020	86
68	2.8	4.0	1.8	-	08.07.2018	0	926	84
69	4.2	5.0	3.4	-	22.05.2018	0	1358	131
70	4.8	7.1	3.1	-	25.05.2018	0	1621	128
71	3.2	4.4	2.2	-	30.06.2018	0	876	92
73	3.7	5.2	2.3	-	04.07.2018	0	1275	88
74	4.2	6.0	2.8	-	31.05.2018	0	1342	122
75	3.0	4.1	2.0	-	19.06.2018	6	955	103
76	2.9	5.8	0.8	21.04.2018	26.05.2018	193	1157	122
77	2.9	4.1	2.0	-	20.06.2018	0	927	102
78	3.7	5.2	2.6	-	31.05.2018	13	1278	122

## Appendix 3

**Table 8.3** - iButtons data for the year 01-10-2018/30-09-2019. MGST: Mean Ground Surface Temperature [°C]; Tmax: mean maximum temperature [°C]; Tmin: mean minimum temperature [°C]; RD: basal-Ripening Date; MD: Melt-out Date; FDD: Freezing Degree Day [degree day]; GDD: Growing Degree Day [degree day]; GSL: Growing Season Length [day].

Plot	MGST	Tmax	Tmin	RD	MD	FDD	GDD	GSL
1	3.6	5.4	2.5	07.04.2019	12.06.2019	108	1356	89
2	3.5	5.0	2.4	13.12.2018	01.07.2019	45	1252	90
3	2.9	4.6	1.7	-	20.07.2019	1	938	50
4	3.3	5.5	1.7	-	03.07.2019	5	1093	67
5	2.0	3.1	1.2	09.12.2018	25.07.2019	29	664	45
6	3.5	4.7	2.6	-	01.07.2019	0	1156	90
8	2.0	2.9	1.5	21.04.2019	08.07.2019	25	653	62
9	2.1	3.1	1.4	04.06.2019	21.07.2019	49	715	49
10	1.9	3.0	1.1	19.05.2019	24.07.2019	57	664	46
11	0.8	1.1	0.6	26.06.2019	05.08.2019	45	205	34
12	2.3	3.9	1.2	-	26.07.2019	7	755	44
13	1.6	2.2	1.1	-	23.07.2019	0	477	47
14	1.6	2.0	1.2	-	25.07.2019	0	425	45
15	3.0	4.4	2.1	-	14.07.2019	0	992	57
16	1.9	2.8	1.3	-	15.07.2019	8	611	55
17	3.4	4.8	2.3	-	25.06.2019	3	1075	75
19	1.9	2.9	0.9	24.04.2019	27.06.2019	215	795	73
20	2.2	3.5	1.2	23.04.2019	06.07.2019	132	820	64
21	2.0	3.0	1.2	09.12.2018	07.07.2019	61	692	63
22	2.5	4.1	1.5	-	21.07.2019	0	811	49
23	1.8	2.0	1.5	-	22.07.2019	1	424	48
24	2.8	3.9	2.0	03.12.2018	03.07.2019	23	880	68
25	3.7	5.4	2.5	-	28.06.2019	0	1165	93
26	2.4	2.8	2.1	26.12.2018	01.07.2019	34	762	69
27	1.1	1.2	1.0	-	04.08.2019	2	160	33
28	2.1	2.8	1.5	03.12.2018	02.07.2019	41	703	68
29	2.0	3.3	1.3	15.12.2018	20.07.2019	43	683	50
30	1.7	3.0	0.8	17.06.2019	18.07.2019	203	762	52
31	3.3	5.1	1.9	-	01.07.2019	3	1065	69
32	2.7	4.3	1.6	-	14.07.2019	2	864	56
34	1.8	2.9	1.2	-	04.08.2019	0	557	35
35	1.9	3.8	0.9	03.06.2019	25.07.2019	77	698	45
36	2.3	3.6	1.6	-	16.07.2019	0	727	54
37	3.2	4.6	2.3	-	19.07.2019	0	1046	72
38	2.3	3.3	1.5	-	23.07.2019	0	697	48
39	2.3	3.9	1.4	-	18.07.2019	0	698	52
40	No data							
41	3.8	5.4	2.7	-	19.06.2019	2	1254	102
42	2.4	3.2	1.7	-	13.07.2019	0	716	57
43	2.0	3.6	0.9	27.04.2019	27.06.2019	394	1022	73
44	1.1	3.3	-0.3	24.04.2019	23.06.2019	705	997	75

45	4.3	4.9	3.7	-	12.06.2019	0	1349	107
46	3.1	4.1	2.3	03.12.2018	16.06.2019	26	1025	84
47	1.8	2.5	1.3	13.05.2019	03.07.2019	144	693	67
48	No data							
49	No data							
50	No data							
51	3.2	4.2	2.4	-	26.06.2019	4	1042	75
52	0.4	1.1	-0.3	19.04.2019	05.06.2019	279	271	-
53	4.1	5.1	3.4	03.12.2018	19.06.2019	17	1361	100
54	3.9	4.9	3.0	03.12.2018	21.06.2019	16	1263	98
55	3.8	4.9	2.8	03.12.2018	23.06.2019	23	1275	78
56	No data							
57	3.2	4.7	2.2	03.12.2018	25.06.2019	38	1081	75
59	No data							
60	3.4	5.0	2.4	25.04.2019	15.06.2019	103	1226	104
61	3.0	3.7	2.2	-	02.07.2019	2	910	68
62	1.1	3.3	-0.3	22.05.2019	27.06.2019	608	890	71
63	0.5	2.3	-0.8	27.05.2019	10.07.2019	736	799	60
64	3.0	4.9	1.7	22.02.2019	27.06.2019	64	1043	73
65	3.4	6.8	1.6	-	26.06.2019	1	1138	74
67	2.3	3.4	1.4	-	22.07.2019	15	755	48
68	2.5	4.4	1.3	-	19.07.2019	6	807	51
69	3.0	4.1	2.2	26.04.2019	20.06.2019	95	1047	101
70	3.9	6.6	2.2	18.04.2019	13.06.2019	112	1469	87
71	2.6	3.9	1.7	-	20.07.2019	1	733	71
73	2.7	4.4	1.5	-	25.07.2019	2	931	45
74	3.4	5.3	2.1	-	25.06.2019	0	1072	76
75	2.3	3.7	1.4	-	11.07.2019	0	693	59
76	1.9	5.2	-0.3	24.05.2019	18.06.2019	471	1076	79
77	2.3	4.2	1.2	-	08.07.2019	0	725	62
78	2.8	5.5	1.2	25.04.2019	26.06.2019	77	962	71

## Appendix 4

**Table 8.4** - List of plant species identified in the 72 vegetation plots and their species cover. Species cover values are reported according to the Braun-Blanquet scale (Braun-Blanquet, 1932). ‘?’: absent; ‘r’: 1-2 individuals; ‘+’: cover < 5 %, few individuals; ‘1’: cover < 5 %; ‘2’: cover 5-25 %; ‘3’: cover 25-50 %; ‘4’: cover 50-75 %; ‘5’: cover 75-100 %.

Species / Plot	1	2	3	4	5	6	8	9	10	11	12	13	14	15	16	17	19	20	21	22	23	24	25	26	27	28	29	30	31	32	34	35	36	37	38	39	40		
Achillea_atrata	r	.	+	r	.	.	r	.	.	.	.	.	1	r	r	.	.	.	.	.	.	.	.	.	+	2	.	.	.	.	.	.	.	1	.	r	.		
Adenostyles_alpina	.	.	.	.	.	.	.	.	.	.	.	.	.	.	.	.	.	.	.	.	.	.	.	.	.	.	.	.	.	.	.	.	.	.	.	.	.	.	
Agrostis_alpina	.	.	.	.	.	.	.	.	.	.	.	.	.	.	.	.	.	.	.	.	.	.	.	.	.	.	.	.	.	.	.	.	.	.	.	.	.	.	
Agrostis_rupestris	.	.	.	.	.	.	.	.	.	.	.	.	.	.	.	.	.	.	.	.	.	.	.	.	.	.	.	.	.	.	.	.	.	.	.	.	.	.	
Agrostis_schraderiana	.	.	.	.	.	.	.	.	.	.	.	.	.	.	.	.	.	.	.	.	.	.	.	.	.	.	.	.	.	.	.	.	.	.	.	.	.	.	
Alchemilla_conjuncta_aggr	.	.	.	.	.	.	.	.	.	.	.	.	.	.	.	.	.	.	.	.	.	.	.	.	.	.	.	.	.	.	.	.	.	.	.	.	.	.	
Alchemilla_fissa	.	.	.	.	.	.	.	.	.	.	.	.	.	.	.	.	.	.	.	.	.	.	.	.	.	.	.	.	.	.	.	.	.	.	.	.	.	.	
Alchemilla_pentaphyllea	.	.	.	.	.	.	.	.	.	.	.	.	.	.	.	.	.	.	.	.	.	.	.	.	.	.	.	.	.	.	.	.	.	.	.	.	.	.	
Alchemilla_splendens	.	.	.	.	.	.	.	.	.	.	.	.	.	.	.	.	.	.	.	.	.	.	.	.	.	.	.	.	.	.	.	.	.	.	.	.	.	.	
Allium_schoenoprasum	.	.	.	.	.	.	.	.	.	.	.	.	.	.	.	.	.	.	.	.	.	.	.	.	.	.	.	.	.	.	.	.	.	.	.	.	.	.	
Androsace_chamaejasme	.	.	.	.	.	.	.	.	.	.	.	.	.	.	.	.	.	.	.	.	.	.	.	.	.	.	.	.	.	.	.	.	.	.	.	.	.	.	
Anthyllis_vulneraria_alpestris	.	.	.	.	.	.	.	.	.	.	.	.	.	.	.	.	.	.	.	.	.	.	.	.	.	.	.	.	.	.	.	.	.	.	.	.	.	.	
Arabis_alpina	.	.	.	.	.	.	.	.	.	.	1	1	1	.	.	.	.	r	.	.	r	.	.	.	+	+	+	1	1	.	.	+	.	.	.	1	1		
Arabis_bellidifolia_sstr	+	.	.	.	r	.	.	+	.	.	.	.	.	.	.	.	.	.	.	.	.	.	.	.	.	.	.	.	.	.	.	.	.	.	.	.	.	.	
Arabis_caerulea	.	.	+	.	r	.	.	.	.	.	1	.	.	.	.	.	.	.	.	.	.	.	.	.	.	.	.	.	.	.	.	.	.	.	.	.	.	.	
Asplenium_viride	.	.	.	.	.	.	.	.	.	.	.	.	.	.	.	.	r	.	+	.	.	.	.	.	.	.	.	.	.	.	.	.	.	.	.	.	.	.	
Aster_bellidiastrum	.	.	.	.	.	.	.	.	.	.	.	.	.	.	.	.	2	.	.	.	.	.	.	.	.	.	.	.	.	.	.	.	.	.	.	.	.	.	.
Astragalus_depressus	.	.	.	.	.	.	.	.	.	.	.	.	.	.	.	.	.	.	.	.	.	.	.	.	.	.	.	.	.	.	.	.	.	.	.	.	.	.	.
Astrantia_major	.	.	.	.	.	.	.	.	.	.	.	.	.	.	.	.	.	.	.	.	.	.	.	.	.	.	.	.	.	.	.	.	.	.	.	.	.	.	.
Athamanta_cretensis	.	.	.	.	.	.	.	.	.	.	.	.	.	.	.	.	.	.	.	.	.	.	.	.	.	.	.	.	.	.	.	.	.	.	.	.	.	.	.
Bartsia_alpina	1	.	.	.	.	1	.	.	.	.	.	.	.	.	1	.	.	.	.	.	.	.	.	.	.	.	.	.	.	.	.	.	.	.	.	.	.	.	
Botrychium_lunaria	.	.	.	.	.	.	.	.	.	.	.	.	.	.	.	.	.	.	.	.	.	.	.	.	.	.	.	.	.	.	.	.	.	.	.	.	.	.	.
Campanula_cenisia	.	.	.	.	.	.	.	.	.	.	.	.	.	.	.	.	.	.	.	.	.	.	.	.	.	.	.	.	.	.	.	.	.	.	.	.	.	.	.
Campanula_cochlearifolia	+	r	.	.	.	.	.	.	.	.	.	.	.	.	r	+	.	.	.	.	.	.	.	.	.	.	.	.	.	.	.	.	.	.	.	.	.	.	
Campanula_rotundifolia	.	.	.	.	.	.	r	.	.	.	.	.	.	.	r	.	.	.	.	.	.	.	.	.	.	.	.	.	.	.	.	.	.	.	.	.	.	.	.
Campanula_scheuchzeri	.	+	+	.	.	+	.	.	.	.	.	.	.	.	.	.	.	.	.	.	.	.	.	.	.	.	.	.	.	.	.	.	.	.	.	.	.	.	.
Carex_atrata_aggr	2	.	.	.	.	.	.	.	.	.	.	.	.	.	r	.	+	.	.	.	.	.	.	.	.	.	.	.	.	.	.	.	.	.	.	.	.	.	
Carex_curvula	.	.	.	.	.	.	.	.	.	.	.	.	.	.	.	.	.	.	.	.	.	.	.	.	.	.	.	.	.	.	.	.	.	.	.	.	.	.	.
Carex_foetida	.	.	.	.	.	.	.	.	.	.	.	.	.	.	.	.	+	.	.	.	.	.	.	.	.	.	.	.	.	.	.	.	.	.	.	.	.	.	.
Carex_ornithopodioides	+	.	.	.	.	.	.	.	.	.	.	.	.	.	.	.	r	.	.	.	.	.	.	.	.	.	.	.	.	.	.	.	.	.	.	.	.	.	.
Carex_rupestris	.	.	.	.	.	.	.	.	.	.	.	.	.	.	.	.	.	.	.	.	.	.	.	.	.	.	.	.	.	.	.	.	.	.	.	.	.	.	.
Carex sempervirens	+	3	.	.	.	+	.	.	.	.	.	.	.	.	+	.	3	.	.	.	.	.	.	.	.	.	.	.	.	.	.	.	.	.	.	.	r	.	
Cerastium_latifolium	.	.	.	+	.	.	.	.	.	.	.	.	.	.	.	.	.	.	.	1	.	.	.	.	.	.	.	.	.	.	.	.	.	.	.	.	.	.	+
Cirsium_spinosissimum	.	.	+	.	.	.	.	.	+	.	.	.	.	.	.	.	.	.	.	.	.	.	.	.	.	.	.	.	.	.	.	.	.	.	.	.	.	.	.
Cystopteris_fragilis	.	.	.	.	.	.	.	.	.	.	.	.	.	.	.	.	r	.	.	.	.	.	.	.	.	.	.	.	.	.	.	.	.	.	.	.	.	.	.
Doronicum_clusii	.	.	.	.	.	.	r	.	.	.	.	.	.	.	.	.	.	.	.	.	.	.	.	.	.	.	.	.	.	.	.	.	.	.	.	.	.	.	.
Doronicum_grandiflorum	.	.	+	1	+	.	1	1	.	.	.	.	.	.	.	.	.	.	.	.	.	.	.	.	.	.	.	.	.	.	.	.	.	.	.	.	.	1	+
Draba_aizoides	.	.	.	.	.	.	.	.	.	.	.	.	.	.	.	.	.	.	.	.	.	.	.	.	.	.	.	.	.	.	.	.	.	.	.	.	.	.	.
Dryas_octopetala	.	.	.	.	.	.	.	.	.	.	.	.	.	.	.	.	.	.	.	.	.	.	.	.	.	.	.	.	.	.	.	.	.	.	.	.	.	.	.
Elyna_myosuroides	.	.	.	.	.	.	.	.	.	.	.	.	.	.	.	.	.	.	.	.	.	.	.	.	.	.	.	.	.	.	.	.	.	.	.	.	.	.	.
Epilobium_anagallidifolium	.	.	.	.	.	.	.	r	r	.	.	1	.	.	.	.	.	.	.	r	.	.	.	.	.	.	.	.	.	.	.	.	.	.	.	.	.	+	1
Erigeron_glabratus	.	.	.	.	.	r	.	+	.	.	.	.	.	.	.	.	.	.	.	.	.	.	.	.	.	.	.	.	.	.	.	.	.	.	.	.	.	.	+
Euphrasia_minima	+	+	r	.	.	2	.	.	.	.	.	.	.	.	1	.	.	.	.	.	.	.	.	.	r	.	.	.	.	.	.	.	.	.	.	.	.	+	.
Festuca_violacea_aggr	1	3	1	.	1	2	.	r	.	.	.	.	+	1	1	1	.	.	.	.	.	.	.	+	+	1	.	.	1	.	.	.	.	1	2	2	.	r	
Galium_anisophyllum	.	.	1	.	.	.	.	.	.	1	.	.	.	.	.	r	.	.	.	.	.	.	.	.	.	.	.	.	.	.	.	.	.	.	.	.	.	.	.
Galium_megalospermum	.	.	.	1	.	.	.	.	.	.	.	.	.	.	.	.	.	.	.	.	.	.	.	.	.	.	.	.	.	.	.	.	.	.	.	.	.	.	.
Gentiana_bavarica	.	.	+	.	.	.	.	.	.	.	.	.	.	.	.	+	.	.	.	.	.	.	.	.	.	.	.	.	.	.	.	.	.	.	.	.	.	.	.
Gentiana_campestris_sstr	.	1	.	.	.	1	.	.	.	.	.	.	.	.	2	.	1	.	.	.	.	.	.	.	.	.	.	.	.	.	.	.	.	.	.	.	.	.	.
Gentiana_clusii	.	.	.	.	.	.	.	.	.	.	.	.	.	.	.	.	.	.	.	.	.	.	.	.	.	.	.	.	.	.	.	.	.	.	.	.	.	.	.
Gentiana_lutea	.	.	.	.	.	.	.	.	.	.	.	.	.	.	.	.	.	.	.	.	.	.	.	.	.	.	.	.	.	.	.	.	.	.	.	.	.	.	.
Gentiana_nivalis	.	.	.	.	.	+	.	.	.	.	.	.	.	.	.	.	.	.	.	.	.	.	.	.	.	.	.	.	.	.	.	.	.	.	.	.	.	.	.
Gentiana_tenella	.	.	.	.	.	.	.	.	.	.	.	.	.	.	.	.	.	.	.	.	.	.	.	.	.	.	.	.	.	.	.	.	.	.	.	.	.	.	.
Gentiana_verna	.	+	+	.	.	.	.	.	.	.	.	.	.	.	.	.	.	.	.	.	.	.	.	.	.	.	.	.	.	.	.	.	.	.	.	.	.	.	.
Geum_montanum	.	.	.	.	.	+	.	.	.	.	.	.	.	.	.	.	.	.	.	.	.	.	.	.	.	.	.	.	.	.	.	.	.	.	.	.	.	.	.
Geum_reptans	.	.	.	.	.	.	.	.	.	.	.	.	.	.	.	.	.	.	.	.	.	.	.	.	.	.	.	.	.	.	.	.	.	.	.	.	.	.	.
Globularia_cordifolia	.	.	.	.	.	.	.	.	.	.	.	.	.	.	.	.	.	.	.	.	.	.	.	.	.	.	.	.	.	.	.	.	.	.	.	.	.	.	.
Gnaphalium_hoppeanum	.	.	.	.	.	r	+	r	+	.	.	.	.	.	.	.	.	.	.	.	.	.	.	.	.	.	.	.	.	.	.	.	.	.	.	.	.	.	.
Hedysarum_hedysaroides	.	.	.	.	.	.	.	.	.	.	.	.	.	.	.	.	.	.	.	.	.	.	.	.	.	.	.	.	.	.	.	.	.	.	.	.	.	.	.
Hieracium_angustifolium	.	.	.	.	.	.	.	.	.	.	.	.	.	.	.	.	.	.	.	.	.	.	.	.	.	.	.	.	.	.	.	.	.	.	.	.	.	.	.
Hieracium_pilosella	.	.	.	.	.	.	.	.	.	.	.	.	.	.	.	.	.	.	.	.	.	.	.	.	.	.	.	.	.	.	.	.	.	.	.	.	.	.	.
Homogyne_alpina	.	+	.	.	.	1	.	.	.	.	.	.	.	.	1	+	1	.	.	.	.	.	.	.	.	.	.	.	.	.	.	.	.	.	.	.	.	+	.
Leontodon_helveticus	.	.	.	.	.	1	.	.	.	.	.	.	.	.	.	.	.	.	.	.	.	.	.	.	.	.	.	.	.	.	.	.	.	.	.	.	.	.	.
Leontodon_hispidus_sl	.	+	.	.	.	+	.	.	.	.	.	.	.	.	.	1	.	.	.	.	.	.	.	.	.	.	.	.	.	.	.	.	.	.	.	.	.	.	.
Leontodon_montanus	.	.	+	1	.	.	.	.	.	.	.	.	.	.	.	.	.	.	.	.	.	.	.	.	.	.	.	.	.	.	.	.	.	.	.	.	.	.	.
Ligusticum_mutellina	.	.	.	.	.	+	.	.	.	.	.	.	.	.	.	.	.	.	.	.	.	.	.	.	.	.	.	.	.	.	.	.	.	.	.	.	.	.	.





Species / Plot	41	42	43	44	45	46	47	48	49	50	51	52	53	54	55	56	57	59	60	61	62	63	64	65	67	68	69	70	71	73	74	75	76	77	78				
Lotus_alpinus	.	.	.	.	+	.	.	.	.	.	.	.	1	.	.	.	.	.	.	.	.	.	.	1	.	.	.	.	.	.	.	.	.	.	.	.			
Lotus_corniculatus_aggr	.	.	.	.	.	.	.	.	1	.	.	.	.	.	.	.	.	.	.	.	.	.	.	.	.	.	.	.	.	.	.	.	.	.	.	.			
Luzula_alpina	.	.	.	.	.	.	.	.	.	.	.	.	.	.	.	.	.	.	.	.	.	.	.	.	.	.	.	.	.	.	.	.	.	.	.	.			
Luzula_lutea	.	.	.	.	.	.	.	.	.	.	.	.	.	.	.	.	.	.	.	.	.	.	.	.	.	.	.	.	.	.	.	.	.	.	.	.			
Minuartia_verna	.	.	.	.	.	.	.	.	.	.	.	.	.	.	.	.	.	.	.	.	.	.	.	+	.	.	.	.	.	.	.	.	.	.	.	+			
Mochringia_ciliata	.	+	.	.	.	.	.	.	.	.	.	.	.	.	.	.	.	.	.	.	.	.	.	.	.	+	.	.	1	.	.	r	.	.	.				
Myosotis_alpestris	.	.	.	.	.	.	.	.	.	.	.	.	+	.	.	.	.	1	.	.	.	.	.	.	.	.	.	.	.	.	.	.	.	.	.	.			
Oxyria_digyna	.	1	.	.	.	.	.	.	.	.	.	.	.	.	.	.	.	.	r	.	.	.	.	.	.	.	.	.	.	.	.	.	.	.	.	.			
Oxytropis_campestris	.	.	.	.	.	.	.	.	.	.	.	.	.	.	.	.	.	.	.	.	.	.	.	.	.	.	+	.	.	.	.	.	.	.	.	.			
Pedicularis_verticillata	.	.	.	.	.	.	.	.	.	.	.	.	.	.	.	.	.	.	.	r	.	.	.	.	.	.	1	.	.	.	.	.	.	.	.	+			
Peucedanum_austriacum	.	.	.	.	.	.	.	.	.	2	.	.	.	.	.	.	.	.	.	.	.	.	.	.	.	.	.	.	.	.	.	.	.	.	.	.			
Phleum_rhaeticum	.	.	.	.	.	.	.	.	.	.	.	.	1	.	.	.	.	.	.	.	.	.	.	.	.	.	.	.	.	.	.	.	.	.	.	.			
Phyteuma_hemispermicum	.	.	.	.	.	.	.	.	.	.	.	.	.	.	.	.	.	.	.	.	.	.	.	.	.	.	.	.	.	.	.	.	.	r	.	.			
Plantago_alpina	.	.	.	.	.	.	.	.	.	.	.	.	r	.	.	.	.	.	.	.	.	.	.	.	+	.	.	.	.	r	.	.	.	.	.	.			
Plantago_atrata_sstr	.	.	.	.	.	.	.	.	.	.	.	.	.	.	.	.	.	.	.	.	.	.	.	.	.	.	.	.	.	.	.	.	.	.	.	.			
Poa_alpina	.	.	.	.	r	r	r	.	.	.	.	r	1	+	1	+	+	2	1	.	+	.	1	+	.	.	.	+	+	1	+	1	.	+	+				
Poa_cenisia	.	.	.	.	.	.	.	.	.	.	.	.	.	.	.	.	.	.	.	.	.	.	.	.	.	.	.	.	.	.	.	.	.	.	.	.	.		
Poa_minor	+	+	.	.	.	.	.	+	.	.	.	.	.	.	.	.	.	.	.	.	.	.	.	.	1	1	.	.	.	.	.	.	.	.	.	.			
Polygonum_viviparum	1	.	.	.	r	.	.	.	1	.	1	.	+	.	.	.	.	+	1	+	.	.	2	1	.	.	1	.	1	.	2	.	.	.	2				
Polystichum_lonchitis	.	.	.	.	.	.	.	.	.	.	.	.	.	.	.	.	.	.	.	.	.	.	.	.	.	.	+	.	.	.	.	.	.	.	.	.	.		
Potentilla_aurea	.	.	.	.	1	.	.	.	.	.	.	.	.	.	.	.	.	.	.	.	.	.	.	.	+	.	.	r	.	.	.	r	.	.	.	.			
Potentilla_brauneana	.	r	.	.	.	.	.	.	.	.	.	.	.	.	.	.	.	.	.	.	.	.	.	.	.	.	.	.	.	.	.	.	.	.	.	.			
Potentilla_grandiflora	.	.	.	.	+	.	.	.	.	.	.	.	.	.	.	.	.	.	.	.	.	.	.	.	.	.	.	.	.	.	.	.	.	.	.	.			
Pritzelago_alpina_sstr	.	+	.	.	.	.	r	+	.	+	.	+	.	+	.	.	.	.	r	r	.	.	.	.	+	r	.	.	.	.	.	.	+	+	r	.			
Pseudorchis_albida	.	.	.	.	.	.	.	.	.	.	.	.	.	.	.	.	.	.	.	.	.	.	.	.	.	.	.	.	.	.	.	.	.	.	.	.	.		
Ranunculus_alpestris	+	r	.	.	.	.	.	.	1	1	.	.	.	.	.	.	.	.	+	.	.	1	+	.	.	.	.	.	.	1	1	.	.	+	.	.			
Ranunculus_glacialis	.	.	.	+	.	.	.	.	.	.	.	.	.	.	.	.	.	.	.	r	.	1	.	.	.	.	.	.	.	.	2	2	+	2	.	.			
Ranunculus_montanus_aggr	+	.	.	.	.	.	.	.	1	.	+	.	+	.	.	.	.	.	+	+	.	.	.	r	.	.	r	.	.	.	.	.	.	.	.	.			
Rhododendron_ferrugineum	.	.	.	.	2	.	.	.	.	.	.	.	.	.	.	.	.	.	.	.	.	.	.	.	.	.	.	.	.	.	.	.	.	.	.	.	.		
Rumex_alpestris	.	.	.	.	.	.	.	.	.	.	.	.	.	.	.	.	.	.	.	.	.	.	.	.	.	.	.	.	.	.	.	.	.	.	.	.	1		
Salix_breviserrata	.	r	.	.	.	.	.	.	.	.	.	.	.	.	.	.	.	.	.	.	.	.	.	.	.	.	.	.	.	.	.	.	.	.	.	.	.		
Salix_reticulata	.	.	.	.	.	.	.	+	.	.	r	.	.	.	.	.	.	.	1	.	.	.	.	.	.	.	.	.	.	.	.	.	.	.	.	.	.		
Salix_herbacea	.	.	.	.	.	.	.	.	.	.	.	.	.	.	.	.	.	.	.	.	.	.	.	.	.	.	.	.	.	.	.	.	.	2	.	.	.		
Salix_retusa	1	.	.	.	r	.	.	.	2	.	r	.	.	.	.	.	.	r	+	.	.	.	.	.	2	1	.	1	.	.	.	.	.	.	.	.			
Salix_serpillifolia	1	.	.	.	.	.	.	.	.	.	.	.	.	.	.	.	.	.	.	1	.	.	.	.	.	.	.	.	.	.	2	2	.	.	.	.			
Saxifraga aizoides	.	1	.	.	.	r	1	+	.	r	+	+	.	+	1	.	r	+	.	1	+	.	.	.	1	.	.	+	.	.	.	.	.	.	.	.			
Saxifraga_androsacea	.	.	.	.	.	.	.	.	.	.	.	.	.	.	.	.	.	.	.	.	.	.	.	.	.	.	.	.	.	.	.	.	.	.	.	.	.		
Saxifraga_biflora	.	.	.	.	.	.	.	.	.	.	.	.	.	.	.	.	.	.	.	.	.	.	.	.	.	.	.	.	.	.	.	.	.	.	.	.	.		
Saxifraga_exarata	.	.	.	.	.	.	.	.	.	.	.	.	.	.	.	.	.	.	.	.	.	.	.	.	.	.	.	.	.	.	.	.	.	1	.	.	.		
Saxifraga_moschata_sl	.	.	.	.	.	.	.	.	.	.	.	.	.	.	.	.	.	.	.	.	.	.	.	.	.	.	.	.	.	.	.	.	.	.	.	.	.		
Saxifraga_oppositifolia	.	.	.	+	.	.	r	+	.	r	.	r	.	.	.	.	.	.	.	.	.	.	.	.	+	.	1	+	.	.	.	.	.	.	.	+	.		
Saxifraga_paniculata	.	.	.	.	.	.	.	.	.	.	.	.	.	.	.	.	.	.	r	r	1	.	.	.	.	.	.	.	.	.	+	.	.	.	.	.	.		
Saxifraga_seguieri	.	.	.	.	.	.	.	.	.	.	.	.	.	.	.	.	.	.	.	.	.	.	.	.	.	.	.	.	.	.	.	.	.	.	1	.	.		
Saxifraga_stellaris	.	+	.	.	.	.	.	.	.	.	.	.	.	.	.	.	.	.	.	.	.	.	.	.	.	.	.	.	.	.	.	.	.	.	.	.	.		
Scabiosa_lucida	.	.	.	.	.	.	.	.	.	.	.	.	.	.	.	.	.	.	.	.	.	.	.	.	.	.	.	.	.	.	.	.	.	.	.	.	.		
Sedum_atratum	.	+	.	.	.	.	.	r	.	r	.	.	.	r	+	.	.	.	.	.	.	.	.	.	.	+	.	.	.	r	+	.	.	.	.	+			
Selaginella_selaginoides	.	.	.	.	r	.	.	.	.	.	r	.	.	.	.	.	.	.	.	.	.	.	.	.	.	.	.	.	.	.	.	.	.	.	.	.	.		
Sesleria_caerulea	2	.	.	.	r	.	.	.	2	.	3	.	.	.	.	.	.	.	.	.	.	.	.	.	.	.	.	.	.	.	.	.	.	.	.	.	2		
Sibbaldia_procumbens	.	.	.	.	.	.	.	.	.	.	.	.	.	.	.	.	.	.	.	.	.	.	.	.	.	.	.	.	.	.	.	.	.	.	.	.	.		
Silene_aucaulis	1	.	.	.	2	.	.	.	.	.	.	.	.	.	.	.	.	.	.	.	.	.	.	.	.	.	.	.	.	1	r	2	1	1	.	.	.		
Silene_vulgaris	.	.	.	.	.	.	.	.	.	.	.	.	r	.	.	.	.	.	.	.	.	.	.	.	.	.	.	.	.	.	.	.	.	.	.	.	.		
Solidago_virgaurea_minuta	.	.	.	.	.	.	.	.	.	.	.	.	.	.	.	.	.	.	.	.	.	.	.	.	.	.	.	.	.	.	.	.	.	.	.	.	.		
Soldanella_alpina	.	.	.	.	.	.	.	.	.	.	.	.	.	.	.	.	.	.	.	.	.	.	.	.	.	r	.	.	.	.	.	.	.	.	.	.	.		
Taraxacum_alpinum_aggr	.	.	.	.	.	.	.	.	.	.	.	.	.	.	.	.	.	.	.	.	.	.	.	.	.	.	.	.	.	.	.	.	.	.	.	.	.		
Thlaspi_rotundifolium_aggr	.	+	r	r	.	.	1	r	.	+	r	+	.	.	.	.	.	+	1	+	.	.	.	r	+	.	.	.	+	.	.	.	.	+	.	+			
Thymus_alpestris	.	.	.	.	.	.	.	.	.	.	.	.	.	.	.	.	.	.	.	.	.	.	.	.	.	.	.	.	.	.	.	.	.	.	.	.	.		
Trifolium_badium	.	.	.	.	.	.	.	.	.	.	.	.	.	.	.	.	.	.	.	.	.	.	.	.	.	.	.	.	.	.	.	.	.	.	.	.	+	.	
Trifolium_thalii	.	.	.	.	.	.	.	.	.	.	.	.	.	.	.	.	.	.	.	.	.	.	.	.	.	.	.	.	.	.	1	.	.	.	.	.	.		
Urtica_dioica	.	.	.	.	.	.	.	.	.	.	.	.	.	+	.	.	.	.	.	.	.	.	.	.	.	.	.	.	.	.	.	.	.	.	.	.	.		
Vaccinium_uliginosum	.	+	.	.	.	.	.	.	.	.	.	.	.	.	.	.	.	.	.	.	.	.	.	.	.	.	.	.	.	.	.	.	.	.	.	.	.		
Veronica_alpina	.	1	.	.	.	.	.	.	.	.	.	.	.	.	.	.	.	.	.	.	.	.	.	.	.	.	.	.	.	.	.	.	.	.	.	1	.		
Veronica_aphylla	.	.	.	r	.	r	.	.	.	.	r	.	.	1	.	.	.	.	.	.	.	.	.	.	.	.	.	.	.	1	.	1	.	.	1	.	r	+	+
Viola_cenisia	.	.	.	.	.	.	.	.	.	.	.	.	.	.	.	.	.	.	.	.	.	.	.	.	.	.	.	.	.	.	.	.	.	.	.	.	.	.	

